GEOMORPHOLOGICAL CHANGE MODELS FOR THE SABIE RIVER IN THE KRUGER NATIONAL PARK

AL Birkhead · GL Heritage · CS James
KH Rogers · AW van Niekerk

WRC Report No 782/1/00

Water Research Commission

Disclaimer

This report emanates from a project financed by the Water Research Commission (WRC) and is approved for publication. Approval does not signify that the contents necessarily reflect the views and policies of the WRC or the members of the project steering committee, nor does mention of trade names or commercial products constitute endorsement or recommendation for use.

Vrywaring

Hierdie verslag spruit voort uit 'n navorsingsprojek wat deur die Waternavorsingskommissie (WNK) gefinansier is en goedgekeur is vir publikasie. Goedkeuring beteken nie noodwendig dat die inhoud die siening en beleid van die WNK of die lede van die projek-loodskomitee weerspieël nie, of dat melding van handelsname of -ware deur die WNK vir gebruik goedgekeur of aanbeveel word nie.

GEOMORPHOLOGICAL CHANGE MODELS FOR THE SABIE RIVER IN THE KRUGER NATIONAL PARK

by

A.L. BIRKHEAD[1], G.L. HERITAGE[2], C.S. JAMES[1],
K.H. ROGERS[1] AND A.W. VAN NIEKERK[1]

[1]Centre for Water in the Environment
University of the Witwatersrand
Private Bag 3, WITS 2050
Johannesburg
South Africa

[2]Department of Geography, Peel Building
University of Salford
Manchester M5 4WP
United Kingdom

Report to the Water Research Commission on the Project
"Scenario Modelling for the Kruger National Park Rivers
Research Programme Decision Support System"

Project Leaders: Professor C.S. James
Professor K.H. Rogers

WRC Report No: 782/1/00
ISBN No: 1 86845 317 0

DEDICATION

Andre van Niekerk
1960 - 1996

This research report is dedicated to the memory of our colleague and co-author, Andre van Niekerk. Andre died tragically in a motor vehicle accident en route from the Kruger National Park in May 1996. Andre contributed significantly to the concepts and research upon which this work is founded, and indeed was the principal author of the original research proposal. Quantification of geomorphological change in complex bedrock influenced systems such as the Sabie River is a perplexing task, and this study was made that much more difficult without the contribution of the key proponent. Andre's absence has been sorely felt by we his colleagues and the wider research community in South Africa. He contributed greatly to state of the art rivers research in South Africa, publishing significant work in the fields of fluvial hydraulics, sedimentology and geomorphology. We extend our sincere sympathies to Andre's wife, Simone, and children Benjamin and Michael.

EXECUTIVE SUMMARY

1 Background and Motivation

The Kruger National Park Rivers Research Programme (KNPRRP) was established to develop understanding of the functioning of the natural environments of the rivers and the methodologies required to define their water quantity and quality requirements under constantly changing climatic conditions and land-use practices in the catchment.

It was recognised early in the programme that ecological functioning of the rivers depends strongly on their physical forms, which are determined by the distribution of sediment accumulations in association with bedrock structures and vegetation. Previous studies carried out by the Centre for Water in the Environment (CWE) were therefore planned and carried out to improve understanding of the nature of this physical template and its dynamic response to changes in the hydrological regime, such as could result from water resources development upstream.

The study of Heritage *et al* (1997a) described the contemporary morphology of the Sabie and Letaba Rivers, the establishment of the temporal pattern of change in the channel morphology, the construction of a conceptual model of channel change, the quantification of catchment processes and their effects at appropriate spatial scales, and the development of rudimentary predictive models for fluvial geomorphological change.

The Sabie and Letaba Rivers were classified according to a hierarchical system (Fig. a). The classification uses the principle of agglomerative association with increasing spatial scale, from groups of morphological units progressing through channel types, reaches, macro-reaches and zones, through to the whole river system. This has enabled the descriptive mapping of the geomorphological structure of the Sabie River, and forms the basis for structuring both conceptual and quantitative models of geomorphological change.

A semi-quantitative sediment transport and storage model was developed by Heritage *et al* (1997a) for predicting change at the channel type scale on an annual basis. The Sabie River in the KNP was divided into "sections" (referred to in this study as cells), based on the five principal channel type categories (single thread, braided, mixed anastomosing, bedrock anastomosing and pool-rapid). Topographical information (surveyed cross-sections), characteristic flow resistance coefficients and rating data were used to determine annual sediment transport capacities based on daily flows. Annual sediment loads were assigned to cells (based on channel type) where these data were not available. The change in storage for the channel type cells was modelled for the period 1959 to 1993, and the results were compared to the change in area of exposed sediment from aerial photographs at fixed points along the Sabie River from 1986 through to 1989. The results showed a complex spatial pattern of change with zones of increased sedimentation immediately downstream of the Saringwa, Nwaswitshaka and Sand River tributaries.

The study carried out by Heritage *et al.* (1997a) laid a solid foundation for understanding the morphological dynamics of the Sabie and similar rivers, but did not produce the predictive methodologies required for the Decision Support System (DSS) being developed within the KNPRRP. Accordingly, their report recommended the following further research (the chapter numbers indicate where the topics are addressed in this report):

- Refinement and verification of the suite of geomorphological change and hydrodynamic models through model application (chapters 2, 3 and 5).
- Integration of geomorphological and ecological studies at the spatial and temporal scales at which geomorphological change can be realistically predicted (chapter 7).
- Development of models (and understanding) for prediction of ecological change in response to geomorphological change (chapters 1, 2, 5 and 7).
- Modelling of geomorphological change along the Sabie River under scenarios specified through the KNP DSS (chapter 6).

The project described in this report was intended to continue the previous work carried out on the Sabie River, and to pursue these recommendations.

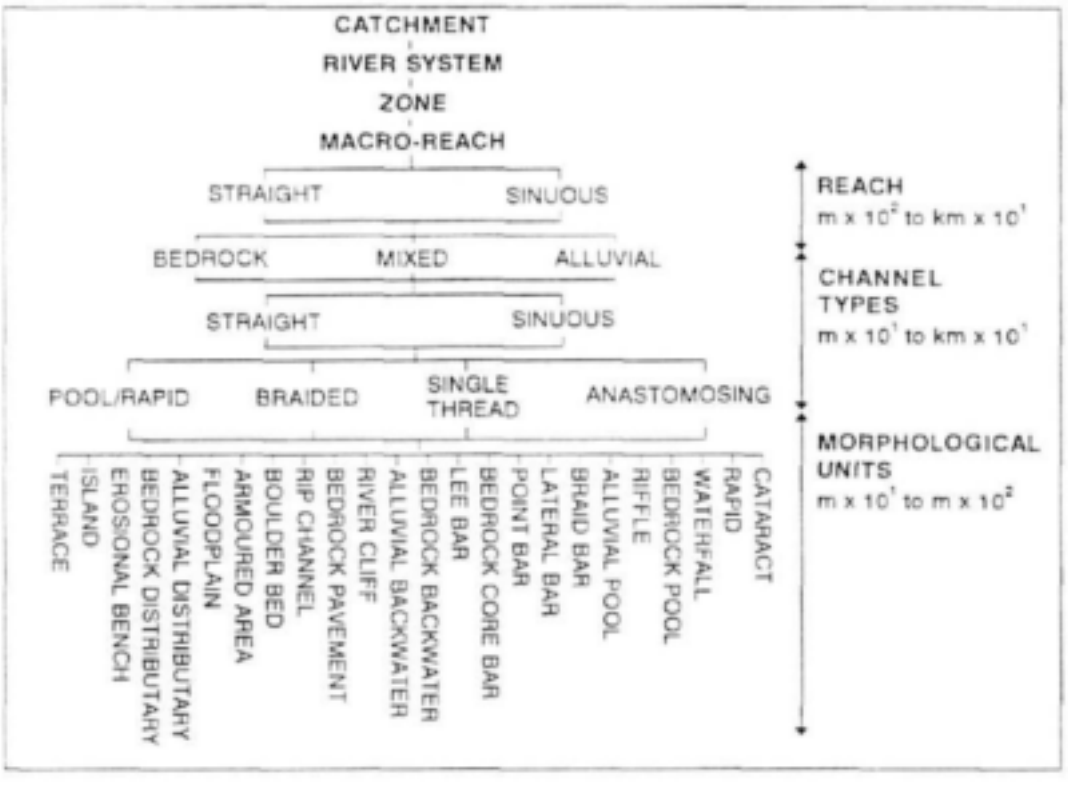

Figure a A hierarchical geomorphological structure of the Sabie River in the Kruger National Park (van Niekerk *et al.*, 1995)

2. Project objectives

The main objective specified for this project was ***the development of geomorphological change models for integration with a Decision Support System for water resource management***. This was to be achieved through pursuit of the following aims:

- ***Refinement, verification and testing of a suite of hydraulic and geomorphological change models developed by the Centre for Water in the Environment (CWE) for use in the Kruger National Park (KNP) Decision Support System (DSS).***

- ***Modelling of geomorphological change on the Sabie River since the early 1900s in order to isolate the effects of past climatic change and anthropogenic influences.***

- *Integration of the results with other research conducted within the KNP Rivers Research Programme.*

3 Major results and conclusions

3.1 Overview of contributions to the understanding and prediction of geomorphological change along the Sabie River

An investigation of the influence of flow regime on the direction and magnitude of geomorphological change along the Sabie River is described in chapter 2. It is demonstrated that, in this semi-arid system, the dominant discharge occurs towards the high magnitude end of the statistical distribution of flood events; the implications of this are discussed with reference to the management of flows to maintain the ecological integrity of the Sabie River.

Previous geomorphological studies (van Niekerk and Heritage, 1993; van Niekerk *et al.*, 1995; Moon *et al.*, 1997; Heritage *et al.*, 1997a) have considered the movement of non-cohesive, medium grained sand within the Sabie River system, since this is the fraction primarily responsible for morphological activity within the active channel. Cohesive fine-grained sediments also occur, however, as large scale consolidated deposits within the incised macro-channel, usually deposited as clay drapes following large flood events. A study of the potential for erosion of consolidated sediments by the infrequent large-magnitude flow events characteristic of semi-arid flow regimes is described in chapter 3, where the results are discussed with relevance to the proposed management of the Sabie River flow regime.

Fluvial geomorphological change is driven by channel hydraulics, whose understanding is a prerequisite for the development of predictive models. The most recent and extensive study concerning channel flow resistance along the Sabie River was undertaken by Broadhurst *et al.* (1997). The hydraulic information generated by this project was limited by hydrological conditions at the time to low and intermediate discharges (up to $80m^3/s$). A large flood in the Sabie River in February 1996 (approximately 2000 m^3/s) provided an opportunity to collect additional high flow hydraulics data, and an extended hydraulics data set is presented in chapter 4. These data are integral to every aspect of this project, and indeed are essential to any study along the Sabie River requiring a translation of discharge into local hydraulic conditions.

Chapter 5 describes the development, calibration and verification of a SEDiment FLux and stOrage model (SEDFLO) for the Sabie River in the KNP. This is an extensive refinement of the channel type based sediment transport model developed by Heritage *et al.* (1997a). Historical data derived from aerial photographic records covering 56 years (1940 to 1996) were used to calibrate and test SEDFLO. Chapter 6 describes the modelling of dynamic sediment storage response to changes in the flow and sediment regimes for different scenarios. The scenarios were based on the instream flow requirement (IFR) recommendations for the Marite, Sand and Sabie Rivers (DWAF, 1997). These represent the most recent flow modification recommendations, from an ecological perspective.

SEDFLO predicts temporal changes in sediment storage (as reflected by bar growth and erosion) for 40 linked channel type cells along the Sabie River. The biota, however, respond to changes at substantially smaller spatial scales, and it has therefore been necessary to develop a model that predicts change at the morphological unit scale. Chapter 7 describes the application and testing of a such a model, which was first developed for predicting change at the unit morphological scale along the Sabie River (KNP) under the auspices of the Biological-abiological LINKS (BLINKS) programme (Heritage *et al.*, 1997b). The conceptual framework of the model is presented, together with a description and justification of the spatial and temporal scales at which it operates and the structure of its input data in relation to SEDFLO predictions. The model is applied to illustrate the nature of changes over the period 1940 to 1996.

3.2 Influence of flow regime on sediment transport characteristics

The transport of sediment through a river reach depends on discharge, and will therefore vary considerably through natural hydrological variations. Simulating sediment movement along the Sabie River required establishing the influence of flow regime (the characteristic pattern of temporal discharge variation) on sediment movement through each of the morphologically distinct channel types used as model cells. This was done by considering the frequency and effectiveness of sediment transport across the flow regime, using measurements of channel geometry, sedimentology, flow resistance and water surface slopes. It was found that, for all the channel types, most sediment transport occurs during large floods. Considering flows over a duration of 5 days, the major flood events account for between 23% and 43% of the potential annual sediment movement, depending on channel type (Table a).

For all alluvial channel types most sediment transport is associated with relatively frequent (up to 2-year return period) floods. For example, flows below the 1.1 year return period account for 39% of potential bulk sediment transport in braided channels. As the influence of bedrock increases, the larger, less frequent floods become progressively more important for bulk sediment transport. The floods responsible for 80% of potential sediment transport through the different channel types are those with return periods up to 2.5 years for braided channels, 3.7 years for single thread channels, 3.8 years for mixed anastomosing channels, 7.0 years for pool-rapid channels, and 7.8 years for bedrock anastomosing channels.

Table a Discharge rates and return periods on the annual maximum time series corresponding to the maximum annual potential sediment transport

Channel Type	Peak annual flow (m^3/s)	Return period (years)	Contribution to annual sediment transport of peak flows over a 5 day duration (%)
Braided	720	12.6	23
Pool-Rapid	721	12.6	35
Single-Thread	561	10.5	32
Mixed Anastomosing	1129	9.0	26
Bedrock Anastomosing	622	12.6	43

The implications of these findings for the management of flows to maintain the ecological integrity of the Sabie River are clear: changes to the present magnitude-frequency regime of flood flows will disrupt the prevailing balance in sediment transport processes and could induce rapid morphological change in the system. The importance of high magnitude, infrequent flows for the maintenance of macro-channel alluvial features has also been emphasised in the inundation frequency study of Heritage *et al.* (1995).

3.3 Influence of flooding on the erodability of cohesive sediments

As well as for sediment transport, large floods are also important geomorphologically because of their ability to erode the cohesive sediment deposited as large scale consolidated bar forms within the incised macro-channel. A measure of the potential for this erosion is provided by a statistical analysis of the frequency distributions of resisting and applied shear stresses, and is discussed with reference to field observations following a large flood in February 1996. The critical resistance to erosion of the cohesive sediments was determined from *in situ* shear vane strength measurements, combined with laboratory testing of disturbed samples. The spatial distribution of maximum shear stresses applied during the flood was determined using measurements of channel geometry, flow resistance, flood stages and water surface slopes.

The analysis shows that 68% of the cohesive sediments along the Sabie River may potentially be entrained by a discharge of approximately 2000 m^3/s. This value is similar (63% to 75%) for all the channel types with the exception of bedrock anastomosing channels, where the deposits have a 91% chance of being eroded at this discharge. The higher probability in the bedrock anastomosing channel types results from the significantly higher applied shear stresses (Table b).

During the flood of February 1996 (the peak was gauged at 1705 m^3/s and 2259 m^3/s, upstream and downstream of the Sand River tributary, respectively) removal of cohesive material was spatially isolated for the sites investigated along the length of the river, with vegetational cover providing increased protection from erosive forces. The proportion of the cohesive bed material eroded during this flood was less than the 68% predicted, although it was difficult to assess accurately because of spatial variability and the presence of more recent overlying deposits.

Although the actual erosion of cohesive material from the Sabie River bed during the flood was less than had been estimated, it is clear that large scale stripping of the macro-channel deposits can occur. The observed erosion was less than estimated because local boundary shear stresses were reduced by in-channel vegetation and also because the flow would have been transporting some catchment-derived sediment and not have entrained its full load from the channel bed. Furthermore, no account was taken of flood duration; longer or multiple floods would have greater potential for eroding cohesive sediments, resulting in stripping levels nearer to the predicted maximum potential. This emphasises the need to manage the riparian vegetation to enable it to continue affording protection to the cohesive bed during extreme flood events, and also to take account of the sediment loads derived from the catchment during floods.

Table b Probability of eroding cohesive sediments (discharge between 1705 m^3/s and 2259 m^3/s)

Channel type	**Spatial composition** (%)	**Probability of erosion** (%)	**Average applied shear stress** (Pa)
Braided	14	63	70
Pool-Rapid	28	66	63
Single-Thread	3	75	80
Mixed Anastomosing	35	63	59
Bedrock Anastomosing	20	91	145
Sabie River	100	68	70

3.4 Extended flow resistance data set

Hydraulic and geomorphological conditions are the primary determinants of physical habitat in rivers, and it is therefore necessary to understand the mechanisms controlling local hydraulic parameters when predicting the impacts of changes in the flow and sediment regimes. Local hydraulic conditions such as flow depth, velocity and bed shear are determined by the total flow resistance of the channel, which represents the aggregate of skin friction, channel form and vegetational resistance components. Broadhurst *et al.* (1997) carried out an extensive study of flow resistance in the Sabie River. The study quantified the total flow resistance at both the morphological unit and channel type (association of morphological units) scales. The flow resistance information was, however, limited to discharges below 40 m^3/s, except for the mixed anastomosing channel type where hydrological conditions during the study permitted measurements up to 80 m^3/s and for one isolated event of 1000 m^3/s.

The large flood event of 14 February, 1996 provided an opportunity to extend this data set. The flood peak was gauged from the road bridges at Kruger Gate and immediately downstream of the Sand River confluence at 1705 m^3/s and 2259 m^3/s, respectively. Peak and receding limb stage levels were recorded at the monitoring sites selected during previous studies.

Multiple linked cross-sectional profiles located at the same representative channel types used by Broadhurst *et al.* (1997) were used to compute the reach averaged total flow resistances according to the Barnes (1967) methodology. Manning's flow resistance coefficient values for the extended data set are plotted in Fig. b. The extended relationships converge at high flows due to the reduced influence of channel type specific hydraulic controls (e.g. channel morphology and vegetation structure).

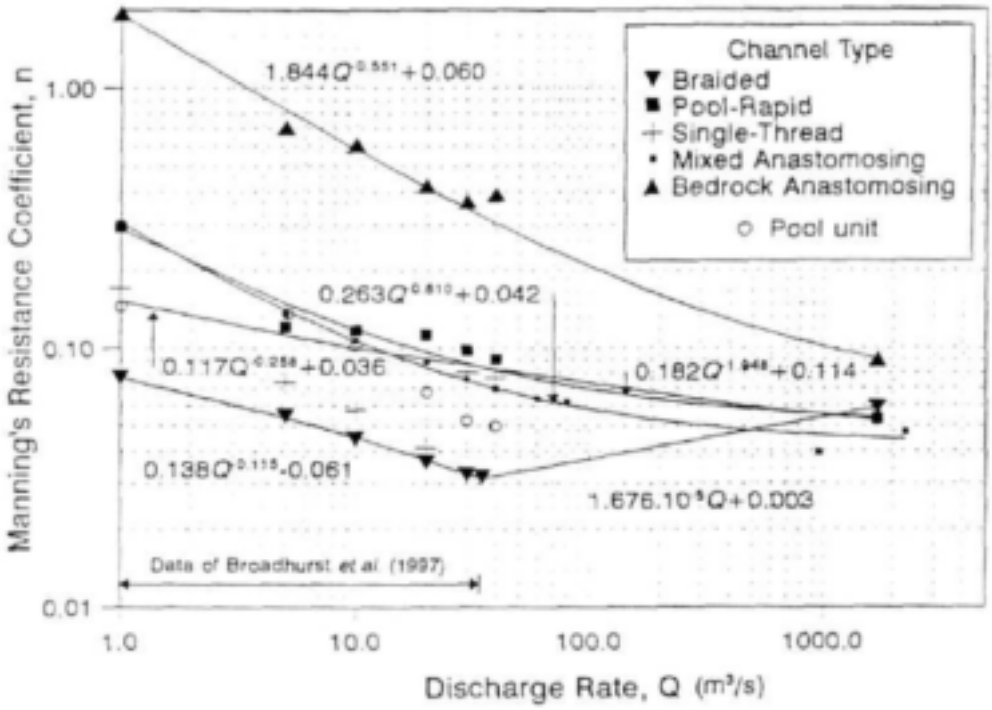

Figure b Variation of Manning's resistance coefficient for representative examples of the five principal geomorphological channel types along the Sabie River (extended from Broadhurst *et al.*, 1997).

3.5 Scenario modelling of temporal sediment storage along the Sabie River

The semi-quantitative sediment flux and storage model, developed for predicting change at the channel type scale on an annual basis by Heritage *et al.* (1997a) has been refined, calibrated and verified using historical data derived from aerial photographs covering 56 years. Modelling is carried out in two phases. The first phase deals with the production of sediment in the catchments of the Sabie River and its tributaries, and the delivery of this eroded source material to the study length of the river in the KNP. In the second phase the transport and storage of the sediment along the river is computed using the Sabie River SEDiment FLux and stOrage model (SEDFLO).

The first phase is performed jointly by the CALSITE and ACRU models. CALSITE was applied to the Sabie River catchment by Donald (1997), and is considered to provide more accurate long-term sediment yields. CALSITE output is in terms of annual sediment yield,

however, and because SEDFLO operates on a daily basis, these annual values were distributed in time according to the daily variations predicted by ACRU .

In SEDFLO the sediment transport along the river is calculated by the widely accepted total load equation of Ackers and White (1973). The model was calibrated for the Sabie River using historical information describing changes in sedimentation obtained from aerial photographs. The photographs provided useful assessments of geomorphological change and changes in coverage by alluvial bars, as illustrated in Fig. c. The 1940 to 1986 and 1944 to 1986 records (Fig. c) were used as a single data set for model calibration by determining the equivalent change over a 46 year period by linear extrapolation of the 1944 to 1986 data where necessary. During the period 1940 to 1986, the braided channel types exhibit the highest individual (cell 2) and average rate of bar growth (5.1%), followed by the pool-rapid (2.3%) and mixed anastomosing (1.5%) channel types. The bedrock anastomosing channel types have remained relatively stable, with an average rate of accumulation of only 0.3% of the total change along the river in the KNP. Only two cells (1 and 21) have been classified as single-thread channel types, and display zero and 2.4% of the total bar growth.

Application of SEDFLO indicates a long-term (1940 to 1986) change in sediment storage for the Sabie River within the KNP of approximately $3.5x10^3$ tons/annum (Fig. d). Shorter-term changes in sediment storage are highly variable, reflecting periods of progressive sediment accumulation interspersed by significant declines during years experiencing large flow events. The average increase in sediment storage during periods of progressive accumulation is as high as $40x10^3$ tons/annum, while the loss of sediment during years experiencing large floods is generally greater than $200x10^3$ tons.

The predicted changes in sediment storage are shown to be realistic when compared with changes in alluviation along the length of the Sabie River and the rate of siltation of the dam at Lower Sabie. The modelling of pre1940 change within the bedrock anastomosing channel types shows significant losses of in-channel sediment storage, and although there are no historical data to test this finding, a sequence of observed change suggests the occurrence of an extreme flood prior to 1940.

The following conclusions have been drawn from the scenario modelling of temporal sediment storage along the Sabie River, using flow regimes derived from IFR recommendations.

- Long-term rates of alluviation increase approximately in proportion to reduced mean annual runoff.

- Transient sediment storage behaviour is reduced by diminished flooding, as illustrated for the Sabie and Sand River IFR scenarios in Figs. e and f. This is likely to impact significantly the spatial and temporal assemblages of geomorphological features and associated aquatic and riparian habitats as irreversible sedimentation reduces the proportional occurrence of bedrock influence in the system.

- In adjusting to new dynamic equilibrium states in response to a reduced flooding regime, alluvial channel types tend to erode whilst pools and (to a lesser degree) mixed

anastomosing channel types tend to aggrade (Fig. g). Loss of storage in braided channel types is likely to result in smaller active channels, incised within the macro-channel infill deposit.

The extent of calibration required when using SEDFLO casts serious doubts on the advisability of using high resolution sediment transport models to describe bulk sediment movement and storage behaviour in complex systems such as the Sabie River. Requirements of greater accuracy with this approach must inevitably lead to impractically high resolution discretization and inappropriate detail in process modelling, with prohibitive data requirements. This approach is also inappropriate at the spatial scale directly influencing biotic response and an alternative, rule-based, modelling technique has therefore been developed for predicting change at the morphological unit scale.

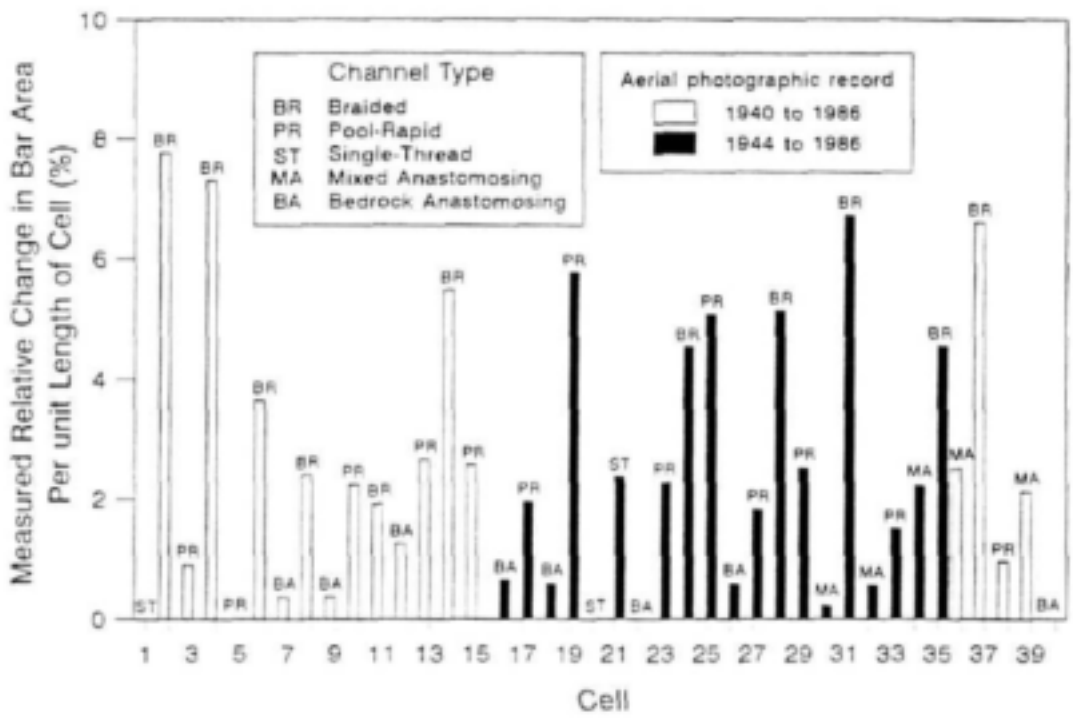

Figure c Change in bar area per unit length of river cell as a percentage of the total change along the Sabie River in the KNP, measured from the 1940/44 and 1986 photographic records.

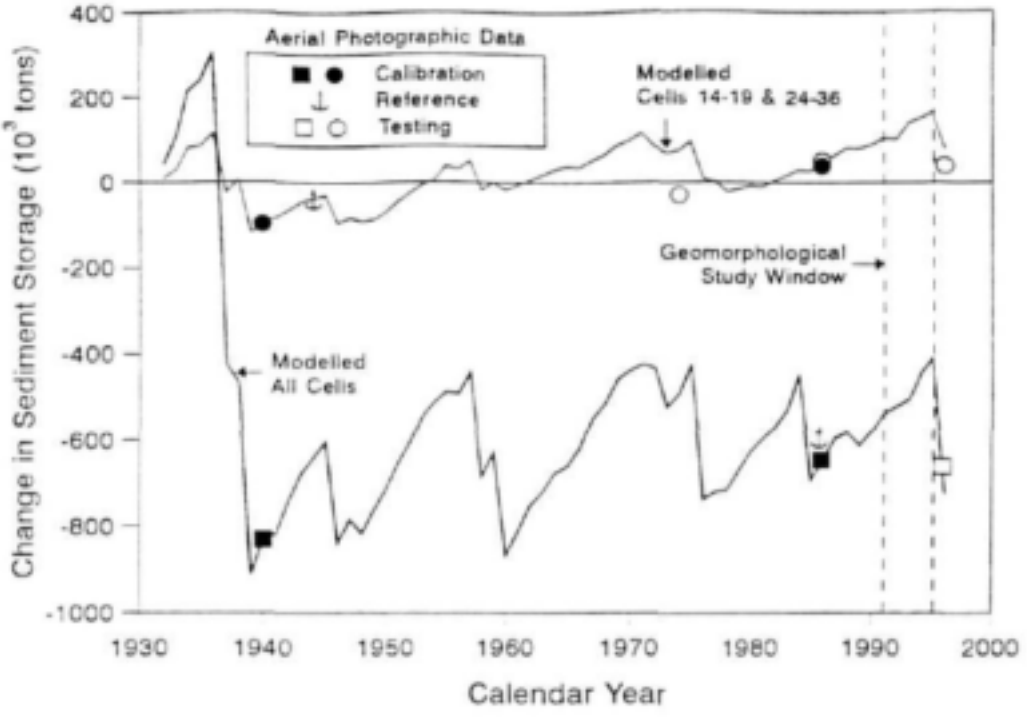

Figure d Plot of modelled change in sediment storage along the Sabie River over the period 1932 to 1996, showing the aerial photographic data used for model calibration and testing.

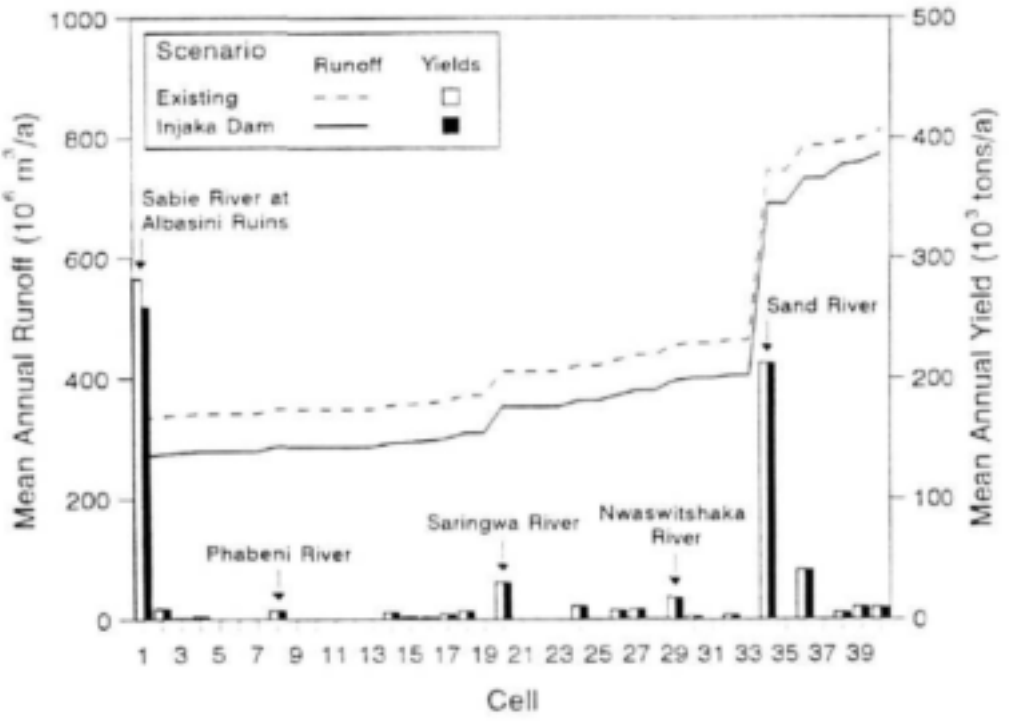

Figure e Mean annual runoff and sediment yields for the Sabie/Sand River IFR scenario, showing existing (historical) conditions.

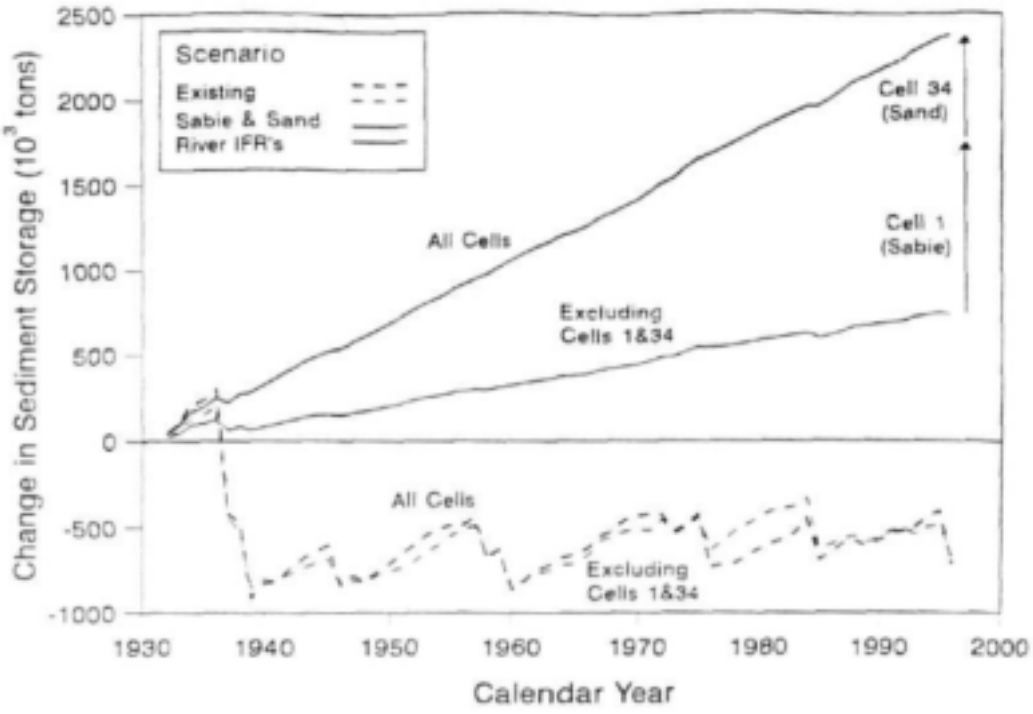

Figure f Plots of modelled changes in sediment storage along the Sabie River for the Sabie/Sand IFR scenario, showing existing (historical) conditions.

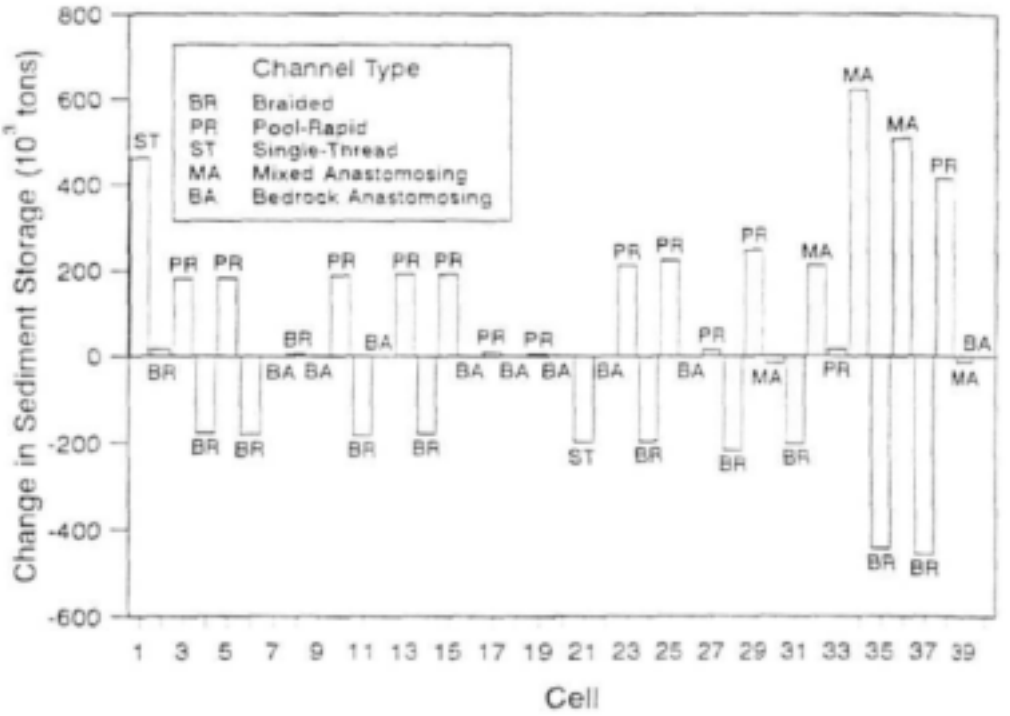

Figure g Net change in sediment storage along the Sabie River over the period 1932 to 1996 for the Sabie/Sand River IFR scenario.

3.6 Rule based modelling of geomorphological unit change along the Sabie River

At the scale appropriate for inferring biological response, volumes of sediment are less important to predict than the forms of deposits. Qualitative, rather than quantitative, description is therefore required. A logical rule-based approach has been developed that describes changes in relative proportions of morphological units constituting the different channel types. This model uses the general trends predicted by SEDFLO and translates them into channel form changes that influence biotic response. The same division of the river into cells and the same principal channel types are used as for SEDFLO. Daily flows are specified by indices representing the categories of base flow, freshette, annual flow or flood, and sediment input to each cell by indices representing the categories of low, reduced, moderate and high. The percentage representation of each morphological unit in a cell is then adjusted on the basis of these indices using rules determined from expert knowledge, field observation, aerial photograph interpretation and space for time substitution techniques.

The model was tested using synthesized flow and sediment flux data from SEDFLO, and the output compared with observed change in the areal coverage by unconsolidated sediment deposits within each of the five representative cells (one for each representative channel type) on the Sabie River. The results were also compared with the gross pattern of erosion and deposition predicted for each representative cell to determine if the modelled patterns of change were similar.

The rule based model appears to predict the direction of change in unconsolidated sedimentary deposits satisfactorily, the results indicating that sediment flux may have a greater influence on channel form than flow variability. Only in the case of the mixed anastomosing cell were predictions consistently poor. In some years expected changes to the macro-channel deposits were not confirmed by the model, possibly due to the lack of knowledge concerning the change dynamics of these features over longer time scales. In some instances, the morphological change predictions were not consistent with the historical aerial photographic data or the bulk change in sediment storage modelled using SEDFLO, and the degree of accuracy varied between the respective channel type cells. Possible reasons for the modelling inaccuracies include inaccuracy of rules due to limited expert knowledge and the assumption of untested morphological change hierarchies. These inadequacies reflect lack of detail, rather than shortcomings in the approach, and these can be supplemented as more knowledge becomes available.

The application of the rule based geomorphological unit change model gives encouraging evidence to support the further development of this methodology as a predictive tool. Further development and refinement, however, requires more data on morphological dynamics at the unit scale for a range of active and macro-channel features. The direct quantification of areal coverage by unit scale morphological features from aerial photographs over the period of record (1940 to 1996) was beyond the scope of this project and will require a protracted desktop study. These data are, however, imperative to any real further developments of the methodology. Continuation of aerial photographic data collection is essential for providing historical records necessary for further model testing.

4 Attainment of objectives

The models presented in this report provide a basis for assessing the impact of water resources development in the Sabie River catchment on the physical characteristics of the river, and hence on biotic response.

The hydraulic and geomorphological change models previously developed by the CWE for use in the KNP DSS have been refined, verified and tested. SEDFLO, which describes the bulk distribution of sediment along the river and changes on a channel type scale, is fully developed and can be applied to predict responses to natural or anthropogenic hydrological changes. Use of the model is described in the appendix to this report and the code is available on the KNPRRP web site (http://www.ccwr.ac.za/knprrp/index.html). This model could be applied to other rivers in Southern Africa but would require substantial field work to obtain the necessary data, and to describe any channel types different from those on the Sabie. The rule-based model for translating SEDFLO output to the morphologic unit scale is not fully developed due to current lack of knowledge of system behaviour at this scale, although the model structure shows potential for its development into a valuable tool.

SEDFLO has been applied to predict the river response to scenarios based on IFR recommendations, to demonstrate the magnitude of possible changes. It has not been used to isolate the effects of past climatic and anthropogenic changes, as originally proposed, because the data currently available are inadequate for making this distinction for input and because the value of this analysis is now considered to be less important than when originally motivated. This application could be carried out after extensive interpretation of climatic and hydrological data, but its value should be carefully reconsidered before doing so.

The model applications have been integrated with other research conducted within the KNPRRP. The scenario modelling undertaken so far used IFR recommendations for the Marite, Sand and Sabie Rivers. The rule-based model was applied in close collaboration with the BLINKS project.

The scenarios modelled provide an indication of the effects of applying existing IFR recommendations, but do not allow for reservoir spillage or different reservoir operation options. Once comprehensive water resource system simulations have been completed, SEDFLO can be used again to refine the predictions presented in this report.

5 Recommendations for further research

Further research is necessary to improve understanding of channel adjustment at the morphological unit scale, in order to enable more reliable rules to be formulated for the rule-based model.

The high level of dependence of SEDFLO on site-specific calibration makes its transferability to other rivers difficult. Further research on novel (e.g. rule-based) modelling approaches should lead to more easily transferable products.

ACKNOWLEDGEMENTS

The funding of this project by the Water Research Commission is gratefully acknowledged. The research in this report represents an extension of previous studies of the geomorphological response to changing flow regimes as well as hydraulic aspects of flow in the Sabie River, Kruger National Park. The contributions and assistance provided by the numerous persons mentioned in the foregoing reports are therefore also acknowledged here.

In addition, particular institutions and individuals contributed directly to this study, and we extend our sincere thanks to the following.

The University of the Witwatersrand, Department of Civil Engineering provided computing facilities, Norman Alexander was always willing to give assistance and advice in the soils laboratory, and J. Galpin gave guidance in the statistical minefield. The Centre for Water in the Environment, and in particular Mrs Wendy Midgley provided continual support. Bernie Moon also assisted with shear vane tests.

Kim Mace from the Department of Environmental Studies at the University of Bradford made invaluable contributions with the analysis of aerial photographs.

The Council for Industrial and Scientific Research (CSIR), and in particular Paul Donald collaborated with us in work on sediment production in the Sabie River catchment.

The University of Stellenbosch, Department of Civil Engineering, and in particular Graham Jewitt gave assistance in procuring the hydrological simulations for the Sabie River catchment under auspices of the abiotic-biotic links project.

The University of Natal, Department of Agricultural Engineering undertook the hydrological and sediment production modelling for the Sabie River catchment.

Bruce Harnett from King's College, University of London, assisted in the soils laboratory.

The South African National Parks provided field and logistical support.

The Steering Committee established by the Water Research Commission for this project made some valuable comments for improvement of the report.

The Steering Committee responsible for this project, consisted of the following persons:

Mr D S van der Merwe	Water Research Commission
Dr S A Mitchell	Water Research Commission
Mrs C M Smit	Water Research Commission (Secretary)
Professor K Rountree	Rhodes University
Dr H Biggs	Kruger National Park
Professor Görgens	University of Stellenbosch

Mr N Armitage	University of Cape Town
Dr J King	University of Cape Town
Dr R McKenzie	WRP Consulting Engineers (Pty) Ltd.
Professor G R Basson	University of Pretoria.

CONTENTS

NOTATION

A	Cross-sectional flow area (m^2)
A	Bar area (m^2)
A	Two dimensional array of coefficients
A_1, A_2	Initial and final bar areas (m^2)
ΔA	Change in bar area (m^2)
a, b, c	Regression coefficients in the Manning resistance vs. discharge relationship
A, m, C	Empirical coefficients in the dimensionless sediment transport relationship
B	One dimensional array of constants
C	Chezy resistance coefficient ($m^{1/2}/s$)
C	Cover and management factor
d	Grain diameter (m)
D	Flow depth (m)
$\bar{D}$	Average flow depth (m)
D_{gr}	Dimensionless grain diameter
d_{35}	Diameter at which 35% of the sediment is finer (m)
d_{50}	Diameter at which 50% of the sediment is finer (m)
Di_p	Delivery index
E	Long-term average annual soil loss (t/ha/annum)
f	Darcy-Weisbach friction factor
F	Flow parameter
F_{cg}	Sediment mobility number for coarse grain size sediments
F_{fg}	Sediment mobility number for fine grain size sediments
F_{gr}	Sediment mobility number for coarse, intermediate and fine grain size sediments
Fr	Froude number
g	Gravitational acceleration constant (9.81 m/s^2)
G	Dimensionless sediment transport
γ	Unit weight of water (ρg, 9810 N/m^3)
ha	hectare (10 000 m^2)
h_n	Water surface elevation at n^{th} cross-sectional profile (m)
$\Delta h_{v_{(i+1)}}$	Velocity head loss between cross-sectional profile i and $i+1$ (m)
h_{v_n}	Velocity head at n^{th} cross-sectional profile (m)
i	Cell index
i	Cross-sectional profile index
I_i	Sediment inflow to the i^{th} cell (tons)
I_p	Plasticity index
j	Cell index
K	Soil erodability factor
$k_{s(i+1)}$	Energy loss coefficient between cross-sectional profile i and $i+1$
l	Bar length (m)
l_1, l_2	Initial and final bar lengths (m)
Δl	Change in bar length (m)
L	Slope length factor
$L_{s(i+1)}$	Reach length between cross-sectional profile i and $i+1$ (m)
μ	Micron (10^{-6} m)

n	Manning resistance coefficient (s/m$^{1/3}$)
n	Sediment type indicator in Ackers and White (1973) equation
N	Number of cross-sectional profiles
O_i	Sediment outflow from the i^{th} cell
P	Supporting conservation practice factor
P	Wetted perimeter (m)
ρ_s	Density of sediment (2650 kg/m^3)
ρ	Density of water (1000 kg/m^3)
Q	Discharge rate (m^3/s)
Q	Event or long term runoff volume (m^3)
Q_s	Mass sediment discharge (m^3/s)
Qs_{pot}	Long-term potential sediment discharge (tons)
q_p	Event peak discharge rate (m^3/s)
R	Rainfall erosivity factor (Jmm10^3/m^2/hr)
R	Regression coefficient
R	Hydraulic radius (m)
S	Slope gradient factor
S	Channel slope
SE	Source erosion
S_f	Energy slope
S_f^h	High flow energy slope
S_f^l	Low flow energy slope
S_v	Shear vane strength (kPa)
S_s	Mass density of sediment relative to that of fluid (2.65)
ΔS_i	Change in sediment storage for the i^{th} cell (tons)
ΔS_i^*	Relative change in sediment storage for the i^{th} cell
τ_a	Average boundary shear stress (N/m^2)
τ_c	Critical boundary shear stress (N/m^2)
τ_o	Shear stress (N/m^2)
θ	Slope of the vane shear strength vs. critical shear stress relationship
t,ton	1000 kg
U	Average flow velocity (m/s)
U_f	Fraction finer than 60μ (%)
u_*	Shear velocity (m/s)
u_*'	Shear velocity related to grain roughness (m/s)
v	Average flow velocity (m/s)
υ	Kinematic viscosity (1.14 10^{-6} at 15 °C, m^2/s)
W	Surface flow width (m)
X	Concentration of sediment transport
X_i	$A_i R_i^{2/3}$ (m$^{8/3}$)
Y_i	$A_i R_i^{1/2}$ (m$^{5/2}$)
Y_i	Catchment sediment yield to the i^{th} cell (tons)
Y_{sd}	Event sediment yield (t)
Z_i	$A_i^2 R_i$ (m^5)

LIST OF ACRONYMS AND ABBREVIATIONS

ACRU	Agricultural Catchments Research Unit
BA	Bedrock Anastomosing
BBM	Building Block Methodology
BLINKS	abiotic-Biotic LINKS
BR	BRaided
CALSITE	CALibrated SImulation of Transported Erosion
CWE	Centre for Water in the Environment
DSS	Decision Support System
DWAF	Department of Water Affairs and Forestry
GIS	Geographical Information System
IFR	Instream Flow Requirement
KNP	Kruger National Park
MA	Mixed Anastomosing
MAR	Mean Annual Rainfall
MUSLE	Modified Universal Soil Loss Equation
PR	Pool-Rapid
ST	Single-Thread
USA	United States of America
USLE	Universal Soil Loss Equation
SEDFLO	SEDiment FLux and stOrage model
SLEMSA	Soil Loss EstiMator for Southern Africa

LIST OF FIGURES

Executive summary

Chapter 1 Introduction

Chapter 2 Influence of flow regime on sediment transport characteristics

Chapter 3 Influence of flooding on the erodability of cohesive sediments

Chapter 4 Channel hydraulics

Chapter 4 Sabie River sediment flux and storage model

Chapter 6 Scenario modelling of geomorphological change

Chapter 7 Rule based geomorphological unit change model

LIST OF TABLES

Chapter 6 Scenario modelling of geomorphological change

Chapter 7 Rule based geomorphological unit change model

1 Introduction

1.1 The rivers of the Kruger National Park

The seven major rivers flowing through the Kruger National Park (KNP) in the Mpumalanga Lowveld (Crocodile, Sabie, Olifants, Letaba, Shingwedzi, Levuvhu and Limpopo Rivers) all rise beyond the western border of the KNP and drain catchments that are being subjected to increasing pressure for their available land and water resources. This pressure arises from the escalating human population growth and associated domestic water demands in the rural areas immediately west of the KNP, coupled with afforestation and agricultural development in the upper catchments. Studies undertaken by the Sabie River Working Group in conjunction with the Department of Water Affairs and Forestry (DWAF) and the Development Bank of Southern Africa have shown that the need for water resource development in the region is so great that it can be justified on purely economic grounds (DWAF, 1994).

Attention has been focused mainly on the Sabie River as the most natural, but imminently threatened and only perennial river flowing through the KNP. Construction of the Injaka Dam on a tributary of the Sabie River is well underway, with the Bushbuckridge transfer pipeline having been completed. The additional water supply will be used primarily to meet domestic requirements, thereby implementing the Government's Reconstruction and Development Programme. It will also provide higher assurance supplies for the agricultural sector and allocation for the conservation of the riverine ecosystems of the area and the associated natural environment (DWAF, 1994)

The Sabie River drains approximately 6000 km^2 of the Mpumalanga Province in the north-east of South Africa (Fig. 1). It is a semi-arid catchment, with a mean annual precipitation varying from 1800 mm over a relatively small area on the Drakensberg escarpment in the west, to 400 mm in the east. This is in sharp contrast to the mean annual evapotranspiration losses of 1400 mm in the west, rising to 1700 mm in the east. Rainfall, and consequently discharge, are highly variable within the KNP, displaying seasonal minima (0.5 m^3/s to 1 m^3/s) in the dry winter months (April to September) and mean summer flows of 15 m^3/s to 20 m^3/s. Extreme flood events have been gauged in excess of 2000 m^3/s (February 1996). Changes in the flow and sediment regimes of the Sabie River are leading to morphological adjustments, with an associated alteration in habitat and water availability for aquatic and riparian fauna and flora (Heritage *et al.*, 1997a). The Sabie River in the KNP is characterised by a wide fringe of riparian vegetation colonising the river banks, where more than 130 indigenous species of shrubs and trees occur. The riverine environment provides essential habitat for fish, reptiles, amphibians, invertebrates, hippopotami, birdlife and browsers that utilise the riparian zone.

A number of projects have been conducted into physical and biotic aspects of the Sabie River and its catchment area, including the geology (Cheshire, 1994), hydrology (Chunnett *et al.*, 1990; Hughes *et al.*, 1996, Jewitt *et al.*, 1997), geomorphology (Heritage *et al.*, 1997a, 1997b), hydraulics (Broadhurst *et al.*, 1997) riparian vegetation (Carter and Rogers, 1995; de Fontaine, 1995; van Coller and Rogers, 1995; van Coller and Rogers, 1996, van Coller *et al.*, 1997) and its water use (Birkhead *et al.*, 1997), fish and invertebrates (Weeks *et al.*, 1996; O'Keeffe *et al.*, 1996), and these should be consulted for detailed information.

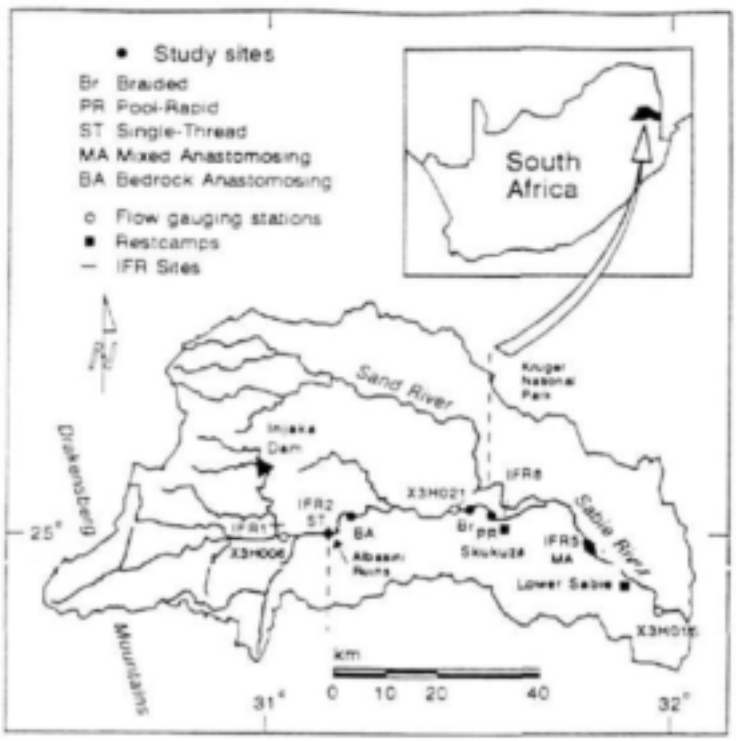

Figure 1 Sabie River catchment and location of study sites and the Injaka Dam

1.2 Project objectives

The main objectives of this project were:

1. Refinement, verification and testing a suite of hydraulic and geomorphological change models developed by the Centre for Water in the Environment (CWE) for use in the KNP Decision Support System (DSS).

2. Modelling of geomorphological change on the Sabie River since the early 1900s in order to isolate the effects of past climatic change and anthropogenic influences.

3. Integration of the results with other research conducted within the KNPRRP.

This project represented a continuation of previous work conducted on the Sabie River in the KNP by the CWE, and it is therefore appropriate to cite the main objectives and findings of two relevant earlier studies upon which much of the work described in this report is based.

1.2.1 The geomorphological response to changing flow regimes of the Sabie and Letaba River systems (Heritage *et al.*, 1997a)

The main objectives pursued in the study included the description of the contemporary morphology of the Sabie and Letaba Rivers, the establishment of the temporal pattern of change in the channel morphology, the construction of a conceptual model of channel change, the quantification of catchment processes and their effects at the appropriate spatial scales, and the development of predictive models for fluvial geomorphological change. The strategy adopted by Heritage *et al.* (1997a) to achieve the above aims and findings pertinent to the present study are discussed below.

The Sabie and Letaba systems were classified according to a hierarchical system (Fig. 2). The classification uses the principle of agglomerative association to increase the spatial scale, from groups of morphological units progressing through channel types, reaches, macro-reaches and zones, through to the whole river system. The classification system has allowed the descriptive mapping of the geomorphological structure of the Sabie and Letaba Rivers, and forms the basis for structuring both conceptual and quantitative models of geomorphological change.

On the Sabie River, five principal channel types are common and readily recognisable, including *alluvial single thread* (fully alluvial, regular single channel river, straight or sinuous planform), *alluvial braided* (alluvial multi-channel network of distributaries), *mixed anastomosing* (multi-channel network of distributaries in both alluvium and bedrock), *bedrock anastomosing* (multi-channel network of stable bedrock distributaries), and *pool rapid* (system of alternating steep bedrock rapids and associated upstream pools).

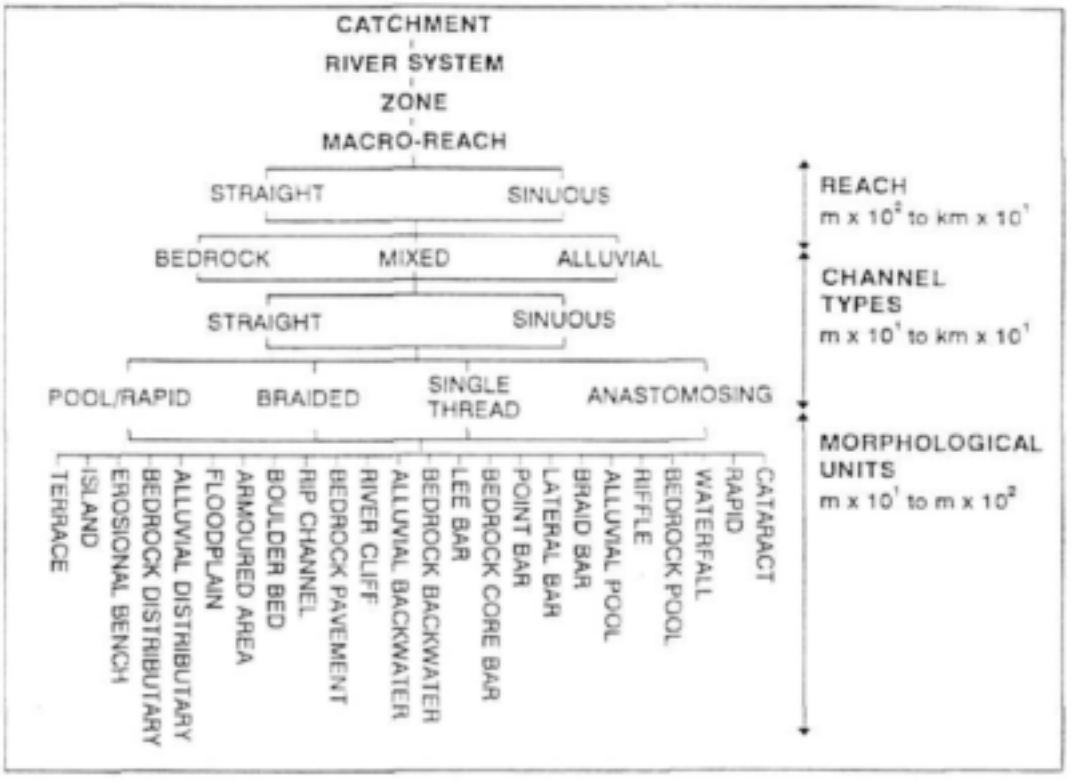

Figure 2 Agglomerate geomorphological hierarchy of the Sabie River in the Kruger National Park (van Niekerk *et al.*, 1995)

The Sabie River channel types identified by Heritage *et al.* (1997a) are used throughout this study and brief descriptions of the five principal types are therefore provided.

Braided

The degree of braiding in the Sabie River, as defined by the number of braid distributaries, is low and appears restricted to the deposition of mid-channel and lateral bars within an active channel whose cohesive banks are well protected by vegetative cover. Geomorphological diversity is lower than for those channel types directly influenced by bedrock. Quantification of the features present along a 4.5 km stretch of braided channel (Fig. 1) revealed that bedrock features were restricted to small rapids. Alluvium is present as bedrock core bars and mid-channel and lateral deposits in the active channel. The pools display some degree of alluviation. The macro-channel areas are also dominated by lateral alluvial features, with rare bedrock outcrops.

Single-Thread

The alluvial single-thread channel type has developed in sections of the Sabie River where alluvium has accumulated to cover any bedrock influence in the macro-channel. The active channel may be straight or sinuous, with the freedom to make planform adjustments restricted by the width of the incised macro-channel. Few geomorphological features exist in the active channel, which is composed largely of deep alluvial pools and rare mid-channel and lateral bars. The macro-channel consists wholly of lateral bars and alluvial bank morphological units.

Pool-Rapid

The pool-rapid channel type is itself geomorphologically diverse and displays many bedrock features. Detailed field investigation of the geological controls revealed a number of reasons for this, including localised geochemical differences and differing lithologies (Cheshire, 1994). These factors create active channel pool-rapid sequences, the scale of which depends on local geological variability and channel gradient. Typically, the rapids are free of sediment apart from occasional boulders and bedrock core bars. The pool areas are more variable ranging from sediment free bedrock areas to bedrock-lined pools incorporating a variety of bar types, particularly mid-channel bars and lateral deposits. The active pool-rapid typically occupies only a portion of the macro-channel width. Large scale sedimentary features have been deposited over much of the bedrock across the remainder of the incised macro-channel.

Mixed Anastomosing

Mixed anastomosing channel types exhibit a high geomorphic diversity, containing multiple bedrock, mixed and alluvial distributary channels that divide and rejoin over a distance much greater than the distributary width. A small percentage of the active distributary channels are filled with alluvial material in the form of lateral, mid-channel and lee bars. Pools also contain some sediment. The macro-channel exhibits extensive lateral alluvial deposits, islands and bedrock core bars. The multi-channel planform appears to be relatively stable, with the river commonly reverting to its old low flow course following floods greater than the capacity of the active channels.

Bedrock Anastomosing

Bedrock anastomosing channels were first identified on the Sabie River by van Niekerk and Heritage (1993) and are dominated by bedrock features. Kale *et al.* (1996) have recognised similar multi-channel bedrock distributary reaches on the Narmada River, India. Typically, the incised macro-channel has widened to extend three to four times the average width and this continues for several kilometres downstream. Geomorphological diversity is high with many features occurring at a low density. Numerous steep gradient active channel bedrock distributaries exist within the incised channel, describing a tortuous route over the resistant rock. These distributaries display very few alluvial features within their bedrock channels, with sediment accumulation being restricted to lateral deposits and alluvium in pools in the form of armoured clastic lags and finer deposits in dead zones. Bedrock features include pools, rapids, cataracts and small waterfalls. The macro-channel is characterised by bedrock core bar deposits (van Niekerk *et al.*, 1995) and occasional larger islands between distributary channels. Elevated bedrock areas are common, forming exposed bedrock pavements.

Channel change was investigated at two temporal scales, including short term (annual) change as evidenced by aerial photographs between 1986 and 1993, and long term (>50 years) change inferred from a single set of aerial photographic records utilising space for time substitution.

A conceptual model was constructed in which the directions of morphological change between ten potential channel types in the continuum from bedrock to alluvial systems were quantified based on aerial photographic interpretations and sediment yield studies. Of the factors influencing change over ecologically relevant timescales, one determinant was identified as static (geology), whilst others were considered to be dynamic over the short term (flow and sediment dynamics) and long term (hydrology and sediment production). Flow variability and magnitude, sediment inputs and channel competence were identified as the principal controls on channel form, and the conceptual model predicts the probable directions of channel type change as a result of altering the control variables.

The quantification of catchment control processes was addressed through sediment production modelling using Geographical Information System (GIS) techniques and a detailed hydrological study of recorded daily flows within the Sabie River catchment. Investigations of flow and sediment dynamics were also undertaken at the regional river and representative channel type scales through extensive field monitoring.

A semi-quantitative sediment transport and storage model was developed for predicting change at the channel type scale on an annual basis. The Sabie River in the KNP was delineated into "sections" (referred to in this study as cells), based on the five principal channel type categories. Topographical information (surveyed cross-sections), characteristic flow resistance coefficients and rating data were used to determine annual sediment transport capacities based on daily flows. Annual sediment loads were assigned to cells (based on channel type) where these data were not available. The change in storage for the channel type cells was modelled for the period 1959 to 1993, and the results were compared to aerial photographs at fixed points along the Sabie River from 1986 to 1989. The results show a complex spatial pattern of change with zones of increased sedimentation immediately downstream of the Saringwa, Nwaswitshaka and Sand River tributaries. To improve its predictive reliability, the semi-quantitative model has been refined, calibrated and tested as described in chapter 5 of this report.

The recommendations for further research suggested by the geomorphological study (and the chapter references where they are addressed within the current report), include:

- Refinement and verification of the suite of geomorphological change and hydrodynamic models through model application (chapters 3 and 5).
- Integration of geomorphological and ecological studies at the spatial and temporal scales at which geomorphological change can be realistically predicted (chapter 7).
- Development of models (and understanding) for prediction of ecological change in response to geomorphological change (chapters 1, 2, 5 and 7).
- Modelling of geomorphological change along the Sabie River under scenarios specified through the Decision Support System (DSS) (chapter 6).

1.2.2 Translating discharge into local hydraulic conditions on the Sabie River: an assessment of channel flow resistance (Broadhurst *et al.*, 1997)

The main objective in the study was to identify and quantify the flow resistance components on the Sabie River and to predict their effects on local hydraulic variables under different flow conditions. The overall objective was achieved through the identification of a spatial flow resistance hierarchical structure within the Sabie River (i.e. representative reaches, channel types, morphological units, cross-sections and distributary channels), an evaluation of the different methods for evaluating flow resistance, the establishment of hydraulic monitoring networks, the quantification of flow resistance at various spatial scales, and the compilation of appropriate guidelines.

1.3 Contribution of the present project towards understanding and predicting geomorphological change along the Sabie River

The ability to predict morphological adjustments rests on quantitative description of the underlying processes of hydraulics and sediment dynamics. The necessary investigations of these fundamentals are described in chapters 1 to 4. The models developed to simulate morphological behaviour at appropriate scales are then presented in chapters 5 to 7.

In temperate systems, the flow regime is dominated by low-magnitude high-frequency flow events and across the flow regime it is these flows that are considered to be responsible for the bulk of potential sediment movement within the system (Wolman and Miller, 1960). In contrast, semi-arid systems often display a more extreme flow regime influenced strongly by high-magnitude short-duration flow events. This can displace the dominant discharge (i.e. that which most influences the channel morphology) away from the low flows towards the less frequent flood events. **Chapter 2** describes an investigation of the frequency and effectiveness of sediment transport along the Sabie River.

Existing geomorphological studies (van Niekerk and Heritage, 1993; van Niekerk *et al.*, 1995; Moon *et al.*, 1997; Heritage *et al.*, 1997a) have addressed the movement of non-cohesive medium grained sand deposits within the Sabie River system, since this fraction is primarily responsible for morphological activity within the active channel. Cohesive fine-grained sediments, however, occur as large scale consolidated deposits within the incised macro-channel, being typically deposited as

clay drapes following large flood events. A study of the potential for eroding consolidated sediments by infrequent large-magnitude flow events, characteristic of semi-arid flow regimes, is described in **chapter 3**.

The most recent and extensive study concerning channel flow resistance along the Sabie River was undertaken by Broadhurst *et al.* (1997). The hydraulic information generated by this project was limited by the hydrological regime to low and intermediate discharges. A large flood experienced by the Sabie River in February 1996 provided an opportunity to collect additional high flow hydraulics data, and an extended hydraulics data set is presented in **chapter 4**. These data are integral to every aspect of this project, and indeed are essential to any study along the Sabie River requiring a translation of discharge into local hydraulic conditions.

Chapter 5 describes the development, calibration and verification of a SEDiment FLux and stOrage model (SEDFLO) for the Sabie River, KNP. It represents an extensive refinement of the channel type based sediment transport model developed by Heritage *et al.* (1997a). Historical data derived from aerial photographic records covering 56 years (1940 to 1996) were used to calibrate and test SEDFLO. **Chapter 6** describes the application of SEDFLO to model the dynamic sediment storage response of the Sabie River within the KNP to changes in the flow and sediment regimes for different scenarios. The scenarios were based on the instream flow requirement (IFR) recommendations for the Marite, Sand and Sabie Rivers (DWAF, 1997), and represent the most recent flow modification recommendations, from an ecological perspective, to date.

SEDFLO predicts temporal changes in sediment storage (as reflected by bar growth and erosion) for 40 linked channel type cells along the Sabie River. The biota, however, respond to changes at substantially reduced spatial scales, and it has therefore been necessary to develop models that predict change at the morphological unit scale (Fig. 2). **Chapter 7** describes the application and testing of a geomorphological model first developed for predicting change at the unit morphological scale along the Sabie River (KNP), under the auspices of the Biological-abiological LINKS (BLINKS) programme (Heritage *et al.*, 1997b). The modelling approach used at this smaller scale is fundamentally different from that used in SEDFLO for predicting gross change in sediment storage along the whole river. At the smaller scale the volumes of sediment are less important than the forms of the deposits, and the problem is therefore one of qualitative description rather than detailed quantification. A novel approach has therefore been used, which applies logical rules (rather than computation) to describe changes in the relative proportions of morphological units (e.g. different types of bars and bedrock features) constituting the different channel types. Information is presented on the conceptual framework behind the model as well as a description and justification of the spatial and temporal scales at which the model operates and the structure of the input data in relation to the channel type sediment flux and storage model developed in chapter 5.

The two models are designed to be applied in sequence at "nested" scales. SEDFLO can describe the change in sediment storage at a channel type scale resulting from changes in catchment sediment yield and hydrology. The rule-based model can then use the SEDFLO output to predict the morphological unit response to the change in sediment storage in the different channel-type cells.

2 Influence of flow regime on sediment transport characteristics

2.1 Introduction

It has long been recognised that alluvial channels demonstrate strong relationships between channel dimensions and flow (Leopold and Maddock, 1953), with the channel adjusting its shape in response to the dominant flow and sediment regime. This concept was extended by Wolman and Miller (1960) with their definition of dominant discharge as the flow (specified in terms of its magnitude and frequency) capable of transporting most sediment across the flow regime given its relative magnitude and frequency. In temperate systems, the flow regime is dominated by low to medium magnitude, high-frequency flow events (Andrews, 1980) and across the flow regime it is these flows that are considered to be responsible for the bulk of potential sediment movement within the system (Fig. 3). In contrast, semi-arid systems often display a more extreme flow regime and the channel morphology is influenced strongly by high-magnitude short-duration flow events. This can shift the dominant discharge away from the low flows towards the less frequent flood events (Fig. 3), as demonstrated by Baker (1977) in central Texas. Wolman and Miller (1960) also noted that the influence of low flows on bulk sediment movement is reduced if the entrainment threshold is elevated and if the flow regime is highly variable. Their study included a theoretical approach concerned with thresholds of transport, backed up with examples from Brandywine, Delaware, where little of the coarsest sediment was moved in comparison with Rio Puerco, New Mexico, where the bulk of material transported was fine.

Several studies have also attempted to attach a return period to the occurrence of the dominant discharge. In alluvial systems, it has been equated with the effective discharge that creates the bankfull channel shape and this has been shown to have a return period on the annual maximum flow series of between 1 and 2 years (Andrews, 1980). Hey (1975) noted a more frequent occurrence for bankfull flow in sand-bed channels. The tendency towards some variability in the return period for bankfull flow was observed by Lewin (1989), which was attributed to non-equilibrium dimensions of the channels due to recent erosion and deposition. Pickup and Warner (1976) noted a bimodal trend in the data for the Cumberland Basin in New South Wales, Australia. A return period flow of 1.15 to 1.4 years was found for the dominant discharge, contrasting with a higher bankfull discharge responsible for shaping the channel through bank erosion.

This chapter describes a study of the frequency and effectiveness of sediment transport along the Sabie River. The river has been divided into a number of morphologically distinct channel types (Fig. 2), each displaying its own hydraulic and sediment transport characteristics. The potential rates of sediment movement were determined across the flow regime using measured data on channel geometry, sediment characteristics, flow resistance and water surface slopes.

2.2 Representative site information

The data required for analysis of sediment transport characteristics were available from work previously carried out on the Sabie River by the CWE (Heritage *et al.*, 1997a; Heritage *et al.*, 1997b; Broadhurst *et al.*, 1997). Sediment transport analyses were undertaken for representative examples of each of the five principal channel types identified along the river (Fig. 1), and

sampling provided the grain-size distribution of the unconsolidated sediments. Generally, the material consists of coarse sand to fine gravels, which represents the characteristic weathering product of the granites within the catchment. Rating relationships have been developed for each site by direct measurement of stage levels and spatial extrapolation of discharge rates from nearby gauging stations (Heritage *et al.*, 1997a). The variation of flow resistance with discharge was determined for each channel type using the Barnes (1967) methodology (refer to chapter 4 and Broadhurst *et al.*, 1997) and these relationships were used to compute potential sediment transport rates.

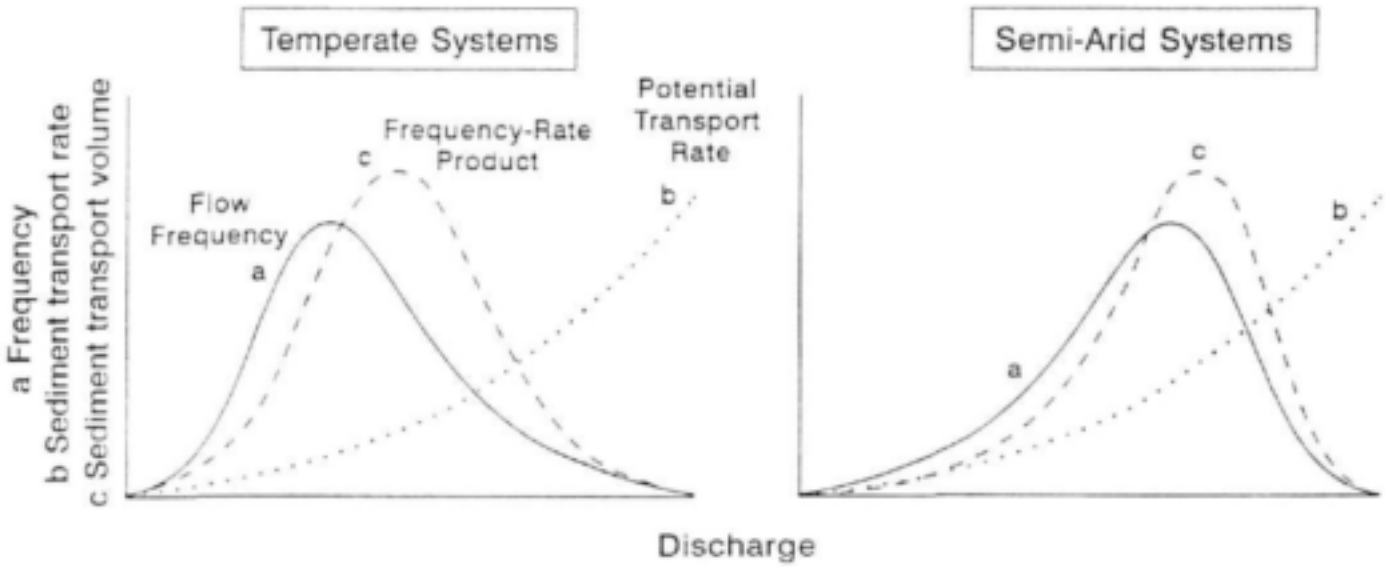

Figure 3 Generalised relationship between magnitude and frequency of discharge and sediment transport in temperate and semi-arid river systems

2.3 Runoff and sediment data

Gauged flow data for the Sabie River are limited by record length, with local gauges (station X3H015 and X3H021) having operated for less than a decade, whilst the record for station X3H006 in the upper catchment extends back to 1959 (Fig. 1). In addition, station maintenance was initially poor, resulting in gaps in the flow record. Furthermore, the older gauges (X3H006) are designed to monitor low flows and consequently flows much above the mean annual flood are not accurately recorded.

A flow simulation exercise was therefore undertaken using the ACRU hydrological model (see chapter 5) to provide a longer and continuous data record (pers. comm., A Pike and G Jewitt). Average daily flows for locations along the Sabie River were simulated using information from the rainfall recording network and gauged flow data. Flows were simulated for the 62 year period of rainfall record (1932 to 1993) and these data were used in conjunction with the flow resistance, water surface slope and bed-material size distribution to compute daily potential sediment transport rates using d_{50} = 1 mm for each channel type using the total load transport equations of

Ackers and White (1973) (refer to chapter 5). Transport rates for the pool units in the pool-rapid channel type were considered in the analysis, since these units exhibit a reduced potential to move material at low flows and therefore represent the critical morphological unit for potential sediment transport analysis.

2.4 Frequency and effectiveness of sediment transport

The potential rates of sediment transport for each channel type, based on the local channel characteristics, are plotted in Fig. 4. Each channel type displays a unique relationship between transport capacity and discharge. The entrainment threshold is lowest in the braided channel, with the rate of increase in potential transport rate being highest in the bedrock anastomosing, followed by pool-rapid, single-thread, mixed anastomosing and braided channel types. The entrainment threshold is lowest in the channel types characterised by low flow resistances (braided, single-thread and mixed anastomosing). As discharge increases and the stage approaches the top of the macro-channel bank, the flow resistances become similar (refer to Fig. 14) and the reversal in relative potential transport rate is primarily a function of relative energy slopes.

Potential sediment transport rates were calculated for each channel type using the 62 year simulated flow sequence and frequency distributions of the data (Fig. 5). The potential bulk sediment transport over the 62 year period is plotted on the y-axis and is obtained by multiplying the median of the transport rate class interval by the frequency of occurrence of that interval. For all cases, the plots display an inverse "J" relationship and few distinct optima exist at rates above the contribution of the lowest transport rate class. Moderate to high transport rates also contribute significantly to the overall potential sediment transport efficiency, particularly in single-thread, pool-rapid and bedrock anastomosing channel types. This results in the distribution of effective sediment movement across a wider range of discharges and indicates the importance of high flow events despite their infrequent occurrence in the 62 year record.

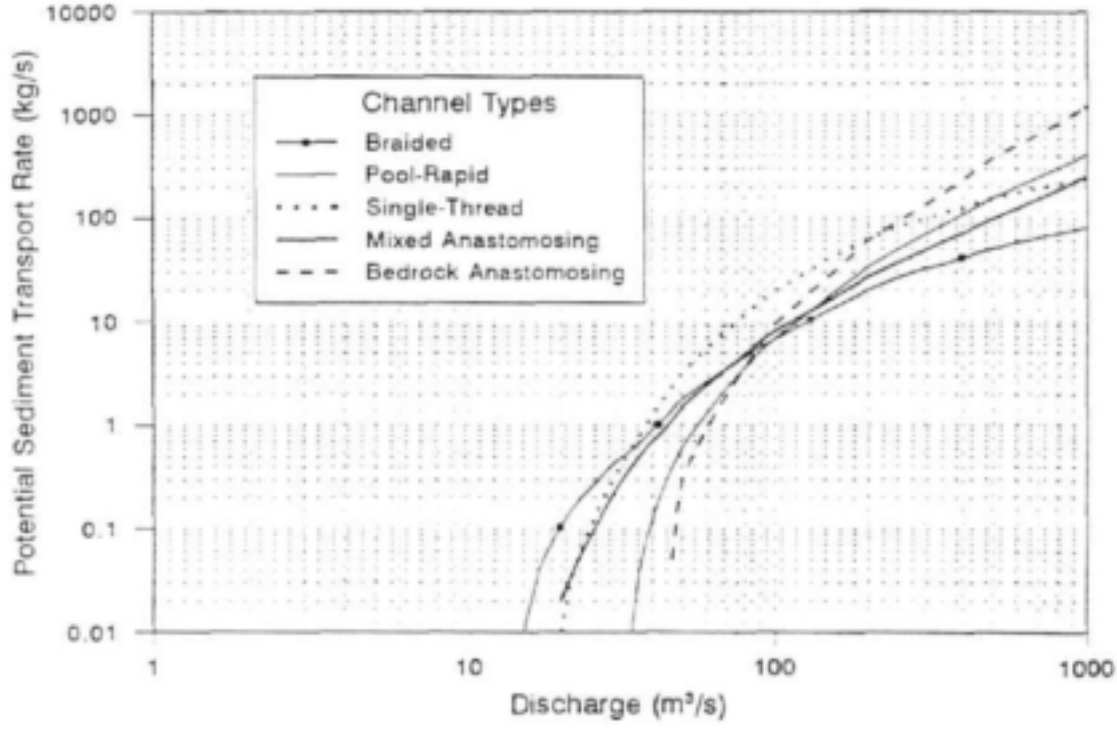

Figure 4 Potential sediment transport rate relationships for the five principal channel types along the Sabie River

The annual maximum series return period curves are plotted in Fig. 6 using the simulated flow sequence data. (The curves for the different channel types do not coincide because they are derived from data at different locations along the river). The curves were used to calculate the return periods of the discharges corresponding to the dominant potential sediment transport rates for each channel type. The return periods and the range of flows responsible for 80% of the potential volume of sediment transported over the period of analysis, are given in Table 1.

The contributions to the potential bulk sediment transport of return period flows less than 1.1 are significant in the braided (39%) and mixed anastomosing (31%) channel types. This results from the lower entrainment thresholds in the braided channel (Fig. 4) and the lower return period associated with peak annual flows in the mixed anastomosing channel (Fig. 6), which is located downstream of a major tributary (Fig. 1). A marginally higher dominant discharge return period of 1.5 exists for the bedrock anastomosing channel. This is attributed to the elevated entrainment threshold (Fig. 4), coupled with higher return periods corresponding to equivalent peak annual flows (Fig. 6). The reduced influence of low flow dominance on bulk sediment movement (as determined by the return periods corresponding with the 80% contribution to the potential sediment transport in Table 1) correlates directly with reduced entrainment thresholds, as noted by Wolman and Miller (1960).

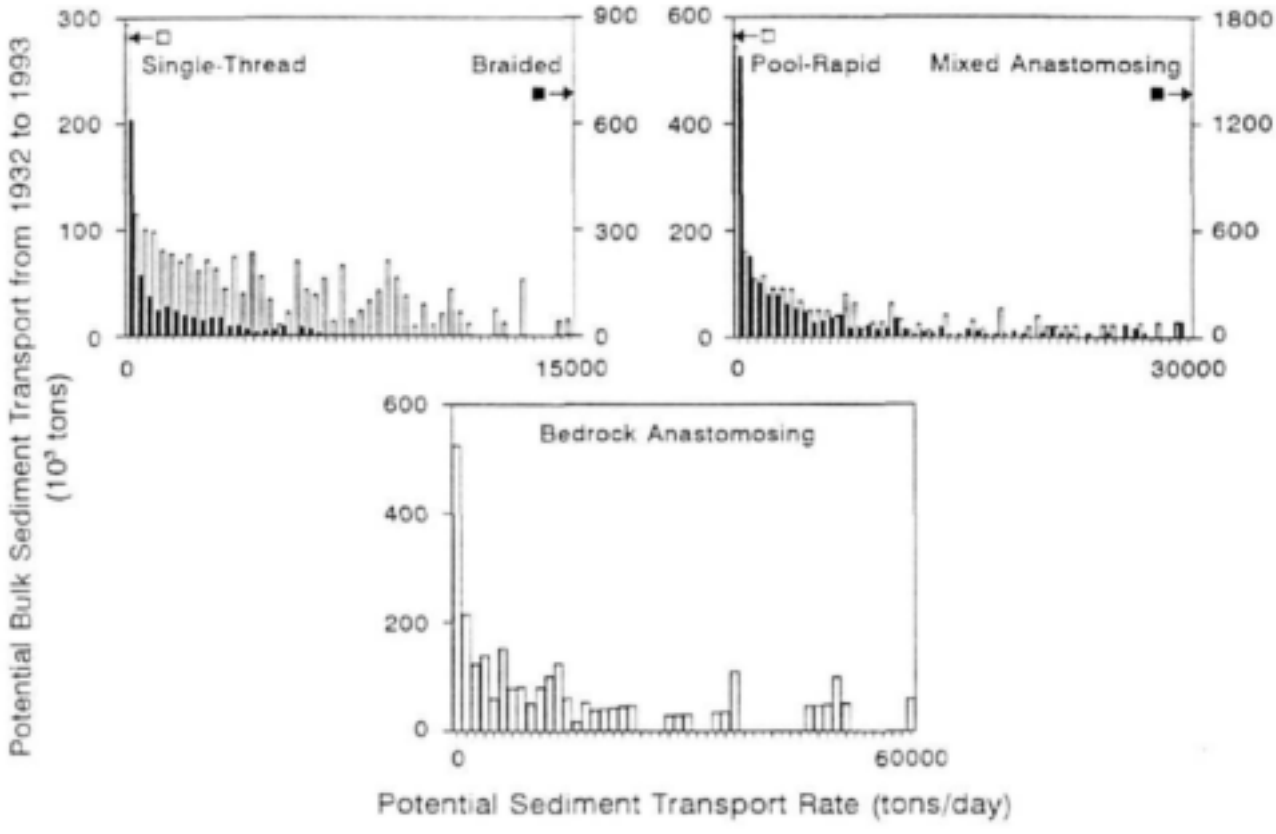

Figure 5 Potential bulk sediment transport for the five principal channel types along the Sabie River

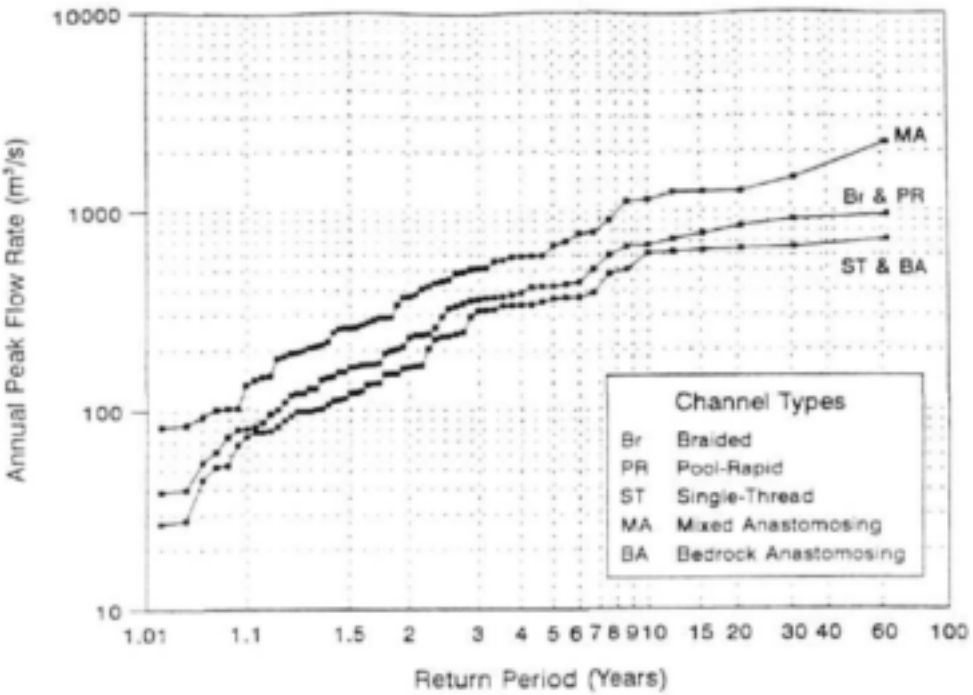

Figure 6 Return periods for the five principal channel types along the Sabie River

Table 1 Discharge rates and return periods on the annual maximum time series corresponding to the dominant potential sediment transport rates

Channel Type	Dominant potential sediment transport rate (tons/day)	Equivalent discharge rate (m^3/s)	Contribution to bulk sediment transport (%)	Return period (years)
Braided	0 - 300 0 - 2400	0 - 70 0 - 264	39 80	1.1 2.5
Pool-Rapid	0 - 600 0 - 13800	0 - 101 0 - 507	23 80	1.2 7.0
Single-Thread	0 - 300 0 - 9000	0 - 52 0 - 320	14 80	1.1 3.7
Mixed Anastomosing	0 - 600 0 - 10200	0 - 92 0 - 573	31 80	1.1 3.8
Bedrock Anastomosing	0 - 1200 0 - 30000	0 - 112 0 - 479	20 80	1.5 7.8

Due to the extremes of flow experienced by the Sabie River, the transport effectiveness of the higher flood flows is somewhat masked by the choice of class interval for the transport frequency analysis, which has to be sufficiently small to display the effects of prolonged winter low flows. Meade and Parker (1989) analysed the time series of annual bulk suspended sediment for a number of rivers in the United States and correlated very high annual bulk transport with extreme flow events. This approach was used here in a modified form to examine the flow and sediment transport data for similar patterns in the Sabie River. Potential annual bulk sediment transport was calculated for each of the channel types and these values are plotted against the return period corresponding to the peak annual flow rate in Fig. 7.

For all the channel types, the highest annual sediment transport correlates with high magnitude flood events on the annual maximum time series (Table 2). Furthermore, the extreme flood events taken over a 5 day duration account for 23% to 43% of the potential annual sediment movement. The reduced sediment transport effectiveness of flows below the 1 in 2 year return period for the pool-rapid and bedrock anastomosing channels should be noted.

2.5 Discussion and conclusions

The results of the sediment transport magnitude and frequency analysis for the five principal channel types along the Sabie River indicate that there is a large degree of dominance in the transport efficiency of low-flows below the 1 in 2 year return period for the predominantly alluvial channel types. This is particularly evident for the braided channel type, where flows below the 1.1 year return period account for 39% of the potential bulk sediment transport. These findings are corroborated by studies reported in the literature for alluvial systems (Andrews, 1980). Moderate and intermediate flows are shown to contribute significantly to sediment transport in the pool-rapid and bedrock anastomosing channels which are characterised by increased bedrock influence. This is noticeable when considering the potential annual bulk sediment transport corresponding to the peak annual flows, where the extreme flood events account for as much as 43% of the annual sediment movement in the bedrock anastomosing channel. The majority of the potential sediment movement (80%) is accounted for by return period flows of less than 7.0 to 7.8 years in the pool-rapid and bedrock anastomosing channel types. Lower return period flows of up to 2.5, 3.7 and 3.8 are responsible for most sediment movement in braided, single-thread and mixed anastomosing channel types, respectively. This illustrates the transport effectiveness of high-magnitude low-frequency flow events in bedrock influenced morphologies within semi-arid systems.

Table 2 Discharge rates and return periods on the annual maximum time series corresponding to the maximum annual potential sediment transport

Channel Type	Peak annual flow (m^3/s)	Return period (years)	Contribution to annual sediment transport of peak flows over a 5 day duration (%)
Braided	720	12.6	23
Pool-Rapid	721	12.6	35
Single-Thread	561	10.5	32
Mixed Anastomosing	1129	9.0	26
Bedrock Anastomosing	622	12.6	43

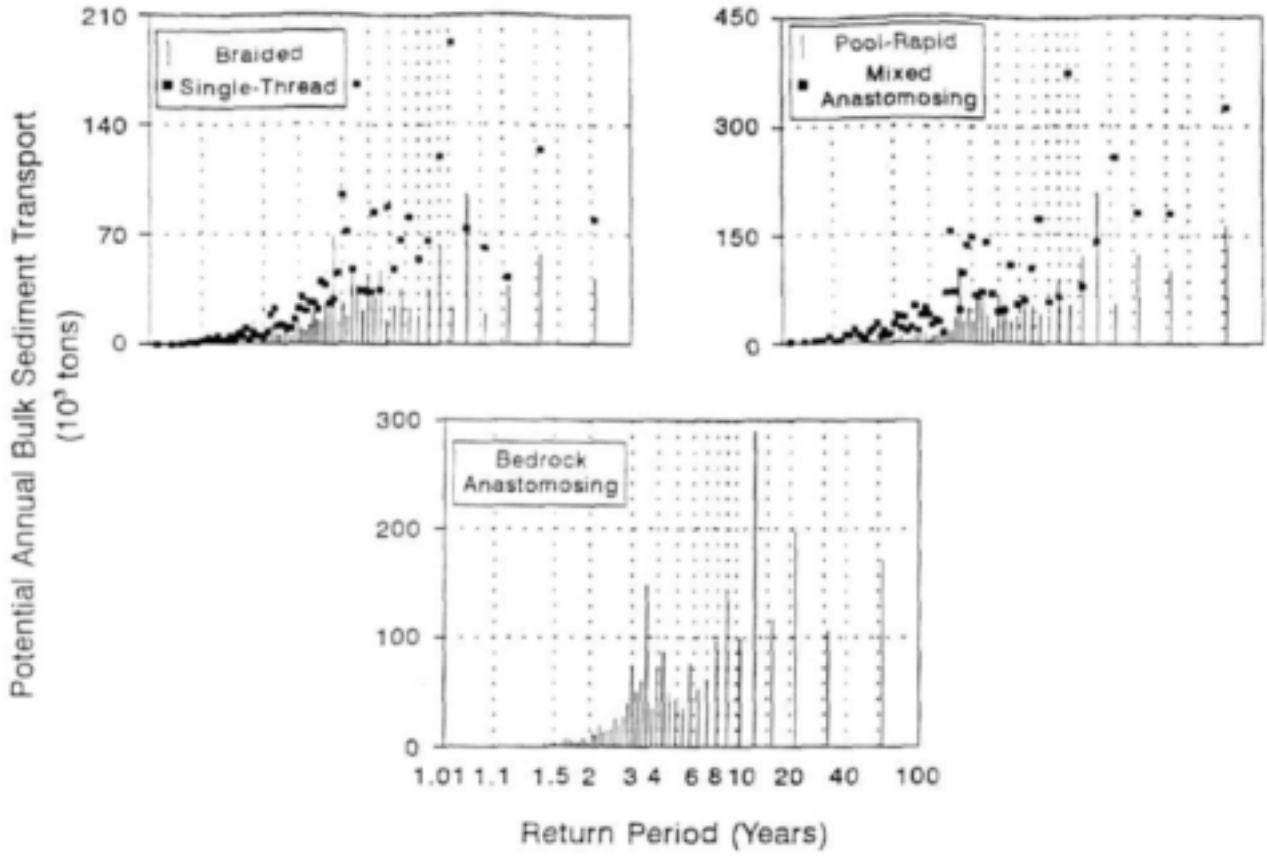

Figure 7 Potential bulk annual sediment transport corresponding to return period on the maximum annual time series for the five principal channel types along the Sabie River

The importance for river morphology of floods with magnitudes in the range that would be expected to by influenced by dam construction has important implications for the management of flows to maintain the ecological integrity of the Sabie River. The existing flood regime must be preserved or replicated in terms of morphological effect to maintain the balance in sediment transport processes and prevent rapid morphological change in the system. The influence of major flood events is also emphasised in the inundation frequency study of Heritage *et al.* (1995), which noted the importance of high magnitude infrequent flows in the maintenance of macro-channel alluvial features.

3 Influence of flooding on the erodability of cohesive sediments

3.1 Introduction

Fluvial geomorphic work is defined in terms of the volume of sediment transported through a reach (Wolman and Miller, 1960) whereas geomorphological effectiveness is defined as the degree of modification of a landform (Wolman and Gerson, 1978). Major floods can both transport large quantities of sediment and significantly modify the fluvial geomorphology if the threshold for erosion is exceeded. River response to large floods has been shown to be highly variable, however. Schumm and Lichty (1963) report large scale sediment loss in response to flooding in the semi-arid Cimarron River, southwest Kansas. Nanson (1986) describes the "catastrophic stripping" of reaches of Charity Creek on the humid coastal region of New South Wales, Australia. In contrast, Moss and Kochel (1978) noted only minor morphologic changes to the lower reaches of the Conestoga River, Pennsylvania (USA), following the Hurricane Agnes flood. Kochel and Baker (1982) also report only minor changes to the distribution of in-channel bars following a flood on the Pecos River, Texas (USA).

A large number of factors have been suggested as influential in determining the geomorphological effectiveness of large floods (Kochel, 1988). Channels are prone to morphologic change if they are characterised by a flashy flow regime, have a high channel gradient, coarse cohesionless unconsolidated bedload, low bank cohesion and a deep confined channel cross-section generating high flood flow velocities and shear stresses. Consolidated silts and clays may also undergo erosion if the applied shear forces exceed the shear strength of the material imparted by the cohesive properties arising from structural and physiochemical forces.

This chapter describes an investigation of the potential for eroding the cohesive fluvial sediment deposited as large scale consolidated bar forms within the incised macro-channel of the semi-arid Sabie River. The critical resistance to erosion of the cohesive sediments was determined from *in situ* shear vane strength measurements combined with laboratory testing of disturbed samples. The spatial distribution of maximum shear stresses applied during a recent flood event is determined using measured data on channel geometry, flow resistance, flood stages and water surface slopes. A measure of the potential for erosion is provided by a statistical analysis of the frequency distribution of resisting and applied shear stresses, and is discussed with reference to field observations following a large flood in February 1996.

3.2 Spatial distribution of cohesive sedimentary deposits and associated riparian vegetation

The bedrock anastomosing, mixed anastomosing and pool-rapid channel types are all heavily influenced by bedrock outcropping within the macro-channel as areas of bedrock pavement. Extensive cohesive deposits are found in the anastomosed sections forming large scale bedrock core bars between the distributary channels (van Niekerk *et al.*, 1995) and these features are heavily vegetated with a community structure dominated by *Breonadia salicina* and *Phyllanthus reticulatus* (van Coller *et al.*, 1997). The distributary channels are characteristically free of sediment or contain minor unconsolidated bar deposits. The pool-rapid channel type is

characterised by cohesive macro-channel lateral bars colonised by *Diospyros mespiliformis*. Active channels display bedrock rapids and some unconsolidated bar features colonised by reeds (*Phragmites mauritianus*) together with occasional consolidated bedrock core bars colonised by *P. reticulatus* and *Combretum erythrophyllum*. The single thread alluvial channel type is uncommon on the Sabie River in the Lowveld. It is characterised by extensive alluvial infill of the macro-channel as macro-channel lateral bars and terraces adjacent to the main channel, colonised by *C. erythrophyllum* and *D. mespiliformis*, and unconsolidated in-channel sandy deposits which are often reeded. The braided channel type is characterised by cohesive macro-channel lateral bar deposits and unconsolidated braid bars dominated by *P. reticulatus* and *C. erythrophyllum*, and lateral bars in the active channel frequently colonised by reeds.

3.3 Hydraulic shear resistance of cohesive sediments

The erodability of channels with cohesive sediments has received much attention in the literature due to its importance for the design of stable engineered channels. A literature survey by the ASCE Task Committee on Erosion of Cohesive Sediments (1968) reveals the interdisciplinary nature of the problem, with most of the work having been carried out by hydraulic and agricultural engineers, as well as soil scientists. Due to the complexity of the subject, most studies have been directed towards field observations and laboratory investigations determining empirical relationships for critical velocity or shear stress. Partheniades and Paaswell (1970) summarise and critically evaluate work ranging from early empirical studies to more recent investigations directed at predicting critical resistance criteria. The majority of the studies relate critical shear stress at the onset of erosion to gross soil properties, including the Atterburg limits (particularly the plasticity index), composition and particle-size distribution, compressive strength, bulk density, hydraulic conductivity, moisture content and void ratio.

The studies documented in the literature consider different combinations of the cited soil parameters in the analyses, making comparisons between studies difficult. Furthermore, the laboratory investigations use different experimental apparatus to model erosion, including hydraulic jet (Dunn, 1959), rotating cylinder (Moore and Masch, 1962), rotating impeller (Thomas and Enger, 1961; Carlson and Enger, 1963), and flume tests (Smerdon and Beasley, 1959; Kampuis and Hall, 1983). In addition, the selection of the point at which scour was considered to occur was relatively subjective. The results, however, generally indicate an increase in critical shear stress with an increase in plasticity index, vane shear strength, compressive strength, clay content and consolidation pressure, whilst critical shear stress displays a general reduction with increasing moisture content and void ratio.

Critical shear stress is most often correlated with vane shear strength (Dunn, 1959; Flaxman, 1963; Espey, 1963; Rectoric and Smerdon, 1964; Kamphuis and Hall, 1983) and plasticity index (US Dept. of Interior, Bureau of Reclamation, 1953; Sunborg, 1956; Dunn, 1959; Smerdon and Beasely, 1959; Carlson and Enger, 1963; Lyle and Smerdon, 1965; Kamphuis and Hall, 1983). The empirical relationship derived by Smerdon and Beasley (1959) (equation 1) is often cited in the literature (e.g. ASCE Task Committee on Erosion of Cohesive Sediments (1968); Partheniades and Paaswell, 1970; Graf, 1972).

$$\tau_c = 0.0034 I_p^{0.84} \quad (1)$$

where
τ_c is the critical shear stress (Pa)
I_p is the plasticity index

The tests were carried out in an open flume with loosely placed soil and no strength measurements were taken. Equation 1 predicts critical shear stresses that are considerably lower than those of other investigations. It is reasonable to expect erosion to be a function of the shear strength of the material, and not related to the plasticity index alone.

The vane shear apparatus provides an indicator of macro soil properties, and is appropriate for in situ testing. The vane shear strength incorporates some measure of the moisture content, degree of compaction and void ratio, all of which have been related to critical shear strength in the literature. The shear strength obtained, however, depends on the rate at which torsion is applied to shear the soil, and this is seldom controlled or standardised under field conditions. Notwithstanding this shortcoming and the need to exercise control during the testing procedure, *in situ* testing is likely to provide information that is more indicative of a material's ability to resist entrainment under field conditions than an analysis of disturbed samples.

Dunn (1959) conducted a laboratory study on consolidated clay samples subjected to erosion by a submerged water jet. The relationship between critical hydraulic shear stress and vane shear strength was assumed to be linear, and in accordance with the form of a generalised theoretical relationship derived for the specific testing procedure. Partheniades and Paasewell (1970) point out that the linear relationship was based on an inadequate number of data points, and therefore is questionable. The data points obtained by Dunn for the sixteen soil types considered, and fitted relationships for four of the soils, are plotted in Fig. 8.

The general relationship between critical shear stress and vane shear strength is given by

$$\tau_c = (S_v + 8.62) \tan\theta \quad (2)$$

where
S_v is the vane shear strength (kPa)
θ is the slope of the linear relationship

The linear relationship derived by Dunn (equation 2) requires further justification even though it was shown to be consistent with the expected theoretical function, since more than two data points were obtained for only four of the soils tested. The validity of Dunn's formulation was assessed by analysing data from various sources and testing procedures, including, rotating cylinder, flume, and field observations (Fig. 8). With the exception of the San Saba silty clay which displayed a large amount of scatter (ASCE Task Committee on Erosion of Cohesive Sediments, 1968) the additional seven soil types generally confirm the linear relationship developed by Dunn. The additional data sets also extend the range of applicability for critical shear stress.

Dunn related the slope of the linear relationship, θ, to three sample identifying indices, namely the plasticity index, percentage finer than 60 μm, and statistical parameters describing the grain size distribution. Of these identifying indices, the plasticity index provided a useful determinant (Fig. 9), but is only applicable for $\theta > 30°$. Furthermore, the value of the plasticity index was not accurately reproduced below 5%. The plasticity index data of Espey (1963) and Rectoric and Smerdon (1964) corroborates and extends the range of validity of the linear relationship suggested by Dunn. This is not the case for the data of Flaxman (1963) and Kamphuis and Hall (1983), which extend over a large range of plasticity indices (3% to 40% and 16% to 38%, respectively) making direct comparison using these data difficult. Dunn also developed a linear relationship between θ and percentage finer than 60 μm over the range 5% to 95%.

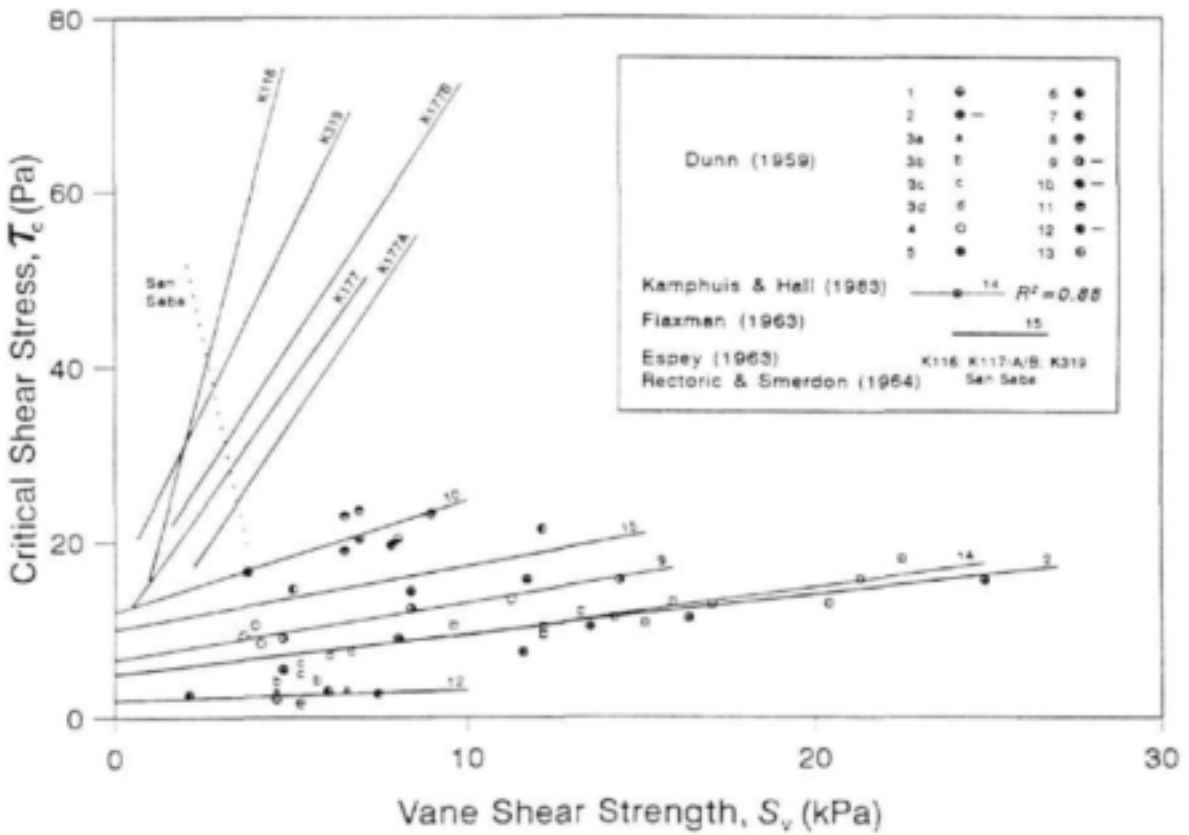

Figure 8 Critical hydraulic shear stress as a function of vane shear strength

Multiple regression was used to develop a relationship for θ as a function of plasticity index and fraction finer than 60 μm, and is given by

$$\theta = 1.285 I_p + 0.398 U_f + 6.276 \qquad 3$$

where

I_p is the plasticity index (%)
U_f is the fraction finer than 60 μm (%)

Data from the literature in the range $0\% \leq I_p \leq 34\%$ and $5\% \leq U_f \leq 95\%$ were used in the analysis, and provide an acceptable linear relationship, yielding, $R^2 = 0.97$. θ determined from equation 2 is plotted against the empirical relationship (equation 3) in Fig. 10.

The *in situ* shear strengths of the cohesive sediments along the Sabie River were determined by performing 300 shear vane tests. Data collection covered the five major channel types, and also included a range of macro-channel and active-channel geomorphological features. No relationship between shear strength and channel type or geomorphological unit was evident, and the data are therefore presented as a frequency distribution in Fig. 11. Disturbed samples corresponding to a range of in situ shear strengths were also selected for laboratory analysis of plasticity index and fraction finer than 60 μm. These data were used to compute the distribution of θ (equation 3), and are plotted in Fig. 12.

The distribution of critical shear strength for the cohesive sediments was determined by computing all possible probabilities of this derived variable according to equation 2, based on the discrete distributions for shear vane strength (Fig. 11) and θ (Fig. 12). The resultant frequency distribution is plotted in Fig. 13.

3.4 Applied shear stresses during extreme flood events

The average boundary shear stress is given by

$$\tau_a = \gamma R S_f \qquad 4$$

where

τ_a is the average boundary shear stress (Pa)
γ ($=\rho g$) is the unit weight of water (N/m^3)
R is the hydraulic radius (m)
S_f is the energy slope

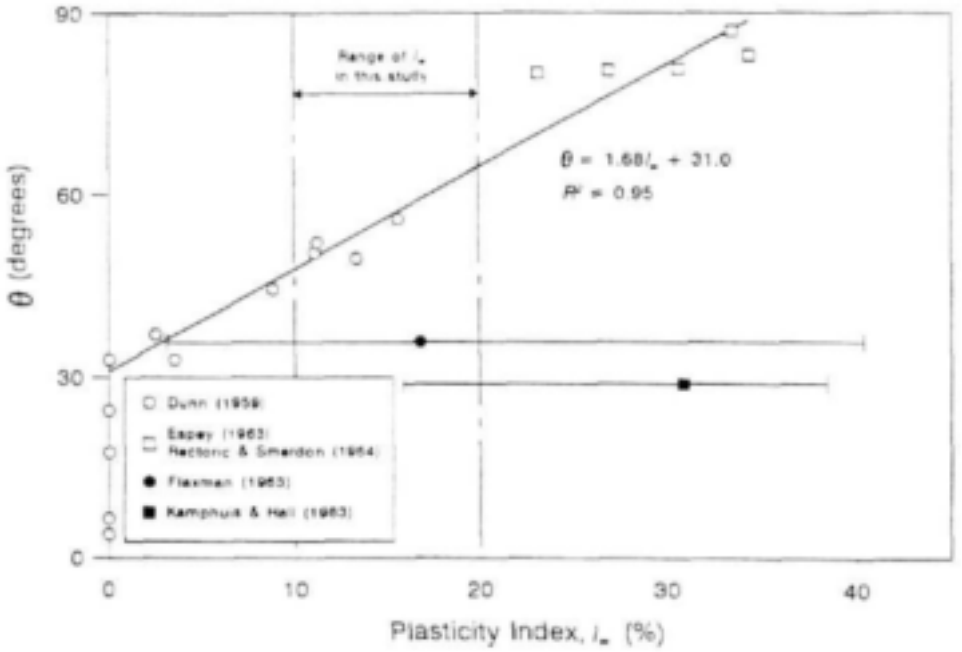

Figure 9 θ expressed as a function of plasticity index

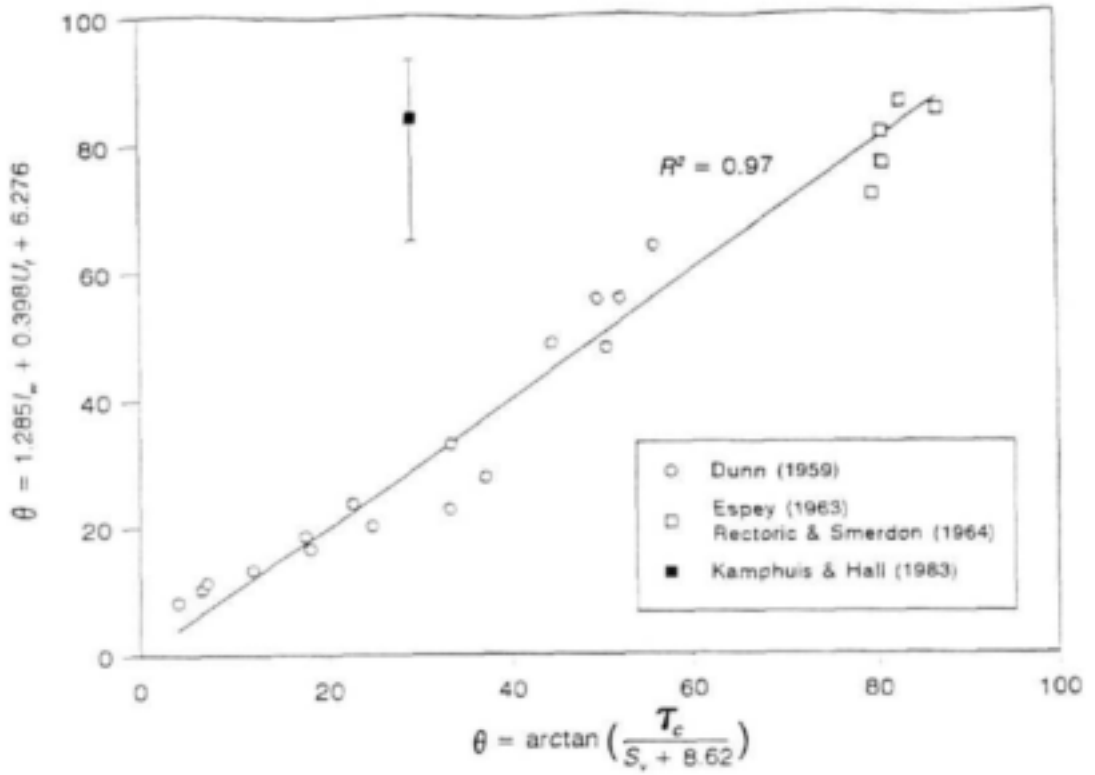

Figure 10 θ determined from equation 2 and empirically as a function of plasticity index and fraction finer than 60 μm (equation 3)

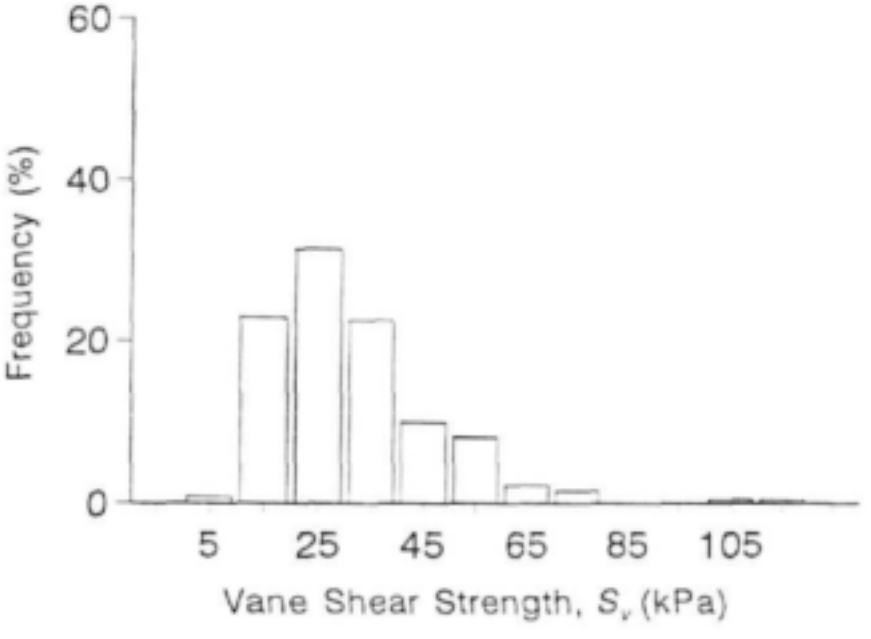

Figure 11 Frequency distribution of shear strength from shear vane tests

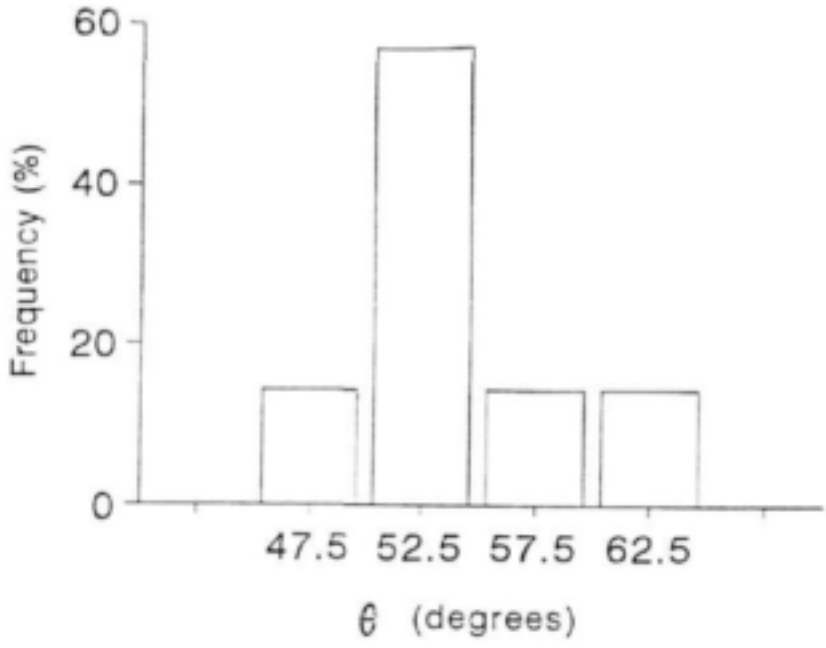

Figure 12 Frequency distribution of θ determined empirically from equation 3

Equation 4 assumes that the total resisting force is dissipated as boundary shear, and no account is taken of form resistance. The approximate distribution of boundary shear stress along a channel cross-section may be determined by assuming that the total stress is distributed linearly according to the variation of flow depth (i.e. flow depth is substituted for hydraulic radius in equation 4 to obtain the local boundary shear stress).

The change in flow resistance concomitant with discharge for five representative reaches, one for each of the channel types, was determined by Broadhurst *et al.* (1997). A recent flood event provided the opportunity to extend the flow resistance relationships (refer to chapter 4), which are presented in Fig. 14 using Manning's total resistance coefficient. It is encouraging to note that the flow resistance tends towards similar asymptotic values for the channel types with increasing discharge. This results from an inclination towards uniform energy slopes as local hydraulic controls become drowned-out in the bedrock influenced river. Topographical and hydraulic data from the representative reaches (Fig. 1) and additional cross-sections surveyed along the river were used to compute the distribution of boundary shear stress corresponding to the flood peak discharge gauged at between 1705 m^3/s and 2259 m^3/s (refer to Table 4). The energy slopes are calculated for sites where no such data were available by making use of the reach-averaged channel-type flow resistance data (Fig. 14).

The frequency distribution of boundary shear stress along the cross-sections was determined by dividing the macro-channel into equal increments and including only those features along the profile where cohesive sediments occur as surface material. In this way, a representative frequency distribution of applied shear may be computed for each channel type (Fig. 13 inset), and also for the Sabie River (Fig. 13), taking account of the proportional composition of the channel types as given in Table 3.

The distribution of applied shear stress (Fig. 13) is bimodal, reflecting the cross-sectional geometry of the macro-channel profiles. The lower mode corresponds to the macro-channel bank and elevated features along the macro-channel floor, whereas the higher mode corresponds to the more incised geomorphological units. Similar distributions occur for each of the channel types with the exception of braided (Fig. 13 inset), which is characterised by a more prismatic macro-channel cross-sectional geometry and hence unimodal distribution. A more rigorous analysis of the distribution of shear stress using turbulent flow analysis will reduce the bimodality due to momentum transfer between regions of deep and shallow flow.

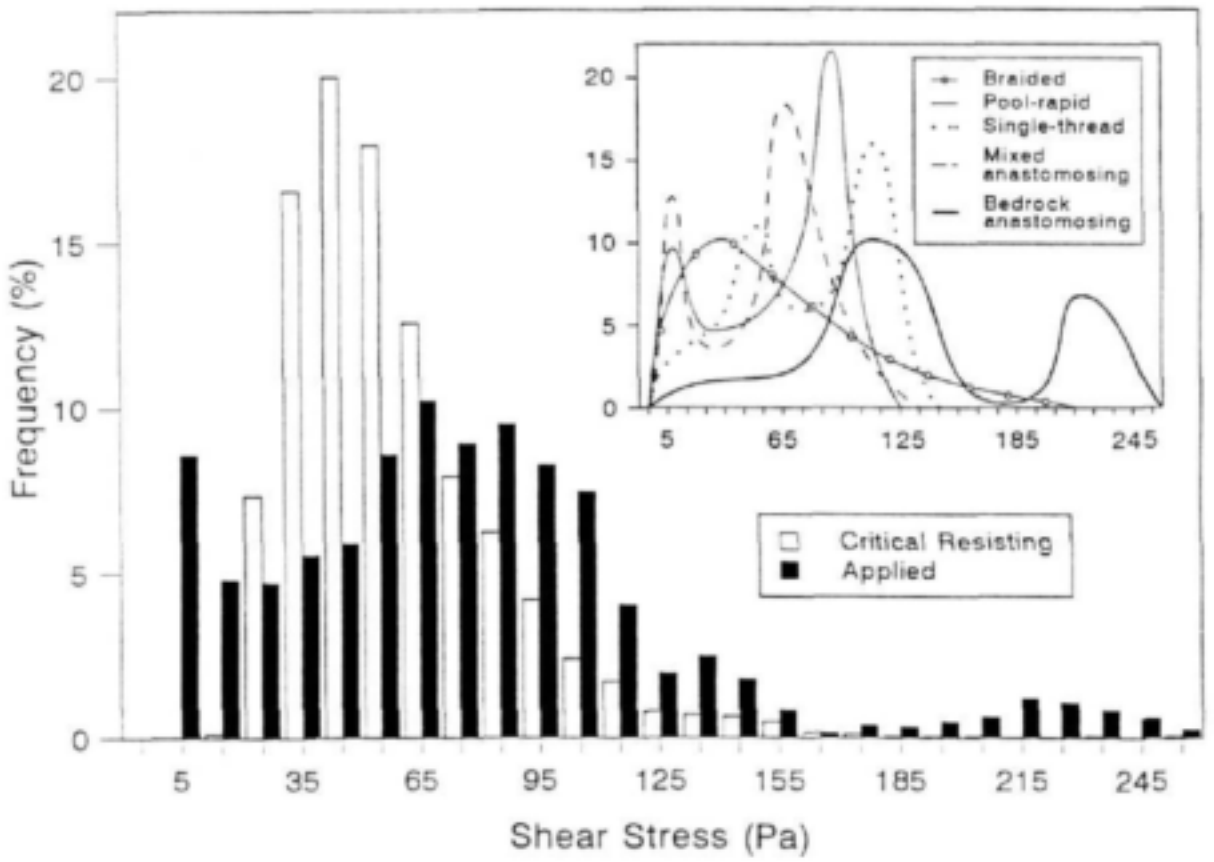

Figure 13 Frequency distribution of critical resisting and applied shear stress (discharge of 1705 m^3/s to 2259 m^3/s) for cohesive sediments along the Sabie River

The probability of eroding the cohesive sediments along the river may be determined by summing the individual probabilities of all possible combinations where the applied shear stress is greater than the critical resisting shear stress. The results of this analysis are given in Table 3 for each of the channel types as well as the composite picture.

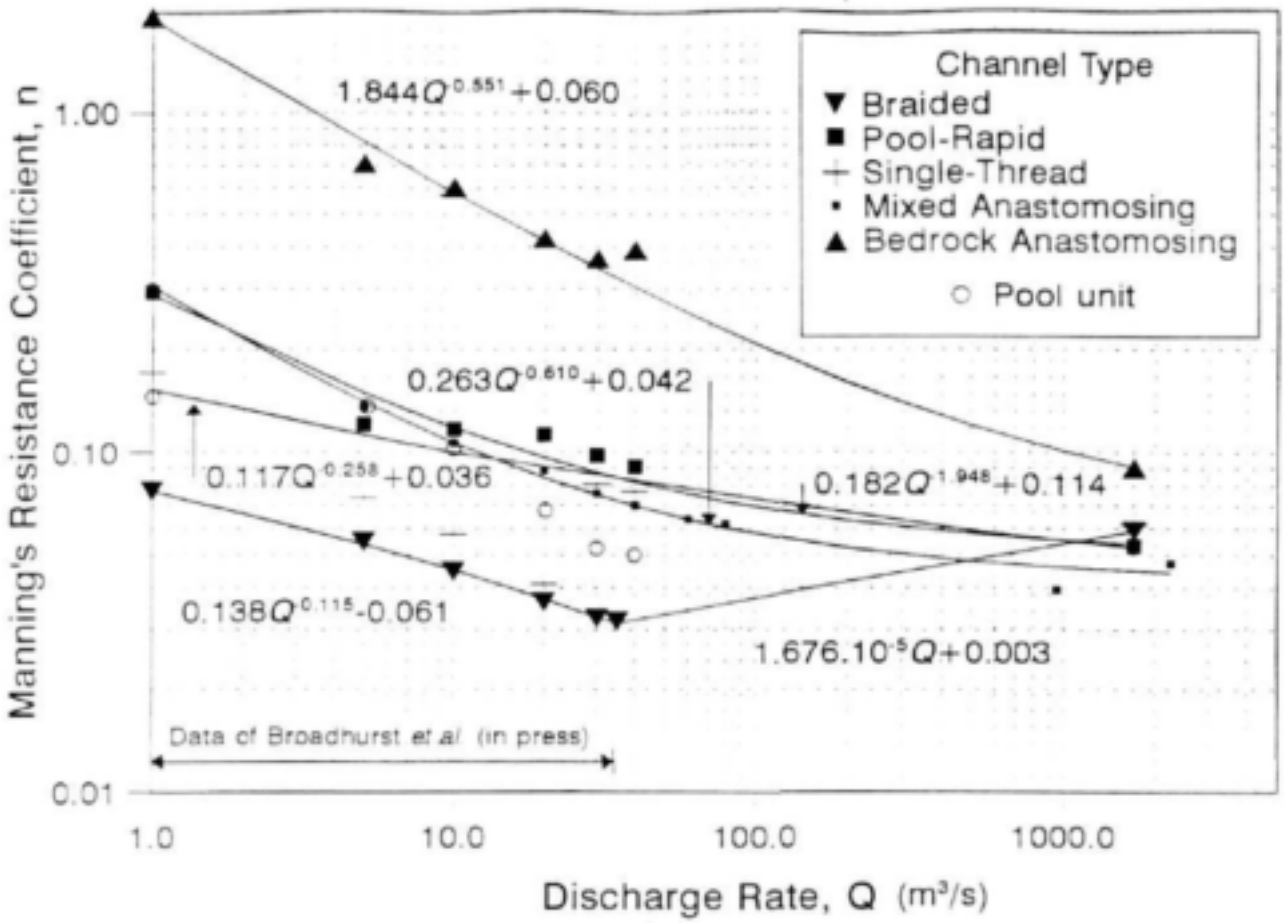

Figure 14 Measured variation of Manning's resistance coefficient with discharge for representative examples of the five principal channel types along the Sabie River (extended from Broadhurst *et al.*, 1997)

Table 3 Probability of eroding cohesive sediments (discharge from 1705 m^3/s to 2259 m^3/s)

Channel type	Spatial composition (%)	Probability of erosion (%)	Average applied shear stress (Pa)
Braided	14	63	70
Pool-Rapid	28	66	63
Single-Thread	3	75	80
Mixed Anastomosing	35	63	59
Bedrock Anastomosing	20	91	145
Sabie River	100	68	70

3.5 Discussion and conclusions

The analysis shows that the cohesive sediments along the Sabie River have a 68% likelihood of being eroded by a discharge of approximately 2000 m^3/s. This value remains relatively consistent (63% to 75%) for all the channel types with the exception of bedrock anastomosing, where the deposits have a 91% chance of being eroded at this discharge. The higher probability in the bedrock anastomosing channel types arise from the significantly elevated shear stresses (Table 3).

Field observations following a flood experienced in February 1996 (peak was gauged at between 1705 m^3/s and 2259 m^3/s, upstream and downstream of the Sand River tributary, respectively, Fig. 1) revealed that the removal of cohesive material was spatially isolated for the sites investigated along the length of the river. The influence of vegetation colonising the macro-channel floor was apparent, with vegetational cover providing increased protection from erosive forces. The proportion of the cohesive bed material that was subjected to erosion during this flood appeared to be less than 68%, although it was difficult to assess due to spatial variability and evidence of recent overlying fluvial deposits.

The actual boundary shear stresses are likely to be considerably lower than those estimated in the analysis. This is because the analysis is based on the assumption that the total resisting force is dissipated along the channel perimeter as boundary shear acting on the surface of the cohesive sediment. The Sabie River is characterised by well developed riparian vegetation, particularly in bedrock anastomosing channel type reaches. Although in-channel vegetation increases the total flow resistance by form drag, it acts to reduce boundary shear. In addition, the root masses bind the sediments further reducing entrainment. The proportion of the total resisting force that may be dissipated as vegetational form drag was apparent in the bedrock anastomosing channel type reaches, where extensive riparian tree mortalities were recorded with trees uprooted by the flow (refer to Fig. 39 for visual evidence of observed change within the representative bedrock anastomosing channel type reach between 1986 and 1996). The bed material along the Sabie River consists predominantly of non-cohesive medium to coarse sands and gravels. Granular material overlying cohesive soils provides protection of the cohesive bed, but mobile sediments act to rapidly abrade underlying cohesive material (Kamphuis, 1990).

The erosion of cohesive materials in a mixed alluvial-bedrock river containing mobile non-cohesive granular sediments and significant in-channel riparian vegetation is complex. This study quantifies the probability of eroding the cohesive sediments along the Sabie River, based on analyses of critical resistance of the local material and applied hydraulic stresses. Although the estimated probability of eroding cohesive material from the Sabie River bed for a large flood event appears to be higher than that observed following an extreme recent flood, the analysis nevertheless shows that there is considerable potential for large scale stripping of the macro-channel deposits. The reduction in hydraulic boundary shear stress resulting from in-channel vegetation is possibly the major reason for the erosion potential being higher than that observed. This is combined with the possibility that the flood was transporting catchment derived sediment at its maximum capacity, and so was not competent to transport additional material eroded from the channel bed. Furthermore, no account was taken of flood duration, where longer duration or multiple floods would have an increased potential to erode cohesive sediments resulting in stripping levels nearer to the predicted maximum potential. This emphasizes the need to adequately manage the riparian vegetation to enable it to continue affording protection to the cohesive bed during extreme flood events.

4 Channel hydraulics

4.1 Introduction

Hydraulic and geomorphological conditions are the primary determinants of the physical habitat in rivers, and it is therefore necessary to understand the mechanisms controlling local hydraulic parameters to predict the effect of altering the flow and sediment regimes on the river. The total flow resistance of a channel determines the local hydraulic conditions (such as flow depth, velocity and bed shear), and represents the sum of several individual resistance components including for example skin, channel form and vegetational resistance elements.

The most recent and extensive study concerning channel flow resistance along the Sabie River was undertaken by Broadhurst *et al.* (1997). The study quantified the total flow resistance at both the morphological unit and channel type (association of morphological units) scales. The flow resistance information was, however, limited to discharges below 40 m^3/s, with the exception of the mixed anastomosing channel type where hydrological conditions during the study permitted measurements of up to 80 m^3/s and for an isolated event of 1000 m^3/s.

4.2 Extending the flow resistance data of Broadhurst *et al.* (1997)

A major flood event on 14 February 1996 provided an opportunity to extend the flow resistance data of Broadhurst *et al.* (1997). The flood peak was gauged from the road bridges at Kruger Gate and immediately downstream of the Sand River confluence at 1705 m^3/s and 2259 m^3/s, respectively. Peak stage levels were recorded at selected monitoring sites located during previous studies (Heritage *et al.* (1997a) and Broadhurst *et al.* (1997) provide a full description and location of monitoring sites along the Sabie River, KNP). Stage levels and discharges on the receding limb of the flood event were also measured.

Representative examples of the common channel types identified by Heritage *et al.* (1997a) along the Sabie River were used by Broadhurst *et al.* (1997) to obtain characteristic channel type flow resistance data. Multiple linked cross-sectional profiles located along the river were used to compute the reach averaged total flow resistances according to the Barnes (1967) methodology. The locations of the representative channel types are given in Fig. 1. Figures 15 to 19 are plots of the longitudinal bed and water surface profiles for the representative channel types for low flow and flood conditions. The macro-channel cross-sectional profiles used for determination of the reach averaged flow resistances are indicated, as are their locations along the river.

Table 4 gives the flood hydraulics and reach averaged flow resistance data.

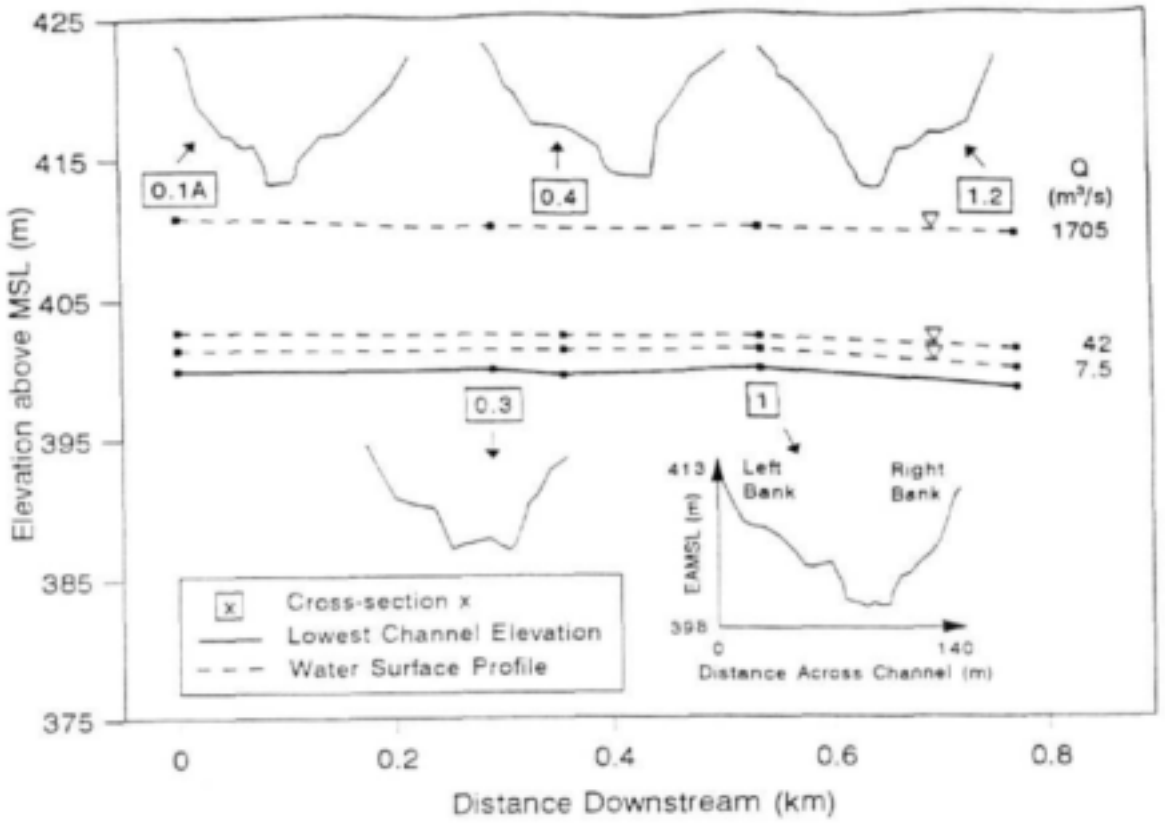

Figure 15 Longitudinal and cross-sectional profiles used for the resistance analysis in the single-thread channel type

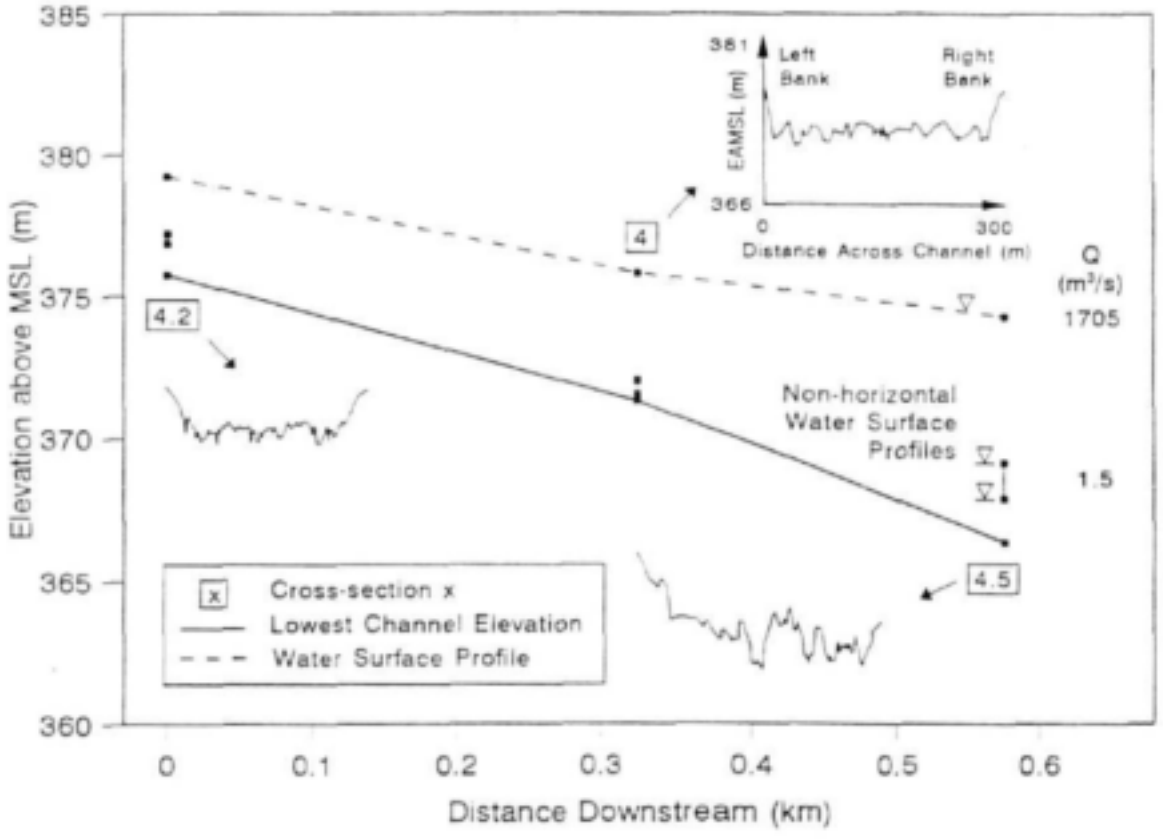

Figure 16 Longitudinal and cross-sectional profiles used for the resistance analysis in the bedrock anastomosing channel type

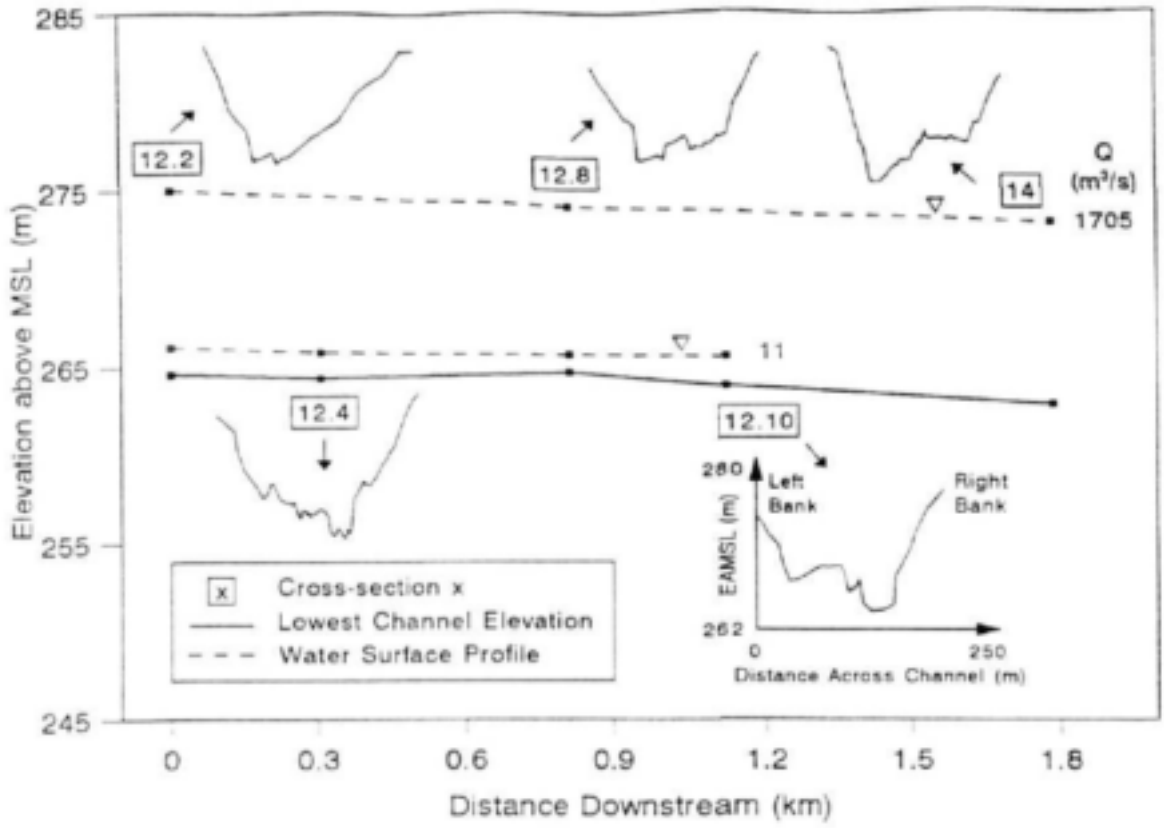

Figure 17 Longitudinal and cross-sectional profiles used for the resistance analysis in the braided channel type

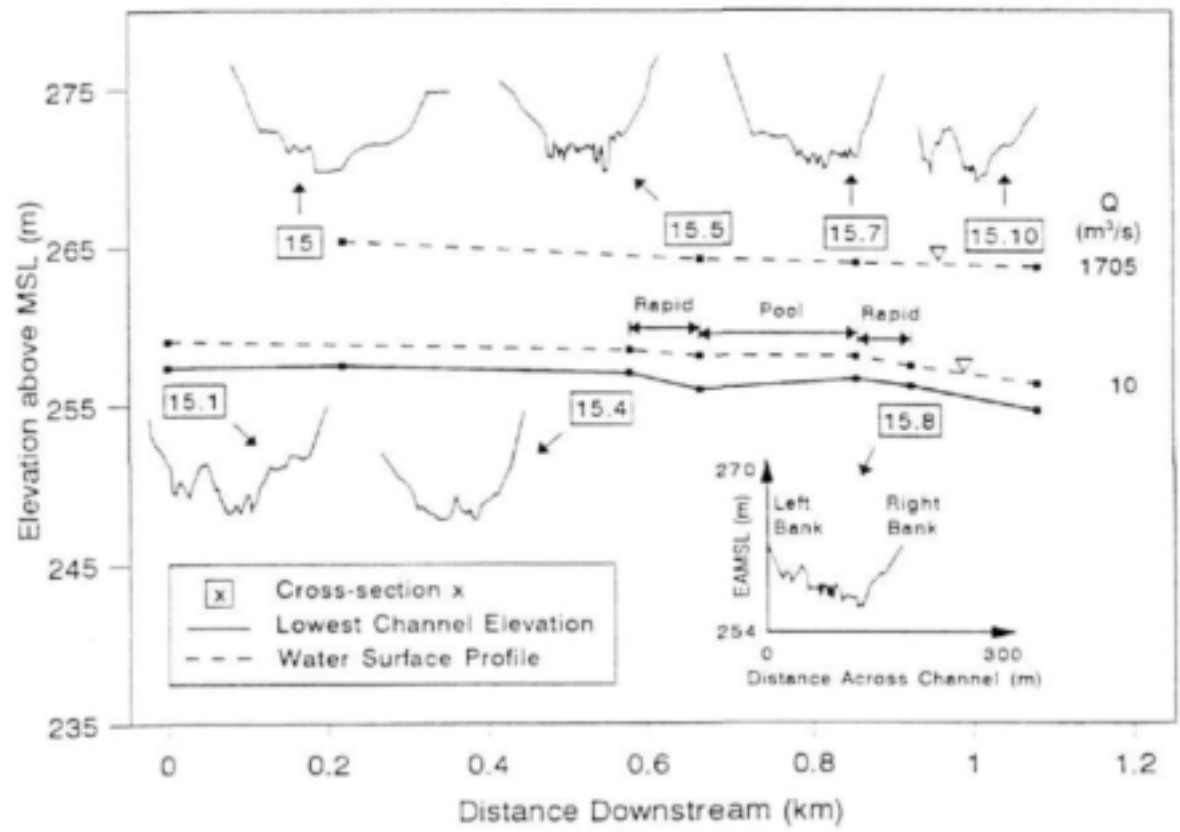

Figure 18 Longitudinal and cross-sectional profiles used for the resistance analysis in the pool-rapid channel type

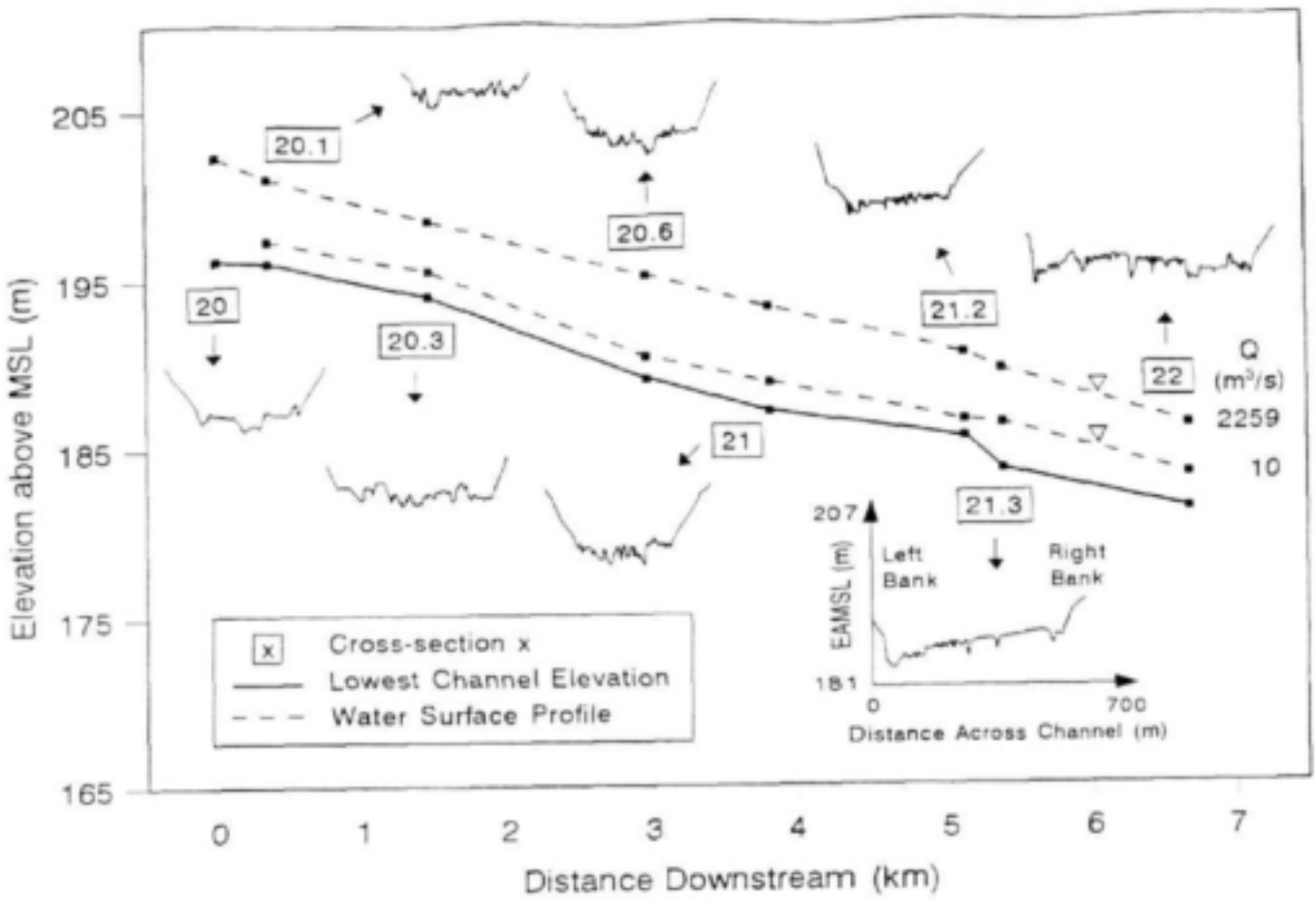

Figure 19 Longitudinal and cross-sectional profiles used for the resistance analysis in the mixed anastomosing channel type

The reach averaged coefficients according to the Manning, Chezy and Darcy-Weisbach resistance formulations are calculated using equations 5 (Barnes, 1967), 6 (Hicks and Mason, 1991) and 7 (Broadhurst *et al.*, 1997), respectively, and are given by

$$n^2 = \frac{1}{Q^2}\left(\frac{\left(h_N - h_1\right) + \left(h_{v_N} - h_{v_1}\right) - \left(k_{12}\Delta h_{v_{12}} + \ldots + k_{i(i+1)}\Delta h_{v_{i(i+1)}} + \ldots + k_{(N-1)N}\Delta h_{v_{(N-1)N}}\right)}{\frac{L_{12}}{X_1 X_2} + \ldots + \frac{L_{i(i+1)}}{X_i X_{i+1}} + \ldots + \frac{L_{(N-1)N}}{X_{N-1} X_N}}\right) \quad 5$$

$$C^2 = Q^2\left(\frac{\frac{L_{12}}{Y_1 Y_2} + \ldots + \frac{L_{i(i+1)}}{Y_i Y_{i+1}} + \ldots + \frac{L_{(N-1)N}}{Y_{N-1} Y_N}}{\left(h_N - h_1\right) + \left(h_{v_N} - h_{v_1}\right) - \left(k_{12}\Delta h_{v_{12}} + \ldots + k_{i(i+1)}\Delta h_{v_{i(i+1)}} + \ldots + k_{(N-1)N}\Delta h_{v_{(N-1)N}}\right)}\right) \quad 6$$

$$f = \frac{8g}{Q^2}\left(\frac{\left(h_N - h_1\right) + \left(h_{v_N} - h_{v_1}\right) - \left(k_{12}\Delta h_{v_{12}} + \ldots + k_{i(i+1)}\Delta h_{v_{i(i+1)}} + \ldots + k_{(N-1)N}\Delta h_{v_{(N-1)N}}\right)}{\frac{L_{12}}{\sqrt{Z_1 Z_2}} + \ldots + \frac{L_{i(i+1)}}{\sqrt{Z_i Z_{i+1}}} + \ldots + \frac{L_{(N-1)N}}{\sqrt{Z_{N-1} Z_N}}}\right) \quad 7$$

where

N	is the number of cross-sectional profiles
h_N	is the water surface elevation at profile N (m)
h_{v_N}	is the velocity head at profile N (m)
$k_{(i+1)}$	is the energy loss coefficient due to acceleration between profile i and $i+1$
$\Delta h_{v_{(i+1)}}$	is the velocity head loss between profile i and $i+1$ (m)
$L_{(i+1)}$	is the reach length between profile i and $i+1$ (m)
X_i	is given by $A_i R_i^{2/3}$ ($m^{8/3}$)
Y_i	is given by $A_i R_i^{1/2}$ ($m^{5/2}$)
Z_i	is given by $A_i^2 R_i$ (m^5)

Figure 14 is a plot of Manning's resistance coefficient as a function of discharge for the extended data set. It is reassuring to note that although the resistance coefficients vary considerably at low flows (0.075 to 2), the trends converge at high flows to values in the range 0.04 to 0.09. This is expected, and arises from the drowning-out of local hydraulic controls and reduced influences of characteristic channel type morphological assemblages as stages approach the upper levels of the macro-channel bank. The resistance coefficients for the mixed anastomosing channel type (0.0395 at 952 m^3/s and 0.0472 at 2259 m^3/s, Table 4) differ from that determined by Broadhurst *et al.* (1997) (0.075 at 1000 m^3/s). The February 1996 flood values are adopted based on the extended number of cross-sections used in the analysis (Broadhurst *et al*'s. (1997) study was limited to 2 cross-sections). With the exception of the single-thread channel type data (which displays a discontinuity at 20 m^3/s to 30 m^3/s, Fig. 14), relationships of the following form have been fitted to the resistance data:

$$n = aQ^b + c \qquad 8$$

where

n	is the Manning resistance coefficient ($s/m^{1/3}$)
Q	is the discharge (m^3/s)

a, b, c are the regression coefficients and are given in Table 5.

4.3 Water surface profile data

In addition to the resistance data, energy slope data are required to characterise the stage discharge or rating relationships and also to determine the total hydraulic shear forces. Water surface slopes may be substituted for energy slopes if the longitudinal change in velocity head is assumed to be negligible. Water surface slopes were measured for the channel type cells along the Sabie River during low flow conditions and for the representative reaches at the flood flow using conventional survey techniques (Table 6 and Fig. 20) (details of these cells and their locations are provided by Heritage *et al.*, 1997a). Where field data were unavailable, the mean channel type slopes are used for the low flow gradients, whilst the regional gradients (from 1:50 000 topographical maps) are used for the flood profiles. Exceptions are the bedrock anastomosing channel type cells, where the low flow slopes provide better estimates of the flood profiles in these high gradient channel types than the spatially averaged regional slopes from the 1:50 000 topographical maps (refer to Table 6, cell 12).

Table 4 Flood hydraulics data and reach averaged resistance coefficients

Channel type	Discharge Q (m^3/s)	Cross-section	Chainage (m)	Bed elevation h_o (mAMSL)	Water surface elevation Z (mAMSL)	Flow area A (m^2)	Wetted perimeter P (m)	Average velocity v (m/s)	Resistance coefficient		
									Manning n	Chezy C	Friction factor, f
Braided	1705	12.2	0	264.58	275.03	1098	185	1.55			
		12.8	812	264.62	274.05	922	159	1.85			
		14	1789	262.79	273.09	930	156	1.83	0.0597	22.50	0.155
Single thread	1705	0.1A	0	399.82	410.83	800	132	2.13			
		0.3	292	399.83	410.02	755	124	2.26			
		1	828	399.83	409.92	769	134	2.22			
		1.2	1601	398.40	409.47	771	131	2.21	0.0617	21.82	0.165
Pool-rapid	1705	15	0	257.53	265.35	945	209	1.80			
		15.5	664	256.03	264.22	754	183	2.26			
		15.7	855	256.65	263.95	699	169	2.44			
		15.10	1080	254.67	263.70	854	174	2.80	0.0535	23.86	0.138
Mixed anastomosing	2259	20	0	196.62	202.29	1108	340	2.04			
		20.1	350	196.08	201.09	913	352	2.47			
		20.3	1457	194.31	198.47	1033	457	2.19			
		20.6	2967	189.11	195.24	1140	344	1.98			
		21	3842	187.15	193.38	1174	333	1.92			
		21.2	5134	185.52	190.45	947	338	2.38			
		21.3	5392	183.61	189.50	1301	509	1.74			
		22	6692	181.25	186.17	1485	626	1.52	0.0395	22.07	0.125
Bedrock anastomosing	1705	4.2	0	375.74	379.22	489	232	3.48			
		4	325	371.30	375.80	957	308	1.78			
		4.5	575	366.37	374.28	1420	347	1.20	0.0901	13.07	0.456

Table 5 Regression coefficients in equation 8

		Coefficient in equation 8		
		a	*b*	*c*
Channel type				
Braided	0 to 35 m^3/s	1.379×10^{-1}	-1.150×10^{-1}	6.058×10^{-2}
	m^3/s	1.676×10^{-5}	1.000	3.045×10^{-3}
	>35 m^3/s	1.815×10^{-1}	-1.948	1.135×10^{-1}
Pool-Rapid		2.631×10^{-1}	-6.097×10^{-1}	4.209×10^{-2}
Mixed Anastomosing		1.855×10^{0}	-5.509×10^{-1}	6.000×10^{-2}
Bedrock Anastomosing				
Morphological unit				
Pool		1.167×10^{-3}	-2.583×10^{-1}	3.576×10^{-2}

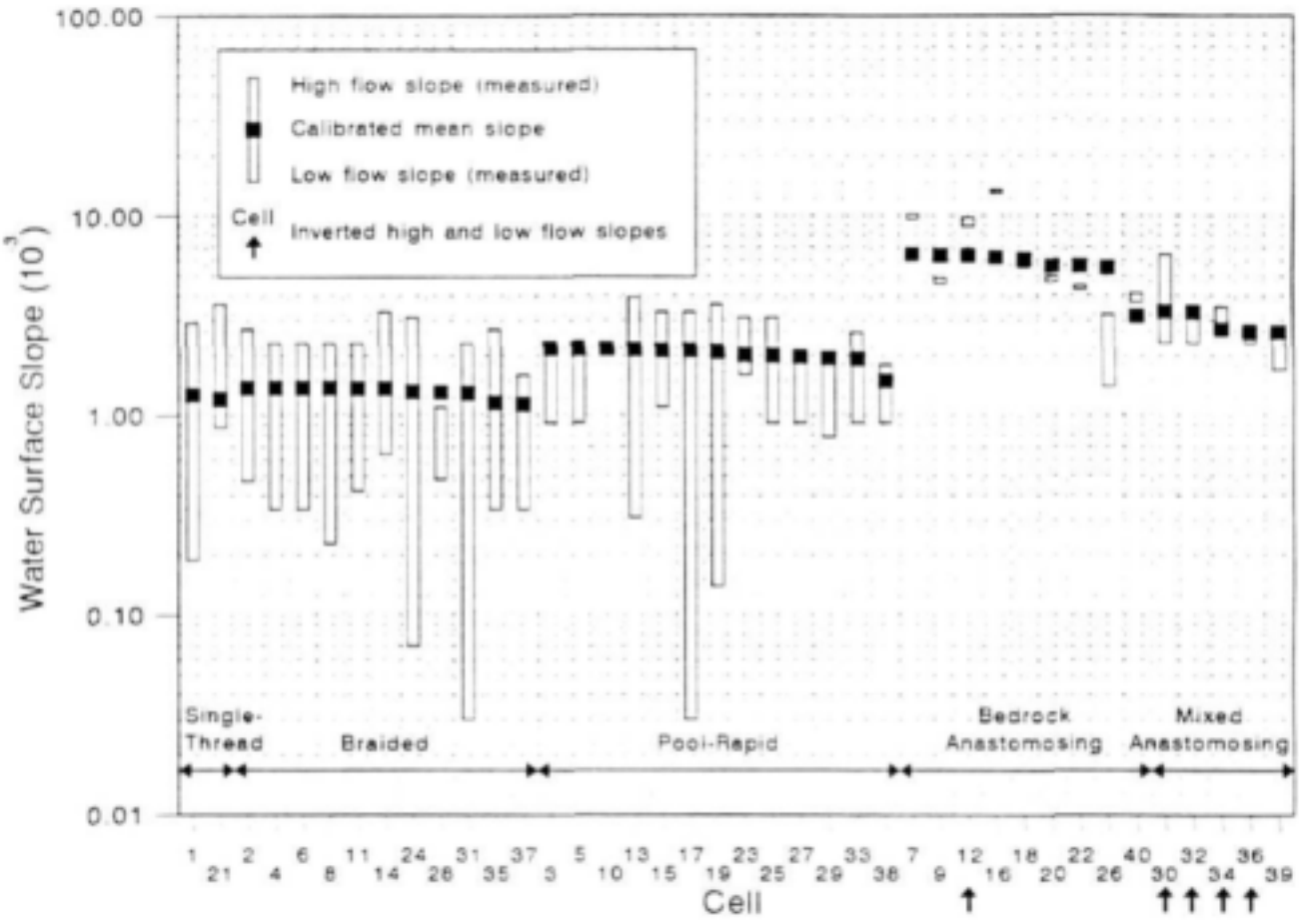

Figure 20 Measured low and high flow water surface slope and calibrated mean energy slope for the channel type cells along the Sabie River

Table 6 Sabie River cell water surface slope data (R - representative channel type; ST - single-thread ; BR - Braided; BA - Bedrock anastomosing; PR - Pool-rapid; MA - Mixed anastomosing; M - mean estimate; KG -Kruger gate, SK - Skukuza restcamp; LS - Lower Sabie restcamp; slopes for pool sections of pool-rapid channel types)

Cell no.	Channel type	Cell length (m)	Regional slope (1:50 000)	Water surface slope		
				Low flow	High flow	Flood data
1	ST[R]	2 610	0.00302	0.00019	flood	0.00290
2	BR	2 450	0.00268	0.00047	regional	
3	PR	350	0.00233	0.00092[M]	regional	
4	BR	300	0.00233	0.00034[M]	regional	
5	PR	300	0.00233	0.00092[M]	regional	
6	BR	300	0.00233	0.00034[M]	regional	
7	BA	1 300	0.00233	0.00972	low flow	
8	BR	1 700	0.00233	0.00023	regional	
9	BA	650	0.00233	0.00463	low flow	
10	PR	700	0.00233	0.00301	regional	
11	BR	1 800	0.00233	0.00042	regional	
12	BA[R]	1 000	0.00571	0.00980	flood	0.00890
13	PR	3 000	0.00394	0.00031	regional	
14	BR	700	0.00331	0.00064	regional	
15	PR	700	0.00331	0.00108	regional	
16	BA	1 600	0.00331	0.01246	low flow	
17	PR	2 400	0.00331	0.00003	regional	
18	BA	1 750	0.00361	0.00548	low flow	
19	PR	800	0.00364	0.00014	regional	
20	BA	1 400	0.00364	0.00473	low flow	
21	ST	800	0.00364	0.00087	regional	
22	BA	1 450	0.00342	0.00432	low flow	
23	PR	1 200	0.00305	0.00163	regional	
24	BR	3 200	0.00305	0.00007	regional	
25	PR	1 300	0.00305	0.00092[M]	regional	
26	BA(KG)	5 700	0.00317	0.00140	regional	
27	PR	4 300	0.00198	0.00092[M]	regional	
28	BR[R]	1 200	0.00167	0.00048	flood	0.0011
29	PR[R](SK)	9 000	0.00178	0.00078	flood	0.0020
30	MA	800	0.00225	0.00640	regional	
31	BR	1 200	0.00225	0.00003	regional	
32	MA	4 000	0.00225	0.00352[M]	regional	
33	PR	2 400	0.00255	0.00092[M]	regional	
34	MA	5 600	0.00284	0.00352[M]	regional	
35	BR	750	0.00265	0.00034[M]	regional	
36	MA[R]	17 500	0.00200	0.00242	flood	0.0023
37	BR	2 300	0.00160	0.00034[M]	regional	
38	PR(LS)	5 000	0.00179	0.00092[M]	regional	
39	MA	11 500	0.00265	0.00173	regional	
40	BA	6 800	0.00408	0.00368	regional	

4.4 Application of the extended hydraulics data

The extended hydraulics data are integral to the components described within this study, and have been utilised as follows:

- The extended flow resistance relationships (Fig. 14) have been used in combination with water surface slopes to model the potential sediment transport within representative examples of the common Sabie River channel types (chapter 2)

- Field data from the flood event in February 1996 have been used to determine the total hydraulic shear force at sites along the Sabie River (chapter 3).

- The extended flow resistance data have been combined with cell-based water surface gradient measurements taken along the Sabie River to characterise the hydraulics and sediment transport relationships (chapter 5).

4.5 Conclusions and recommendations

Hydraulics data corresponding to an extreme flood event have been used to extend the (low to intermediate) hydraulic relationships determined by Broadhurst *et al.* (1997) for the channel types along the Sabie River. The extended flow resistance relationships are shown to converge at high flows due to the reduced influence of channel type specific hydraulic controls (e.g. channel morphology, vegetation structure).

Further development and validation of the "non-horizontal" model described by Broadhurst *et al.* (1997) was beyond the scope of this study. There is a demand, however, for significant work on the hydraulics of bedrock dominated channels, since these morphologies have a widespread occurrence in South African rivers. This need has become increasingly apparent during recent hydraulics investigations for instream flow requirement assessments for a number of Southern African rivers.

The isolation and quantification of individual resistance components needs to be addressed in order to improve the transferability of channel type flow resistance values to similar channel environments. Consequently, a separate project has been initiated to study the flow through reedbeds based primarily on experimental work within a controlled environment. The reed species *P. maritianus* consistutes a large proportion of the in-channel riparian vegetation along the Sabie River, and this project provides the means to isolate and quantify form and bed resistance components.

5 Sabie River SEDiment FLux and stOrage model

5.1 Introduction

A semi-quantitative sediment flux and storage model was developed for predicting change at the channel type scale on an annual basis by Heritage *et al.* (1997a). The refinement, calibration and verification of this model, based on historical data derived from aerial photographs covering 56 years, are described in this chapter. The Sabie River SEDiment FLux and stOrage model (SEDFLO) consists of two integral components. The first component deals with the production of sediment across the catchment landscape and the delivery of this eroded source material to the study length of the river in the KNP. This includes lateral inputs from tributaries. The second component of the model deals with the differential transport of the sediment along the river system.

5.2 Sediment production, yield and delivery

Sediment production refers to the process whereby soil is eroded and subsequently redistributed due to continuing landform development. *Sediment yield* is the total temporal sediment outflow from a watershed or drainage basin measurable at a cross-section or reference point. The rate at which sediment is delivered from major watercourses is usually considerably less than the rate at which it is eroded from the land surface (Vanoni, 1975). A considerable proportion of the material is stored at intermediate locations wherever the entrainment capacity of the flow is insufficient to sustain transport. The *sediment delivery ratio* is the percentage of onsite eroded material (source erosion) that is transported to a given reference point further downstream, and therefore accounts for the sediment storage and reworking of dislodged material across the catchment and within watercourses.

Catchment sediment production has been identified as a principal factor determining channel form and dynamics in the Sabie River (Heritage *et al.*, 1997a). It is therefore necessary to quantify the sediment yields from the Sabie River subcatchments in order to predict geomorphological change within this system. Sediment yields may be determined by actual observations through streamflow sampling and reservoir surveys. Unfortunately, these data are not available for the Sabie River catchment. Consequently, empirical methods have been used to obtain estimates of the sediment yields from the Sabie River subcatchments.

5.2.1 Sediment yield maps of Rooseboom *et al.* (1992)

Rooseboom *et al.* (1992) collated all available information relevant to sediment yields in South Africa and developed a yield map for the region. The early efforts to quantify potential sediment yields revealed that sediment availability is the determining factor in sediment yield processes throughout Southern Africa. A statistical analysis on a regional basis was performed to overcome the wide variability in sediment yields, and a method for estimating sediment yields for catchments with no observed data was developed. This approach gives a value of

155 t/km^2/annum for the Sabie River catchment. The nature reserves do not fall into any of the nine characteristic regions identified by Rooseboom *et al.* (1992), and a value of 155 t/km^2/annum is therefore allocated to this landuse in Table 7.

5.2.2 GIS modelling of van Niekerk and Heritage (1994)

A detailed study of development potential and management of water resources in the Sabie River catchment was commissioned by the DWAF (Chunnett *et al.*, 1990). Based on this study, landuse and slope/erodability classes were captured on the ArcInfo GIS. These covers were used to delineate regions of equal sediment yield potential based on the sediment yield recommendations for relative degrees of land degradation and slope/erodability information of Chunnett *et al.* (1990). The modelling of van Niekerk and Heritage (1994) produced the annual sediment generated in the important subcatchments for existing and undisturbed conditions (Table 7).

5.2.3 ACRU model

The Agricultural Catchments Research Unit (ACRU) model is a multipurpose and multilevel integrated catchment model that simulates sediment yield at a daily time step (Schulze, 1989). The model uses the Modified Universal Soil Loss Equation (MUSLE) to predict the daily sediment yield from the 56 Sabie River subcatchments (Fig. 21).

The Universal Soil Loss Equation, USLE (Wischmeier and Smith, 1978) was originally developed for use in the USA and has received extensive application for estimating sediment production. The USLE provides a long term average annual soil loss due to sheet and rill erosion, and excludes soil loss due to concentrated flow and gully formation.

The USLE has the general form (Vanoni, 1975)

$$E = R\,K\,L\,S\,C\,P \qquad 9$$

where

E is the long-term average annual soil loss (t/ha/annum)
R is the rainfall erosivity factor (J.mm.10^3/m^2/hr)
K is the soil erodability factor (dimensionless)
L,S are slope length and gradient factors, respectively (dimensionless)
C is the cover and management factor (dimensionless)
P is the supporting conservation practice factor (dimensionless)

The USLE has been modified for application in semi-arid environments by the techniques described by Crosby *et al.* (1983) and McPhee and Smithen (1984). The USLE was modified by Williams (1975) by replacing the rainfall erosivity factor (R) in equation 9 with a runoff factor. The modified equation (MUSLE) eliminates the need for a sediment delivery ratio and is applicable for individual storm events (Williams and Berndt, 1972), and is given by:

$$Y_{sd} = 11.8(Q\ q_p)^{0.56}KLSCP \qquad 10$$

Table 7 Simulated sediment yields for the Sabie River subcatchments

Subcatchment	**Area** (km^2)	**Annual Yields** (t/km^2)						Ratio CALCITE : ACRU (average)
		van Niekerk & Heritage (1994)		**Rooseboom *et al.* (1992)**	**CALSITE** Donald (1997)	**ACRU**		
		Present	Natural			Average	Maximum	
Upper Sabie	770	328	300	155	76	66	211	1.15
Maritsane	472	345	299	155	42	162	386	0.26
North Sand	254	403	298	155	226	26	105	8.71
Sand	1910	402	300	155	234	36	116	6.50
Middle Sabie	1466	379	299	155	196	26	85	7.54
Lower Sabie	1389	247	247	155	18	6	25	2.97
Catchment	6261	349	288	155	143	39	120	3.67

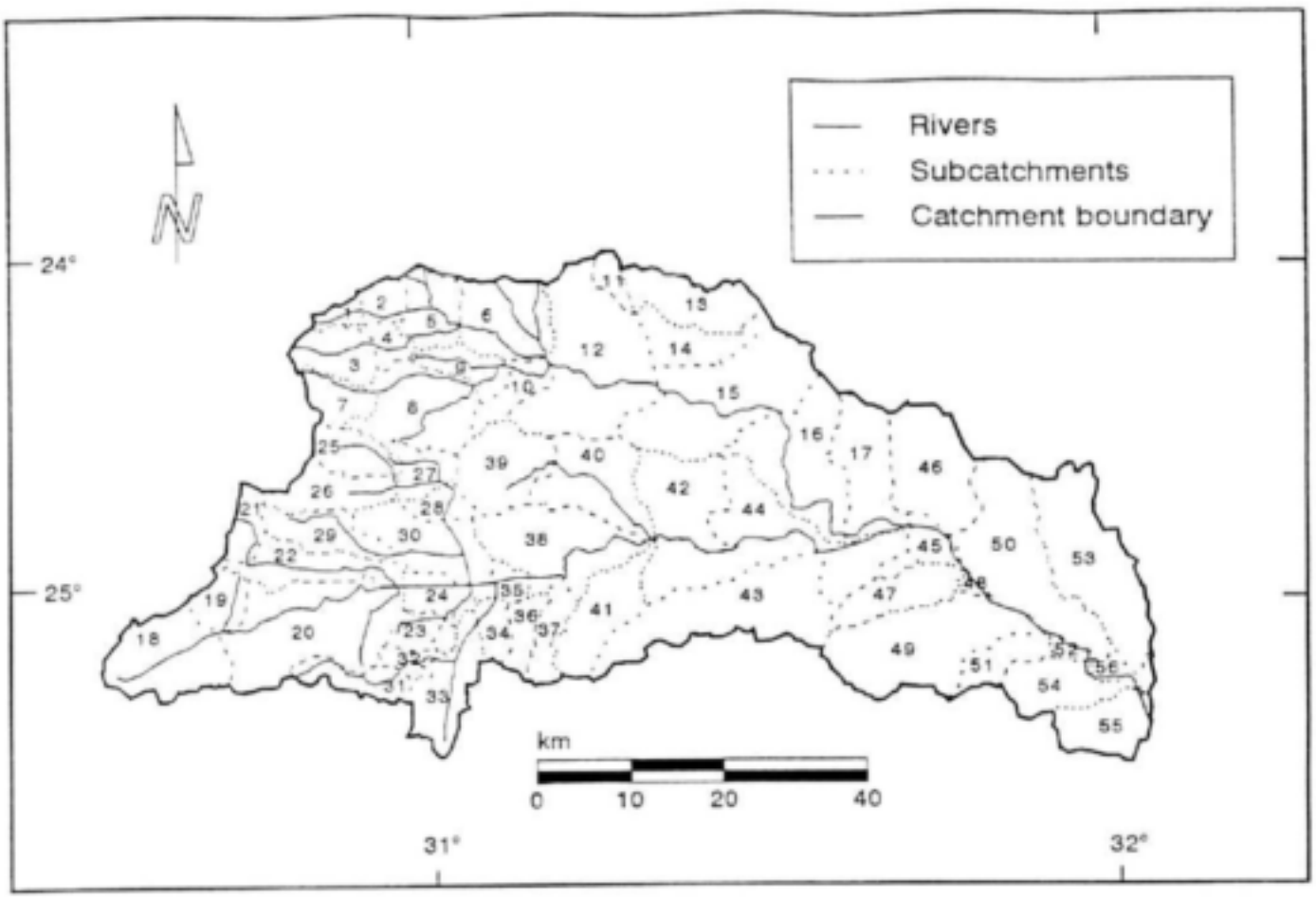

Figure 21 Fifty-six subcatchments used in ACRU to model the hydrology and sediment production in the Sabie River catchment (Jewitt *et al.*, 1997).

where

Y_{sd} is the sediment yield from the event (t)
Q is the event runoff volume (m^3)
q_p is the event peak discharge rate (m^3/s)

The daily sediment yields from the subcatchments illustrated in Fig. 21 have been simulated using the MUSLE in the ACRU model. These have been aggregated to provide the tributary inputs to the Sabie River in the KNP at tributary junctions, as well as distributed inputs from those subcatchments adjacent to the river without any major tributaries discharging into the Sabie (e.g. subcatchment 38). The sediment yield data have been aggregated for the six major subcatchments and the 61 years of simulated data (1932 to 1993) have been used to produce average annual and maximum annual values (Table 7), based on the assumption that the simulation period is sufficiently long for the purpose of predicting long-term annual sediment yields.

5.2.4 CALSITE model

The CALibrated SImulation of Transported Erosion (CALSITE) model is a catchment management tool for simulating soil erosion and sediment yield. CALSITE was developed

initially for use in the Magat basin, Philippines and has subsequently been used in the upper Mahaweli catchment (Sri Lanka), Khon Kaen (Thailand) and the Cameron Highlands (Malaysia) (Bradbury, 1994). The model has been modified for semi-arid conditions and applied to the Sabie River catchment by Donald (1997). CALSITE predicts long-term mean annual sediment yields, with the data requirements including MAR, land cover, soil maps, topographical information and the locations of watercourses (Donald *et al.*, 1995). The catchment is divided into pixels (typically 150 m square), and the sediment yield from each pixel is determined by factoring the source erosion according to the delivery ratio.

5.2.4.1 Source erosion

The Soil Loss EstiMater for Southern Africa (SLEMSA) (Elwell, 1978) was developed in Zimbabwe as an adaptation of USLE. USLE and SLEMSA have similar empirical determinants (equation 9), but have been shown to produce very different results with SLEMSA shown to predict far greater source erosion values for the Sabie River catchment (Donald *et al.*, 1995). This is attributed to the unrealistic slope factor in SLEMSA, and consequently the USLE has been used in CALSITE to model source erosion.

5.2.4.2 Delivery index

In CALSITE the delivery ratio is determined by empirical calibration of a *delivery index*. The delivery index is the ratio of limiting sediment concentration transporting capacity to the concentration at the source (Bradbury, 1994). It can be determined through a physically-based function derived from elevation data, independent of runoff data, such as Bradbury's (1994) equation:

$$DI_p = \frac{P_a^{2.32} \min(F^{0.66} S^{1.44})}{SE} \qquad 11$$

where

DI_p	is the delivery index
P_a	is the annual rainfall (mm)
$min()$	is the limiting value of the quantity within () along the flow path
F	is a flow parameter, representing the number of converging flow paths on a particular grid cell
S	is the channel slope (degrees)
SE	is the source erosion (t/ha/annum)

The coefficient values in equation 11 are derived from studies by Amplett and Dickenson (1989), Govers (1990) and Atkinson (1991).

The delivery index defined by equation 11 is then transformed to a delivery ratio through a calibration procedure, such as that described in the following section.

5.2.4.3 Calibration of sediment delivery for the Sabie River catchment

The calibration procedure is based on the premise that discrepancies between the predicted and measured sediment yields are due to an incorrect delivery ratio, rather than source erosion which is assumed to be accurately represented (Bradbury, 1994). The delivery index (equation 11) is converted to a delivery ratio in the range zero (all source erosion is deposited) to unity (all source erosion is transported) by multiplying the delivery index by a scaling factor. The scaling factor is given by ratio of the predicted catchment yield (delivery index multiplied by source erosion) to the observed value. If no observed data are available, as is the case for the Sabie River catchment, an estimated delivery ratio based on empiricism may be used (e.g. Williams and Berndt, 1972).

Rather than apply an empirical delivery ratio developed for a catchment where the conditions influencing sediment delivery may be significantly different, the Umgeni River catchment in the Kwazulu-Natal Province was used to calibrate a delivery ratio. Both the Sabie and Umgeni River catchments fall into region four delineated by Rooseboom *et al.* (1992), and therefore similar sediment production characteristics may be assumed. The sediment delivery indices (equation 11) for the Umgeni River catchment were calibrated using sediment surveys from three reservoirs with records of greater than eight years. The calibrated sediment ratios ranged from 0.40 to 0.45, and an average value of 0.43 was applied to the source erosion from the Sabie River catchment. The sediment yield results for the Sabie River catchment are given in Table 7.

5.2.5 Comparison between sediment yield estimates

The simulated sediment yields for the six major subcatchments (Fig. 22) using the different methodologies described are given in Table 7. The GIS modelling of van Niekerk and Heritage (1994) produces upper range values for both present and natural conditions, whilst the ACRU modelling using the MUSLE provides the lowest estimates for all the subcatchments. The long-term average annual sediment yield predicted using CALSITE (143 t/km^2/annum) for the Sabie River catchment compares favourably with the 155 t/km^2/annum of Rooseboom *et al.* Both CALSITE and ACRU predict lower sediment yield values for the Upper and Lower Sabie subcatchments, whilst the low yield from the Maritsane subcatchment (42 t/km^2/annum) simulated using CALSITE is not confirmed by the ACRU results, which show the highest yield (162 t/km^2/annum) for this region. CALSITE shows above average yields from the North Sand, Sand and Middle Sabie catchments, which is also the case though to a lesser degree for the present day conditions predicted by van Niekerk and Heritage (1994). The ACRU model, however, shows average to below average yields from these heavily degraded subcatchments.

Based on the simulated yields from empirical data and the yields of Rooseboom *et al.* (1992) derived from statistical analyses of observed data, the CALSITE model is considered to provide the most accurate representation of the long-term sediment yields for the Sabie River subcatchments. This is partly attributed to the significant effort that was invested by Donald (1997) in the application of CALSITE to the Sabie River catchment. Since daily sediment data are required for the Sabie River sediment flux model, the ACRU data for the 56 subcatchments are factored according to the long-term average annual sediment yields predicted by CALSITE for each of the major six subcatchments (Table 7). The temporal variability of sediment inputs to the Sabie River (daily, monthly and annual) are therefore modelled using ACRU, whilst the magnitude of the yields are provided by CALSITE.

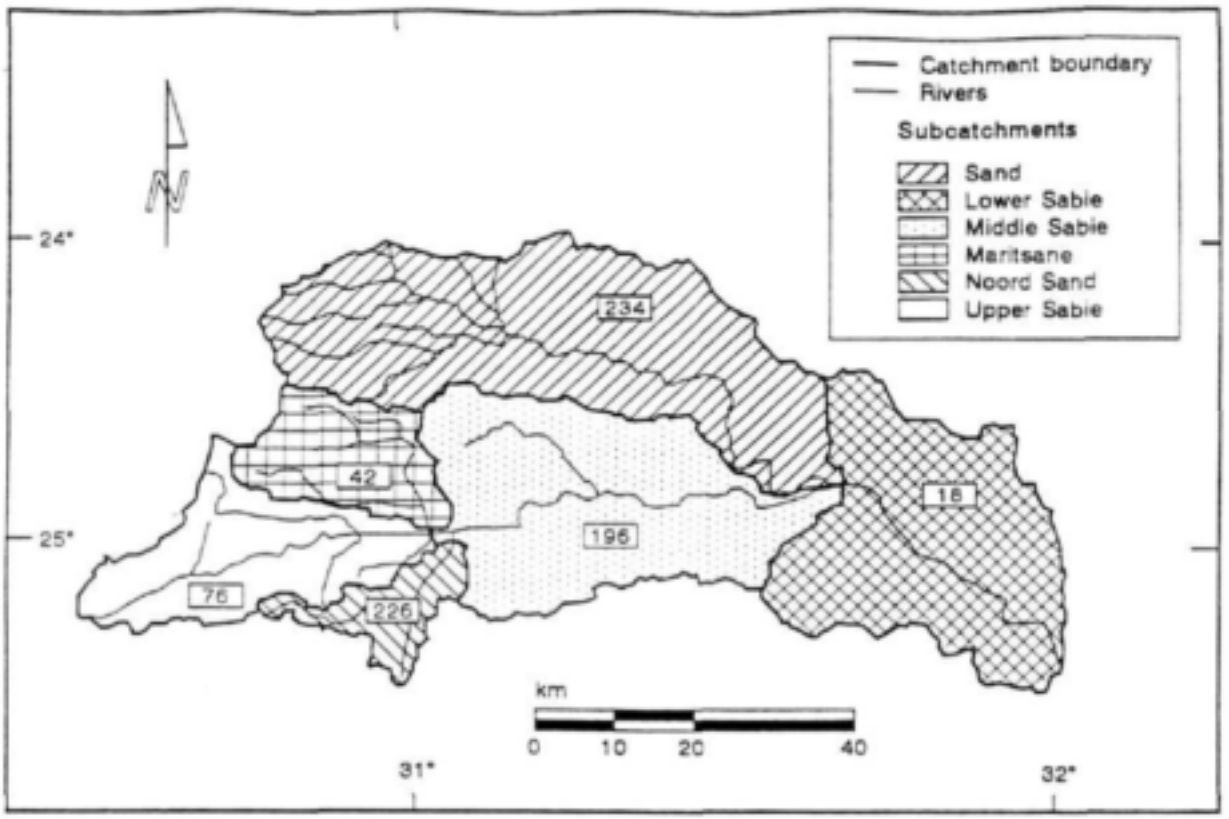

Figure 22 Delineation of the Sabie River catchment into six major subcatchments for which the sediment yield estimates are compared in Table 7. (Numbers are Calsite predictions in t/km^2).

5.3 Modelling sediment transport

5.3.1 Approaches for computing total load

The second integral component of SEDFLO is the prediction of the total (bed plus suspended) sediment (or bed material plus wash) load transported along the river. There are two basic approaches to determining the bed material load:

The *indirect* approach whereby a bed load computation (e.g. van Rijn (1984), Engelund and Hansen (1967) and Meyer-Peter and Müller (1948)) is used to define a concentration close to the bed, and then the Rouse equation (Rouse, 1937) and a velocity distribution are applied to compute the suspended load. The total load is then given by the sum of the bed plus suspended loads. This is the approach used by Einstein (1950) and van Rijn (1984). This methodology works well under equilibrium conditions but has some conceptual flaws when applied to non-equilibrium conditions, e.g. nonuniform flow, as discussed by James (1987). Van Rijn (1986) has, by introducing some artificial adjustments, used the method quite successfully for nonuniform conditions but the conceptual inadequacies remain.

There are also various *direct* approaches which are based on the idea that no distinction between bed load and suspended load is necessary. The total load can therefore be related directly to flow and sediment parameters. Colby (1964), for example, related total bed material load to the average flow velocity. Ghosh *et al.* (1981) computed total bed material load by applying the diffusion-convection model for suspended load through the bed layer, while accounting for high

concentration effects using Hunt's (1954) approach. One important class of methods for computing total load relates sediment discharge to stream power. This approach was used by Bagnold (1966) for determining bed load and suspended load, and more recently by Ackers and White (1973) and Yang (1973) for computing total load directly. The Ackers and White (1973) method has arguably become the most universally accepted approach for computing total load, and is applied here.

5.3.2 Ackers and White (1973) approach

Ackers and White (1973) proposed a method for computing sediment discharge which applies to grain sizes greater than 0.04 mm and for lower regime flow conditions (no data for Froude numbers greater than 0.8 were used for calibration).

Sediment transport is determined as a function of *sediment mobility*, which depends on grain size and density and the flow condition. The flow condition is defined in terms of the shear velocity. The total shear velocity is used when considering fine (suspended) sediments. For coarse sediment calculations, an effective shear stress is used which is related to the average flow velocity in the same way as the total shear velocity is related to flow velocity for a plane bed. For transitional sizes a weighted combination of the plane bed equivalent and total values is used, depending on grain and fluid characteristics. The relationship between sediment discharge and grain mobility is defined by the conversion of applied stream power to the useful work rate of moving sediment.

5.3.2.1 Sediment mobility

For *coarse sediments* the mobility is defined by the ratio of the effective applied shear stress on the bed to the resistance to movement of the top layer of particles. This can be expressed as

$$F_{cg} = \frac{u_*'}{\sqrt{g\,d\,(S_s - 1)}} \qquad 12$$

where

F_{cg} is the coarse grain sediment mobility number
g is the gravitational acceleration constant (m/s^2)
d is the grain diameter (m)
S_s is the mass density of sediment relative to that of fluid
u_*' is the shear velocity related to grain roughness (m/s)

The shear velocity u_*' can be determined from the relationship between mean flow velocity (U) and flow depth (D), i.e.

$$\frac{U}{u_*'} = \sqrt{32}\log\frac{10\,D}{d_{35}} \qquad 13$$

For *fine sediments* the mobility is represented by the ratio of the total shear velocity to sediment fall velocity, which can be expressed as

$$F_{fg} = \frac{u_*}{\sqrt{g\,d\,(S_s - 1)}} \qquad 14$$

where
u_* is the shear velocity (m/s)

The sediment mobility is the square root of the Shields parameter for incipient motion, with u_* defined appropriately for coarse and fine sediments.

A general relationship for mobility of coarse, fine and transitional sediments can be written as

$$F_{gr} = \frac{u_*^{\,n}\, u_*^{\,(1-n)}}{\sqrt{g\,d\,(S_s - 1)}} \qquad 15$$

with
$n = 0$ for coarse sediments, and
$n = 1$ for fine sediments

For intermediate sediments, the value of n (indicating the relative importance of u_* and u'_*) depends on the size and density of the sediment particles and the fluid viscosity, as expressed by the dimensionless grain diameter

$$D_{gr} = d\left(\frac{g\,(S_s - 1)}{\nu^2}\right)^{1/3} \qquad 16$$

where
D_{gr} is the dimensionless grain diameter
ν is the kinematic viscosity of water (m^2/s)

From data, the following relationships for n were derived.

$$n = 0 \text{ for } D_{gr} > 60 \qquad 17$$

$$n = 1.0 - 0.56 \log D_{gr} \text{ for } 1 \le D_{gr} \le 60 \qquad 18$$

Equation 17 applies to coarse sediments and equation 18 to transitional and fine sediments.

5.3.2.2 Sediment transport

A sediment transport relationship was developed by defining the efficiency of the applied stream power in transporting sediment. The applied stream power is given by $\tau_o' U$ for coarse grains and $\tau_o U$ for fine grains, where U is the depth-averaged flow velocity and τ_o and τ_o' are the total and

grain roughness components of boundary shear stress. It is hypothesized that efficiency depends on the mobility number, F_{gr}. Below some critical value of the mobility number there will be no sediment movement and therefore the efficiency is zero. As the mobility number increases above this critical value, sediment discharge and the efficiency will increase.

By combining the efficiency (the rate of work done in moving bed load or maintaining suspension divided by the applied stream power) with the mobility number, the dimensionless sediment transport can be defined as

$$G_{gr} = \frac{XD}{S_s d}\left(\frac{u_*}{U}\right)^n \qquad 19$$

where
X is the concentration of sediment transport, i.e. the mass flux per unit mass flow rate

From measured data, an empirical relationship was obtained between the dimensionless sediment transport (G_{gr}) and the mobility number (F_{gr}) with the form

$$G_{gr} = C\left(\frac{F_{gr}}{A} - 1\right)^m \qquad 20$$

Values for C, A and m are dependent on D_{gr}, as follows:

For $D_{gr} > 60$ (coarse sediment):

$$A = 0.17 \qquad 21$$

$$m = 1.50 \qquad 22$$

$$C = 0.025 \qquad 23$$

For $1 \le D_{gr} < 60$ (fine and transitional sediment):

$$A = \frac{0.23}{\sqrt{D_{gr}}} + 0.14 \qquad 24$$

$$m = \frac{9.66}{D_{gr}} + 1.34 \qquad 25$$

$$\log C = 2.86 \log D_{gr} - (\log D_{gr})^2 - 3.53 \qquad 26$$

A represents the critical value of F_{gr} at which transport is initiated.

The procedure for applying the method is as follows. (Ackers and White (1973) recommend representing graded sediments by the d_{35} size, i.e. the size for which 35% of the sediment in the mixture is finer).

1. Compute the dimensionless grain size from equation 16.

2. Compute values of n, m, A and C using equations 17, 18 and 21 to 26.

3. Compute F_{gr} from equation 15.

4. Compute G_{gr} from equation 19.

5. Convert G_{gr} to the mass concentration using equation 19, i.e.

$$X = G_{gr} S_s \frac{d_{35}}{D} \left(\frac{U}{u_*} \right)^n \qquad 27$$

6. Compute the total mass sediment discharge (Q_s) from

$$Q_s = X Q \qquad 28$$

where
Q_s is the mass sediment discharge (tons/s)
Q is the volumetric water discharge (m^3/s)

5.4 Historical records on sedimentation

Calibration of SEDFLO requires historical records of the changes in sedimentation. Aerial photographs provide a useful means of assessing the vector (direction and magnitude) of the geomorphological change along a river. The spatial and temporal extent as well as the resolution (photographic scale) of the available record are provided in Table 8.

Table 8 Aerial photographic record for the Sabie River

Exposure date	Photographic scale	Cell coverage
1940	1:35 000	1 to 15, 36 to 39
1944	1:20 000	14 to 36
1965	1:60 000	1 to 40
1974	1:30 000	14 to 19, 24 to 36
1977	1:30 000	36 to 40
1986	1:10 000	1 to 40
1996	1:10 000	1 to 40

Although the temporal aerial photographic coverage (Table 8) extends from 1940 to 1996, the spatial coverage is limited, with only three of the seven records covering the whole river in the KNP. In addition, only the last two records (1986 and 1996) are at photographic scales that facilitate accurate quantitative analyses of changes in the river morphology using photogrammetry. Additional fixed-point aerial photographs are available for selected sites along the river from 1989 (see Heritage *et al.*, 1997a), but these records are of limited use in assessing the long-term changes in sedimentation along the entire extent of the Sabie River in the KNP. The scale of the 1965 record is also too coarse (1:60 000) to provide useful data of the change in sedimentation between the 1940s and 1970s records.

Ideally, sedimentation data derived from the aerial photographic records should be subdivided for calibration and verification purposes. A portion (preferably 50%) of the data should be used for model calibration and thereafter the predictive ability of the model assessed using the remaining data. The data required to calibrate a sediment transport (or storage) model along the Sabie River in the KNP need to cover the full extent of the river, since the change in sediment storage for a given cell is a function of the sediment discharge from the upstream cell, lateral inputs from tributaries and the sediment movement through the cell under consideration. Unfortunately, the period covered by the data record (1940 to 1996) cannot readily be subdivided whilst maintaining full spatial coverage. Based on the existing record, sedimentation data derived from the 1940/44 and 1986 aerial photographs are used to calibrate SEDFLO, whilst the partial coverage of the 1977 and full coverage of the 1996 data sets are used to assess the predictive accuracy of the model.

5.4.1 Changes in sedimentation from aerial photographic analysis

5.4.1.1 Photogrammetric analysis

Photogrammetry is the process of obtaining information about the physical environment by measuring and interpreting photographic images. The basis for determining elevations (and hence topography) from aerial photographs is made possible by stereoscopic parallax, defined as the change in position of an image between photographs caused by the shift in observational position. A stereo-model of the land surface is formed by viewing the stereo-pair overlap through a stereoscope. Control points are required on the stereo-model, ideally located at each of the corners of the stereo-model, and must be surveyed in the field.

Photogrammetry was used to provide a sedimentary base-state as at 1986 prior to inundation in 1989 of the dam on the Sabie River at the Lower Sabie restcamp (Fig. 1). The study is described in full by Birkhead *et al.* (1995). The approximate vertical and horizontal resolution that could be achieved using the 1986 1:10 000 aerial photographic record (Table 8) was of the order 0.25 m and 1.0 m, respectively. The vertical resolution is too coarse to obtain meaningful estimates of changes in volumetric storage, and the survey of control points necessary to develop stereo-models of the Sabie River in the KNP would be prohibitive. Furthermore, the print scale of the earlier photographic records will result in reduced resolution, as will the masking effect of the water level and riparian vegetation cover along the river.

5.4.1.2 Temporal and spatial bar dynamics

Changes in sedimentation may be assessed from aerial photographs by evaluating the degree of bar establishment and accumulation in aggrading systems, whilst a general reduction in the coverage by these features may be expected in eroding systems. The use of temporal bar coverage as a quantitative indicator of changes in sedimentation is based on the following assumptions:

- Sediment is deposited and eroded primarily as alluvial bars, and the aerial coverage by these features therefore provides a suitable indicator of the overall change in sedimentation.

- The relationship between change in bar area and associated volumetric storage is linear.

Analyses of aerial photographs and field observations reveal that the first assumption is reasonable for predominantly alluvial channel types (alluvial single thread and braided channel types), whilst there appears to be an increased tendency for sediment to deposit as overbank features during intermediate to high flow events in the bedrock influenced pool-rapid and mixed anastomosing channel types.

For all channel types, extensive deposits of fine-grained sediments from suspension during the recession of large flood events have been noted. This material forms cohesive deposits along the sides of the macro-channel banks and well established and vegetated bars that are elevated above the macro-channel floor. The erodability of these deposits has been addressed in chapter 3. Bedload is considered to be primarily responsible for large-scale changes in river morphology along the Sabie River, and the fluvial deposits within the active channel are constituted mainly of fine sands to fine gravels (Birkhead *et al.*, 1996).

The direct quantification of the plan areal coverage by alluvial deposits for each set of aerial photographs of the Sabie River (Table 8) (to an acceptable degree of accuracy) would require a protracted desktop study. Unfortunately, such an undertaking was beyond the scope of this project, and an indirect means was therefore used to determine the change in bar area. The net change in length of all alluvial bar features (including braid, lee, point and lateral bars) was determined for each of the cells between the available photographic records (Table 9). For example, braided cell 2 experienced a net increase in bar length per unit length of river of 0.496 over the period 1940 to 1986, whilst a net reduction of 0.049 was experienced over the period 1986 to 1996.

Relationship between bar length and area

The lengths and corresponding plan areas of all bars within representative examples of four channel types (single-thread, braided, mixed anastomosing and bedrock anastomosing) were measured using the 1944, 1974, 1986 and 1996 aerial photographs (Table 10). The bedrock anastomosing channel type was excluded from the analysis due to the difficulty in accurately differentiating between alluvial features and bedrock outcrops below the extensive closed canopy of riparian vegetation. This is not problematic, however, since analyses of aerial photographs reveal that bedrock anastomosing channel types have remained relatively stable in terms of dynamic sediment storage (Table 9).

Figure 23 is a plot of bar area against bar length for 77 individual units. The data displays a non-linear relationship between bar length and area, with increased scatter concomitant with larger features. The non-linear relationship is expected and results from the fact that bars do not only develop (or erode) longitudinally (which would result in a linear relationship). Furthermore, the increased scatter with size is reasonable and reflects the increased number of determinants that potentially influence development of these features. These determinants may include for example the stabilisation and sediment trapping ability of vegetation (particularly the abundant reed species *P. maritianus*), as well as the coalescing of braid bars with macro and active channel lateral bars.

A regression analysis ($R^2 = 0.90$) gives the following significant relationship between bar length and area (the probability (p) that R^2 is not significantly different from zero is 0.001):

$$A = 1.356\ l^{1.54} \qquad 29$$

where

A is the bar area (m^2)

l is the bar length (m)

The value of the power coefficient in equation 29 (1.54) is reasonable and expected to lie in the range 1 to 2. If bars developed only longitudinally the power would be unity, whereas if the units developed concentrically then the length (diameter) would be raised to the power 2. No distinct differentiation in the plotting positions and hence relationships for the different bar types are evident, and the single relationship (equation 29) for all types is appropriate.

Table 9 Net change in length of alluvial bars between records for the cells along the Sabie River (ST -Single-thread; BR - Braided; BA - Bedrock anastomosing; PR - Pool-rapid; MA - Mixed anastomosing; * - first aerial photographic record)

Cell no.	Channel type	Net change in bar length per unit length of river (10^{-2})						
		1940	1944	1965	1974	1977	1986	1996
1	ST	*					0.0	0.5
2	BR	*					49.6	-4.9
3	PR	*					5.7	-14.3
4	BR	*					46.7	-16.7
5	PR	*					0.0	-6.7
6	BR	*					23.3	-26.7
7	BA	*					2.3	0.0
8	BR	*					15.3	1.2
9	BA	*					2.3	9.2
10	PR	*					14.3	-8.6
11	BR	*					12.2	-6.1
12	BA	*					8.0	0.0
13	PR	*					17.0	-3.3
14	BR	*	8.6		5.7		20.7	2.9
15	PR	*	0.0		2.1		14.3	11.4
16	BA		*		3.8		0.0	0.0
17	PR		*		-1.7		13.1	3.8
18	BA		*		0.0		3.4	0.0
19	PR		*		13.1		20.6	11.3
20	BA		*				0.0	5.7
21	ST		*				13.8	0.0
22	BA		*				0.0	-1.4
23	PR		*				13.3	-5.8
24	BR		*		0.6		25.9	-9.4
25	PR		*		7.3		22.3	-20.8
26	BA		*		0.0		3.4	1.8
27	PR		*		-1.4		12.0	-1.4
28	BR		*		1.7		28.3	6.7
29	PR		*		0.0		14.7	0.6
30	MA		*		1.3		0.0	23.8
31	BR		*		5.0		34.2	-10.8
32	MA		*		1.3		2.0	5.0
33	PR		*		5.0		3.8	1.5
34	MA		*		5.4		7.6	1.4
35	BR		*		5.3		21.3	-2.7
36	MA	*			1.0		15.0	-4.8
37	BR	*				22.2	20.0	4.8
38	PR	*				0.5	5.6	-0.7
39	MA	*				1.3	12.3	0.2
40	BA			*		0.0	0.0	1.5

Table 10 Representative channel type bar data

Channel type	Cell no.	Length of river analysed (m)	No. of bars analysed			
			Braided	Lateral	Point	Lee
Braided	28	1200	11	2	1	
Pool-Rapid	29	1500	5	2		4
Single-Thread	1	1200	6	4		
	21	800	2	2		
Mixed Anastomosing	36	6360	15	20		3

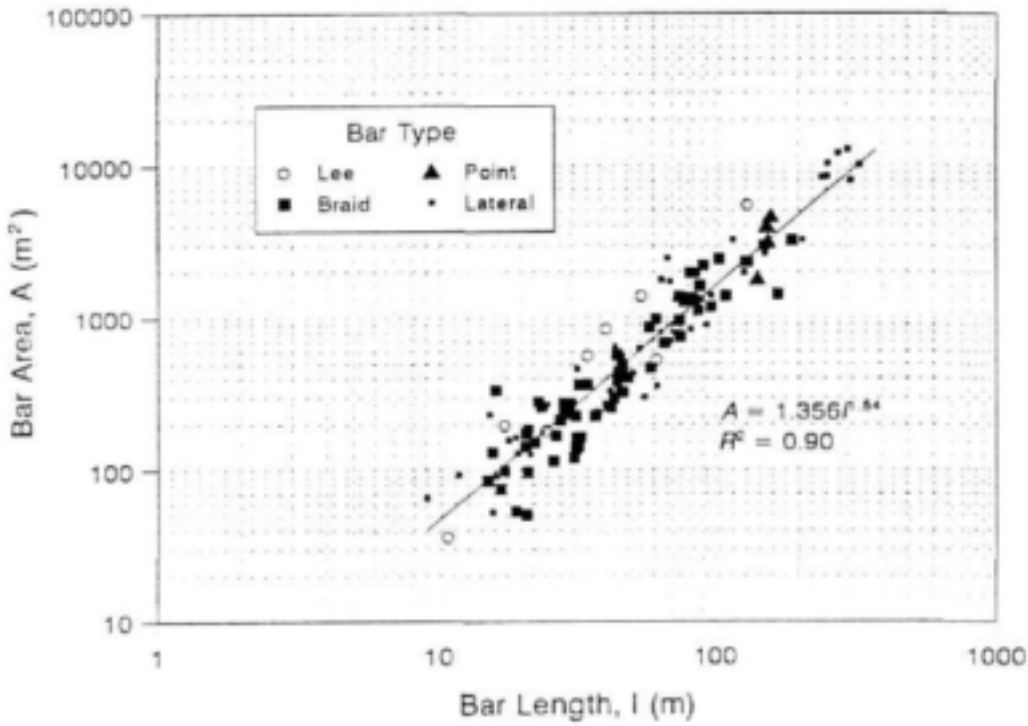

Figure 23 Relationship between bar length and area for 77 units within representative channel types along the Sabie River.

Relationship between change in bar length and change in bar area

A general relationship between the estimated change in bar area for a given change in bar length may be derived from equation 29

$$\Delta A = A_2 - A_1 = 1.356\ (l_2^{1.54} - l_1^{1.54}) \qquad 30$$

where

ΔA is the change in bar area (m^2)
A_1 is the initial bar area (m^2)
A_2 is the final bar area (m^2)
l_1 is the initial bar length (m)
l_2 is the final bar length (m)

The final bar length is given by $l_2 = l_1 + \Delta l$, and equation 30 may be written as

$$\Delta A = 1.356\ ((\Delta l + l)^{1.54} - l^{1.54}) \qquad 31$$

where
l is the initial bar length (m)

Therefore, the change in area is a function of not only the change in length, but also the initial bar length, a consequence of the non-linear relationship between these two parameters.

Figure 24 is a plot of the measured vs. predicted change in bar area using measured data between successive photographs of the representative channel types (Table 10) and applying equation 31. The line ($y = x$) representing an exact fit between measured and predicted values is also indicated. Although the non-linear relationship (equation 31) for change in bar area displays a large amount of scatter with regression coefficient $R^2 = 0.57$, it is nevertheless significant at less than the 0.001 probability level.

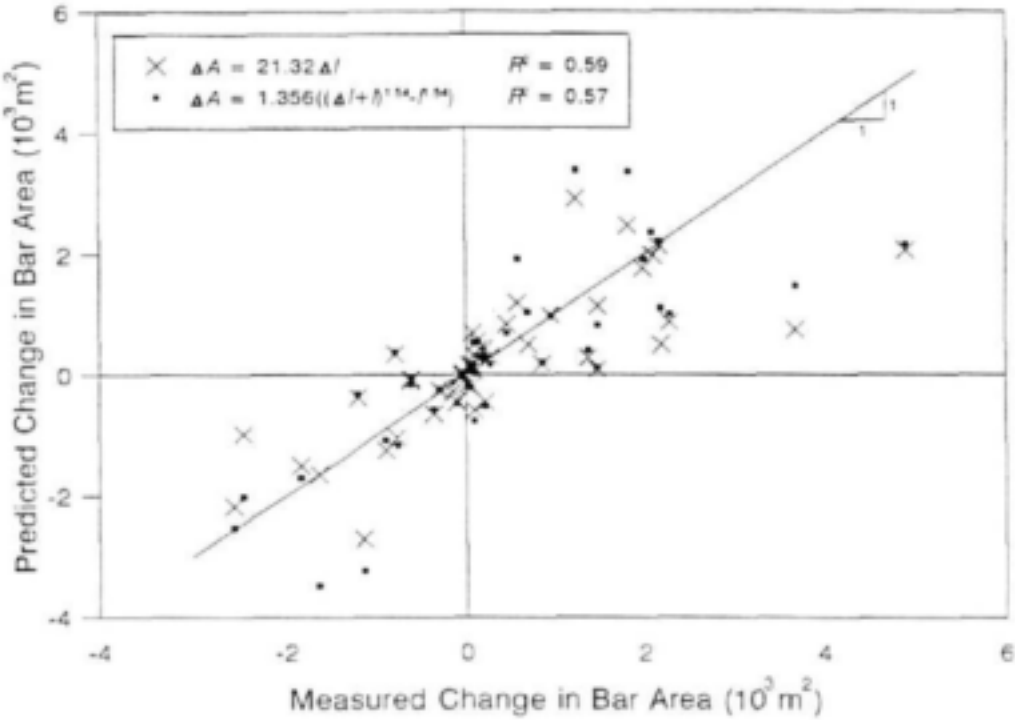

Figure 24 Measured vs predicted change in bar area using both linear regression and the non-linear equation 31.

A linear relationship ($\Delta A = 21.32\Delta l$, Fig. 24) was also fitted to the measured change in area and change in length data, and somewhat unexpectedly yields a marginally better correlation (R^2= 0.59). The inability of the non-linear equation to yield better estimates than the linear formulation is attributed to the inherent scatter in the data, as well as the smaller sample size (47 data points) against which equation 31 is plotted. The linear relationship is, however, much easier to apply to the change in length data (Table 9), since it may be applied to the net change in length rather than to individual bar units as would be required by the non-linear function. The linear relationship was consequently adopted.

The 1940 to 1986 and 1944 to 1986 records (Table 9) are used as a single data set for model calibration by determining the equivalent change over a 46 year period by applying a linear extrapolation to the 1944 to 1986 data. Figure 25 is a plot of the measured relative change in bar area per unit length of cell from 1940 to 1986. The braided channel types exhibit the highest individual (cell 2) and average rate of bar growth (5.1%), followed by the pool-rapid (2.3%) and mixed anastomosing (1.5%) channel types. The bedrock anastomosing channel types have remained relatively stable, with an average rate of accumulation of only 0.3% of the total change along the river in the KNP. Only two cells (1 and 21) have been classified as single-thread channel types, and display zero and 2.4% of the total bar growth.

The aerial photographic data (Table 9) are specified as relative change within each cell in Table 11 to reflect the proportion (length) of river occupied by each cell. For example, braided cell 2 has experienced an increase in bar area by 7.84% of the total absolute change for the river over the period 1940 to 1986, whilst a 2.94 % reduction in relative bar area has been recorded from 1986 to 1996. Since only net accumulation of bars has been recorded over the period 1940 to 1986, the sum of the change is 100% (Table 11), whilst the sum of the change from 1986 to 1996 is -14.47%, reflecting net loss of alluvial bars over the last decade. The relative changes recorded in Table 11 are plotted in Fig. 26, Fig. 27 and Fig. 28 for the periods 1940 to 1986, 1944 to 1974 and 1986 to 1996, respectively. Since the change in Table 11 is expressed as relative values between records and only partial spatial coverage is available for the 1974 data set, the overall change from 1940 to 1986 can not be equated to the sum of the change from 1944 to 1974 and 1974 to 1986.

Whereas the longer-term changes (Fig. 26) show net accumulation of alluvial bars, the shorter term changes (Fig. 27 and Fig. 28) are more variable, displaying both accumulation and reduction of alluvial features. For example, mixed anastomosing cell 36 displays net accumulation over the periods 1944 to 1974 and 1974 to 1986, whereas this trend is reversed over the last decade (1986 to 1996). The recent reduction in alluvial bars is ascribed to the recent extreme flood experienced in February 1996 (peak gauged at 2259 m^3/s at the Sabie-Sand River confluence, Fig. 1), which resulted in the net loss of bars along the river by 14.47% (Table 11).

5.5 Solution procedure

SEDFLO predicts the temporal change in storage for the 40 linked cells, each of which is characterised as one of the five principal channel types. The solution procedure involves a simple temporal and spatial sediment mass balance as illustrated in Fig. 29 for three linked cells over two discrete time-steps. Figure 30 is a schematic illustrating the division of the Sabie River into 40 linked cells, showing major tributaries, subcatchments and the locations of other features (e.g. restcamps, roads and railway line crossings) along the river in the KNP. The sediment yield data (Table 7) for the 56 Sabie River subcatchments (Fig. 21) and the sediment transport potential (computed according to Ackers and White, 1973) is specified as daily time series for each of the channel type cells.

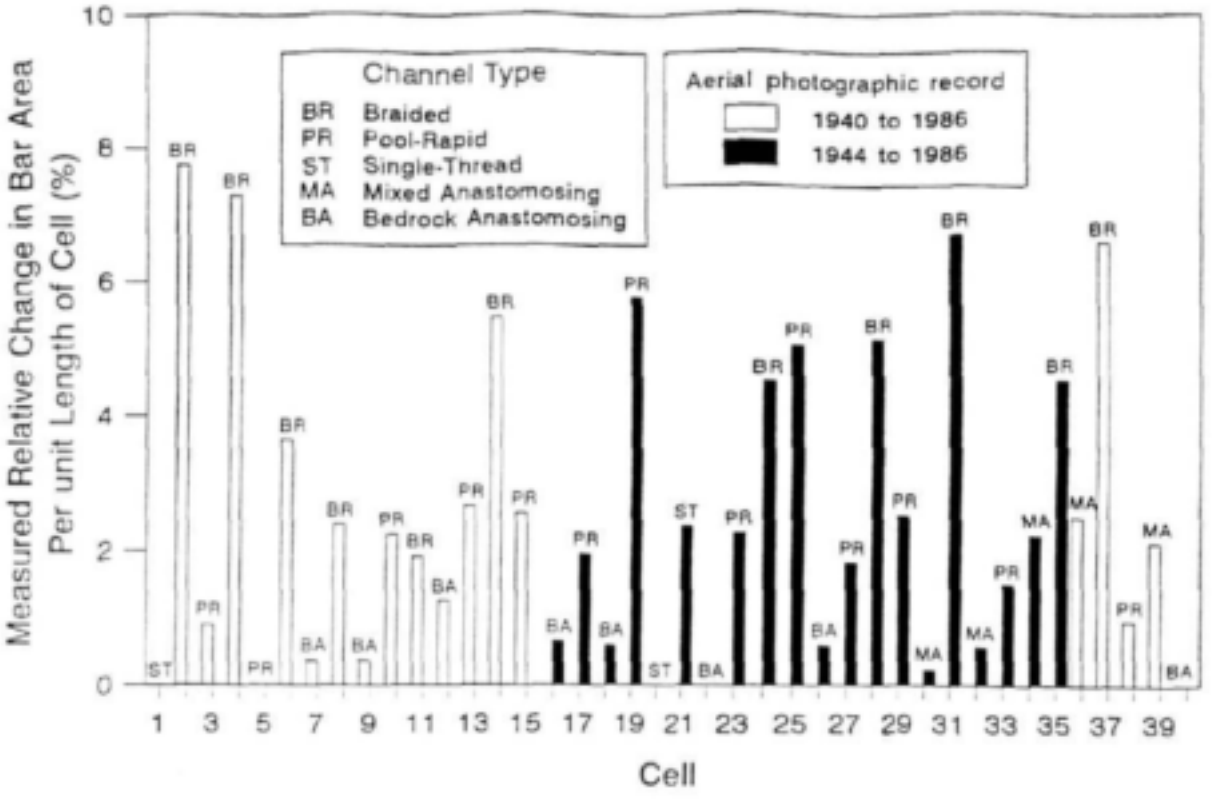

Figure 25 Change in bar area per unit length of cell as a precentage of the total change along the Sabie River (KNP), measured from the 1940/44 and 1986 aerial photographic records

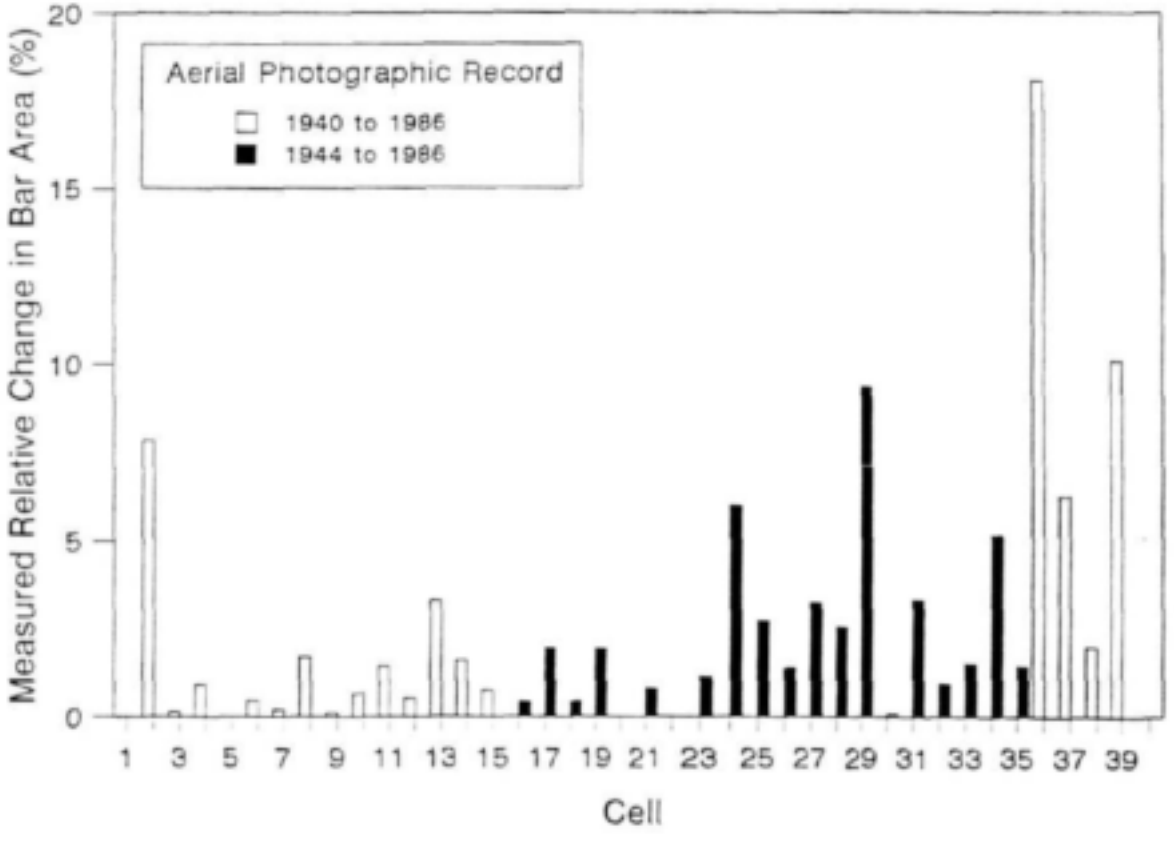

Figure 26 Change in bar area as a percentage of the total change along the Sabie River (KNP), measured from the 1940/44 and 1986 aerial photographic records

Table 11 Net relative change in area of alluvial bars between records for the cells along the Sabie River (ST -Single-thread; BR - Braided; BA - Bedrock anastomosing; PR - Pool-rapid; MA - Mixed anastomosing; * - first aerial photographic record)

Cell no.	Channel type	Net relative change in bar area (%)			
		1940 to 1986	1944 to 1974	1974 to 1986	1986 to 1996
1	ST	0.00			7.99
2	BR	7.84			-2.94
3	PR	0.13			-1.23
4	BR	0.90			-1.23
5	PR	0.00			-0.49
6	BR	0.45			-1.96
7	BA	0.19			0.00
8	BR	1.68			0.50
9	BA	0.10			1.47
10	PR	0.65			-1.48
11	BR	1.42			-2.69
12	BA	0.52			0.00
13	PR	3.29			-2.43
14	BR	1.58	3.28	1.80	0.50
15	PR	0.74	1.21	1.24	1.96
16	BA	0.43	5.00	0.00	0.00
17	PR	1.93	-3.36	3.90	2.23
18	BA	0.42	0.00	0.74	0.00
19	PR	1.90	8.62	2.04	2.22
20	BA	0.00			1.96
21	ST	0.78			0.00
22	BA	0.00			-0.50
23	PR	1.13			-1.71
24	BR	5.99	1.58	10.27	-7.37
25	PR	2.72	7.81	3.59	-6.63
26	BA	1.37	0.00	2.40	2.51
27	PR	3.22	-4.95	6.40	-1.48
28	BR	2.54	1.68	4.21	1.97
29	PR	9.35	0.00	16.40	1.32
30	MA	0.07	0.86	0.00	4.67
31	BR	3.32	4.94	5.09	-3.18
32	MA	0.93	4.28	0.99	4.90
33	PR	1.49	9.87	1.13	0.88
34	MA	5.14	24.88	5.28	1.92
35	BR	1.41	3.27	1.98	-0.50
36	MA	18.06	14.40	32.54	-20.58
37	BR	6.26			2.71
38	PR	1.97			-0.86
39	MA	10.09			0.56
40	BA	0.00			2.50
Sum		100.00	83.38	100.00	-14.47

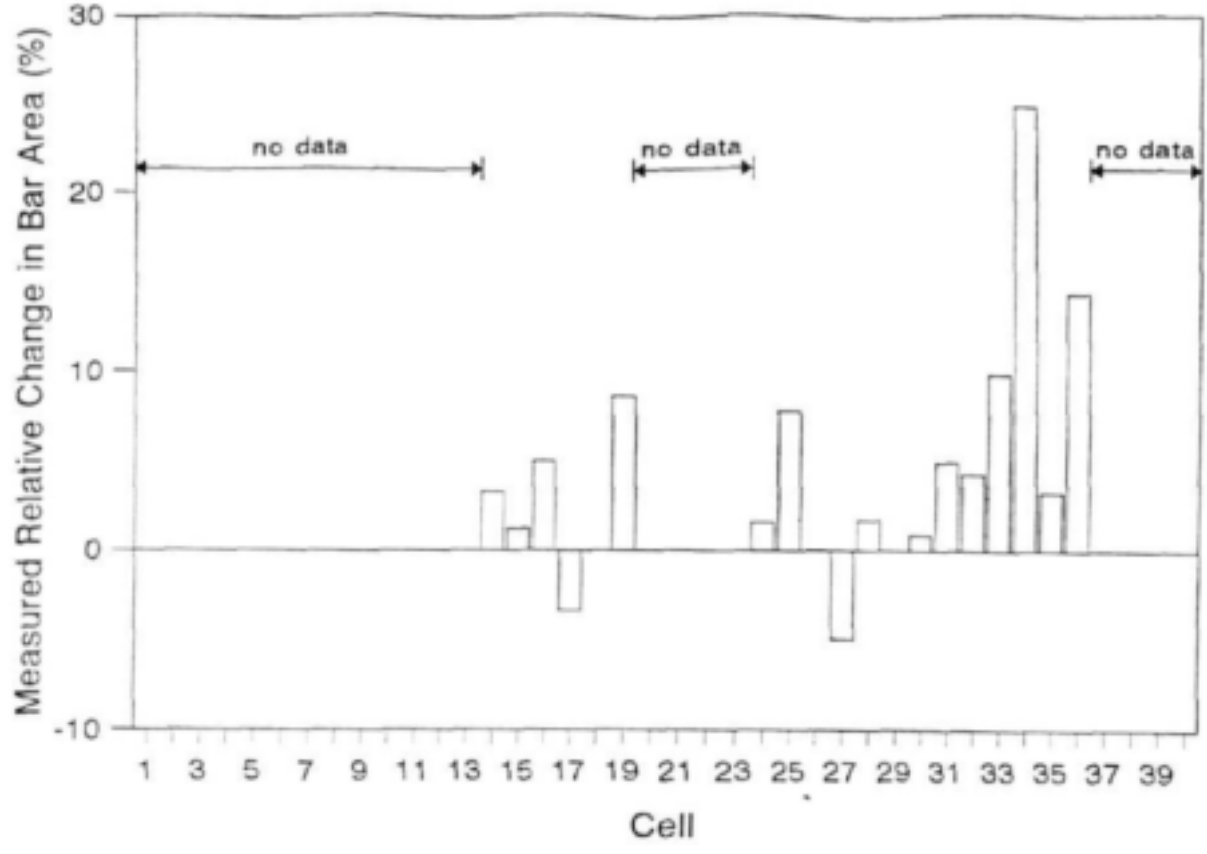

Figure 27 Change in bar area as a percentage of the total change along the Sabie River (KNP), measured from the 1944 and 1974 aerial photographic records.

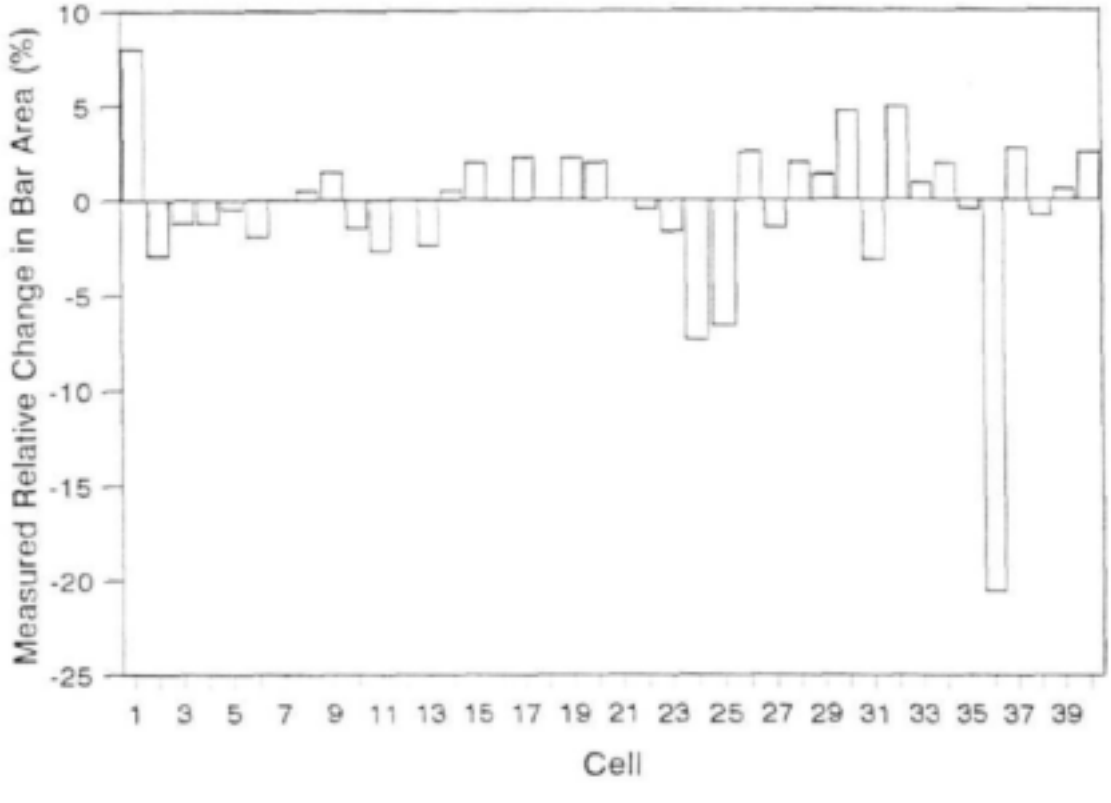

Figure 28 Change in bar area as a percentage of the total change along the Sabie River (KNP), measured from the 1986 and 1996 aerial photographic records.

5.5.1 Time series of sediment yields

The yield time series for the subcatchments of the Sabie-Sand River system have been converted into river cell equivalents by aggregating those subcatchments comprising the major tributaries (Table 12). For those cells where inputs from the adjacent catchment are from a number of minor tributaries (subcatchments 38, 42, 44, 45, 48, 50, 52 and 56), the yields were proportioned according to the relative sizes of the rivers. The modelled runoff from each of the subcatchments (specified in millimetres per day) was also converted to an equivalent average volumetric discharge rate (m^3/s) for each river cell. As discussed previously, no account was taken of the temporal sediment storage within the tributaries feeding into the Sabie River (i.e. sediment is not routed along the influent tributaries). This is likely to result in considerable overestimates in the sediment delivery (assuming that the dynamic sedimentation patterns within the tributaries are comparable to the net measured sedimentation along the Sabie River (Table 11)), and emphasizes the importance of differentiating between sediment yield and delivery, where sediment delivery is the discharge at a location along the river channel and takes account of the intermediate storage within the upstream channel network.

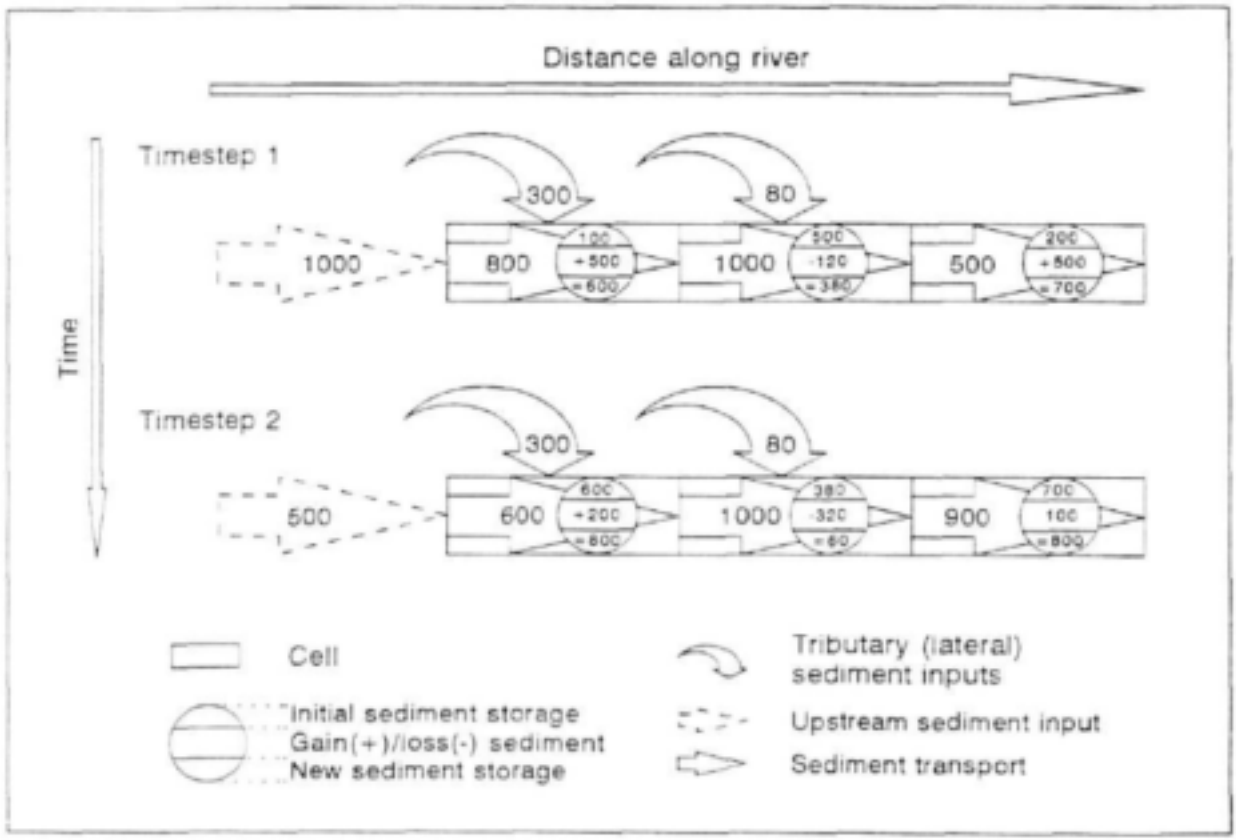

Figure 29 Sediment mass balance for three linked cells over two discrete time steps (after Heritage *et al.*, 1997a).

5.5.2 Time series of sediment transport potential

The time series of sediment transport capacities for the river cells were computed by developing characteristic transport potential relationships (as tabulated data) for each of the channel type cells. The daily flow time series were then used to interrogate these data and compute the potential sediment transport time series.

Table 12 Tributaries corresponding to ACRU subcatchments

Tributary/Input	ACRU Subcatchments
Sabie River at Albasini Ruins	18 to 35
Phabeni River	36 & 37
Mtshawu River	41
Saringwa River	39 & 40
Nwaswitshaka River	43
Sand River	1 to 17
Nwatindlopfu River	46
Nwatinwambu River	47
Nwatimhiri River	49
Lubyelubye River	51
Mosehla River	54
Mnondozi River	53
Nhlowa River	55

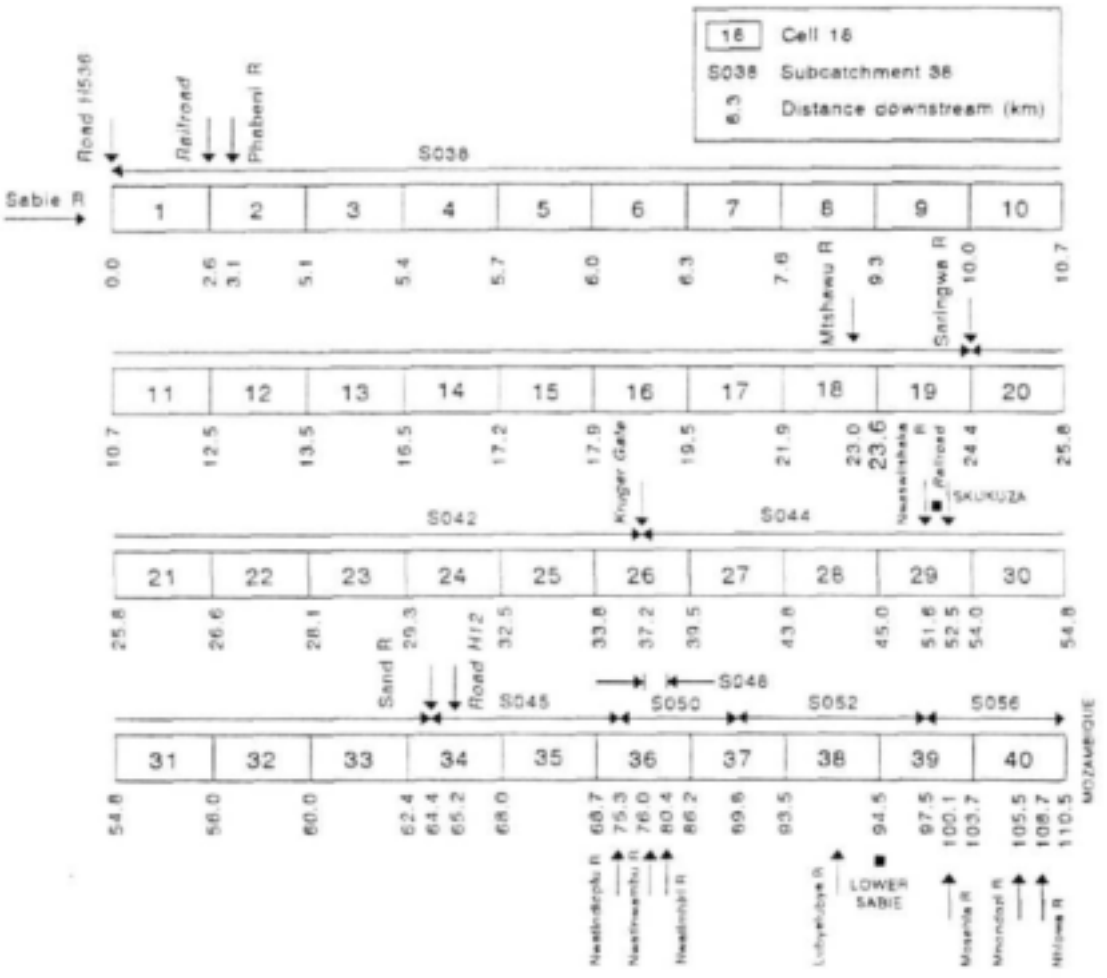

Figure 30 Division of the Sabie River into channel type cells, showing the major tributaries, subcatchments and locations of other features (e.g. restcamps, road and railway line crossings) along the River.

5.5.2.1 Sediment transport potential data

Geometric parameters

For each of the five principal channel types, three or four cross-sections from the representative channel type reaches (Figs. 15 to 19 for the single-thread, braided, pool-rapid, mixed anastomosing and bedrock anastomosing channel types, respectively) have been used to compute the cross-sectional flow areas (A) and wetted perimeters (P) corresponding to a range of flow depths (D) up to the macro-channel bank-full levels. In addition, the values of the parameter representing the *geometric* determinants in the Manning's resistance relationship were also calculated (Table 13), given by

$$Q = \frac{1}{n}\frac{A^{5/3}}{P^{2/3}}S_f^{1/2}$$

$$\therefore \quad \frac{Qn}{S_f^{1/2}} = \frac{A^{5/3}}{P^{2/3}} \qquad 32$$

where the left and right-hand terms represent groupings of the *hydraulic* and *geometric* determinants, respectively.

Table 13 Example of the geometric data computations for the cross-sections in single-thread cell 1

Flow depth D (m)	Cross-section 0.3			Cross-section 0.4		
	A (m²)	P (m)	$\frac{A^{5/3}}{P^{2/3}}$	A (m²)	P (m)	$\frac{A^{5/3}}{P^{2/3}}$
0.0	0.00	0.00	0.00	0.00	0.00	0.00
0.5	3.17	16.56	1.05	8.41	24.34	4.14
1.0	16.69	37.98	**9.65**	21.39	28.03	17.86
1.5	37.20	42.96	33.79	35.81	30.35	40.00
2.0	59.03	45.96	70.03	51.02	32.19	69.36
2.5	82.15	48.44	116.83	65.36	33.85	101.35
etc.						

Hydraulic parameters

In the same way that representative cross-sections are used for cells of the same channel type, the flow resistance relationships plotted in Fig. 14 are also considered transferable to similar channel types along the river system. Uniqueness in hydraulic behaviour (and sediment transport potential) between cells of the same channel type is introduced through the energy slope. Energy slope is considered to be synonymous with water surface slope, which assumes that the longitudinal change in velocity head ($v^2/2g$) is small and may be neglected. Water surface slopes

have been measured during low flow conditions for most of the river cells (Table 6). The low flow water surface slopes for the pool units have been applied in the pool-rapid channel type cells. Pool units are characterised by a low-flow energy gradient resulting from backing-up upstream of bedrock outcrops. Hydraulic conditions within pools are therefore critical for sediment transport analysis during low flows. Mean channel type low flow water surface slope estimates were applied where no data are available. High flow slope data were measured for the representative channel types during the extreme flood event experienced in February 1996. These data were compared to the regional channel slopes scaled off 1:50 000 topographical maps in Table 14. The average absolute error between the surveyed flood profiles and the slopes derived from aerial photographs is 23%, indicating that regional data may be used to approximate high flow water surface slopes within a reasonable level of accuracy.

Table 14 Comparison between flood water surface slopes and regional (1:50 000) slopes

Representative channel type	Water surface slopes		Flood peak discharge (m^3/s)	Error (%)
	1:50 000	Flood		
Braided	0.0017	0.0011	1705	+ 54
Pool-Rapid	0.0018	0.0020	1705	- 10
Single-Thread	0.0030	0.0029	1705	- 3
Mixed Anastomosing	0.0020	0.0023	2295	- 13
Bedrock Anastomosing	0.0057	0.0089	1705	- 36
|Average|				23

Significant changes (increases) in slope are generally encountered at bedrock anastomosing channel types. The contour intervals on the 1:50 000 topographical maps are 20 m, and the regional slopes are therefore averaged over a number of cells (Table 6). For this reason, the low-flow water surface slopes are used in the bedrock anastomosing channel type cells to provide improved estimates of the high flow energy slopes where field data are not available. For the bedrock anastomosing representative channel type cell (cell 12), the measured low flow water surface slope (0.0098) better approximates the measured flood water surface slope (0.0089) than the regional topographical channel slope (0.0057). Figure 20 is a plot of the water surface slopes categorised according to channel type. The single-thread, braided and pool-rapid channel types display large deviations between the low and high flow water surface gradients compared with the mixed anastomosing data, whilst the bedrock anastomosing channel type cells are characterised by a significantly increased mean slope.

The energy slope at a particular location along the river is a function of the local hydraulic controls, and is best determined by computing the generally non-uniform flow profile (see Birkhead *et al.*, 1995). Such hydraulic computations are impractical for the Sabie River owing to the extensive degree of bedrock control, combined with the complex cross-sectional morphologies and spatial distributions of flow resistance (sedimentological and vegetational). It

is for these reasons that representative channel type cross-sections have been applied and that a function is introduced to compute intermediate energy slopes between the measured low and high flow values. This function is given by

$$S_f = S_f^h + \frac{S_f^l - S_f^h}{1 + (0.01Q)^2} \qquad 33$$

where

S_f^h is the high flow energy slope
S_f^l is the low flow energy slope
Q is the discharge (m^3/s)

Equation 33 results in slopes that equate to the low flow slopes at zero discharges and are asymptotic to the high flow gradients at flood discharges. The energy slopes are plotted as a function of discharge rate for the representative channel types in Fig. 31. Observations of hydraulic behaviour along the Sabie River revealed that local hydraulic controls (bedrock outcrops) are generally drowned at discharges much above 200 m^3/s. The coefficients in equation 33 have therefore been selected such that the energy slopes materially equate to the high flow slopes at this discharge.

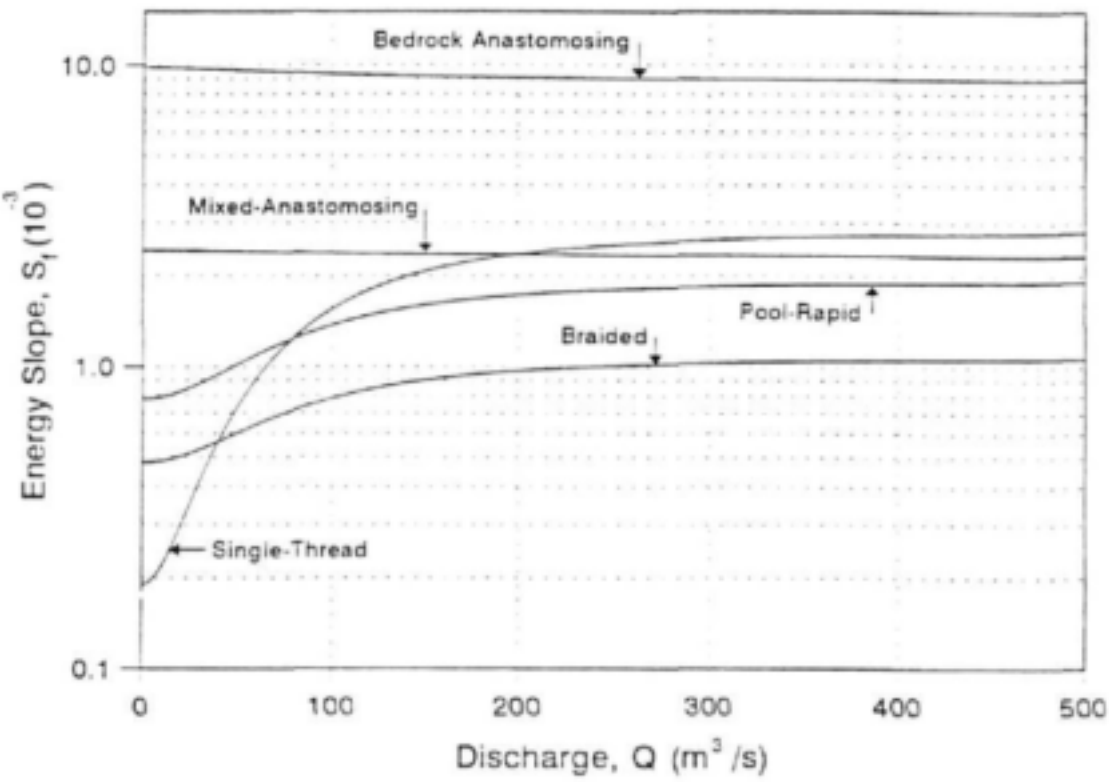

Figure 31 Plot of energy slopes as a function of discharge for the representative channel types.

For each of the cells, the flow resistance coefficient (n), energy slope (S_f) and a *hydraulic* parameter consisting of the hydraulic determinants in the Manning's resistance relationship (equation 32) were computed for a range of discharges (Table 15).

Rating data

The rating (i.e. stage-discharge) data for each of the cell cross-sections were obtained by determining the flow depth corresponding to a given discharge rate that has the same geometric and hydraulic parameter values, i.e. the solution of Manning's resistance relationship (equation 32). For example, the flow depth corresponding to a discharge of 2.0 m^3/s for cross-section 0.3 in cell 1 is 1.0 m (refer to Tables 13, 15 and 16). Linear interpolation is used to compute *geometric* and flow depth parameter values in Table 13. The value of applying this solution procedure is that the *geometric* parameter data need only be determined for the representative channel type cross-sections whereas the *hydraulic* parameter data are unique to each cell. This is useful, since the *hydraulic* parameter data were updated during model calibration, whereas the *geometric* data remained unchanged. Table 16 is an example of the hydraulic data that are computed for each of the representative cross-sections within each river cell.

Table 15 Example of the hydraulic data computations for single-thread cell 1

Discharge Q (m^3/s)	n	S_f	$\frac{Qn}{S_f^{1/2}}$
0.0	0.0773	0.00190	0.00
1.0	0.0773	0.00190	5.61
2.0	0.0668	0.00191	**9.67**
3.0	0.0625	0.00192	13.52
4.0	0.0583	0.00194	16.72
5.0	0.0540	0.00197	19.26
etc.			

The average boundary shear stress (τ or τ_o) is given by equation 4. The remaining tabulated hydraulic parameters are given by

$$\bar{D} = \frac{A}{W} \qquad 34$$

$$U = \frac{Q}{A} \qquad 35$$

$$u^* = \sqrt{gRS_f} = \sqrt{\tau/\rho} \qquad 36$$

Table 16 Modelled hydraulic parameters and potential sediment transport for cross-section 0.3 in the single-thread cell 1, with d = 1 mm

Discharge Q (m³/s)	**Flow depth** D (m)	**Flow depth** $\bar{D}$ (m)	**Surface width** W (m)	**Flow area** A (m²)	**Wetted perimeter** W (m)	**Mean flow velocity** U (m/s)	**Froude number** Fr	**Shear stress** τ (N/m²)	**Sediment transport** Qs (kg/s)
0	0.00	0.00	0.00	0.00	0.00	0.00	0.00	0.00	0.00
1	0.83	0.36	30.40	11.06	30.67	0.09	0.05	0.67	0.00
2	1.00	0.44	37.65	16.70	37.99	0.12	0.06	0.82	0.00
5	1.24	0.64	41.07	26.17	41.51	0.19	0.08	1.22	0.00
10	1.45	0.83	42.16	35.04	42.68	0.29	0.10	1.75	0.00
20	1.65	1.01	43.17	43.78	43.76	0.46	0.15	2.87	0.01
50	1.85	1.18	44.19	52.24	44.86	0.96	0.28	8.36	3.60
100	2.14	1.43	45.66	65.19	46.44	1.53	0.41	x.28	22.01
200	2.71	1.90	48.57	92.11	49.57	2.17	0.56	42.98	71.76
500	4.54	2.58	76.65	197.79	78.19	2.53	0.50	69.38	179.43
1000	6.44	3.87	93.70	362.51	95.73	2.76	0.45	106.74	280.19
2000	9.95	5.74	132.57	756.80	135.83	2.64	0.35	158.14	348.31

$$R = \frac{A}{P} \quad 37$$

$$Fr = \frac{U}{\sqrt{gD}} \quad 38$$

where

$\bar{D}$	is the average flow depth (m)
W	is the surface flow width (m)
R	is the hydraulic radius (m)
ρ	is the water density (kg/m^3)
Fr	is the Froude number

The average flow depth ($\bar{D}$) rather than the maximum flow depth (D) was used to compute the sediment transport (equation 19), since this is a more appropriate measure of the effective flow depth within the generally complex cross-sectional profiles (Figs. 15 to 19). The potential rate of sediment transport was computed according to the Ackers and White (1973) methodology described in 5.3.2. The effective sediment discharge for a cell is the lowest occurring at any position within the cell. Therefore, the lowest predicted value based on the representative cross-sections within a cell was used to compute the time series of potential sediment transport.

5.6 Model calibration

The need to calibrate SEDFLO arises from the uncertainty inherent in both the modelled sediment yields and potential transport values. As discussed previously, observed sediment yield and transport data through reservoir surveys and streamflow sampling are not available for the Sabie River catchment. Moreover, sediment transport rates are difficult to measure directly in this semi-arid environment where temporal and spatial variation at a river cross-section means that direct point sampling of mobile sediment is likely to bear little resemblance to mean transport volumes (Moon *et al.*, 1997). For these reasons, the yield estimates and sediment transport values are calibrated using the historical data from analyses of the aerial photographs.

5.6.1 Critical analyses of modelled inputs

5.6.1.1 Sediment transport

Analysis of the grain size distributions of sediment samples from active channel features along the Sabie River yields a median grain size (d_{50}) of 1 mm. This size is used to characterise the alluvial material responsible for changes in sediment storage as determined by bar dynamics, and is applied in the potential transport analysis.

Figure 32 is a plot of the long-term (1940 to 1986) bulk potential sediment transport (Qs_{pot}) against runoff volume (Q) for the 40 cells along the Sabie River computed using the Ackers and White (1973) methodology. The increase in runoff from 22×10^6 m^3 to 35×10^6 m^3 corresponds to

Sand River inflow over the period 1940 to 1986 ($13x10^9$ m^3). The data display a large amount of scatter, with no unique spatial relationship along the river for the cell data. The cell data are differentiated based on channel types, and simple power relationships have been fitted. The distinction between channel types reflects the representative channel type flow resistance and geometric data used in the computations. The scatter within the data for each channel type reflects different energy slopes, which are unique to the cells, with the exception of data derived using mean low flow slopes. Although the scaling coefficients vary considerably (0.028 to 0.192), the power coefficients are less variable, ranging from 0.708 to 1.021 for the mixed anastomosing and braided/single-thread channel types, respectively. This implies that the functional relationship between sediment discharge and flow is consistent across channel types over the long-term. It is interesting to note that the highest potential sediment transport is for alluvial single thread and braided channel types, whereas the lowest bulk transport is for the bedrock anastomosing channel type. This implies that the alluvial channel types will generally erode, whilst the bedrock dominated channel types will generally deposit. This is not supported by data derived from photographic records (Fig. 25), which reveals net sedimentation in the alluvial channel types and relative stability within the bedrock anastomosing cells.

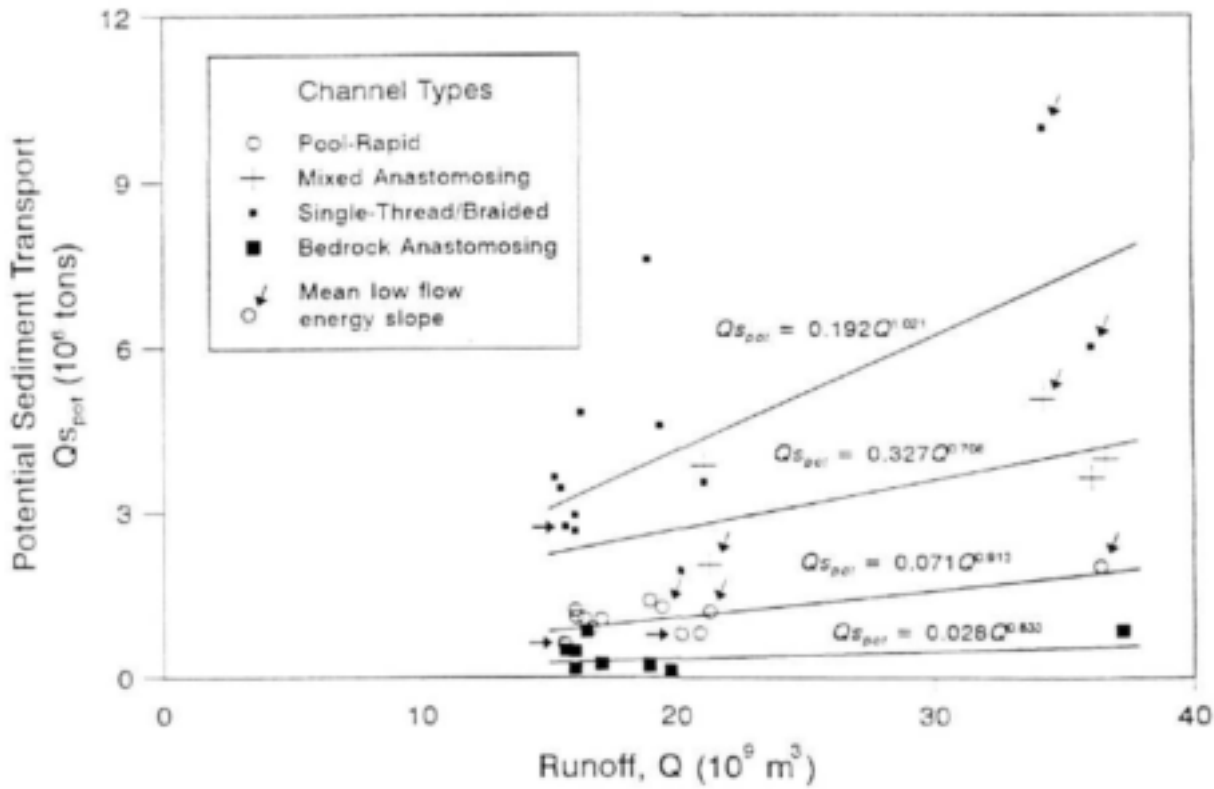

Figure 32 Runoff vs potential sediment transport for each of the 40 cells along the Sabie River over the period 1940 to 1986.

The predictive accuracy of sediment transport models (refer to 5.3.1) varies considerably. Furthermore, these models have been derived using flume data and observations from alluvial rivers and therefore their applicability within bedrock and vegetation influenced systems such as the Sabie River is highly questionable. Assuming a general functional relationship between long-term sediment discharge and runoff for the extent of the river (and that it is suitably predicted by

the transport model), scaling factors may be determined that will result in the minimum deviation between the channel type relationships (Fig. 32) and a unique long-term bulk sediment transport runoff relationship (independent of channel type). Scaling factors for the channel type data in Fig. 32 are given in Table 17, and were determined by calculating the ratio of the average area under the channel type power relationships (60.9×10^{15} tons.m^3) to the individual areas, over the volumetric runoff range 15×10^9 to 38×10^9 m^3. For example, the scaling factor (0.486) for the braided/single-thread channel type is given by the ratio of the average area under all channel type relationships (60.9×10^{15}) to the actual area under the braided/single-thread curve (125.4×10^{15})

Table 17 Channel type scaling factors applied to sediment transport data (Fig. 32)

Channel type	Area under curve (10^{15} tons m^3)	Scaling factor
Braided/Single-thread	125.4	0.486
Mixed anastomosing	76.0	0.801
Pool rapid	32.5	1.878
Bedrock anastomosing	9.8	6.200

Applying the scaling factors in Table 17, a more realistic long-term sediment discharge function is developed for the extent of the river (Fig. 33), and is given by

$$Qs_{pot} = 0.132Q^{0.916} \qquad 39$$

with Qs_{pot} in 10^6 tons and Q in 10^9 m^3.

The parameter value of the power coefficient (0.916) is reasonable, since if the power deviated significantly from unity, then the reduced (power < 1) or elevated (power > 1) transport potential downstream of influent tributaries must be concomitant with a major change in channel geometry and/or energy slope. No such morphological adjustments or changes in water surface slopes are, however, apparent downstream of major tributaries along the length of the Sabie River in the KNP.

5.6.1.2 Sediment yields

Figure 34 is a plot of the modelled mean annual runoff and sediment yields along the length of the Sabie River in the KNP for the period 1940 to 1986. The inputs from the Sabie River upstream of Albasini Ruins, the Saringwa River, the Sand River, and smaller tributaries are indicated. The disproportionately large modelled inputs from the Sand and Saringwa Rivers, relative to the corresponding increases in runoff, are apparent.

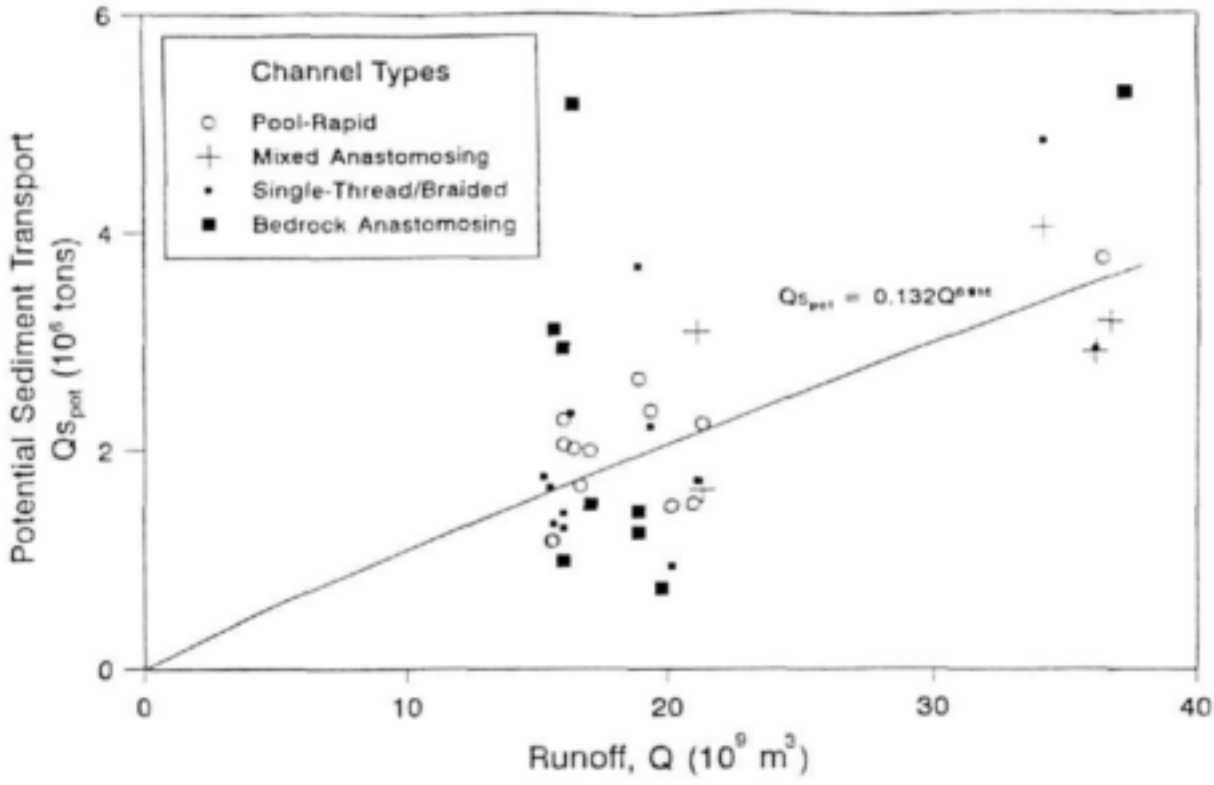

Figure 33 Runoff vs potential sediment transport factored according to channel type for each of the 40 cells over the period 1940 to 1986

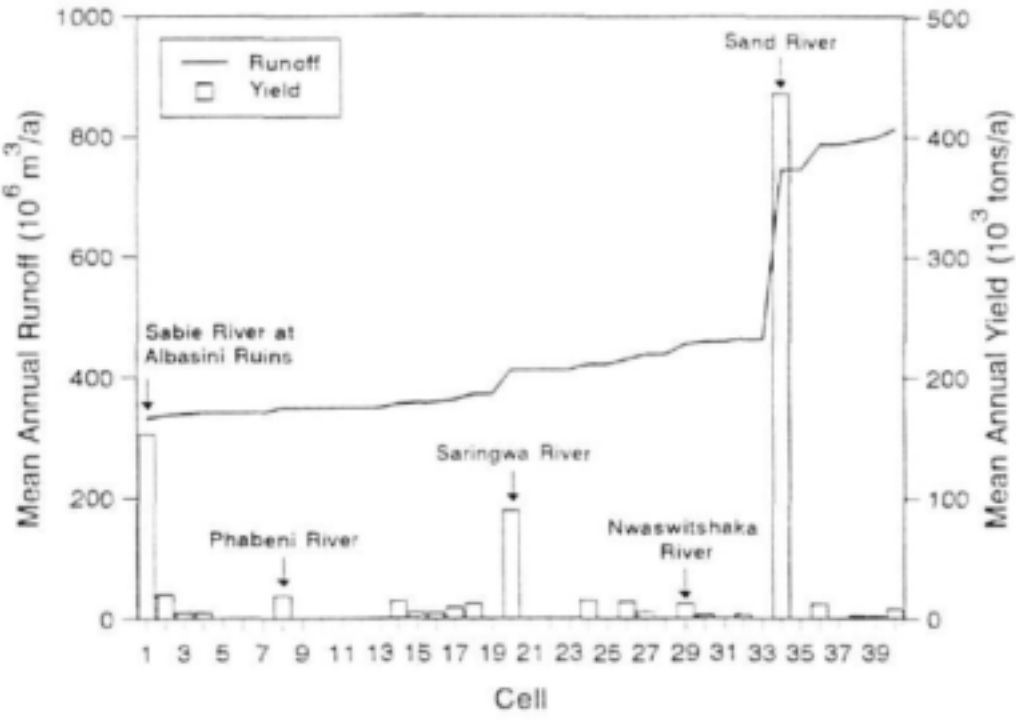

Figure 34 Mean annual runoff and sediment yields from the tributaries along the Sabie River in the KNP

5.6.2 Model calibration using historical data

Based on the mean annual sediment yields over the period 1940 to 1986 (Fig. 34), and the relative changes in sediment storage derived from historical aerial photographic data (Table 9, 1940 to 1986), there exists a unique solution for sediment transport for each of the cells along the river. The derivation of this solution follows.

The sediment mass balance (or conservation of mass) for each cell along the river is given by

$$\Delta S_i = I_i - O_i \qquad 40$$

where
i is the cell index
ΔS_i is the change in storage for the i^{th} cell
I_i is the inflow to the i^{th} cell
O_i is the outflow from the i^{th} cell

Equation 40 may be written as

$$\Delta S_i = Y_i + Qs_{i-1} - Qs_i \qquad 41$$

where
Y_i is the catchment sediment yield to the i^{th} cell
Qs_i is the sediment outflow from the i^{th} cell

The relative change in sedimentation is given by

$$\Delta S_i^* = \frac{\Delta S_i}{\sum_{j=1}^{n} \Delta S_j} \qquad 42$$

where
ΔS_i^* is the relative change in storage for the i^{th} cell
j is the cell index
n is the index for the most downstream cell

and the total change in absolute sedimentation along the river is given by

$$\sum_{j=1}^{n} \Delta S_j = \sum_{j=1}^{n} Y_j - Qs_n \qquad 43$$

Combining equations 41, 42 and 43 with all the unknowns on the left hand side of the equality sign gives the following relationship for the sediment outflow as a function of the catchment yields and the relative change in sedimentation along the river

$$-Qs_{i-1} + Qs_i - \Delta S_i^* Qs_n = Y_i - \Delta S_i^* \sum_{j=1}^{n} Y_j \qquad 44$$

It is convenient to write equation 44 in the form

$$AQs = B \qquad 45$$

where

A is the two-dimensional array of coefficients
Qs is the one-dimensional array of sediment discharge
B is the one-dimensional array of constants

and are given by

$$\begin{pmatrix} 1 & & & & & & \Delta S_1^* \\ -1 & 1 & & & & & \Delta S_2^* \\ & \ddots & \ddots & & & & \vdots \\ & & -1 & 1 & & & \Delta S_i^* \\ & & & \ddots & \ddots & & \vdots \\ & & & & -1 & 1 & \Delta S_{n-1}^* \\ & & & & & -1 & 1-\Delta S_n^* \end{pmatrix} \begin{pmatrix} Qs_1 \\ Qs_2 \\ \vdots \\ Qs_i \\ \vdots \\ Qs_{n-1} \\ Qs_n \end{pmatrix} = \begin{pmatrix} Y_1 - \Delta S_1^* \sum_{j=1}^{n} Y_j \\ Y_2 - \Delta S_2^* \sum_{j=1}^{n} Y_j \\ \vdots \\ Y_i - \Delta S_i^* \sum_{j=1}^{n} Y_j \\ \vdots \\ Y_{n-1} - \Delta S_{n-1}^* \sum_{j=1}^{n} Y_j \\ Y_n - \Delta S_n^* \sum_{j=1}^{n} Y_j \end{pmatrix} \qquad 46$$

Various methods of solution are available for solving a set of simultaneous equations such as represented by equation 45, including both iterative and direct solution procedures. Iterative methods are generally incorporated into solution procedures to alleviate the necessity of solving large systems of simultaneous equations. The direct solution technique LU decomposition with forward and backward-substitution as discussed by Press *et al.* (1989) is used to solve equation 45. The method utilises Crout's algorithm with partial and implicit pivoting to decompose the array of coefficients into lower and upper triangular systems. A routine for forward and backsubstitution is implemented on the LU decomposed array of coefficients (A) and the array of constants (B), to return the solution of the sediment outputs (Qs) from each cell.

Figure 35 is a plot of the computed bulk sediment transport against runoff for each of the 40 cells along the Sabie River over the period 1940 to 1986 using the above solution procedure. The cells corresponding to the Sabie River at Albasini Ruins (cell 1) as well as the Saringwa (cell 20) and Sand River (cell 34) tributaries are indicated. A simple power relationship has been fitted to the data, yielding a power coefficient value of 1.748. The relationship is sensitive to the relative yields predicted for the Sabie River at Albasini Ruins, the Saringwa and Sand River tributaries. This value exceeds that obtained for the bulk potential transport analysis (0.916, Fig. 33), and results from the disproportionately large modelled yields from the Sand and Saringwa Rivers, relative to the corresponding increases in runoff. The implications of a power coefficient value that deviates substantially from unity have been discussed. Due to the uncertainty inherent in the sediment yield predictions (Table 7), a relationship between bulk sediment transport and runoff with the power coefficient value derived from the potential transport analysis, is considered a more realistic representation. The fitted relationship is therefore given by

$$Qs = 1.071Q^{0.916} \qquad 47$$

Calibrated yields for the cells with sediment inputs from the catchment were determined by applying equation 47, and are given in Table 18 and plotted in Fig. 36 together with the yields modelled using CALSITE/ACRU. As expected (from the difference between the assumed power relationship and uncalibrated yield point data (Fig. 35)), the Sabie River input increases (by a factor of 1.85), whereas the yields from both the Saringwa and Sand River are reduced (by 0.35 and 0.49, respectively). The net change introduced by calibration of the yields (Table 18) is a reduction by only 20%, from 845.3×10^3 tons/annum to 685.7×10^3 tons/annum over the period 1940 to 1986.

Using the calibrated yields (Table 18) sediment discharges through each of the linked cells, based on the measured relative change in sediment storage (Table 11), were computed (Table 19). These discharges represent the total fluxes through the river system (i.e. the sum of the bed material and wash load, where the wash load is the fine-grained fraction of the suspended load which is transported through the system). The proportion of the total catchment yield represented by the 1 mm grain size is determined by the scaling factor between the sediment discharge runoff relationships (Figs. 33 and 35), and is 12.3% (0.132/1.071). It is reassuring to note that this is comparable to the 10% applied by Heritage *et al.* (1997a), based on approximate analyses of relative grain size distributions of samples extracted from the catchment and active channel features along the Sabie River. The average annual change in sediment storage (10^3 tons/annum) of the representative grain size (d = 1 mm), and the relative changes are also given in Table 19 (cf. historical data for the period 1940 to 1986 in Table 11).

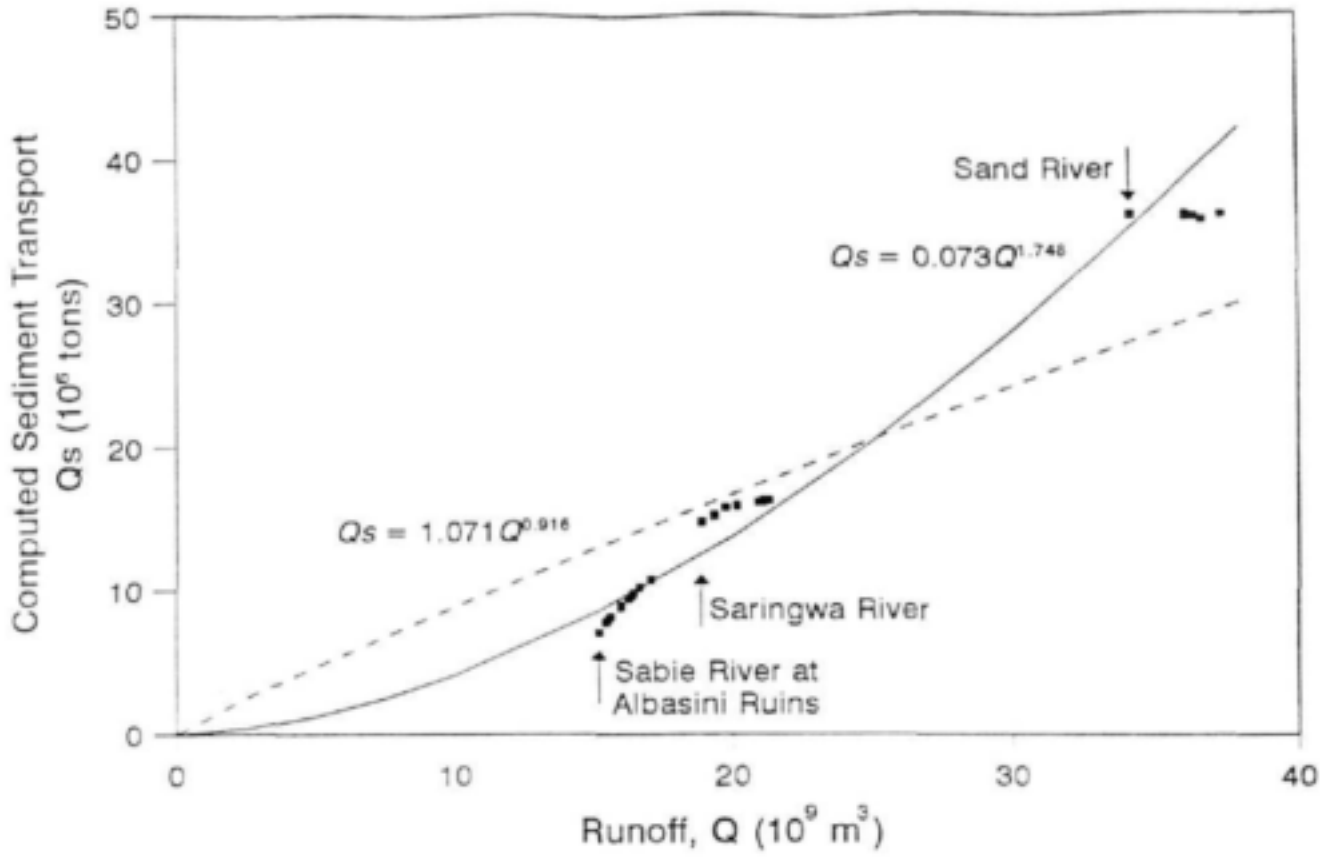

Figure 35 Computed sediment transport as a function of runoff for each of the 40 cells over the period 1940 to 1986.

The calibrated sediment discharge and storage data imply that the long-term changes in sediment storage are small compared with the total sediment flux through the river system (Table 19). The average annual sediment accumulation along the Sabie River (1940 to 1986) is $3.3x10^3$ tonxbetween Albasini Ruins and the Sand River confluence (62.4 km), and $2.4x10^3$ tons downstream of the confluence (48.1 km). The average annual sediment load ranges from $34.8x10^3$ to $46.8x10^3$ tons for the upper reach, rising to $78.8x10^3$ tons at the Mozambique border. Therefore, the change in storage of the representative grain size accounts for only 7% and 3% of the transported material upstream and downstream of the Sand River confluence, respectively. This is a reasonable finding, since in order for the river system to be displaying net alluviation along its length (Fig. 25) without any marked increases in sedimentation immediately downstream of tributary inputs, the system must be transporting a load greater than the changes in storage. It is interesting to note that the predicted changes in storage per unit length of river downstream of the Sand River confluence (50 tons/km/annum) are comparable to those upstream (52 tons/km/annum), although the predicted sediment load (and runoff) doubles downstream of the confluence.

Table 18 Calibrated mean annual yields for the period 1940 to 1986

Cell and main tributaries		Mean annual yields (10^3 tons/a)		Factor
		ACRU/ CALSITE	Calibrated	
1	Sabie River at Albasini Ruins	152.7	282.6	1.85
2	Phabeni River	19.9	8.9	0.45
3		4.7	1.5	0.31
4		4.7	2.2	0.47
8		18.8	7.2	0.38
14		14.0	5.7	0.41
15		4.7	2.0	0.43
16		4.7	1.6	0.34
17		9.3	4.4	0.47
18	Mtshawu River	12.6	7.0	0.56
20	Saringwa River	89.4	30.7	0.34
24		15.0	11.0	0.73
26		13.7	7.5	0.55
27		5.3	8.4	1.58
29	Nwaswitshaka River	12.0	18.3	1.52
30		2.6	2.9	1.10
32		2.6	3.8	1.42
34	Sand River	435.9	212.7	0.49
36	Nwatinlopfu, Nwatinwambu, Nwatinhiri Rivers	11.8	41.3	3.50
38	Lubyelubye River	2.1	5.6	2.64
39	Mosehla River	1.5	10.3	7.00
40	Mnondozi, Nhlowa Rivers	7.3	10.1	1.38
Sum		**845.3**	**685.7**	**0.80**

A general long-term transport relationship (independent of channel type) has been applied to calibrate the model (Fig. 33). To achieve this, the cell based energy slopes are calibrated and a single slope value is applied in the sediment transport model. The rationale for using a single slope rather than low and high flow slopes as applied originally (Fig. 31 and equation 33) arises from the need to keep the number of calibrated determinants to a minimum. This is understandably at the expense of a more realistic representation that cannot be uniquely parameterised, however. The calibrated energy slopes are given in Table 20 and plotted in Fig. 20. The calibrated slopes generally fall within the range of measured slopes, as expected.

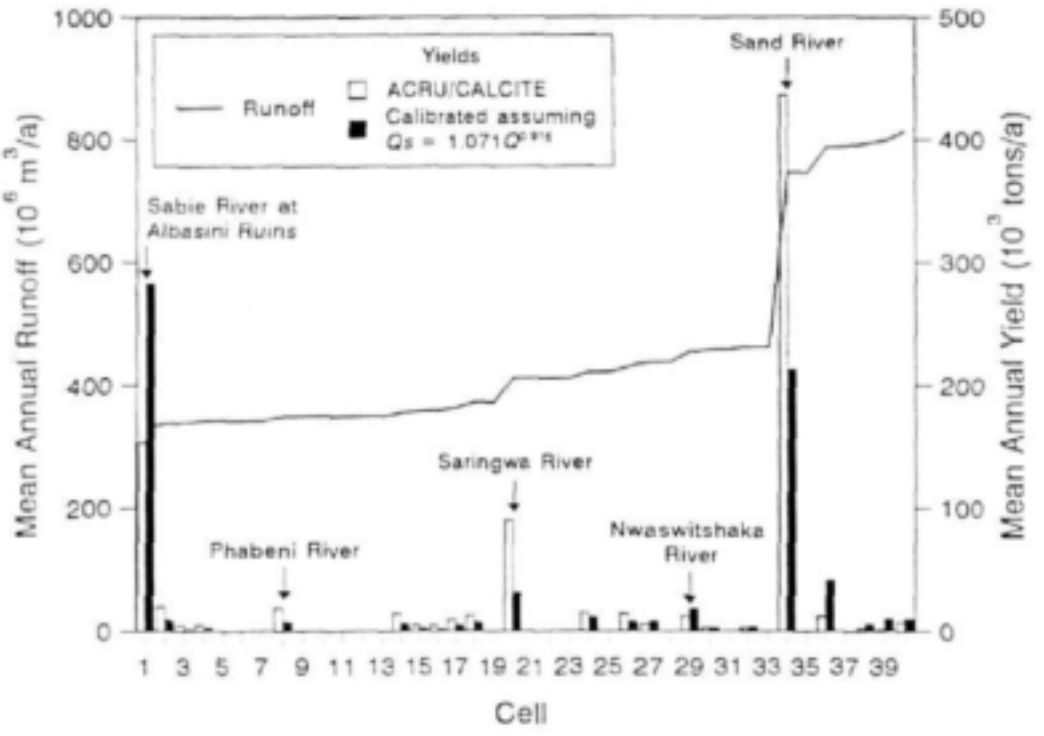

Figure 36 Mean annual runoff and sediment yields calibrated applying a power relationship (equation 47) between long-term sediment discharge and runoff

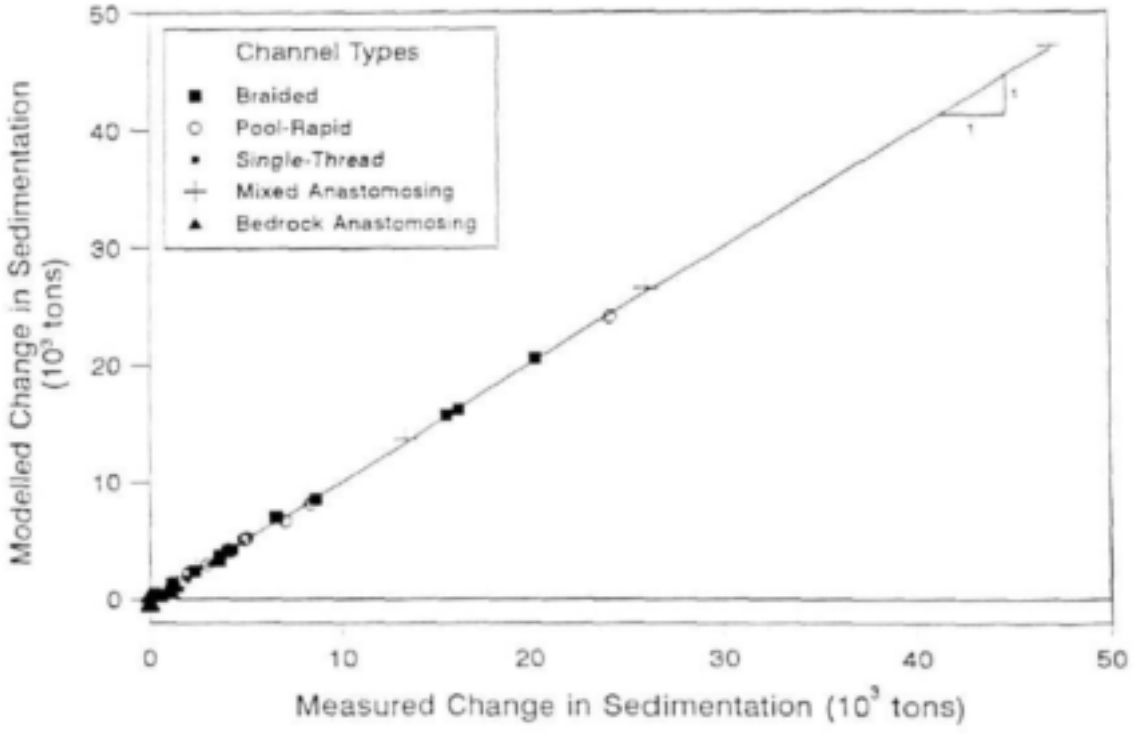

Figure 37 Calibration of the cell based energy slope to produce agreement between modelled and measured change in sedimentation from aerial photographs for the period 1940 to 1986

Table 19 Calibrated mean annual sediment discharge and change in cell storage for the period 1940 to 1986

Cell	Mean annual sediment discharge (10^3 tons/a)			Mean annual change in sediment storage (d = 1 mm)	
	ACRU/ CALSITE	Calibrated total load	d = 1 mm (12.3% total load)	(10^3 tons/a)	% of total
1	152.7	282.6	34.8	0.00	0.0
2	167.8	287.9	35.5	0.44	7.8
3	172.4	289.3	35.6	0.00	0.1
4	176.6	291.1	35.9	0.05	0.9
5	176.6	291.1	35.9	0.00	0.0
6	176.3	290.9	35.8	0.02	0.5
7	176.2	290.8	35.8	0.01	0.2
8	193.9	297.2	36.6	0.09	1.7
9	193.9	297.2	36.6	0.00	0.1
10	193.5	296.9	36.6	0.03	0.6
11	192.6	296.2	36.5	0.08	1.4
12	192.3	296.0	36.5	0.02	0.5
13	190.3	294.5	36.3	0.18	3.3
14	203.4	299.5	36.9	0.08	1.6
15	207.7	301.2	37.1	0.04	0.7
16	212.1	302.6	37.3	0.02	0.4
17	220.3	306.1	37.7	0.10	1.9
18	232.6	312.9	38.6	0.02	0.4
19	231.5	312.1	38.4	0.10	1.9
20	320.8	342.8	42.2	0.00	0.0
21	320.4	342.4	42.2	0.04	0.8
22	320.4	342.4	42.2	0.00	0.0
23	319.7	341.9	42.1	0.06	1.1
24	331.0	350.1	43.1	0.33	6.0
25	329.4	348.9	43.0	0.15	2.7
26	342.3	355.7	43.8	0.07	1.4
27	345.6	362.6	44.7	0.18	3.2
28	344.1	361.4	44.5	0.14	2.5
29	350.5	375.5	46.3	0.52	9.3
30	353.1	378.4	46.6	0.00	0.1
31	351.1	376.9	46.4	0.18	3.3
32	353.1	380.2	46.8	0.05	0.9
33	352.2	379.5	46.8	0.08	1.5
34	785.0	589.9	72.7	0.29	5.1
35	784.2	589.3	72.6	0.07	1.4
36	785.1	622.3	76.7	1.01	18.1
37	781.3	619.4	76.3	0.35	6.3
38	782.2	624.1	76.9	0.11	2.0
39	777.6	629.8	77.6	0.56	10.1
40	784.9	639.9	78.8	0.00	0.0
Sum				5.64	100.0

Table 20 *Calibrated energy slopes for the cells along the Sabie River (ST - Single -thread; BR - Braided; BA - Bedrock anastomosing; PR - Pool-rapid; MA - Mixed anastomosing)*

Cell	Channel Type	Calibrated energy slope
1	ST	0.00127
2	BR	0.00138
3	PR	0.00217
4	BR	0.00138
5	PR	0.00216
6	BR	0.00138
7	BA	0.00644
8	BR	0.00137
9	BA	0.00637
10	PR	0.00215
11	BR	0.00137
12	BA	0.00635
13	PR	0.00214
14	BR	0.00136
15	PR	0.00213
16	BA	0.00623
17	PR	0.00212
18	BA	0.00609
19	PR	0.00210
20	BA	0.00566
21	ST	0.00121
22	BA	0.00566
23	PR	0.00201
24	BR	0.00132
25	PR	0.00200
26	BA	0.00551
27	PR	0.00197
28	BR	0.00130
29	PR	0.00195
30	MA	0.00331
31	BR	0.00129
32	MA	0.00329
33	PR	0.00192
34	MA	0.00269
35	BR	0.00116
36	MA	0.00264
37	BR	0.00115
38	PR	0.00149
39	MA	0.00261
40	BA	0.00314

Figure 37 is a plot of the modelled change in cell sedimentation (applying the calibrated energy slopes in Table 20) against the equivalent measured change for the period 1940 to 1986. The equivalent measured change is derived from the relative percentage change data by proportioning the overall modelled change (Table 21) according to the measured cell based relative change in Table 11 (i.e. 180.3×10^3 tons = 100%).

5.7 Model verification

The change in sediment storage is computed on an annual basis by accumulating the daily sediment transport and yield values and performing a mass balance for each linked river cell. Figure 38 is a plot of the modelled annual changes in sediment storage for the period 1932 to 1996. Changes are plotted for the whole river and also for only those cells covered by the 1944 record (refer to Table 8). The modelled changes are expressed relative to the start of the simulation (1932). The measured data derived from the aerial photographic records are expressed in equivalent (mass) units and are plotted as point data. The data used to calibrate the model are coincident with the simulated values in 1986 (relative to the 1940 reference), as required. The modelled and measured (equivalent based on the 1940 to 1986 calibration) data for assessing the predictive performance is given in Table 21.

Table 21 Comparison between modelled and measured change in sediment storage along the Sabie River (**bold** : calibration data)

Period	Cells	Change in sediment storage (10^3 tons)		|Error| (10^3 tons/a)
		Modelled	Aerial photographic data	
1940/44 to 1986	All	**180.3**	**180.3**	-
	14 to 19 & 24 to 36	**142.9**	**142.9**	-
1944 to 1974	14 to 19 & 24 to 36	111.1	9.3	3.4
1974 to 1986	14 to 19 & 24 to 36	-27.9	74.3	8.5
1986 to 1996	All	-72.0	-7.4	6.5
	14 to 19 & 24 to 36	32.2	-5.4	3.7

The long-term (1940 to 1986) change in sediment storage for the extent of the river in the KNP is approximately 3.5×10^3 tons/annum. Shorter-term changes in sediment storage are significantly more variable (Fig. 38), reflecting periods of progressive sediment accumulation (e.g. 1939 to 1945, 1948 to 1957, 1960 to 1971, 1976 to 1984, 1985 to 1995), interspersed by significant reductions during years experiencing large flow events. The average increase in sediment storage during periods of progressive accumulation is as high as 40×10^3 tons/annum, while the loss of sediment (as reflected by the reduction in unconsolidated alluvial bars) during years experiencing large floods is generally greater than 200×10^3 tons (approximately 300×10^3 tons for the recent flood in 1996). It is difficult to objectively assess the performance of the model as reflected by

the error in sediment storage given in Table 21, with values ranging from $3.4x10^3$ to $8.5x10^3$ tons/annum for the interpolated and extrapolated 1974 and 1996 data points, respectively. This is due to the large temporal variability resulting primarily from the influence of extreme flows, for example, although the maximum error in storage prediction ($8.5x10^3$ tons/annum) represents more than twice the long term average accumulation, it is only 3% of the sediment removed from storage during the 1996 flood. Nevertheless, the predicted and measured data for 1996 compare well, with the modelled trend showing a progressive accumulation from 1985 to 1995 (Fig. 38), followed by an abrupt loss of storage in 1996. The existing (long-term) aerial photographic data, however, reveal only a minor loss between 1986 and 1996.

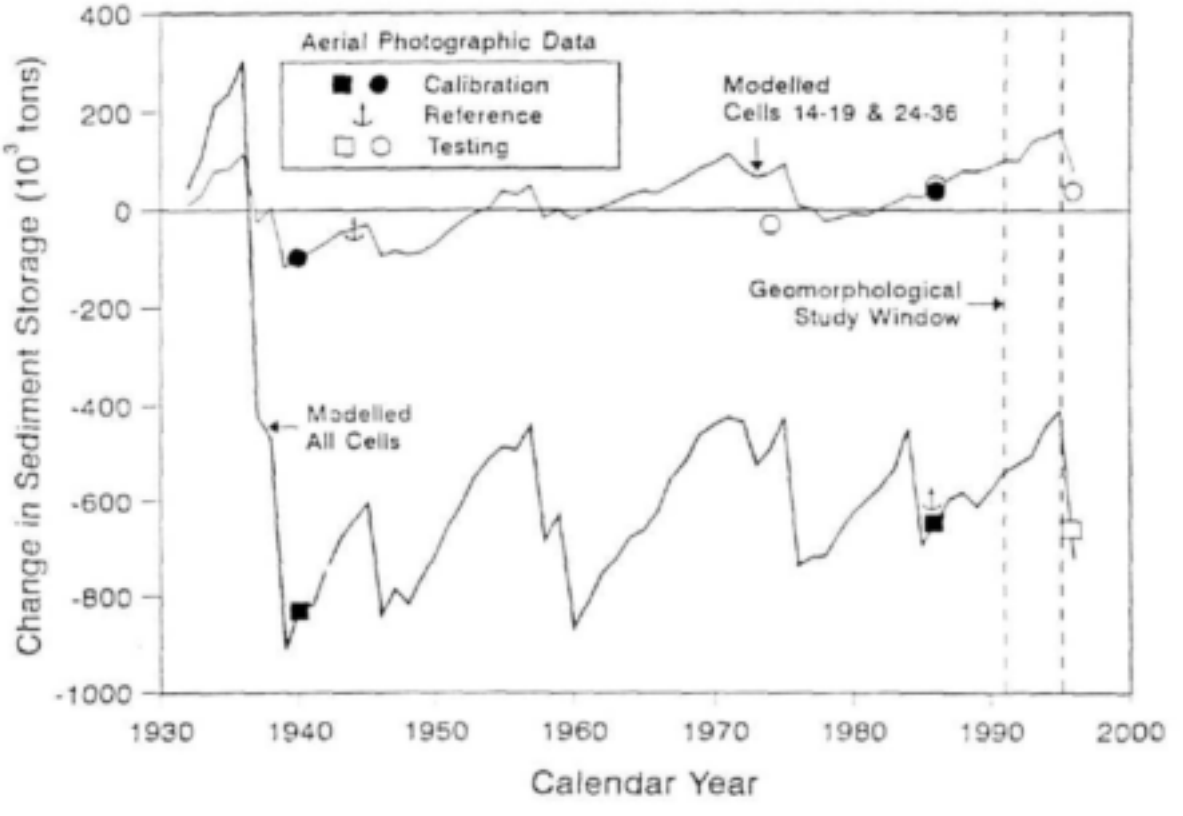

Figure 38 Plot of modelled change in sediment storage along the Sabie River for the period 1932 to 1996, showing the data points derived from aerial photographic data for model calibration and testing.

Low-flow aerial photographs of selected reaches along the Sabie River for the years 1986, 1989 and 1992 have been examined to quantify morphological unit change (Heritage *et al.*, 1997a). The degree of erosion or sedimentation was evaluated in terms of the type and coverage by new sedimentary features observed within selected examples of channel types between 1986 and 1989 (period of average runoff) and between 1989 and 1992 (period of reduced runoff). Some 400 changes in morphological unit presence and extent were recorded within the four channel types

considered (Table 22) (no aerial photographs are available for single-thread channels). Change between 1986 and 1989 was minimal, with both erosion and deposition recorded in mixed anastomosing and mixed pool-rapid reaches, and minor deposition within bedrock anastomosing and braided reaches. A reduction in flow between 1989 and 1992 corresponded with a net increase in coverage by exposed sediments. In particular, mixed anastomosing channel types displayed an increase in lateral and mid-channel bars and, similarly, mixed pool-rapid reaches exhibited increased sedimentary coverage, particularly by lateral bars. Bedrock anastomosing areas showed a response similar to that observed during the 1986-1989 period, with braided channel types recording an increase in net exposed sediment constituted principally as braid-bars (Table 22). From these aerial photographic data, sedimentation appears to have occurred during both average (1986-1989) and reduced periods of flow (1989-1992). Bedrock influenced channel types that contain a sedimentary influence (mixed pool-rapid and mixed anastomosing) appear to have accumulated sediment at an increased rate during periods of reduced flow.

The predicted increase in sedimentation from 1986 to 1992 is therefore corroborated by the additional data, as is the significant loss of unconsolidated sediment storage in 1996 by the combination of the intermediary and 1986-1996 aerial photographic data.

Table 22 Changes in sediment presence and coverage by morphological units for reaches within the principal channel types along the Sabie River, KNP (after Heritage *et al.*, 1997a).

Channel type	1986 to 1989		1989 to 1992	
	Change in sediment coverage (m^2)	Morphological unit change	change in sediment coverage (m^2)	Morphological unit change
Pool-Rapid	510 413 570 857 -946	Lateral bar Lee bar Rip channel	1866 395 11198 4901 9663	Lateral bar Lee bar Rip channel Mid-channel bar
Bedrock Anastomosing	1314	Lateral bar	938	Mid-Channel bar Lateral bar
Mixed Anastomosing	1624 -2152 0 761 267	Mid-channel bar	6038 3620 3632 2634 -130	Lateral bar Mid-channel bar Rip channel Lee bar
Braided	1956	Mid-channel bar	1125	Braid bar
Single-Thread	-	-	-	-

Observed channel change on the Sabie River reveals that the system is not in a state of dynamic equilibrium, but is rather evolving (Heritage *et al.*, 1997a). Previous studies (Heritage *et al.*, 1997a; Vogt, 1992; Chunnett *et al.*, 1990) indicate that the river has experienced a net increase in sedimentation over the period 1940 to 1986, once again confirmed by the present analysis of change as reflected by bar dynamics. Aerial photographic data reveal that the change is spatially and temporally dynamic and complex. For example, Chunnett *et al.* (1990) observed from the 1944 and 1986 aerial photographs that of fifty hippopotamus pools in 1986, seven did not exist in 1944, twelve were smaller in 1944, five were larger in 1944, and six remained unaltered. This variability is also displayed by the shorter term changes in bar formation (Fig. 38), where both accumulation and reduction of alluvial features are predicted.

It is reassuring to note that the modelled change in sediment storage is realistic. The average annual accumulation per length of river (51 tons/km/annum), translates into a volumetric accumulation of 1.2 m^3 per metre length of river (applying a porosity of 25% characteristic of the unconsolidated sand deposits along the Sabie River (Birkhead and James, 1998)) from over the period 1940 to 1986. Although this estimate may seem somewhat low (based on short-term field observations), the value is in fact most realistic given the spatial variability of observed changes in unconsolidated sediment storage (i.e. bedrock anastomosing channel types have displayed no significant change in storage (Fig. 25)).

A dam on the Sabie River at the Lower Sabie restcamp was constructed in 1986, with the primary objective of providing wildlife habitat and game viewing opportunities. A survey of the dam was undertaken in 1995, and is discussed in full by Birkhead *et al.* (1995). Although the river level and vegetation cover (particularly *P. mauritianus*) were found to mask sedimentary in-channel features, the data nevertheless revealed that the sediment profile in 1995 (as determined by sonar and ground-penetrating radar surveys) was below the pre-impoundment river water level in 1986. It is of interest to determine the predicted sediment load transported by river immediately upstream of the dam, and to compare this with the dam capacity. The modelled sediment discharge from 1987 to 1995 is 385×10^3 tons, which translates into a volumetric load of approximately 200×10^3 m^3. The survey area extended to 850 m upstream of the dam wall, and showed no significant reduction in capacity (380×10^3 m^3 in 1995) between 1987 and 1995. Analysis of aerial photographs, however, reveals extensive reed development further upstream for 1.5 km, and this has been attributed to increased siltation in the upper reaches of the dam's influence (Birkhead *et al.*, 1995). The approximate capacity of this impounded region is 300×10^3 m^3 as at 1995 (from sonar surveys). The data support the hypothesis that the post-impoundment delta deposit generally associated with reservoir sedimentation by bedload transport (Linsley *et al.*, 1992) had not yet by 1995 progressed to the basin extending 850 m upstream of the dam wall. The average annual sediment discharge into the dam (1987 to 1995) is 22×10^3 m^3/annum, whereas the long-term (1932 to 1996) value is significantly higher at 44×10^3 m^3/annum, reflecting the increased load in years experiencing large floods (e.g. 1996). The estimated total volumetric load for 1996 alone is 175×10^3 m^3, commensurate with the cumulative load over the nine previous (dry) years. Based on the long-term sediment load and assuming 100% trapping efficiency, the dam will effectively be completely silted by 2008. This lifespan (21 years) is comparable with dams constructed along the Letaba River in the 1970s, which are now completely silted.

The plots of modelled change in sediment storage (Fig. 38) show the same temporal trends for both the whole river and the section covered by cells 14 to 19 and 24 to 39. The plotting positions vary considerably, however, with that covering the whole river displaying more significant losses during years experiencing large floods. The reason for the offset between the plots, particularly during the late 1930s, arises from the influence of the bedrock anastomosing channel type cells, with only two out of total nine cells incorporated in the plot of the partial river coverage (refer to Table 9). The model has been calibrated between 1940 and 1986, and the bedrock anastomosing channel type cells have remained relatively stable over this period. The modelling of pre-1940 change within the bedrock anastomosing cells produces significant erosion of in-channel sediment, and there are no historical data to test this finding. Figure 39 provides a sequence of observed change for the representative bedrock anastomosing channel type cell (cell 12) for the years 1940, 1986 and 1996. The 1940 exposure shows a river devoid of any sediment and riparian vegetation, and suggests the recent occurrence of an extreme flood or series of events. The 1986 photograph reveals considerable colonisation by riparian vegetation. A good proportion of the riparian vegetation was uprooted by the 1996 floods (maximum discharge of 1705 m^3/s at this site, refer to Fig. 16), with the braid bar in the upstream pool having been completely removed and bars downstream of the anastomosing channel significantly reduced in size. Based on the record, it is not possible to determine the pre-1940 sediment storage status of the bedrock anastomosing channel types and consequently the potential for large scale erosion of in-channel sediment.

Figure 38 is re-plotted in Fig. 40, allowing no change in the sediment storage dynamics of the bedrock anastomosing channel type cells. The plots in Fig. 40 agree closely and illustrate the scale differences between the plots in Fig. 38 introduced by large scale erosion in the bedrock anastomosing channel type cells during the late 1930s.

5.8 Conclusion

The model presented in this chapter (SEDFLO) is able to describe the change in sediment storage in each of the 40 defined cells (each characterized as one of the principal channel types) along the Sabie River within the KNP in response to flows and sediment deliveries input on a daily basis. It is therefore useful for predicting relative increases or decreases in sediment accumulation in identified channel-type reaches in response to changed hydrological regimes associated with anthropogenic or climate change influences. The next chapter describes the application of the model to simulate the river response to simplified flow scenarios based on instream flow requirement (IFR) specifications. Chapter 7 describes a modelling technique for translating river response at the channel type scale to more ecologically meaningful responses at the morphological unit scale.

A visual interface for the SEDFLO model has been developed to facilitate its use and is described in the appendix to this report. The model code is available on the Kruger National Park Rivers Research Programme web site: http://www.ccwr.ac.za/knprrp/index.html .

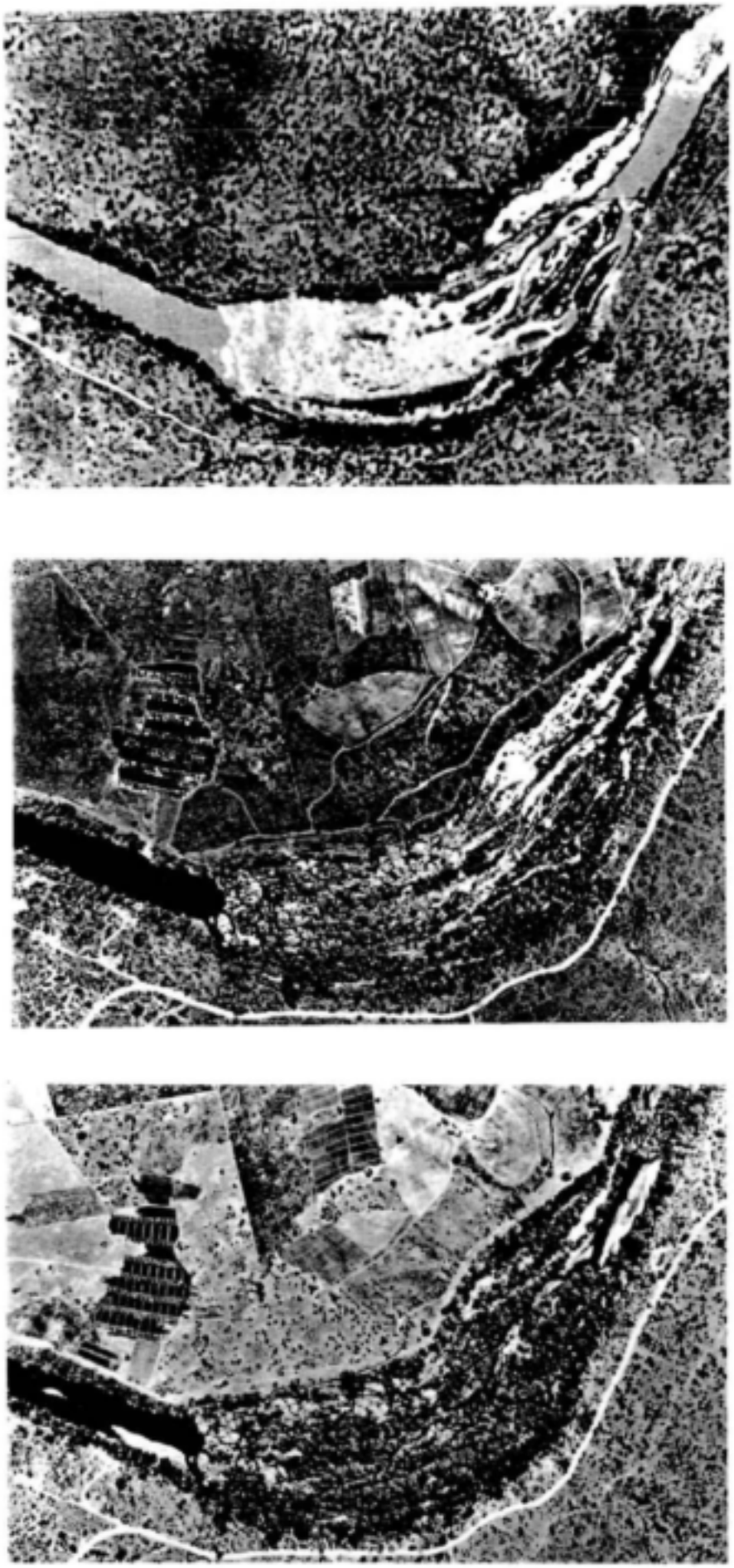

Figure 39 Sequence of observed change within the bedrock anastomosing channel type (Fig. 1) between the years 1940, 1986 and 1996 (top to bottom). Flow is from left to right.

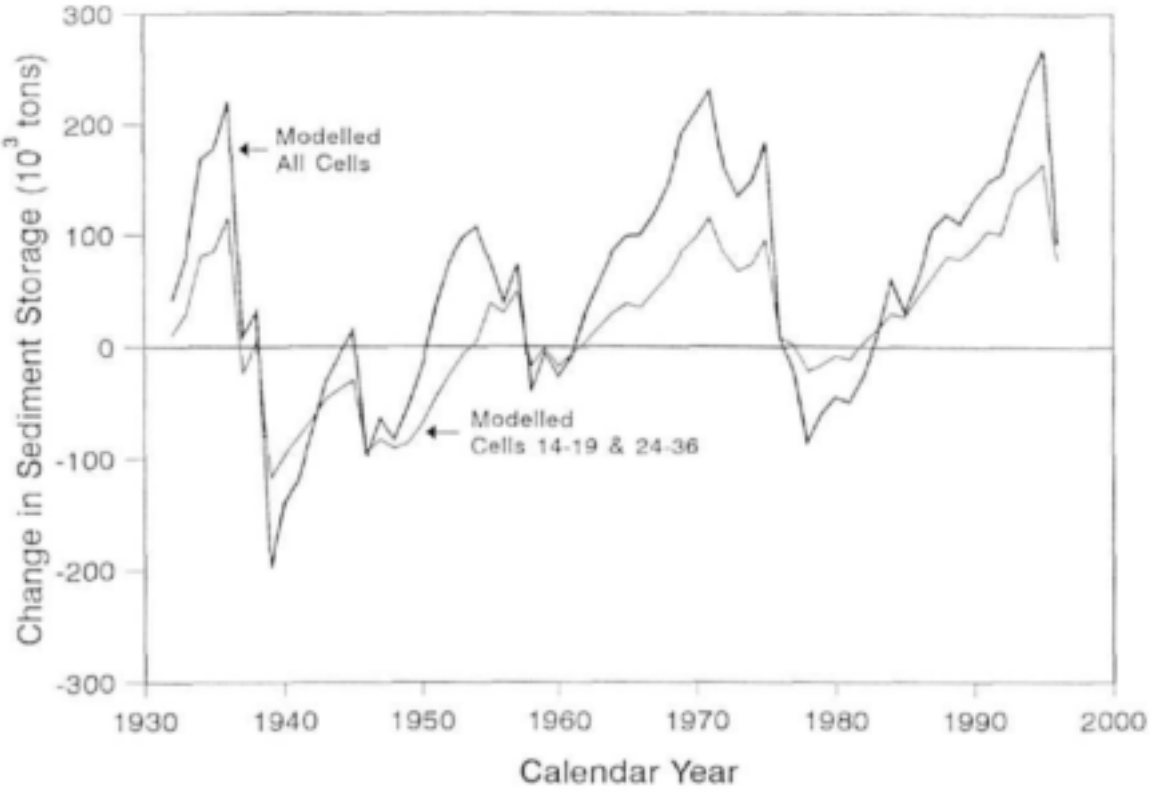

Figure 40 Plot of modelled change in sediment storage along the Sabie River for the period 1932 to 1996, allowing no change in the sediment storage within the bedrock anastomosing channel type cells.

6 Scenario modelling of geomorphological change

6.1 Introduction

The calibrated SEDiment FLux and stOrage model (*SEDFLO*) developed and tested in chapter 5 is applied to synthesize the temporal and spatial changes in sediment storage along the Sabie River in response to three flow scenarios. In order to model scenarios that are realistic, flow recommendations determined from an Instream Flow Requirements (IFR) assessment using the Building Block Methodology (BBM) are used (refer to the proceedings of the IFR workshop for the Sabie-Sand River system, DWAF, 1997).

Changes in river sedimentation for the period 1932 to 1996 are considered in the scenario modelling, and the results are compared to those predicted using the historical flow and sediment regimes over the past 64 years, i.e. Fig 38.

6.2 Flow scenarios

6.2.1 Injaka Dam

The Injaka Dam on the upper Marite River (Fig. 1) and associated Bushbuckridge transfer pipeline were found to be the most economical first phase of the Sabie River Government Water Transfer Scheme (DWAF, 1994). Water released from the dam into the Marite River will augment flow in the Sabie River to provide primarily for domestic needs as well as irrigation, while some of the water will be transferred by the pipeline to the Sand River subcatchment for similar purposes. The main features of the Injaka Dam and Bushbuckridge transfer pipeline are given in Table 23.

The instream flow requirements for IFR site 1 located on the Marite River immediately upstream of its confluence with the Sabie River (Fig. 1) are used for the Injaka Dam scenario. The modelling of the operation of the Injaka Dam based on the IFR recommendations is yet to be undertaken and therefore the existing application of the IFR represents a situation somewhat worse than envisaged based on the existing environmental recommendations, since the flows that will overtop the wall are not included. The drought IFRs are also excluded, since this will involve an analysis to determine the seasons (from 1932 to 1996) that may objectively be classified as drought periods. The finalised maintenance flows (base and higher) as documented in Table 16.3 of the proceedings of the Sabie-Sand IFR workshop (DWAF, 1997) are used. The timing of the higher flows has been determined to coincide with the elevated flows of the Sabie River, as would be envisaged under optimal reservoir operation (refer to Hughes *et al.*, 1997).

Figure 41 is a plot of the mean annual runoff along the Sabie River, based on the flow recommendation at IFR site 1. The existing (historical) runoff is also indicated. The temporal sediment inputs to the Sabie River from the Marite River tributary have been reduced by the yields (as calibrated in SEDFLO) for ACRU subcatchments 25, 26 and 27, i.e. a trapping efficiency of 100% is assumed for the Injaka Dam. The modelled yields from these subcatchments within the foothills of the Drakensberg mountains are small, as illustrated by the reduction in mean annual sediment yield for the most upstream cell (cell) (Fig. 41).

Table 23 Main features of the Injaka Dam and Bushbuckridge transfer pipeline

Injaka Dam	
Catchment area	209 km^2
Mean annual runoff	$101x10^6$ m^3
Storage capacity	$123x10^6$ m^3
Water surface area at full supply level	795 ha
Wall height	51 m
Crest length	550 m
Bushbuckridge transfer pipeline	
Maximum annual transfer volume	$25x10^6$ m^3
Static head	96 m

Figure 42 is a plot of the modelled change in sediment storage within the Sabie River (KNP) for the Injaka Dam scenario. Plots of the temporal storage minus the contribution of the most upstream cell (cell 1) and the cell at the Sand River confluence (cell 34) are included. The net change in sediment storage within these cells is indicated by the vertical arrows to the right of the graphs, and reveal that extensive deposition is predicted for the upstream cell (cell 1). This arises from the fact that reduced runoff will transport less sediment (except if the runoff is distributed primarily as high magnitude, short duration flow events), and this sediment is likely to deposit within the upstream river network (i.e. between the dam wall and the Sabie River confluence). It is necessary therefore to isolate these junction cells from the river so as not to obtain a distorted indication of the overall change in sedimentation along the river.

It is interesting to note that the Injaka Dam scenario shows only a slight increase in the overall trend of net alluviation within the Sabie River from the 1940s to present (excluding cells 1 and 34). More importantly, it reveals a reduction in the dynamic behaviour of the sediment storage. This results primarily from lower magnitude flows which have been shown (chapter 5) to be responsible for the erosion of alluvial bars and a highly variable pattern of temporal sediment storage within the overall trend of net alluviation. Figure 43 is a plot of the net changes in sediment storage for the channel type cells over the period 1932 to 1996. The results at first appear difficult to explain, with the braided channel types generally showing net erosion and the pool-rapid channel types (and mixed anastomosing to a lesser degree) displaying overall deposition. The observed long-term change (Fig. 25) shows the braided channel to display the highest rate of sediment accumulation per unit river length, and this trend would be expected to continue at an accentuated rate. Further consideration, however, reveals that the results are realistic given the differences in sediment transport characteristics between bedrock influenced pools (the critical feature in terms of sediment transport within the pool-rapid channel types) and the alluvial braided channel types.

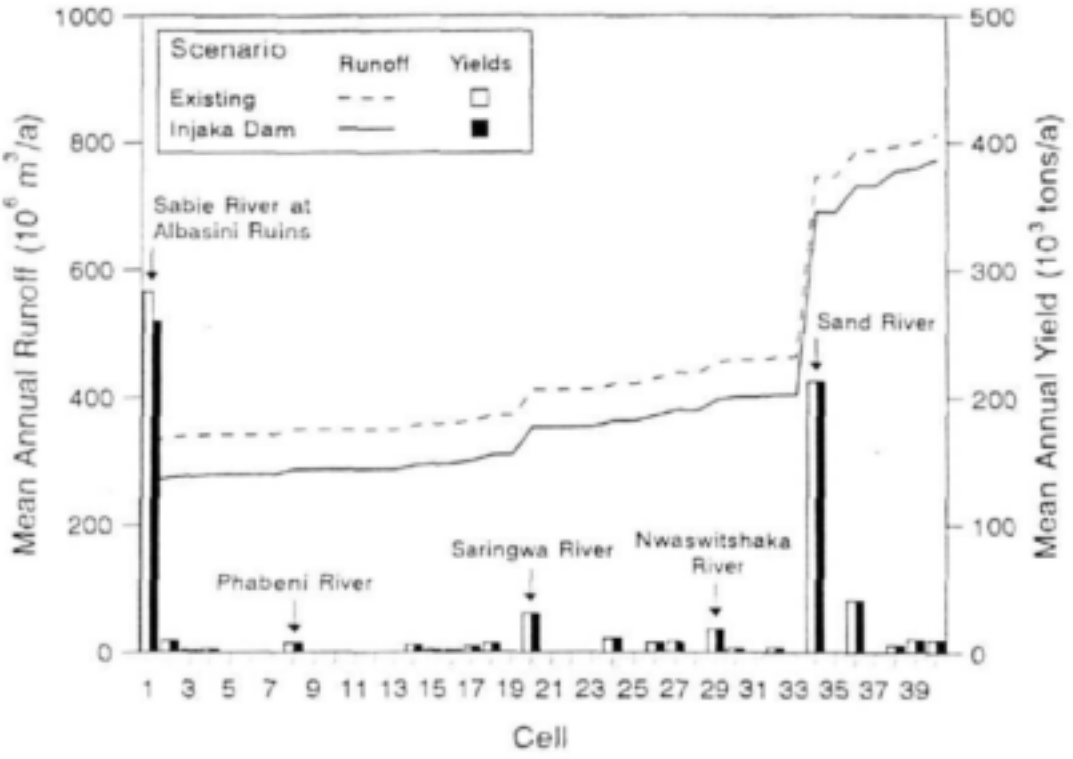

Figure 41 Mean annual runoff and sediment yields for the Injaka Dam IFR scenario showing existing (historical) conditions.

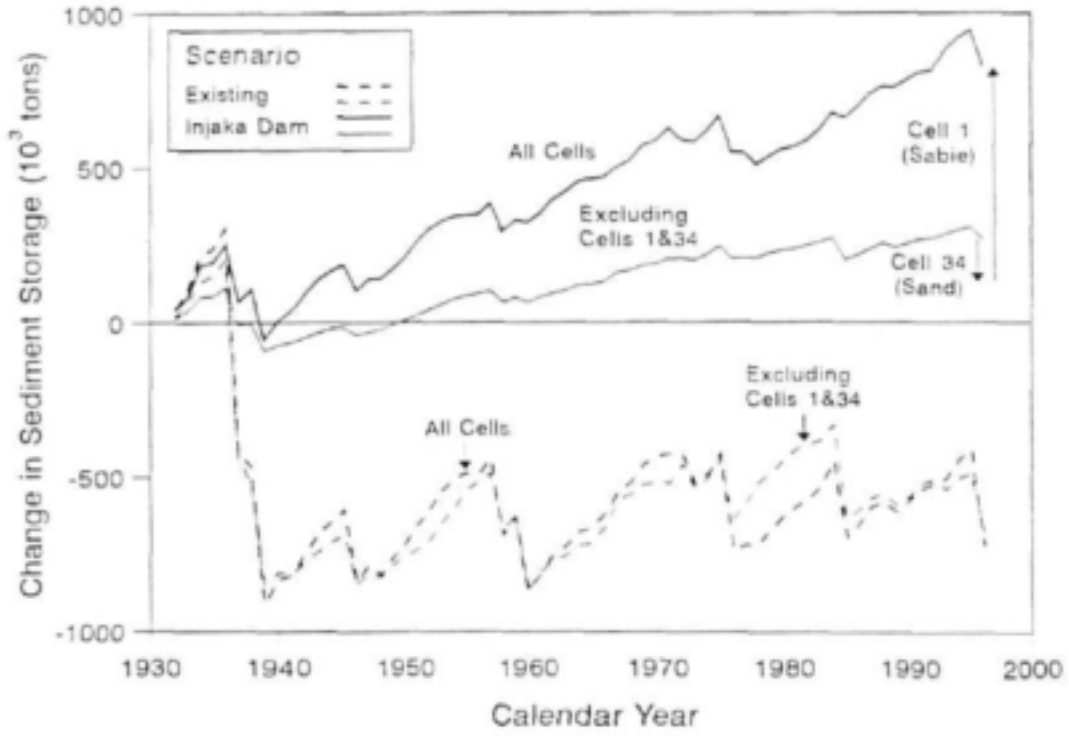

Figure 42 Plots of modelled changes in sediment storage along the Sabie River for the Injaka Dam IFR scenario, showing existing (historical) conditions.

Braided channel types display a more uniform energy gradient than the stepped profiles characteristic of pool-rapid channel types. Bedrock outcrops occur in the pool-rapid channels in areas displaying local change in bedrock resistance as a result of lithological and structural variability (Cheshire, 1994). The result are regions of low energy (gradually varied flow) backup constituting pools upstream of bedrock outcrops and high energy (rapidly varied) flow through bedrock and boulder rapids. Consequently, sediment in braided channels experiences incipient motion at lower discharges than pool units within pool-rapid channels, as confirmed by the potential transport relationship plotted in Fig. 4 for the representative channel types. It is inconceivable to consider two adjacent alluvial cells (in the absence of intervening tributaries) where the actual sediment transport discharge relationships (covering the range of flows in the river) do not intersect (Fig. 4). The consequence would be channels that indefinitely accumulate sediment or erode their beds. Clearly, for a system in dynamic equilibrium, the transport relationships will intersect, and this reflects different proficiencies at transporting sediment across the flow regime. A pool-rapid channel type displays a higher transport capability at higher flows, whereas a braided channel has a lower entrainment threshold and therefore a higher transport proficiency at lower flows.

This explains the general erosion predicted for the braided channel type cells and the general aggradation within the pool-rapid channels (Fig. 43) resulting from the reduced flooding regime of the river. It is important to note, however, that this will not occur indefinitely, but rather reflects the short-term change to an altered flow and sediment regime. Morphological adjustments will result in changes to the transport characteristics of the channel, and new functional transport relationships will develop with time.

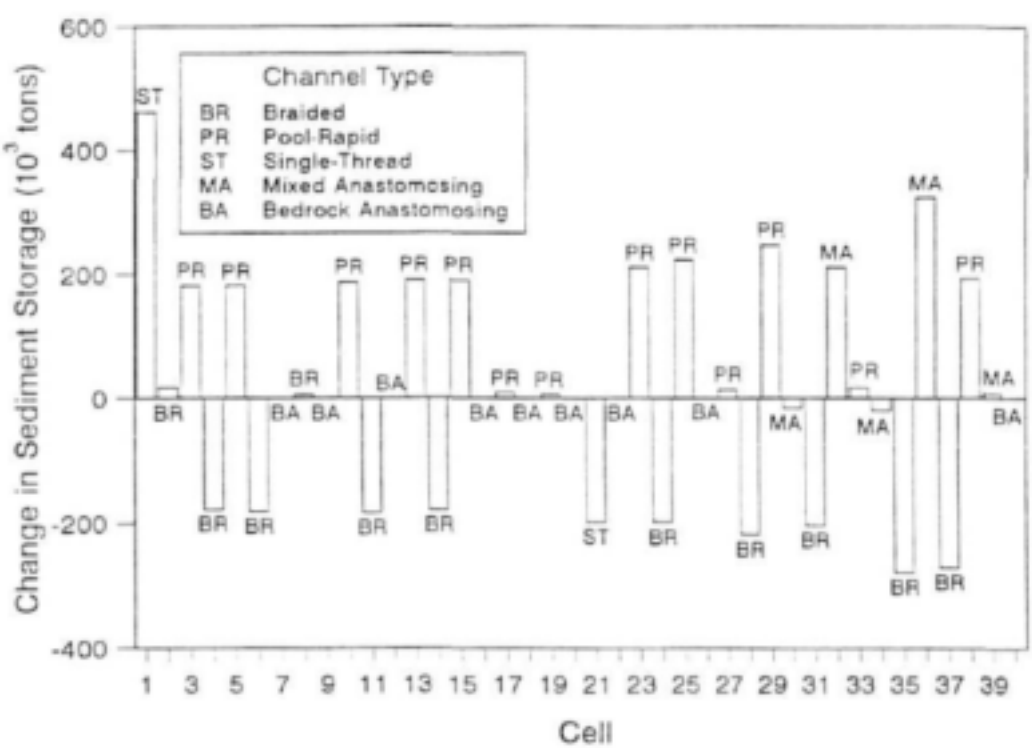

Figure 43 Net change in sediment storage along the Sabie River over the period 1932 to 1996 for the Injaka Dam IFR scenario.

6.2.2 Injaka Dam and Sand River IFR recommendations

For the second scenario, the Injaka Dam development is combined with the flow recommendations for the Sand River (IFR site 8, Fig. 1) immediately upstream on the Sabie River confluence, as proposed during the IFR workshop (DWAF, 1997). As with the Injaka Dam scenario, only the IFR maintenance (base and higher) flows are used. The application represents a situation worse than envisaged based on the existing environmental recommendations. This is because flood flows are not incorporated in the analysis due to lack of information pertaining to future water resources developments in the Sand River catchment, including operation of the Bushbuckridge transfer pipeline from the Injaka Dam.

As discussed previously, a reduction in runoff is concomitant with a loss of sediment load, and the modelled sediment yields from the Sabie River tributaries for the historical conditions (1932 to 1996, Fig. 36) cannot be assumed. In order to determine the reduced yields, a sediment transport/storage analysis such as developed here for the Sabie River needs to be undertaken for the tributaries subjected to reduced runoff. This is, however, beyond the scope of the present study. An approximate means of determining the sediment load from the Sand River is undertaken by applying the annual long-term historical relationship between sediment discharge and runoff. Figure 44 is a plot of the annual sediment discharge against runoff for the most upstream cell (cell 1) and cell 34 (Sand River at its confluence with the Sabie River). Reasonable power relationships have been fitted to the data which displays considerable scatter as would be expected given the variability of the flow regimes. The relationship for the Sand River is used to compute the (reduced) annual sediment load entering the Sabie River system as a function of the annual flow volume (based on the IFR recommendations).

Figure 45 is a plot of the mean annual runoff along the Sabie River, based on the flow recommendations at IFR site 1 (Marite River) and IFR site 8 (Sand River). The significant reductions in the mean annual runoff and associated sediment load from the Sand River (cell 34) is illustrated and compared with existing (historical) conditions.

Figure 46 is a plot of the modelled change in sediment storage within the Sabie River (KNP) for the combined Injaka Dam and Sand River IFR scenario. Significant alluviation is predicted downstream of the Sand River confluence (cell 34) and although deposition is likely, the magnitude of the modelled increase in storage may be attributed to overestimating the annual sediment loads carried by the Sand River. This scenario also shows only a slight increase in the overall rate of net alluviation excluding cells 1 and 34. The response, however, reveals a further reduction in the dynamic behaviour of the sediment storage due to the loss of variability (particularly flooding) from the historical flow regime. The changes in sediment storage along the river are plotted in Fig. 47. The cells downstream of the Sand River confluence show the same directional responses predicted for the Injaka Dam scenario (Fig. 43), with the exception of mixed anastomosing cell 34 which has altered its response from marginal erosion to large scale deposition.

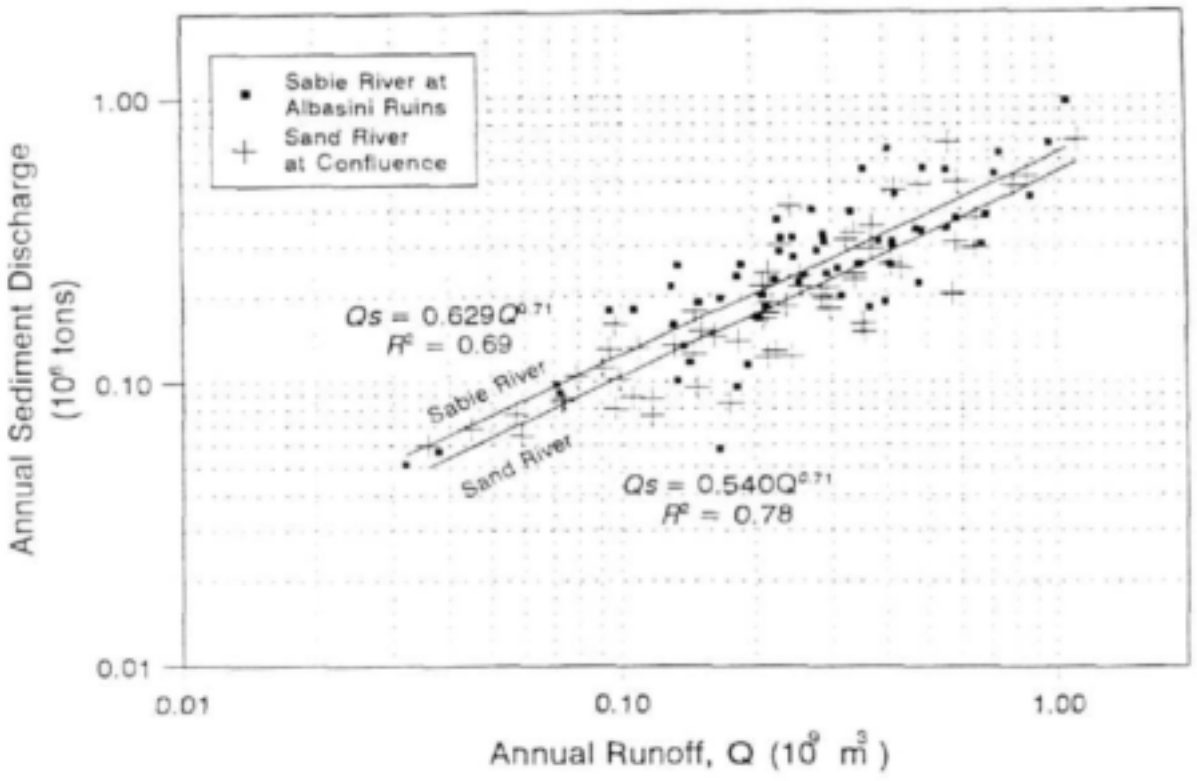

Figure 44 Relationship between annual sediment discharge and runoff for the Sabie River at Albasini Ruins and the Sand River at its confluence with the Sabie River.

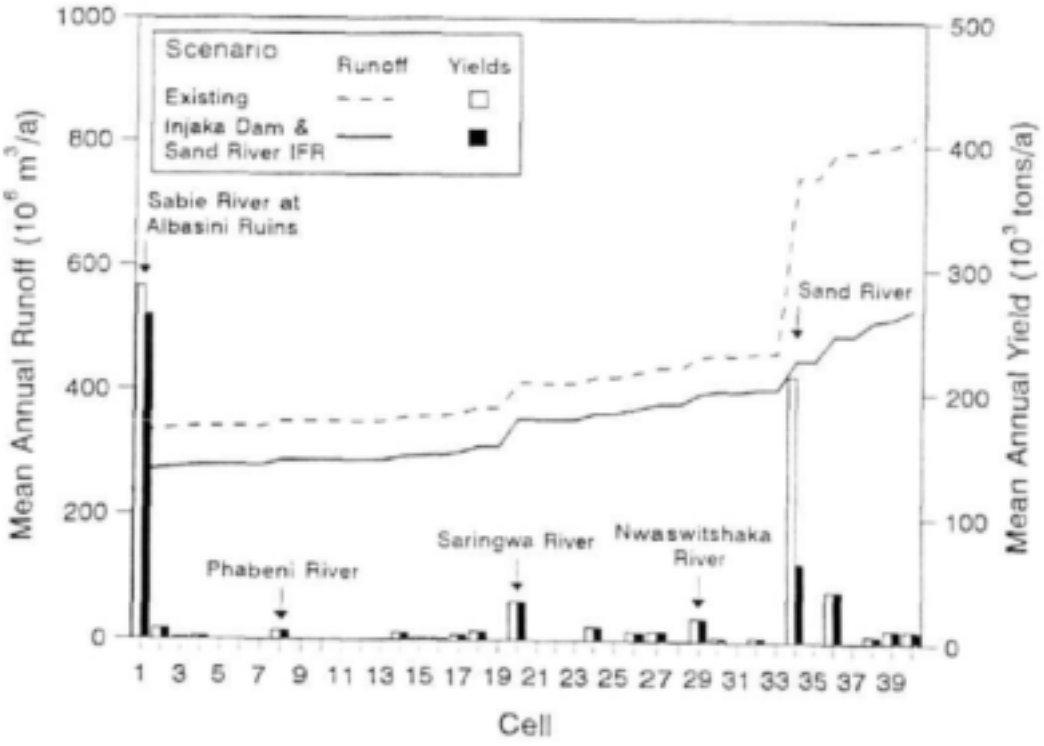

Figure 45 Mean annual runoff and sediment yields for the Injaka Dam and Sand River IFR scenario, showing existing (historical) conditions.

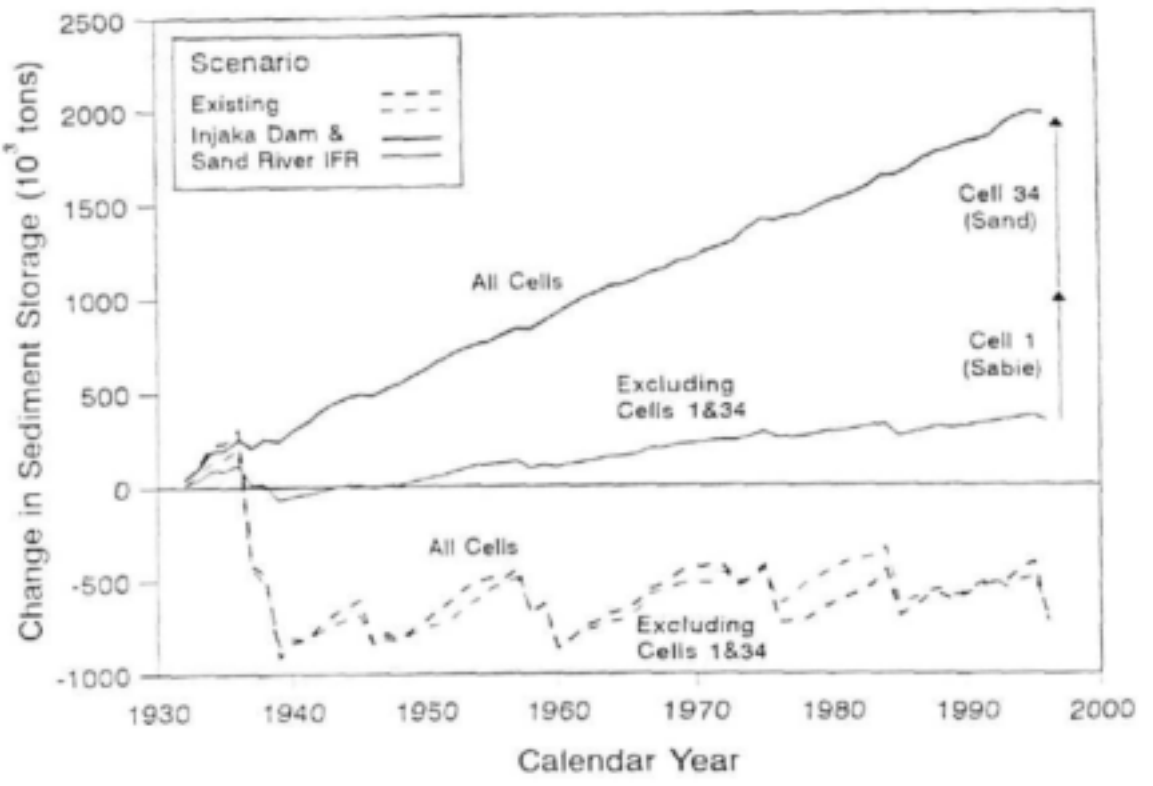

Figure 46 Plots of modelled changes in sediment storage along the Sabie River for the Injaka Dam and Sand River IFR scenario, showing existing (historical) conditions

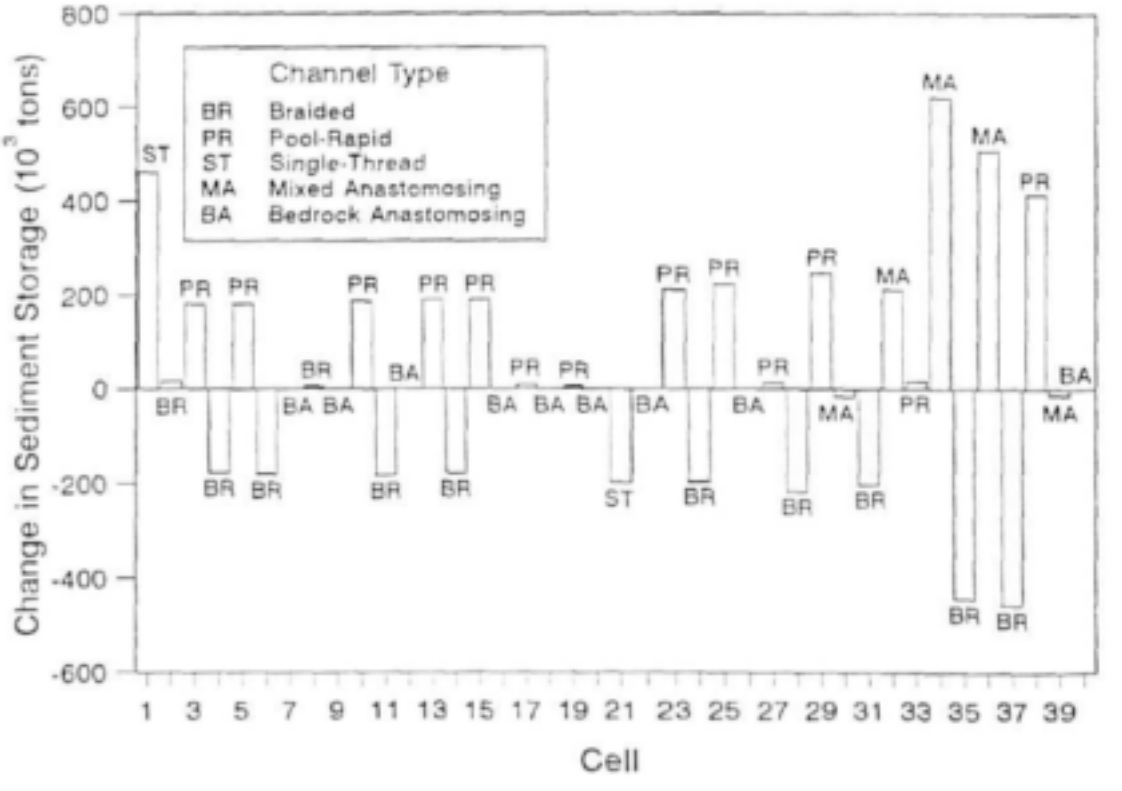

Figure 47 Net change in sediment storage along the Sabie River over the period 1932 to 1996 for the Injaka Dam and Sand River IFR scenario

6.2.3 Sabie and Sand River IFR recommendations

For the third scenario, the altered Sand River flow and sediment regime used in scenario two is combined with the flow recommendations for the Sabie River at Albasini Ruins (IFR site 2, Fig. 1). As with the previous applications, only the IFR maintenance (base and higher) flows are used. The annual sediment discharge relationship for the Sabie River (Fig. 44) is used to compute the (reduced) annual sediment load entering the Sabie River system at cell 1 as a function of the annual flow volumes.

Figure 48 is a plot of the mean annual runoff along the Sabie River. The further reductions in the mean annual runoff and associated sediment load from upstream contributions (cell 1) are illustrated. Figure 49 is a plot of the modelled change in sediment storage for the combined Sabie River and Sand River IFR scenario. Further alluviation is predicted upstream of Albasini Ruins (cf. Fig. 42). This scenario produces approximately twice the net historical rate of alluviation along the Sabie River, excluding the contribution of cells 1 and 34. The short-term variability in temporal storage is essentially lost, resulting in a constant rate of overall alluviation. The changes in sediment storage along the river are plotted in Fig. 50. The directional changes in storage are as predicted for the second scenario (Fig. 47). It is interesting to note that the mixed anastomosing and pool-rapid channel type cells immediately downstream of the Sand River confluence display extensive deposition, whilst the braided cells reveal accentuated erosion.

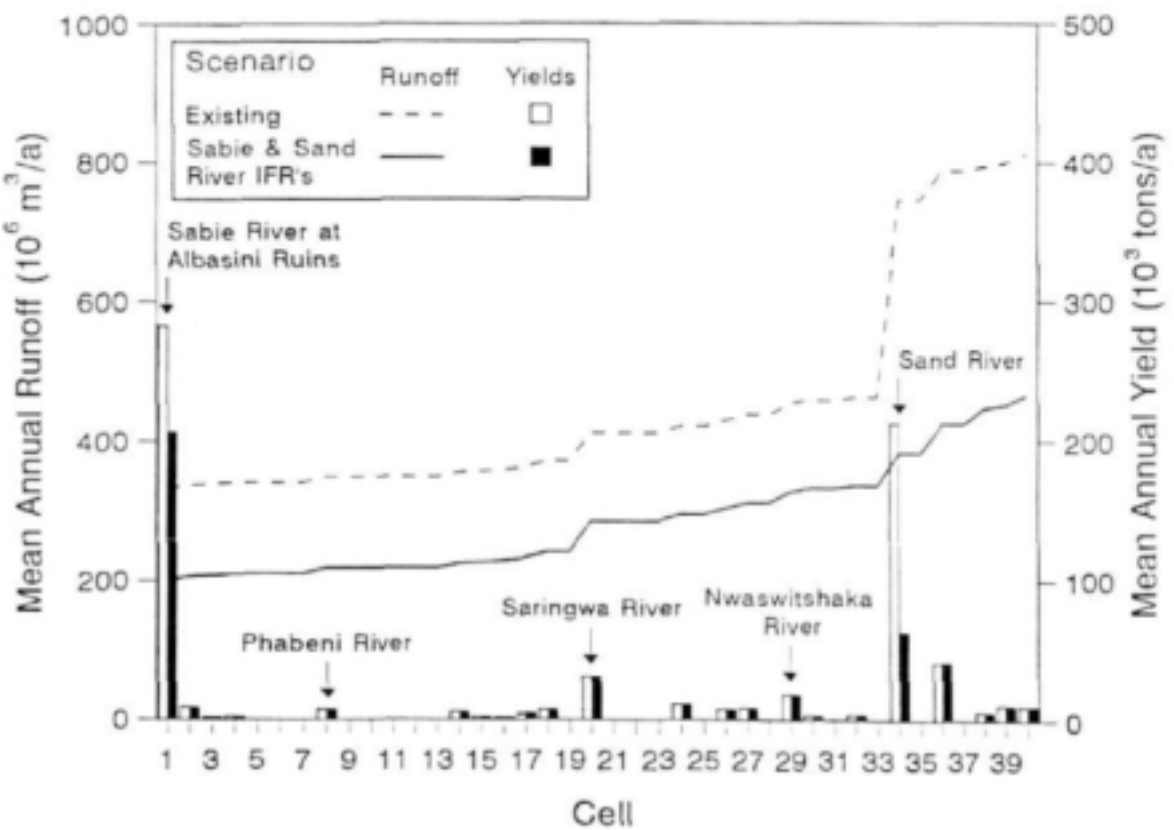

Figure 48 Mean annual runoff and sediment yields for the Sabie River and Sand River IFR scenario, showing existing (historical) conditions.

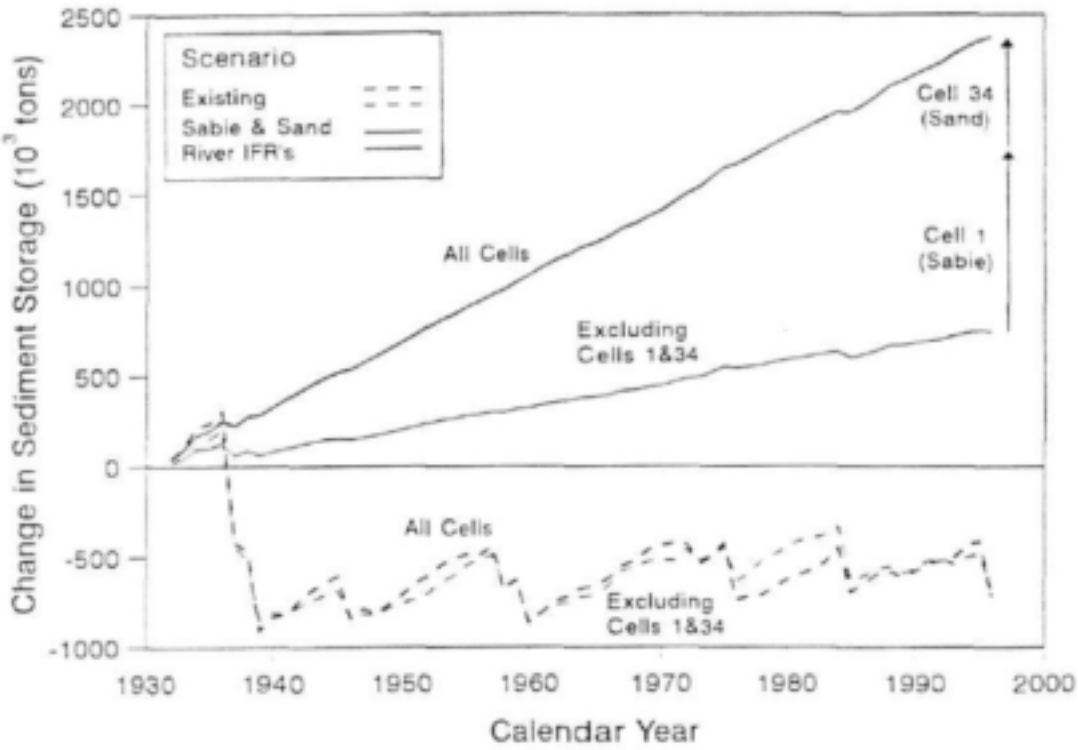

Figure 49 Plots of modelled changes in sediment storage along the Sabie River for the Sabie River and Sand River IFR scenario, showing existing (historical) conditions

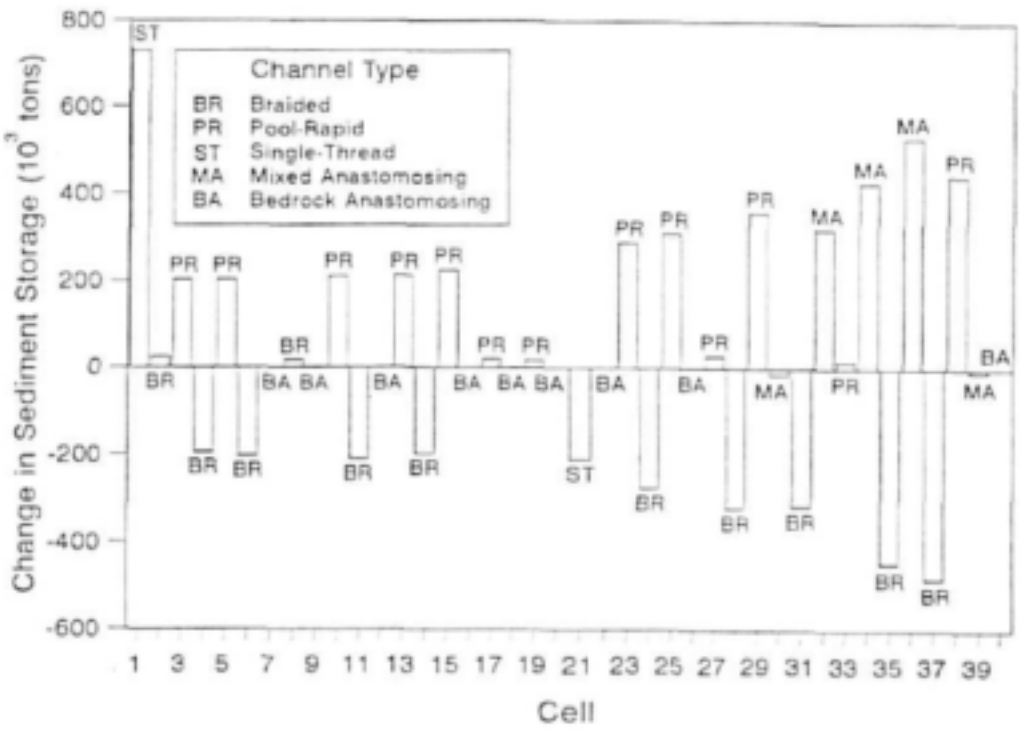

Figure 50 Net change in sediment storage along the Sabie River over the period 1932 to 1996 for the Sabie River and Sand River IFR scenario.

6.3 Conclusions

The sediment storage response of the Sabie River within the KNP has been modelled at a channel type scale using SEDFLO with flow regimes representing different upstream water resources development scenarios. The scenario flows are based on specified instream flow requirements only, and not on detailed reservoir simulations; they therefore do not include high flows resulting from reservoir spillage. More realistic scenario flow sequences are to be produced by system simulation in another project within the KNPRRP, and should form the basis for further application of SEDFLO.

The following conclusions are drawn from the scenario modelling:

- The long-term rates of alluviation (excluding the most upstream and Sand River confluence cells) increase approximately proportionately with reduced MAR.

- The reduction of dynamic sediment storage behaviour resulting from diminished flooding influence is clearly noticeable. This is likely to impact significantly on the spatial and temporal assemblages of geomorphological features and associated aquatic and riparian habitats, since under conditions of reduced flooding, irreversible sedimentation will systematically reduce the proportional occurrence of bedrock influence within the system.

- In order to achieve a new dynamic equilibrium in response to a reduced flooding regime, alluvial channel types display a tendency to erode whilst pools and (to a lesser degree) mixed anastomosing channel types show a tendency to aggrade. Loss of storage within braided channel types is likely to result in a smaller active channel incised within the macro-channel infill deposit.

SEDFLO predicts gross changes in sediment storage along the river, which is insufficient for inferring biological response at smaller scales. The gross changes must therefore be translated into morphological characteristics associated with habitat. A modelling approach developed for this purpose is described in the following chapter.

7 Rule based geomorphological unit change model

7.1 Introduction

This chapter describes the application and testing of a rule based geomorphological unit change model, first developed for predicting change at the unit morphological scale along the Sabie River (KNP), under the auspices of the Biological-abiological LINKS (BLINKS) programme (Heritage *et al.*, 1997a). Information is presented on the conceptual framework behind the model, including a description and justification of the spatial and temporal scales at which the model operates and the structure of the input data in relation to the channel type sediment transport and storage model (SEDFLO) presented in chapter 5.

The form of inputs and outputs to and from the model are discussed with respect to the morphologic template, hydrological regime and sediment production. In addition, matrices of rules for each of the channel type sub-models are presented for each generic channel type and justified with reference to field evidence of channel change on the Sabie River. The model is tested using modelled flow and sediment flux data from SEDFLO (chapter 5), and the output is compared to observed change in the area of unconsolidated sediment deposits within each of the five representative cells (one for each representative channel type) on the Sabie River. Furthermore, the results are also compared to the gross pattern of erosion and deposition predicted for each representative cell to determine if the modelled patterns of change are similar. The limitations of the rule based model are discussed, and recommendations are suggested that will result in an improved predictive accuracy.

7.2 Data requirements

The geomorphology model is designed to accept discharge and sediment flux data for any cell on the Sabie River in the form of annual values computed from daily flow and sediment flux simulations. The Sabie is sub-divided into 40 linked cells which represent the spatial extent of alternating channel types (bedrock, mixed and alluvial anastomosing, bedrock and mixed pool-rapid, alluvial single-thread and braided) along the river (Fig. 30 and Table 9). Variable inputs to the model consist of hydrological and sediment index values.

7.2.1 *Geomorphological data*

The geomorphology of the Sabie River has been intensively studied (van Niekerk and Heritage, 1993; van Niekerk *et al.*, 1995; Moon *et al.*, 1997; Heritage *et al.*, 1997a). As a result, a geomorphological hierarchy has been developed that structures the river on the basis of the association of geomorphological units (Tables 24 and 25) to form channel types (Fig. 2).

Five channel types characterise the system (bedrock, mixed and alluvial anastomosing, bedrock and mixed pool-rapid, alluvial single-thread and braided), and these have been combined to form three generic channel types (anastomosing, pool-rapid and single-thread/braided), which constitute the geomorphological basis of the geomorphology model. The changes in morphologic assemblage are predicted independently for each of these generic channel types.

Table 24 *Description of the major morphological units found on the Sabie River in the KNP.*

Morphological unit	Description
Rapid	Steep bedrock sections, high velocity concentrated flow
Bedrock pavement	Horizontally extensive area of exposed rock
Isolated rock	Discrete small outcrop of bedrock
Pool (bedrock, mixed and alluvial)	Topographic low point in the river channel associated with a downstream bedrock or alluvial control
Braid bar	Accumulation of sediment in mid-channel causing the flow to diverge over a scale that approximates to the channel width
Lateral bar	Accumulation of sediment attached to the side of the channel, may occur sequentially downstream as alternate bars
Point bar	Accumulation of sediment on the inside of a meander bend
Bedrock core bar	Accumulation of finer sediment on top of bedrock in bedrock anastomosing areas
Lee bar	Accumulation of sediment in the lee of flow obstructions
Distributary (bedrock, mixed and alluvial)	Individual active channel in an anastomosing system
Island	Large mid channel sediment accumulation that is rarely inundated
Anastomosing bar	Accumulation of coarser sediment on top of bedrock in bedrock anastomosing areas
Macro-channel lateral bar	Large accumulation of fine sediment on the sides of the incised macro-channel
Pool	Topographical low, may be bedrock, mixed or alluvial, termed apical when on outer bend of meander/sinuous reach
River cliff	Near-vertical bank of river normally associated with outer bend of meander/sinuous reach
Rip channel	Equivalent to chute, small high flow channel on inside of point bar or lateral bar feature
Riffle	Topographical high associated with gravel-bed rivers as part of pool-riffle sequence
Floodplain	Accumulation of contemporary alluvial material from overbank flooding and lateral aggradation (meander migration)
Terrace	Accumulation of older alluvial material associated with previous higher level river floodplain now elevated above contemporary channel as a result of incision
Cutoff	Abandoned length of river no longer permanently connected to the main river as a result of meander migration or avulsion
Levee	Raised linear feature adjacent to the main channel composed of overbank sediments
Boulder bed	Area of very coarse sediment accumulation (>128 mm)
Armoured bed	Area of coarse sediment accumulation (64-128 mm)
Waterfall	Vertical disruption to channel bed
Cateract	Series of small waterfalls

The model utilises this baseline geomorphological template consisting of the alternating generic channel types along the river (Fig. 30) as a basis on which to route sediment inputs from the sub-catchments. Continuity of sediment movement is achieved through erosion or deposition of material in each cell in response to the balance of erosive forces and sediment inputs (Fig. 29). Internally, the changing sediment balance within each channel type results in a change in the geomorphological composition at the scale of morphologic unit, and these are modelled using a rule based expert system (Heritage *et al.*, 1997b)

Each of the generic channel types is initially defined by a base morphologic state as determined by quantitative analysis of 21 kms of river channel within the KNP (Table 26). In the anastomosing generic channel type, mixed anastomosing channels display an increased percentage of anastomosing bars (35%) at the expense of bedrock core bars, which reduce to 11%. This is coded into the rules.

Through this approach, long term channel change can be usefully modelled at the scale of geomorphological unit (pools, rapids, bar types, etc.), and new geomorphological associations following channel change can be predicted using the geomorphological model and data on the flow regime and sedimentation.

Table 25 Morphological composition of the common channel types found on the Sabie River in the KNP.

Channel type	Description	Morphological units
Alluvial single thread	Uniform single channel river. Limited bedrock outcrops or braid bars associated with active channel. May be bedrock or alluvial.	Lateral bar (1), Pool (1), Rock pool (1), River cliff (2), Apical pool (2), Point bar (2), Rip channel (2), Riffle (2), Rapid (2), Floodplain (2), Terrace (2).
Alluvial braided	Multi-channel system with impermanent distributaries in alluvium. Channel convergence and divergence occurs on the scale of channel width.	Braid bar (1), Alluvial distributary (1), Lateral bar (1), Point bar (2), Rip channel (2), Cutoff channel (2), Armoured area (2), Floodplain (2), Terrace (2), Alluvial backwater (3), River cliff (3), Levee (3), Apical pool (3).
Mixed anastomosing	Multi-channel system of distributaries in bedrock and alluvium	Rock pool (1), Rapid (1), Alluvial pool (1), Bedrock core bar (1), Rock distributary (1), Alluvial distributary (1), Cataract (2), Waterfall (2), Boulder bed (2), Armoured area (2), Lee bar (2), Rock backwater (2), Alluvial backwater (2) alluvial bars (2).
Bedrock anastomosing	Multi-channel system of permanent bedrock distributaries. Sediment may accumulate on topographic highs.	Rock pool (1), Rapid (1), Bedrock core bar (1), Cataract (1), Waterfall (1), Rock distributary (1), Boulder bed (2), Armoured area (2), Lee bar (2), Rock backwater (2).
Mixed pool-rapid	System of shallow faster steeper bedrock dominated rapids and associated upstream backwater pools	Rock pool (1), Rapid (1), Bedrock core bar (2), Lateral bar (2), Lee bar (2), Cataract (2), Boulder bed (2), Armoured area (2), Floodplain (2), Rock distributary (2), Terrace (2), Rock backwater (2), Braid bar (3), Pool (3), Riffle (3) Alluvial distributary (3),
(1) = Definite occurrence, (2) = Probable occurrence, (3) = Rare occurrence		

Table 26 Morphologic composition of the generic channel types on the Sabie River within the KNP.

Morphologic unit	Generic channel type		
	Anastomosing (%)	Pool-rapid (%)	Alluvial (%)
Braid bar	3	1	15
Lateral/point bar	5	20	20
Lee bar	2	1	
Bedrock core bar	51	10	
Anastomosing bar	5		
Rapid	5	4	1
Isolated rock	2	1.5	1
Bedrock pool/distributary	9	2.5	
Mixed pool/distributary	15	15	3
Alluvial pool/distributary	1	20	35
Island			
Bedrock pavement	2		
Macro-channel lateral bar		25	25

7.2.2 Hydrological data

The daily average flow hydrology was simulated using the ACRU model (refer to 5.2.3). The flow regime has been divided into four categories according to the standard deviation from the median flow (Table 27), and are used to drive the channel change matrices presented in Table 28. Category 1 is baseflows, which are considered geomorphologically insignificant due to their inability to transport sediment (refer to Fig. 51). Freshettes (category 2) may alter some instream morphological units and flows of the order of the annual flood (category 3) are competent to redistribute significant volumes of unconsolidated sediment and may also result in the erosion of some consolidated deposits. Major floods (category 4) will overtop the active and seasonal distributary channel network (see Heritage *et al.*, 1997a) and have the ability to alter the morphology of areas between these channels by modifying macro-channel features such as bedrock core bars, islands and macro-channel lateral bars. Category 1 flows are less than one standard deviation below the median flow for the period of record; category 2 includes flows between the median and 1 standard deviation less than the median; category 3 incorporates flows between the median and 1 standard deviation above the median; and category 4 flows are greater than one standard deviation above the median.

7.2.3 Sedimentation data

Sediment enters the Sabie River at tributary junctions, with many of these flowing only ephemerally and introducing sediment sporadicaly. These sediment inputs are reworked by the perennial flows within the Sabie River according to local channel competence as defined by the

channel type. The annual sediment inputs to each of the channel type cells are provided by SEDFLO (chapters 6 and 7). The sediment transport data are categorised into states based on the standard deviations from the median as for the flow states (Table 27).

Table 27 Categorisation of the flow and sedimentation parameters used to define the process states in the geomorphological model, with the median flow and sediment input values assigned indices of 1.

Flow regime category			**Sediment input category**		
Flow state		Flow index range	Sedimentation state		Sedimentation index range
Base	**(1)**	< 0.68	**Low**	**(1)**	< 0.68
Freshette	**(2)**	0.68 to 1.0	**Reduced**	**(2)**	0.68 to 1.0
Annual flow	**(3)**	1.0 to 1.32	**Moderate**	**(3)**	1.0 to 1.32
Flood	**(4)**	> 1.32	**High**	**(4)**	> 1.32

7.3 Rule development and coding

The magnitude and direction of change at the morphologic unit scale has been determined from expert knowledge gained through extensive field experience, detailed examination of temporal aerial photographic sequences, and space for time substitution techniques (Vogt, 1992; van Niekerk and Heritage, 1993; van Niekerk and Heritage, 1994; Heritage and van Niekerk, 1994; Carter and Rogers, 1995; Heritage *et al.*, 1997a; Broadhurst *et al.*, 1997; Moon *et al.*, 1997). The rules are presented as a set of matrices defined by the controlling flow and sediment flux indices. Three matrices have been constructed to simulate geomorphological change in the three generic channel types whose baseline geomorphological state is defined by the parameter values in Table 26. The anastomosing channel matrix defines changes for bedrock, mixed and alluvial anastomosing channel types; the pool-rapid matrix covers changes in bedrock and mixed pool-rapids and the alluvial matrix concerns change within braided and alluvial single-thread channels.

The change matrices give the percentage change in morphological unit as a function of the flow and sediment indices, and are presented as Tables 29, 30 and 31 for the pool-rapid, alluvial and anastomosing generic channel types, respectively. The pool morphologic units are listed twice, the first value accounts for changes between alluvial deposits, and the second value represents internal redistribution of sediment. In the case of the pool-rapid channel type, the matrix values imply that braid bars increase during a year when the flow regime displays a freshette or the annual flood combined with moderate to high sediment indices. Conversely, bars are eroded during years experiencing a major flood but reduced or low sediment inputs. For the case of the anastomosing channel type, the formation of anastomosing bars is favoured in years where major floods occur coupled with a high sediment ratio. This is in contrast to years experiencing a major flood linked to a moderate sediment ratio, where bedrock core bars are considered to aggregate.

Table 28 Channel type switching rules for the Sabie River channel types

Generic channel type	Sabie River channel types		Geomorphological unit			
			Bedrock pools	Bedrock core bars or anastomosing bars	Rapids	Braid bars
Anastomosing	Bedrock anastomosing		> 10%	< 80%		
	Mixed anastomosing		0% to 10%	< 80%		
	Alluvial anastomosing		0%	< 80%		
Pool-rapid	Bedrock pool-rapid			> 80%	> 5%	
	Mixed pool-rapid			> 80%	2% to 5%	
Alluvial	Braided	Mixed			< 2%	> 10%
		Alluvial			< 2%	> 10%
	Single thread	Mixed			< 2%	0% to 10%
		Alluvial			< 2%	0% to 10%

Table 29 Morphologic unit change matrix for the pool-rapid generic channel type

Morphological unit	Sediment ratio high				Sediment ratio moderate				Sediment ratio reduced				Sediment ratio low			
	Base	Freshette	Annual	Flood	Base	Freshette	Annual	Flood	Base	Freshette	Annual	Flood	Base	Freshette	Annual	Flood
Braid bar	1	4	5	2	1	3	4	2		-2	-4	-3	-1	-3	-4	-5
Lateral point bar	1	3	4	2	1	2	3	2		-2	-2	-3	-1	-3	-4	-5
Lee bar	2	4	3	2	2	3	2	2		-2	-2	-3	-2	-3	-3	-5
Bed core bar			1	2				1	-1			-1			-1	-2
Anastomosing bar																
Rapid			-1	-2				-1				1			1	2
Isolated rock																
Bedrock pool	-2	-2	-2	-1	-2	-2	-2	-1		1	2	2	1	2	2	3
Mixed pool	-1	-2	-3	-2	-1	-2	-3	-1		2	3	3	1	2	4	4
Alluvial pool	-1	-7	-7	-3	-1	-4	-4	-4	1	3	4	4	2	5	6	8
Bedrock pool	-2	-2	-2	-1	-1	-1					1	2	1	2	3	5
Mixed pool	-4	-5	-8	-6	-3	-4	-3	-2	1	2	3	3	1	2	5	5
Alluvial pool	6	7	10	7	4	4	3	2	-1	-2	-4	-7	-2	-4	-8	-10
Island																
Pavement				3				-5								3
Macro lateral bar				3				-5								-3

Table 30 Morphologic unit change matrix for the alluvial generic channel type

Morphological unit	Sediment ratio high				Sediment ratio moderate				Sediment ratio reduced				Sediment ratio low			
	Base	Freshette	Annual	Flood	Base	Freshette	Annual	Flood	Base	Freshette	Annual	Flood	Base	Freshette	Annual	Flood
Braid bar		2	4	8		1	3	6		3	4	5		-1	-8	-12
Lateral point bar		2	4	8		1	3	6		-6	-8	-10		-2	-8	-10
Lee bar																
Bed core bar																
Anastomosing bar																
Rapid			-1													1
Isolated rock			-1													1
Bedrock pool																
Mixed pool			-1	-2			-1	-2		1	1	2			6	12
Alluvial pool		-4	-7	-14		-2	-5	-10		2	3	3		3	10	10
Bedrock pool																
Mixed pool																
Alluvial pool																
Island																
Pavement				-3				-5								3
Macro lateral bar				3				5								-3

Table 31 Morphologic unit change matrix for the anastomosing generic channel type

Morphological unit	Sediment ratio high				Sediment ratio moderate				Sediment ratio reduced				Sediment ratio low			
	Base	Freshette	Annual	Flood	Base	Freshette	Annual	Flood	Base	Freshette	Annual	Flood	Base	Freshette	Annual	Fllood
Braid bar			1	2			0.5	1		-0.5	-1	-2		-1	-2	-3
Lateral/point bar			1	2			0.5	1		-0.5	-1	-2		-1	-2	-3
Lee bar				1												-1
Bed core bar			1	3			1	5			1				-2	-8
Anastomosing bar			1	5			1	3			-1	-2			-2	-8
Rapid				-2				-1				1				2
Isolated rock				-1				-0.5				0.5				1
Bedrock distributary			-1	-1				-1								
Mixed distributary			-1	-3				-3				-1				-3
Alluvial distributary				1										3		-1
Bedrock distributary				-2			-0.5	1		1	1	3		1	3	4
Mixed distributary				-3			-0.5	1			1	1		1	2	3
Alluvial distributary				1				0.5								-1
Island																
Pavement			-2	-3			2	-3				2			4	10
Macro lateral bar																

Overall, the matrices may be seen to function in two ways. Active channel features respond to baseflows to generate minor changes: under low sediment inputs there will be minor erosion, while minor deposition will occur under high sediment input conditions. Changes are muted as the flows are not generally competent to redistribute sediment. As flows increase through freshettes to the annual maximum flows and finally flood flows, these changes are accentuated such that major erosion occurs under low sediment inputs and major deposition occurs under high sediment inputs (Fig. 51).

The macro-channel geomorphic system responds differently to the flow and sediment conditions. Under baseflows and freshettes there is no change to the macro-channel features as they are not inundated. Under flows of the order of the annual maximum flood there will be some minor erosion given low sediment inputs altering to minor deposition given high sediment inputs. Given an extreme flood these effects are intensified with major deposition under high sediment input conditions and major erosion under low sediment input conditions (Fig. 51).

A set of change rules have been imposed on each matrix as follows:

- Erosion of alluvial features within the active channel (braid bars, lateral bars, point bars, lee bars) results in a similar percentage gain of submerged morphologic features (bedrock pools, mixed pools, alluvial pools).

- Erosion of alluvial features beyond the active channel (bedrock core bars, anastomosing bars, islands, macro-channel lateral bars) results in a similar percentage gain in bedrock features (bedrock pavement, rapids, isolated rock).

- There is internal redistribution of sediment within the submerged features (bedrock pools, mixed pools, alluvial pools) in response to erosion and deposition.

- Where features are totally eroded, a hierarchy has been set up that transfers the loss to another alluvial feature. The order is: bedrock core bar, anastomosing bar, island and macro-channel lateral bar for the features beyond the active channel; and lee bar, lateral bar/point bar, alluvial pool, mixed pool, for in-channel morphologic units.

Switching between channel types is controlled by a set of critical morphological unit values. Two principal pathways are coded into the model, the first accounts for changes within anastomosing channels and the second between pool-rapid, braided and single-thread channels. The channel type switching rules are defined in Table 28. The proportional composition of bedrock core bars (80%) and rapids (2%) are used as the controlling geomorphic units to define the switching between anastomosing and pool-rapid, and pool-rapid and alluvial generic channel types, respectively.

A factor has been introduced that controls the overall extent of morphological change in response to a certain annual flow series. This factor reduces or increases the rate of change for all units based on the original matrix values and is designed to prevent the model from eroding or depositing units at a rate that is considered unrealistic. This prevents the model from operating the erosive redistribution rules too frequently following the complete loss of a unit.

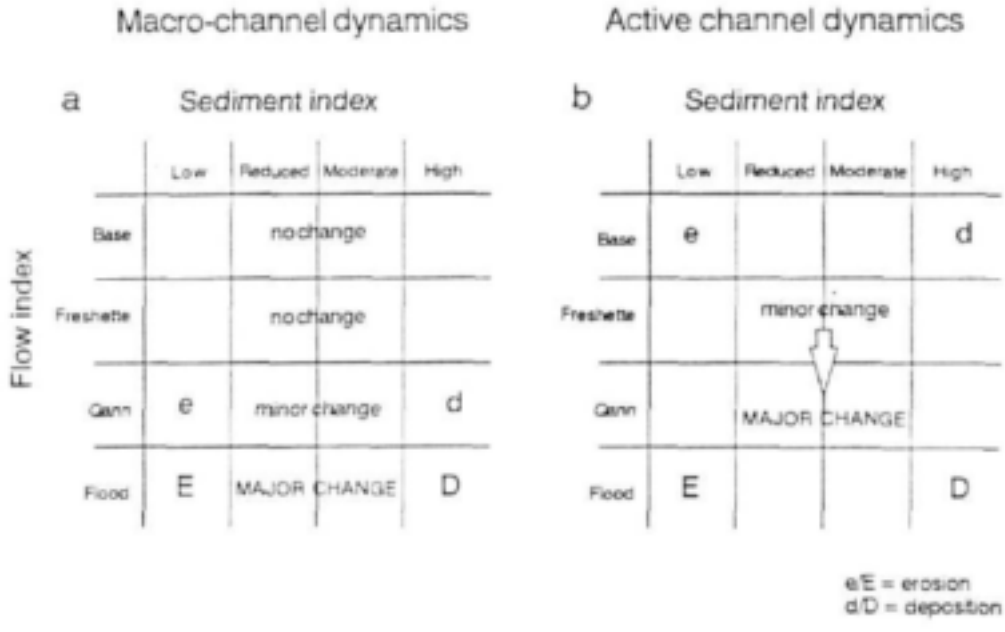

Figure 51 Active and macro-channel geomorphological response to flow and sediment regimes

In summary, the model initially assigns the base geomorphological state to the cell under investigation (Table 26). An annual timestep is then applied to alter the geomorphological state in response to the flow and sediment categories (Table 27). The geomorphic composition is changed according to the unit percentage change values corresponding to the cell generic channel type (Tables 29 to 31). An internal check is applied to determine the redistribution of sediment between bars and pool/distributary sediments. If a unit is eroded completely and falls below zero, then the erosion redistribution rules are invoked with the eroded unit set to zero and the excess erosion transferred to the next most vulnerable unit in the erosion hierarchy. Internal consistency is thus maintained. Finally, the model provides a check for change of channel type (Table 28) prior to invoking the next time step (Fig. 52).

7.4 Model verification

The model is tested by comparison with historical records of geomorphological change derived from aerial photographic records, and also using the erosion and sedimentation trends predicted by SEDFLO (refer to chapter 5). The first test involves the prediction of change in morphological composition for five representative channel type cells (one for each of the common channel types along the Sabie River) from 1932 to 1996. The results are compared with measurements of change in unconsolidated bar area recorded using aerial photographs over the periods 1940/44 to 1974, 1974 to 1986 and 1986 to 1996 (Table 32). The second test involves a more detailed

comparison of trends in bulk erosion and deposition as predicted for each representative cell by SEDFLO (Fig. 53) against the rule based unconsolidated sediments dynamics. Finally, conclusions are drawn concerning the stability of macro-channel features in response to the periods having experienced flooding during 1936 and 1939, 1954 and 1960, and 1985 and 1986. It is during these large flood events that macro-channel features are expected to be altered by fluvial processes, whereas at lower flows the stage does not inundate these units.

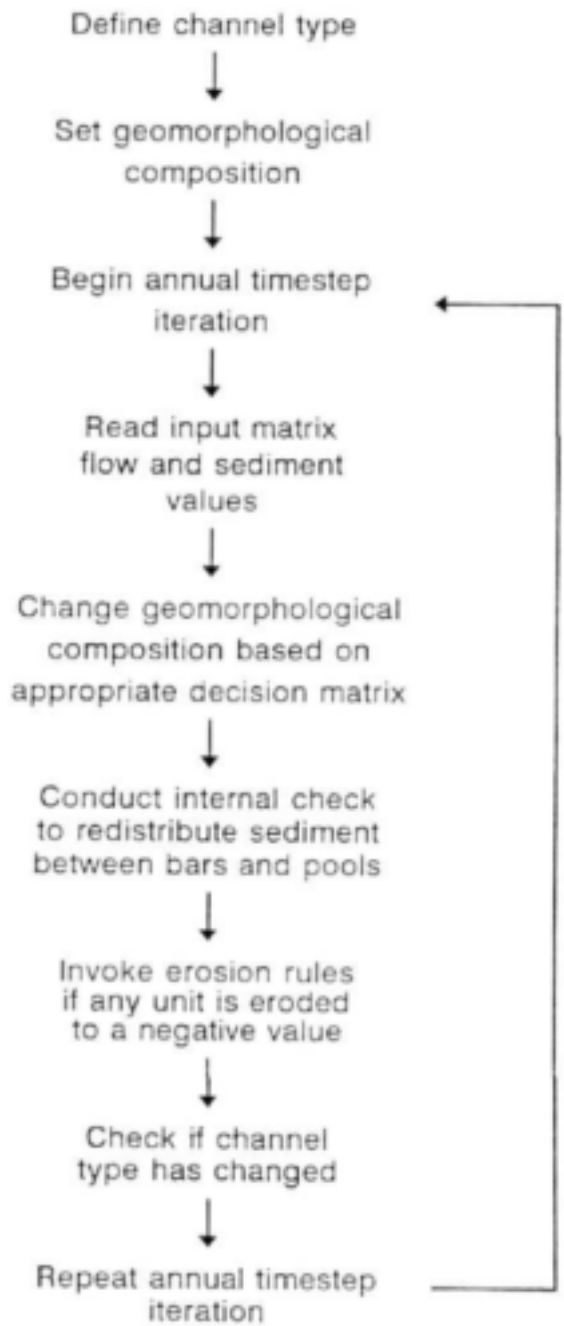

Figure 52 Flow diagram for the operation of the rule based geomorphological unit change model.

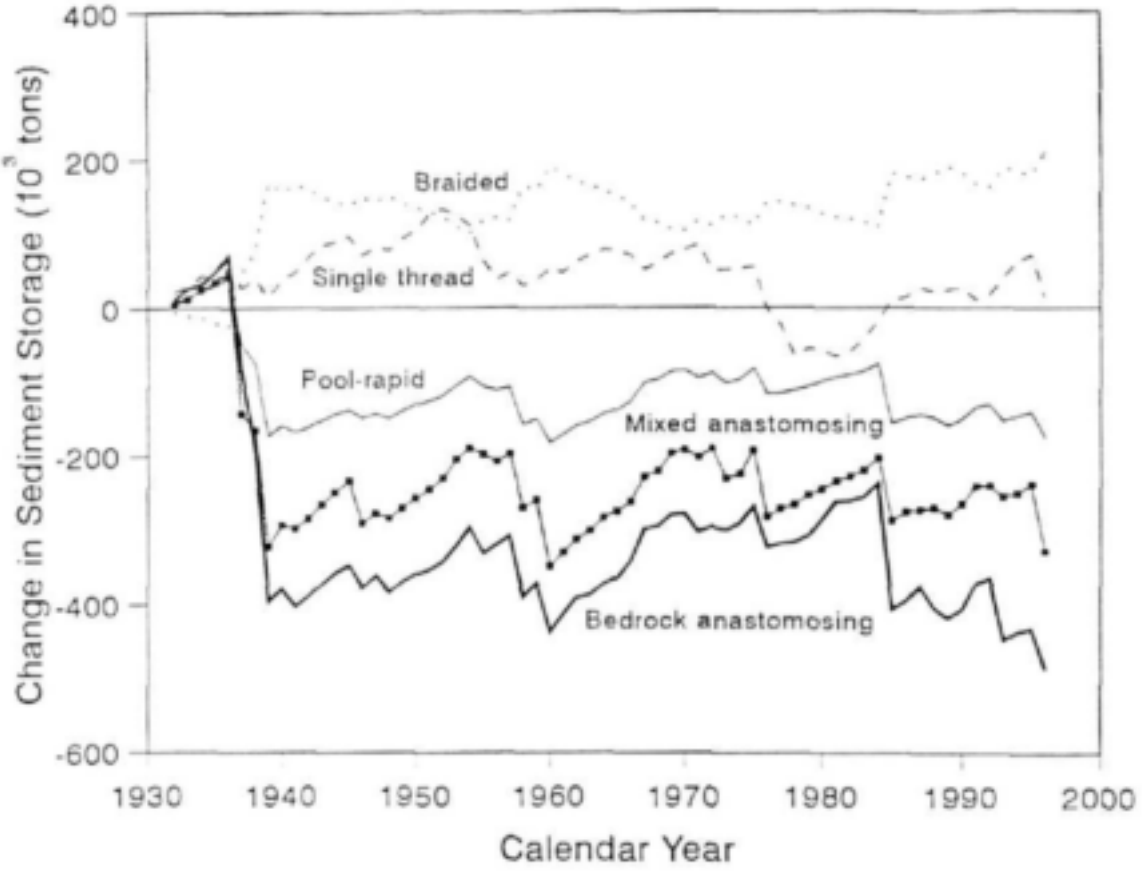

Figure 53 Modelled change in sedimentation using SEDFLO for each of the representative channel type cells along the Sabie River.

Table 32 Aerial photographic records of geomorphological change for representative channel type cells along the Sabie River

Channel type	*Aerial photographic record*			
	1940/44 to 1974	1974 to 1986	1944 to 1986	1986 to 1996
Braided	✓	✓	✓	✓
Pool-rapid	✓	✓	✓	✓
Single-thread			✓	✓
Mixed anastomosing	✓	✓	✓	✓
Bedrock anastomosing			✓	✓

7.4.1 Input data

The hydrological and sediment flux input data are calculated in three ways to generate flow and sediment input matrices:

The first input data matrix (Table 33) is based on the annual flow data (categorised into base flows, freshettes, annual flood flows and extreme flood flows based on the standard deviation from the median, Table 27), combined with sediment input data which is given by the sum of the upstream flux and tributary contributions (Fig. 29) as modelled by SEDFLO.

The construction of matrix 1 input data is summarised as follows:

- The derivation of a cell based annual flow index based on four flow categories.
- The derivation of a cell based sediment index based on four sediment categories that include upstream and tributary contributions.

Table 33 Matrix 1 input data

Sediment\flow index		Base flow (1)	Freshette flow (2)	Annual flow (3)	Flood flow (4)
Low sediment input	(1)	1,1	1,2	1,3	1,4
Reduced sediment input	(2)	2,1	2,2	2,3	2,4
Moderate sediment input	(3)	3,1	3,2	3,3	3,4
High sediment input	(4)	4,1	4,2	4,3	4,4

Table 33 defines sixteen sub-categories of conditions which, for the purpose of constructing the following matrices, are numbered in order from left to right in succeeding rows, i.e. (1,1) is sub-category 1, (1,4) is sub-category 4, (2,1) is sub-category 5, and so on up to (4,4) which is sub-category 16. The second (Table 34) and third (Table 35) input data matrices utilise the change in sediment storage data predicted by SEDFLO for each representative channel type cell. Several combinations of flow and dynamic sediment storage may result in similar patterns of channel change, and therefore no unique equivalent to the matrix presented in Table 33 exists. Consequently, matrix 2 places the emphasis for change on the influence of the sediment regime, whereas matrix 3 places the emphasis for change on the flow regime. For example, if the annual change in sediment storage for a particular cell falls into sub-category 8, then this is equivalent to an annual flow-reduced sediment input according to the matrix 2 input (Table 34), and a base flow-reduced sediment input according to the matrix 3 input (Table 35).

The construction of the input data for matrices 2 and 3 is summarised as follows:

- The derivation of a cell based annual change in sediment storage index based on sixteen categories corresponding to the number of possible combinations in the 4 x 4 input matrix (Table 33).

Table 34 Matrix 2 input data

Sediment\flow index		Base flow (1)	Freshette flow (2)	Annual flow (3)	Flood flow (4)
Low sediment input	(1)	1	2	4	7
Reduced sediment input	(2)	3	5	8	11
Moderate sediment input	(3)	6	9	12	14
High sediment input	(4)	10	13	15	16

Table 35 Matrix 3 input data

Sediment\flow index		Base flow (1)	Freshette flow (2)	Annual flow (3)	Flood flow (4)
Low sediment input	(1)	7	5	2	1
Reduced sediment input	(2)	8	6	4	3
Moderate sediment input	(3)	9	11	13	14
High sediment input	(4)	10	12	15	16

7.5 Results and discussion

The geomorphological changes predicted for each representative channel type cell are presented in Figs. 54 to 68, where Figs. 54 to 58, 59 to 63, and 64 to 68 provide the results of applying matrix 1 (Table 33), 2 (Table 34) and 3 (Table 35) input data, respectively. The change rate correction factors given in Table 36 are applied to moderate the change in geomorphological composition as tabulated in Table 29, 30 and 31.

Table 36 Rate of change correction factors

Generic channel type	Factor
Alluvial	0.3
Pool-rapid	0.3
Anastomosing	0.6

Under these conditions for example, a braid bar in the alluvial generic channel type matrix (Table 30) subjected to a flood flow regime and high sediment flux will display an annual change of 2.4% (0.3 (Table 36) multiplied by 8% (Table 30)).

In all cases, considerable initial change is predicted which moderates and becomes slightly more stable. The degree of change also varies between channel types, with the pool-rapid cell displaying a greater tendency to change its morphologic composition than the other channel type cells. Similarly, individual morphologic units can be seen to display differing sensitivities with the active channel unconsolidated sedimentary features (braid and lateral bars) changing at a more rapid rate than consolidated sedimentary features such as macro-channel lateral bars and bedrock core bars.

The results of applying input matrix 1 (Figs. 54 to 58) show that for the single-thread channel type cell, morphological diversity is maintained with the loss of some lateral bars to braid bars during the first twenty years of simulation, while alluvial pools also decline as the in-channel bar features are enlarged. The macro-channel features remain largely unchanged. Results for the bedrock anastomosing channel type cell reveal a tendency to erode the unconsolidated in-channel sediment to create bedrock distributaries, while bedrock core bars are maintained. The braided cell displays an increase in the dominance of braid bars, while macro-channel features are maintained. The pool-rapid channel type cell reveals a more complex pattern of change, with variations in the dominance of braid and lateral bars in the active channel at the expense of mixed and alluvial

pools. The macro-channel features again remain stable. Finally, the mixed anastomosing channel type cell appears to accumulate unrealistic proportions of sediment in the active channels as well as excessive coverage by anastomosing bars.

The results from the application of input matrix 2 (Table 34) for the single thread cell reveal an accumulation of unconsolidated bars at the expense of alluvial pools (Fig. 59). In time, lateral bars are eroded to form pools and braid bar area declines. The bedrock anastomosing cell (Fig. 60) shows a rapid loss of in-channel sediment as bedrock pools begin to dominate, while the bedrock pavement also expands to dominate the macro-channel. The braided cell displays excessive sedimentation of lateral bar deposits (Fig. 61). In the pool-rapid cell (Fig. 62), morphological diversity is maintained although a slight alluviation of active channel pools and increased bar coverage is predicted. The mixed anastomosing cell displays marginal changes in morphology, with an initial increase followed by a loss of in-channel bar deposits (Fig. 63).

Application of input matrix 3 (Table 35) shows a rapid and unrealistic rise of in-channel bar deposits in the single thread cell (Fig. 64). The morphology in the bedrock anastomosing cell appears more stable, with the initial loss of in-channel sediment as pools are scoured and a marginal build up of bedrock pavement (Fig. 65). The braided cell also displays unreasonable changes, with lateral bars covering much of the active channel area (Fig. 66). Alluvial pools, braid and lateral bars dominate the geomorphology of the pool-rapid cell (Fig. 67). Finally, the mixed anastomosing cell displays a gradual loss of sediment to expanding bedrock pools in the distributaries, while macro-channel features remain stable (Fig. 68).

In general, the predicted responses to input matrix 3 are unrealistic, sediment either accumulates too rapidly or integral geomorphological features are eroded (alluvial pools in the mixed anastomosing cell). Matrices 2 and 3 predict more realistic morphological changes.

Table 37 Abbreviations for the geomorphological units used in Figs. 54 to 68.

Abbreviation	Geomorphological unit	Abbreviation	Geomorphological unit
brd	Braid bar	bedp	Bedrock pool
lat	Lateral bar	mixp	Mixed pool
lee	Lee bar	allp	Alluvial pool
bcb	Bedrock core bar	isl	Island
anas	Anastomosing bar	pmt	Pavement
rap	Rapid	mlt	Macro-channel lateral bar
iso	Isolated rock		

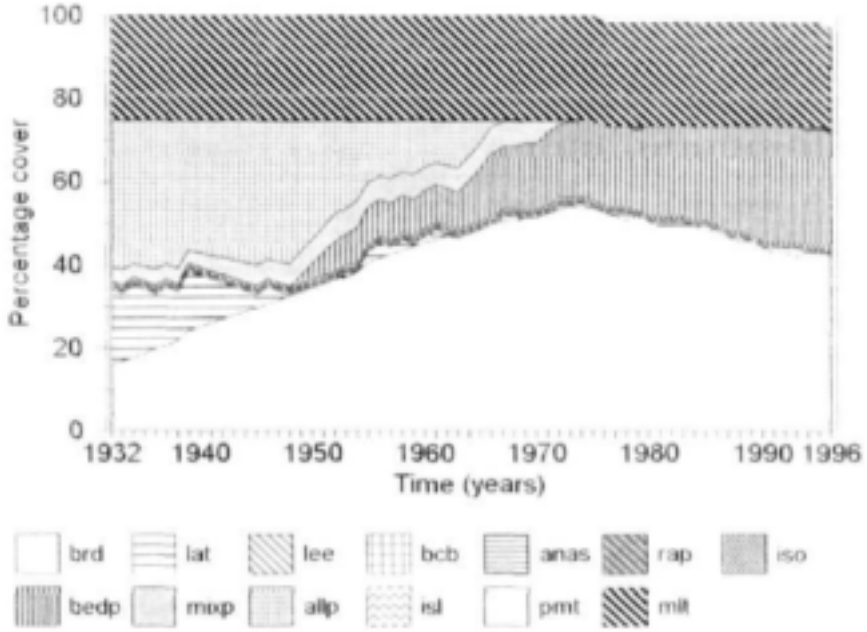

Figure 54 Predicted morphologic unit change for the single-thread representative channel type cell based on input matrix 1 (Table 33), with the abbreviations for the morphologic units given in Table 37.

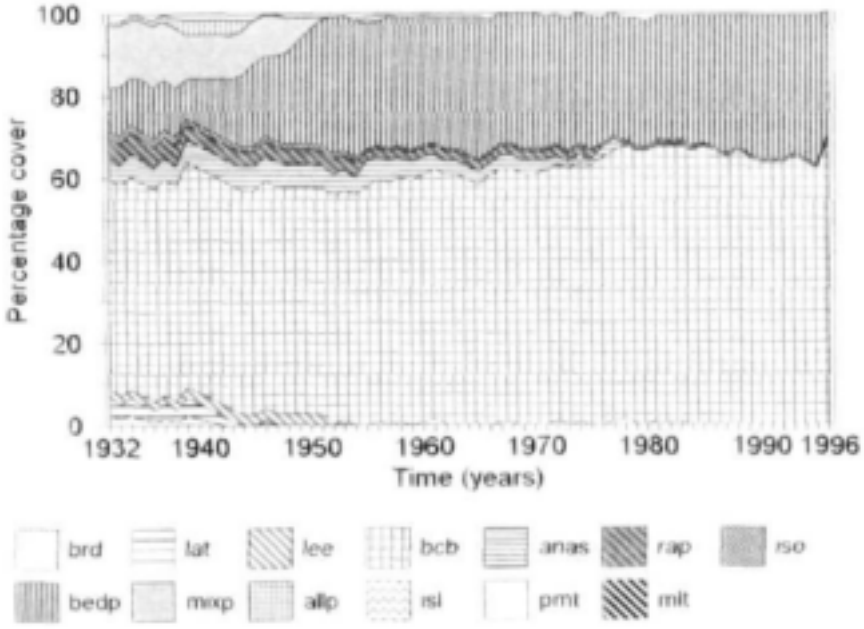

Figure 55 Predicted morphologic unit change for the bedrock anastomosing representative channel type cell based on input matrix 1 (Table 33), with the abbreviations for the morphologic units given in Table 37.

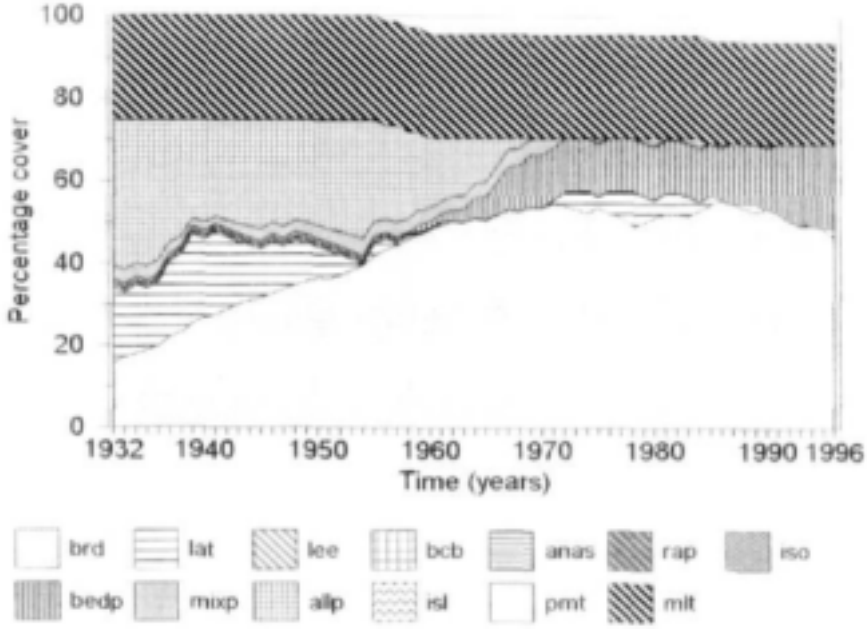

Figure 56 Predicted morphologic unit change for the braided representative channel type cell based on input matrix 1 (Table 33), with the abbreviations for the morphologic units given in Table 37

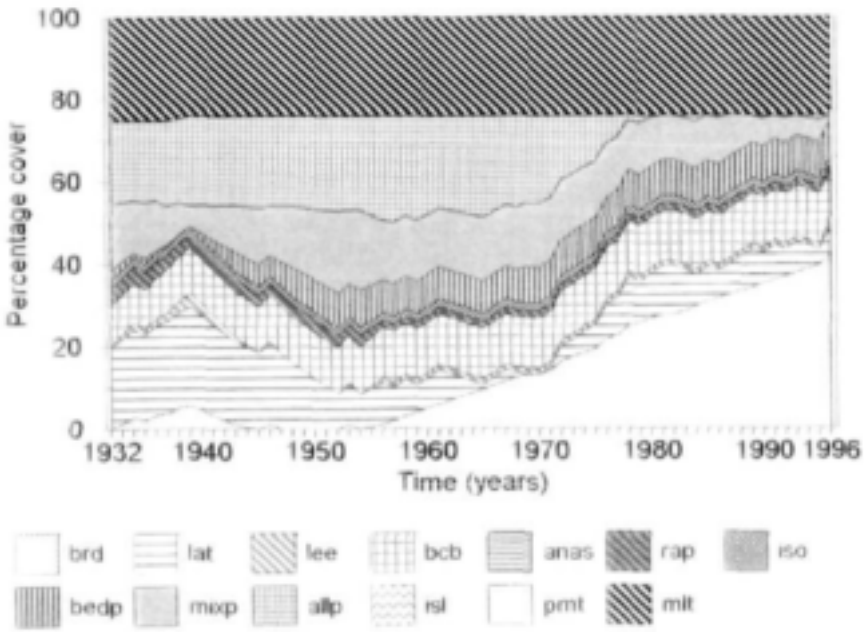

Figure 57 Predicted morphologic unit change for the pool-rapid representative channel type cell based on input matrix 1 (Table 33), with the abbreviations for the morphologic units given in Table 37

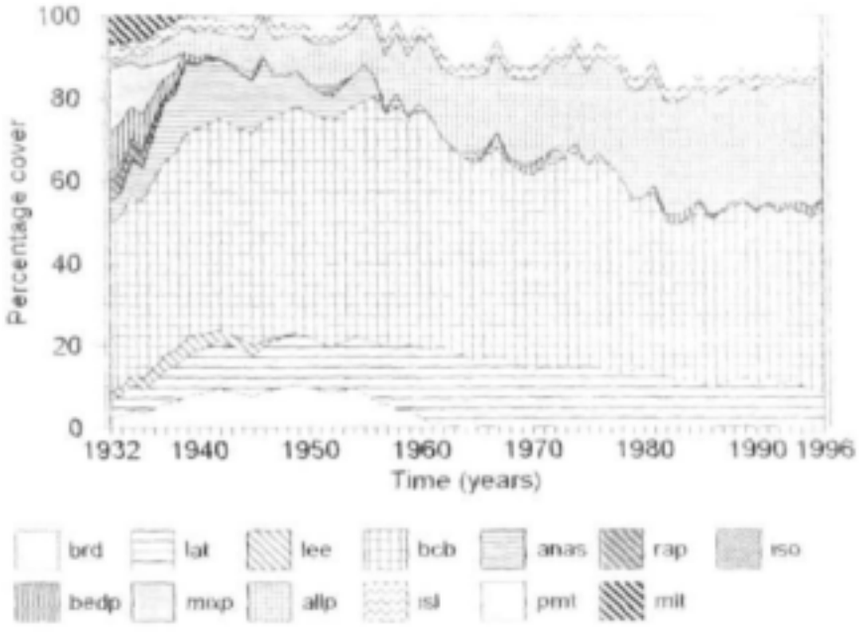

Figure 58 Predicted morphologic unit change for the mixed anastomosing representative channel type cell based on input matrix 1 (Table 33), with the abbreviations for the morphologic units given in Table 37

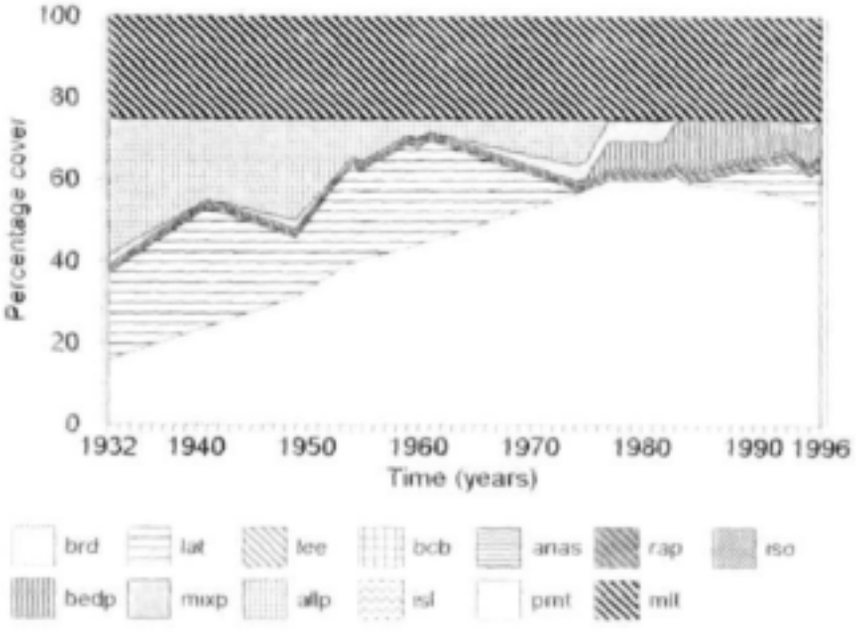

Figure 59 Predicted morphologic unit change for the single-thread representative channel type cell based on input matrix 2 (Table 34), with the abbreviations for the morphologic units given in Table 37

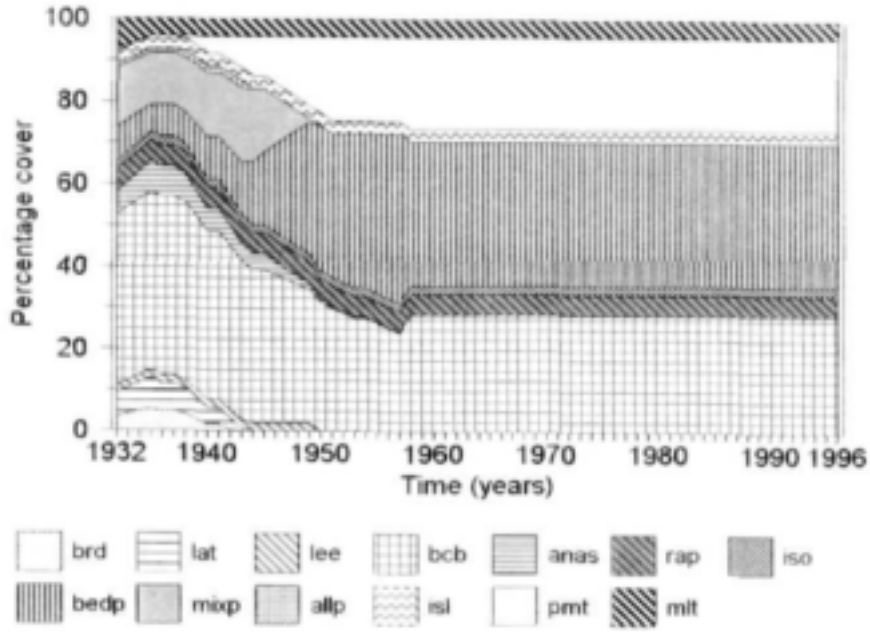

Figure 60 Predicted morphologic unit change for the bedrock anastomosing representative channel type cell based on input matrix 2 (Table 34), with the abbreviations for the morphologic units given in Table 37.

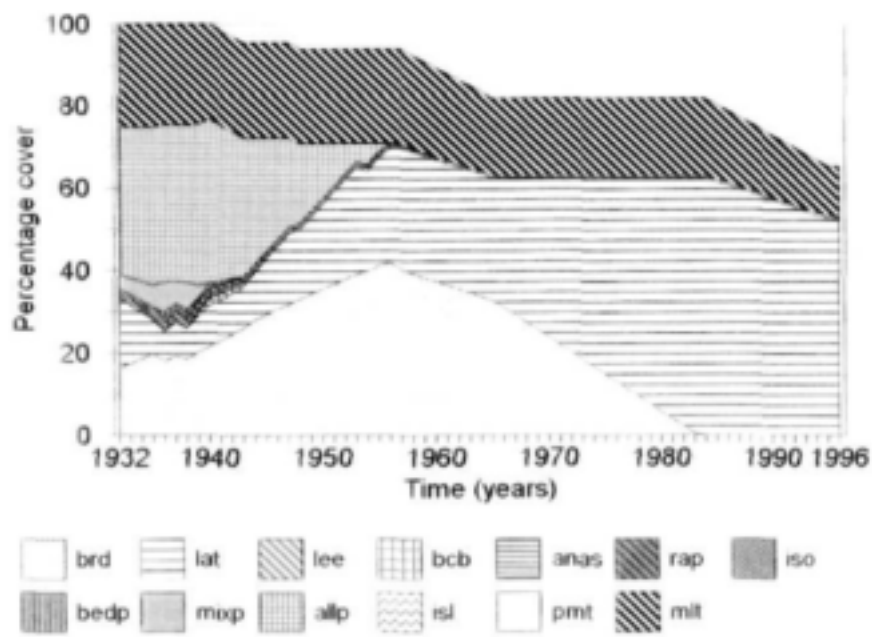

Figure 61 Predicted morphologic unit change for the braided representative channel type cell based on input matrix 2 (Table 34), with the abbreviations for the morphologic units given in Table 37.

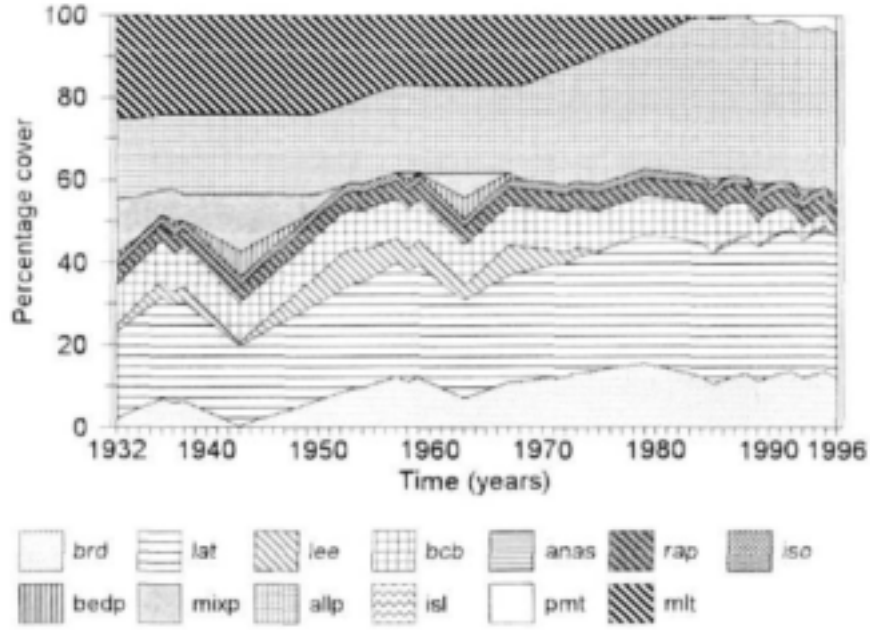

Figure 62 Predicted morphologic unit change for the pool-rapid representative channel type cell based on input matrix 2 (Table 34), with the abbreviations for the morphologic units given in Table 37.

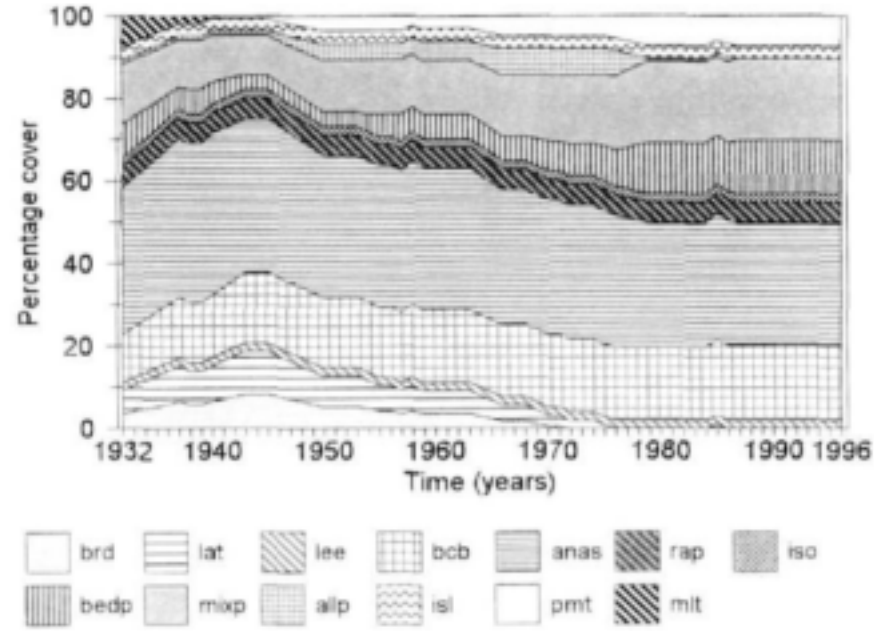

Figure 63 Predicted morphologic unit change for the mixed anastomosing representative channel type cell based on input matrix 2 (Table 34), with the abbreviations for the morphologic units given in Table 37.

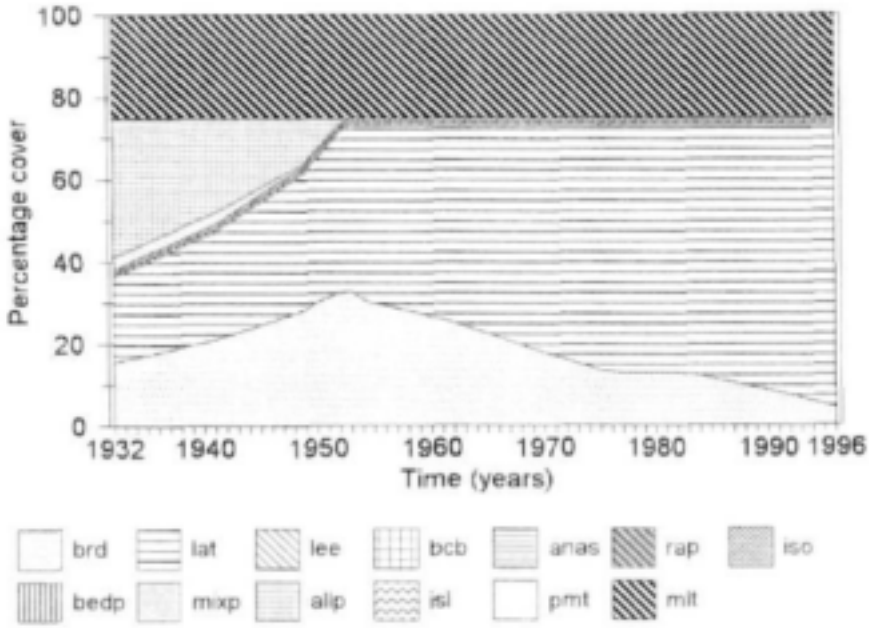

Figure 64 Predicted morphologic unit change for the single-thread representative channel type cell based on input matrix 3 (Table 35), with the abbreviations for the morphologic units given in Table 37.

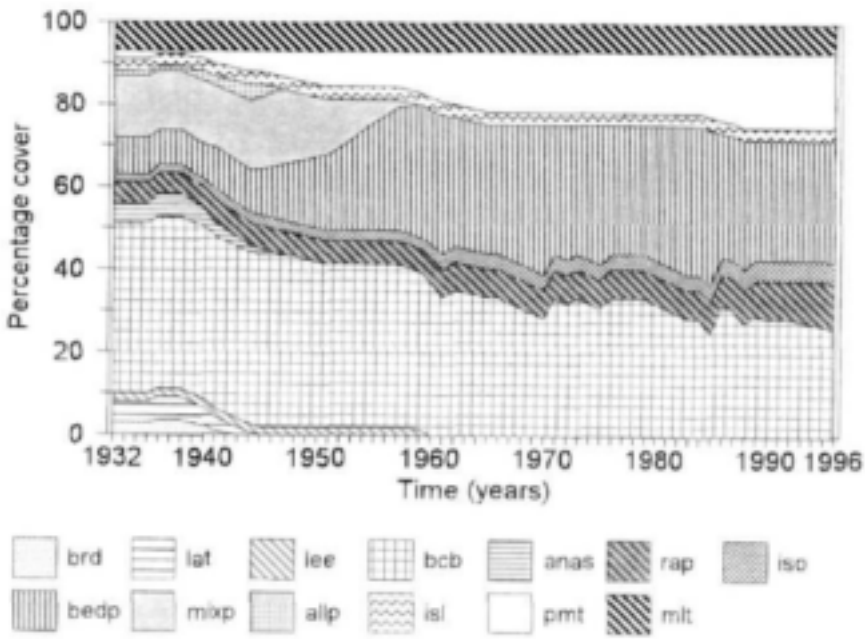

Figure 65 Predicted morphologic unit change for the bedrock anastomosing representative channel type cell based on input matrix 3 (Table 35), with the abbreviations for the morphologic units given in Table 37.

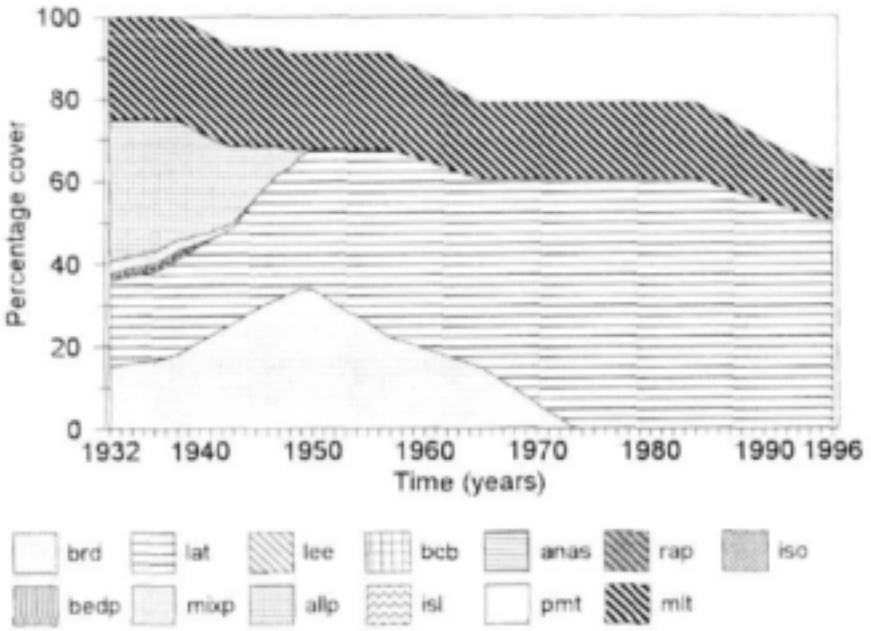

Figure 66 Predicted morphologic unit change for the braided representative channel type cell based on input matrix 3 (Table 35), with the abbreviations for the morphologic units given in Table 37.

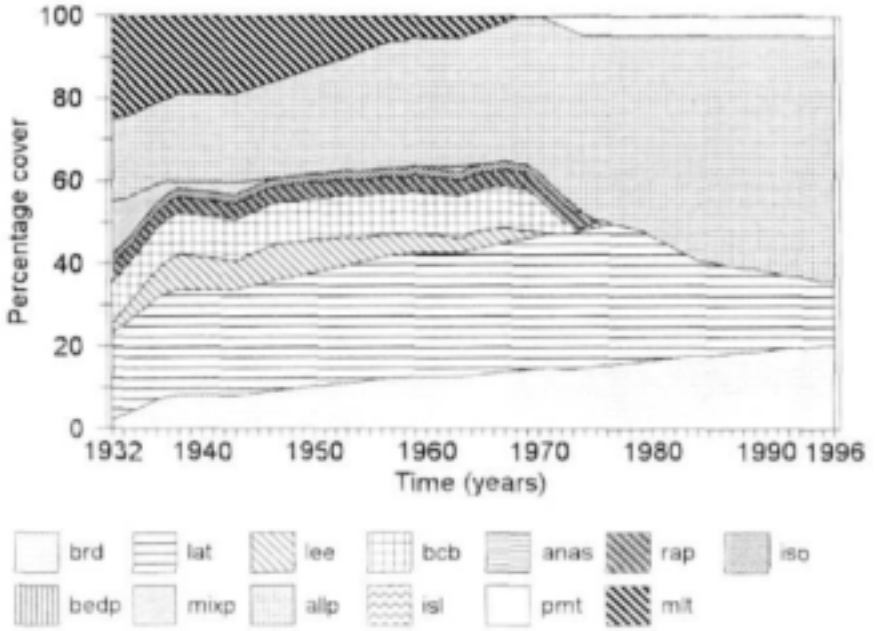

Figure 67 Predicted morphologic unit change for the pool-rapid representative channel type cell based on input matrix 3 (Table 35), with the abbreviations for the morphologic units given in Table 37.

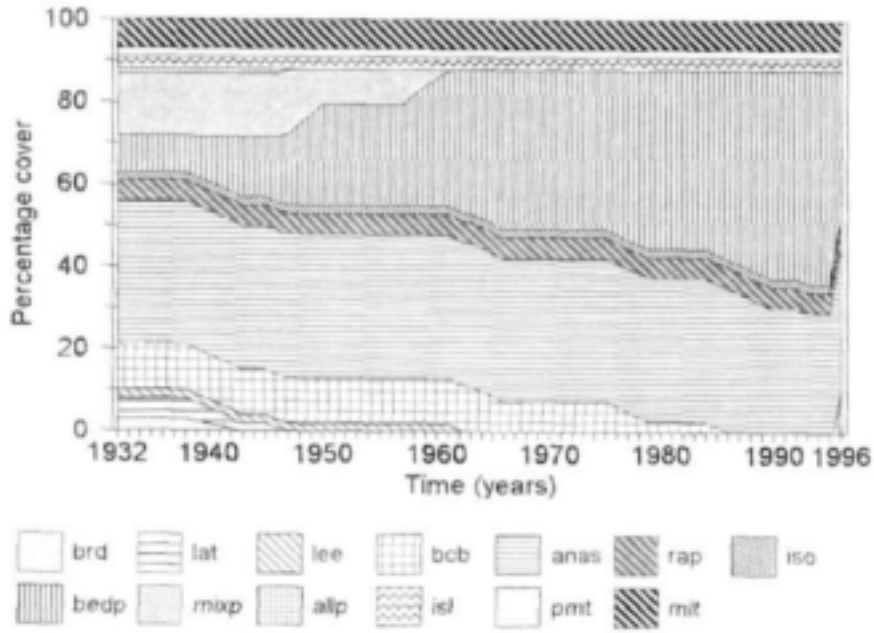

Figure 68 Predicted morphologic unit change for the mixed anastomosing representative channel type cell based on input matrix 3 (Table 35), with the abbreviations for the morphologic units given in Table 37.

The modelled changes were compared with the aerial photographic record and against the expected response to periods of low and high flows. Comparison with changes derived from the aerial photographs (Figs. 69 to 73) indicate that input matrix 1 predicts well up to 1974 for the single-thread cell, while matrices 2 and 3 provide improved predictions through to 1996. Historical change in the bedrock anastomosing cell indicates initial sedimentation to 1986 after which the cell morphology remains stable to 1996. The results from the input matrices indicate erosion to 1974 followed by a period of stability. Aerial photographs of the braided cell show no change in sediment area up to 1974 followed by increased alluviation. All the input matrices result in this trend to 1974 but predict slight erosion between 1974 and 1996. Matrices 1 and 3 predict the observed change in the pool-rapid cell well. In contrast, the predicted changes correspond poorly with observed change in the mixed anastomosing cell. Generally, matrix 3 predicts the observed changes most consistently particularly in the pool-rapid and single thread cells.

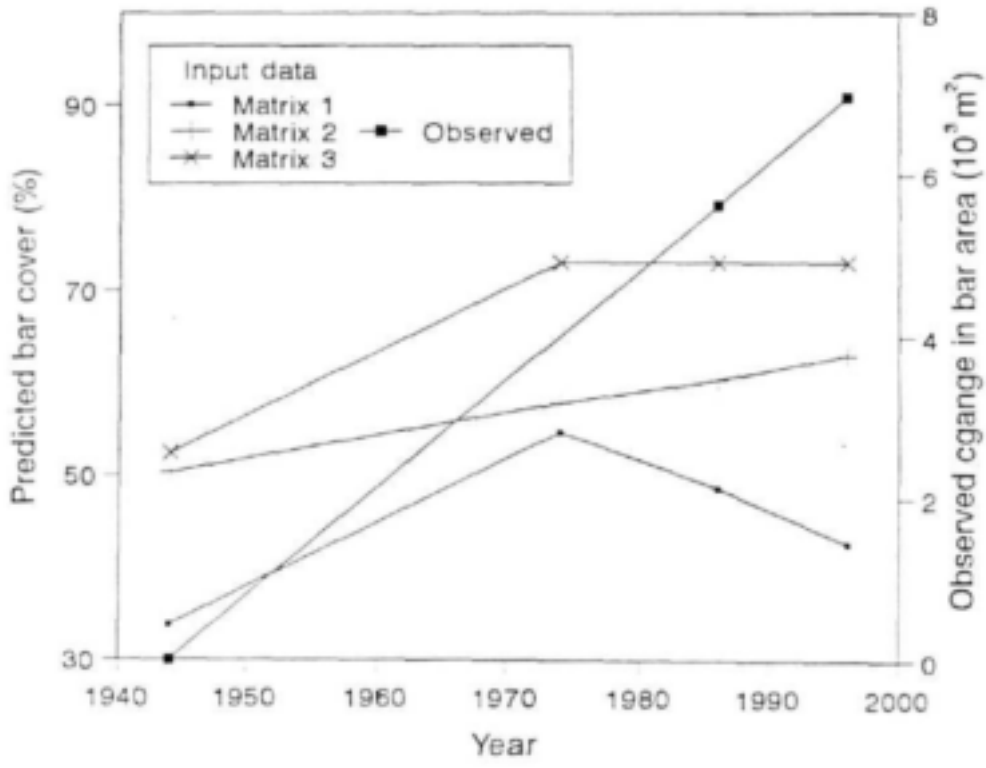

Figure 69 Comparison between observed and predicted change to unconsolidated sediment in the single-thread channel type cell.

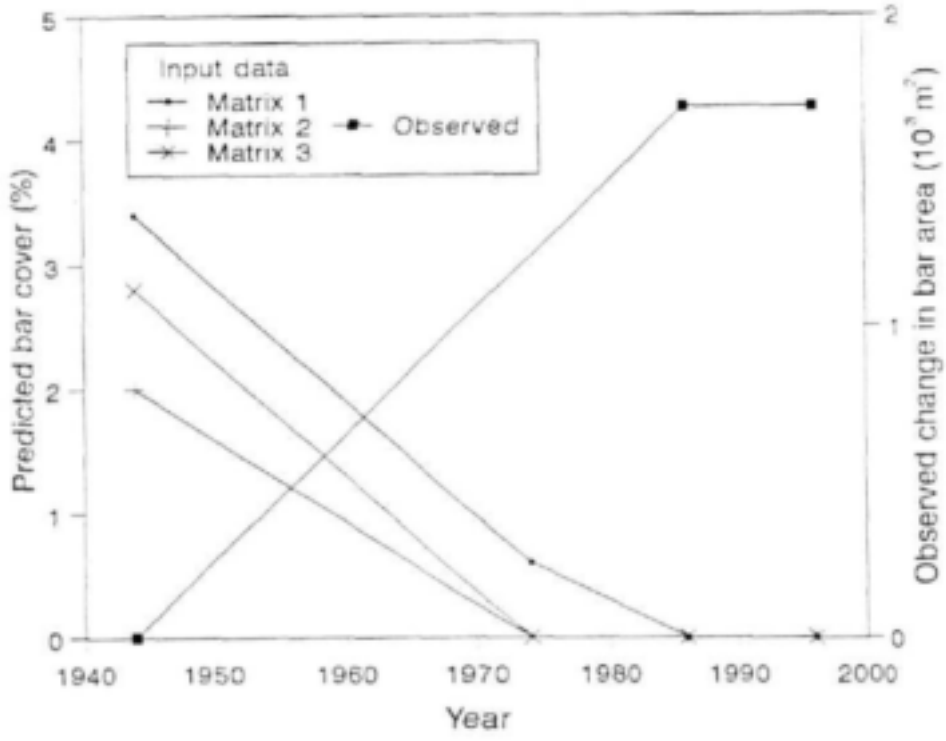

Figure 70 Comparison between observed and predicted change to unconsolidated sediment in the bedrock-anastomosing channel type cell.

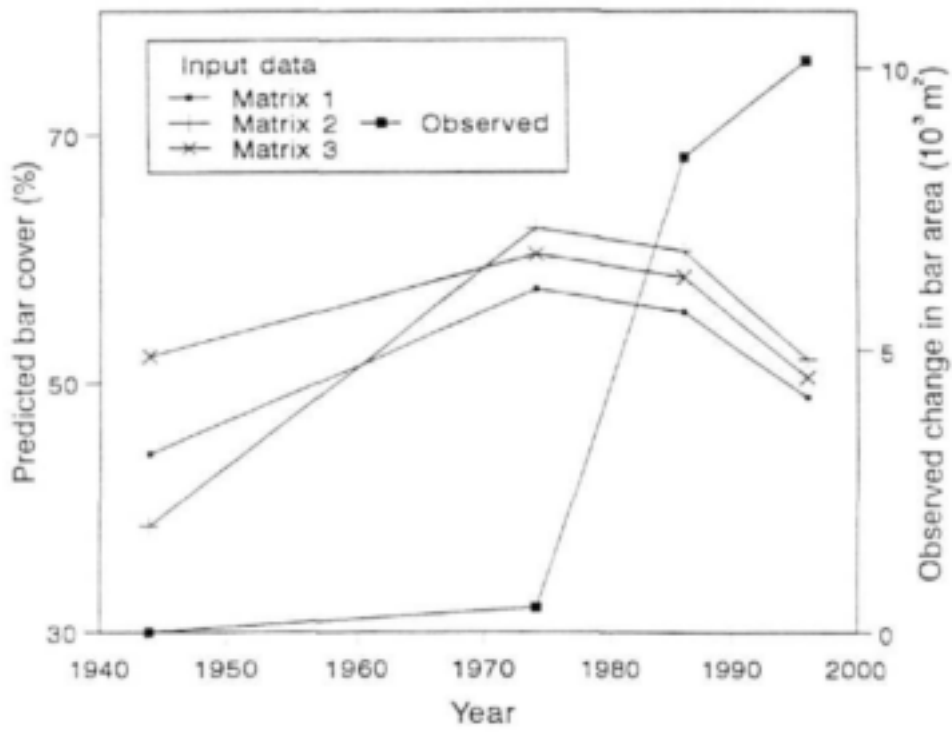

Figure 71 Comparison between observed and predicted change to unconsolidated sediment in the braided channel type cell.

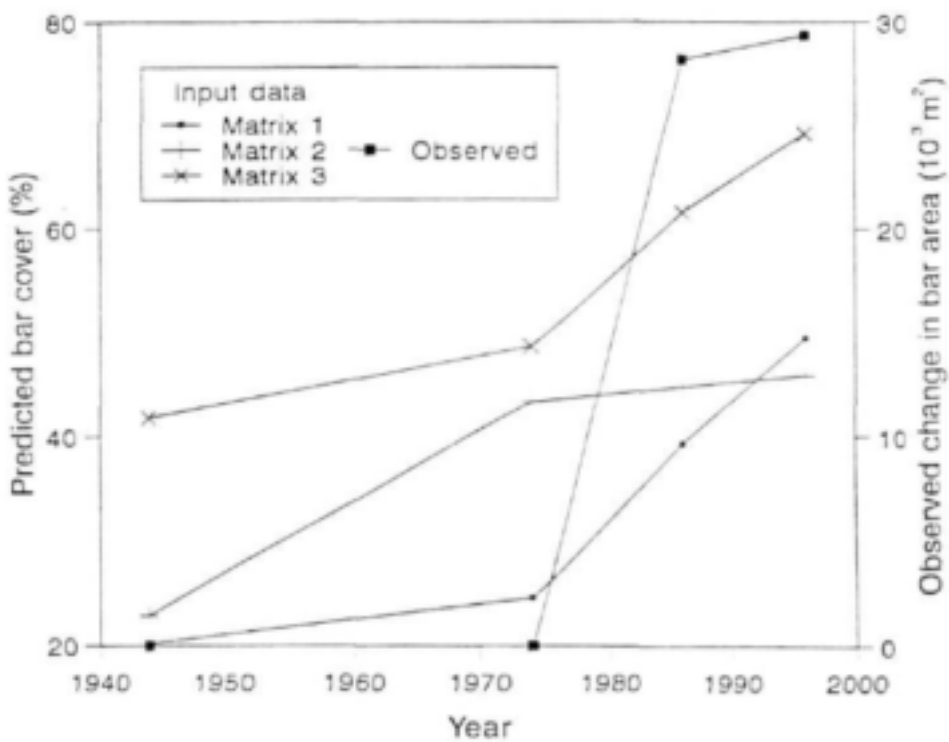

Figure 72 Comparison between observed and predicted change to unconsolidated sediment in the pool-rapid channel type cell.

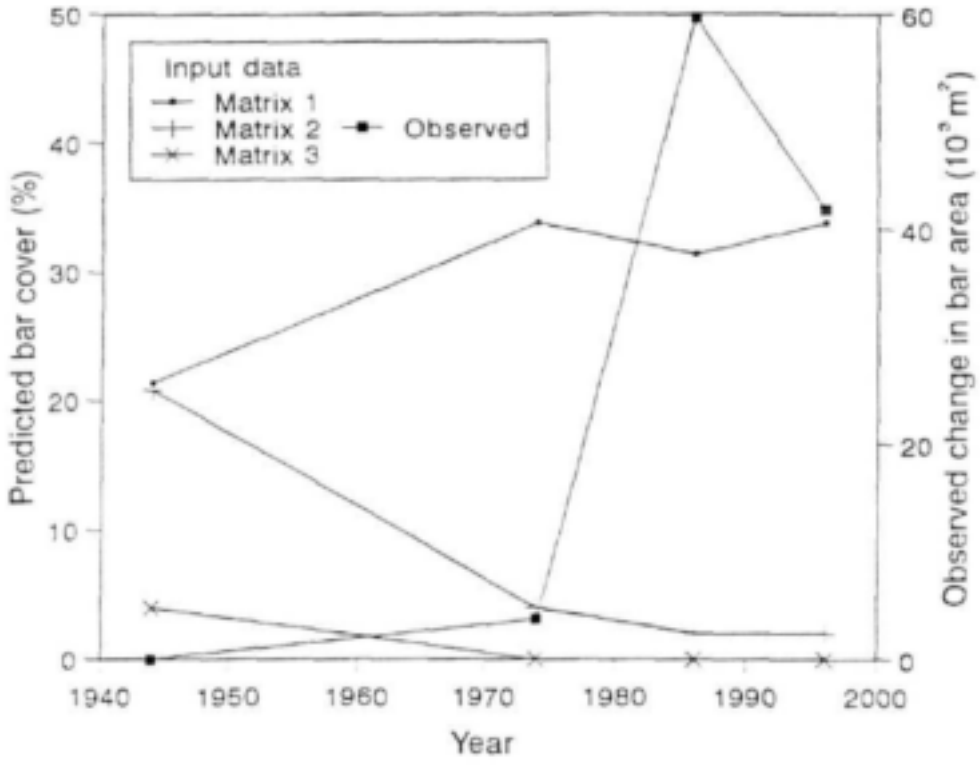

Figure 73 Comparison between observed and predicted change to unconsolidated sediment in the mixed-anastomosing channel type cell.

The erosion and sedimentation trends predicted by SEDFLO indicate periods of reduced flow magnitude and frequency from 1932 to 1936, 1939 to 1954, 1960 to 1975, 1976 to 1984 and 1985 to 1995. Higher flows are evident over the periods 1936 to 1939, 1954 to 1960, 1975 to 1976, 1984 to 1985 and 1995 to 1996 (Fig. 40). The model predictions (Figs. 74 to 78) have been examined to determine their ability to replicate the trends in erosion and deposition associated with the periods of reduced and elevated flows.

Results for the single-thread cell (Fig. 74) show a general poor correspondence between the SEDFLO and rule based model trends. Application of input matrix 3 produces increased sedimentation between 1939 and 1954, the reduction in unconsolidated sediment between 1954 and 1960, and marginal changes thereafter. In the bedrock anastomosing cell there is little correspondence between geomorphological change and the sediment and flow regime, with changes again subdued after 1960 (Fig. 75). Predictions of morphological change are improved for the braided cell, particularly using input matrix 1. Matrices 2 and 3 fail to model the effects of the 1939 to 1960 flows (Fig. 76). Matrix 2 results in a high correspondence to the predicted sediment changes in the pool-rapid cell, whereas matrices 1 and 3 result in more subdued changes (Fig. 77). All predictions of geomorphological change show a poor comparison with the changes in sedimentation in the mixed anastomosing cell (Fig. 78).

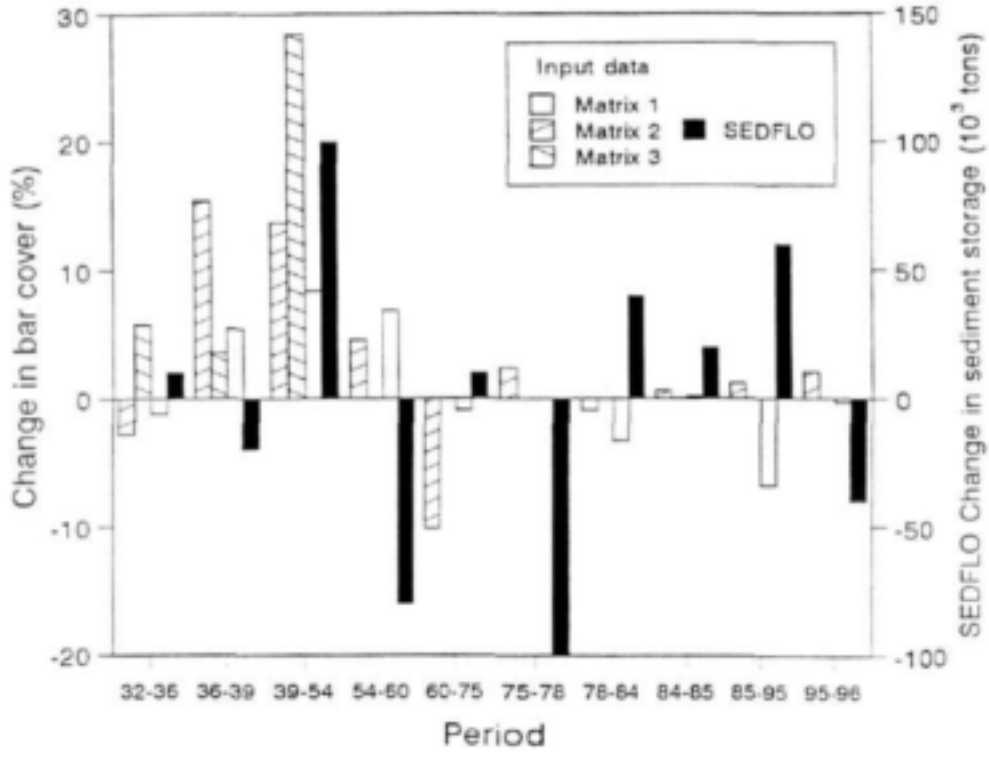

Figure 74 Comparison of trends in erosion and deposition predicted by SEDFLO and the rule based geomorphology model for the single-thread channel type cell.

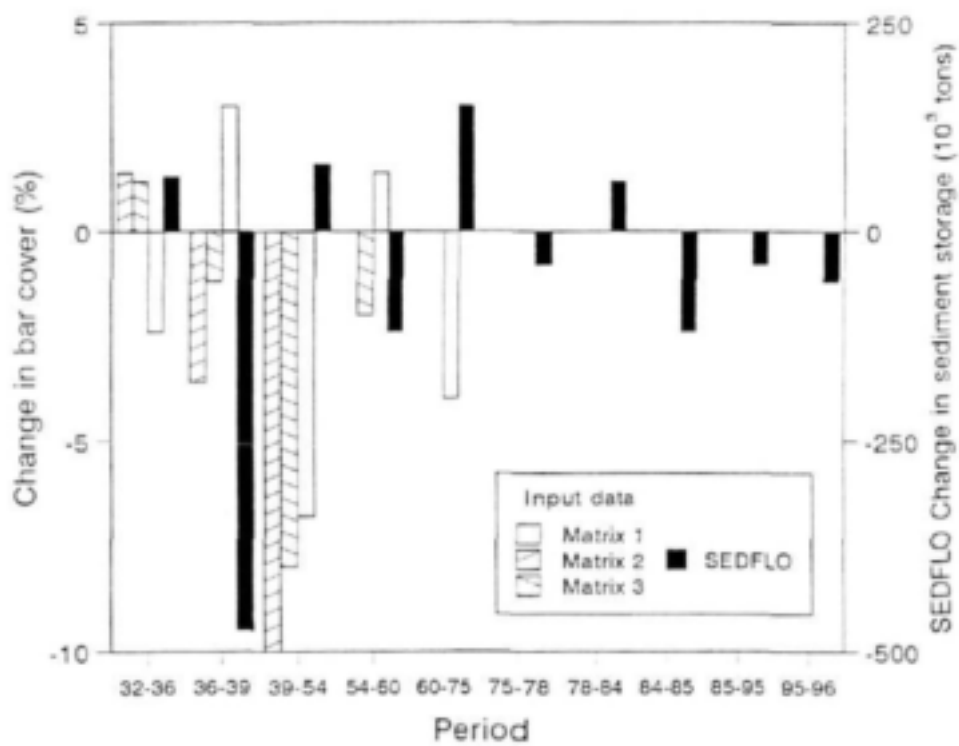

Figure 75 Comparison of trends in erosion and deposition predicted by SEDFLO and the rule based geomorphology model for the bedrock-anastomosing channel type cell.

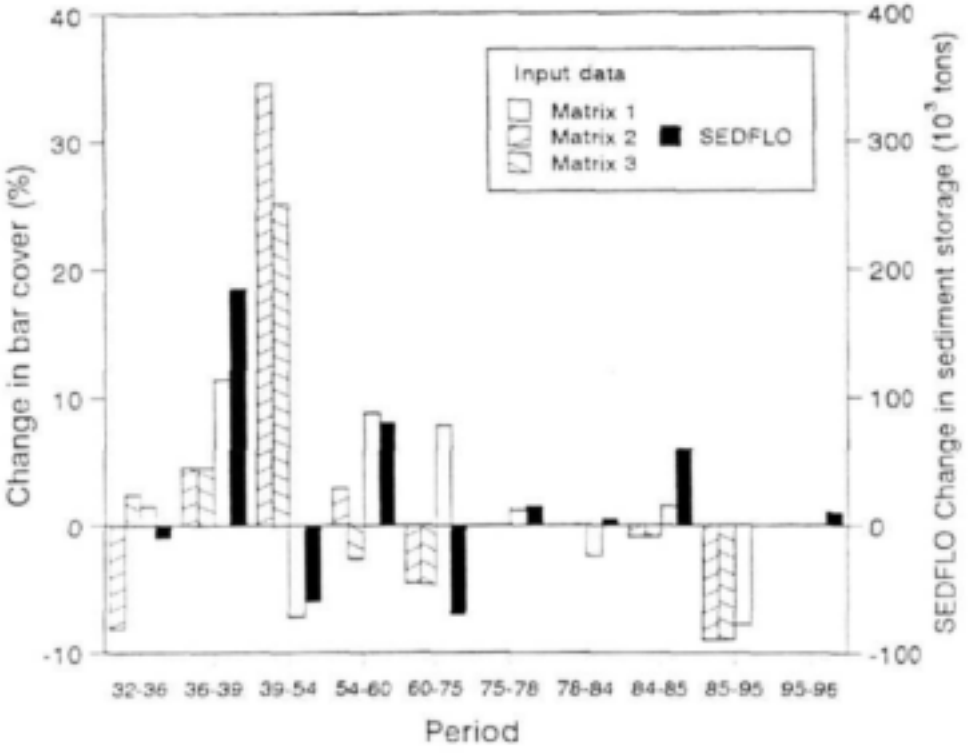

Figure 76 Comparison of trends in erosion and deposition predicted by SEDFLO and the rule based geomorphology model for the braided channel type cell

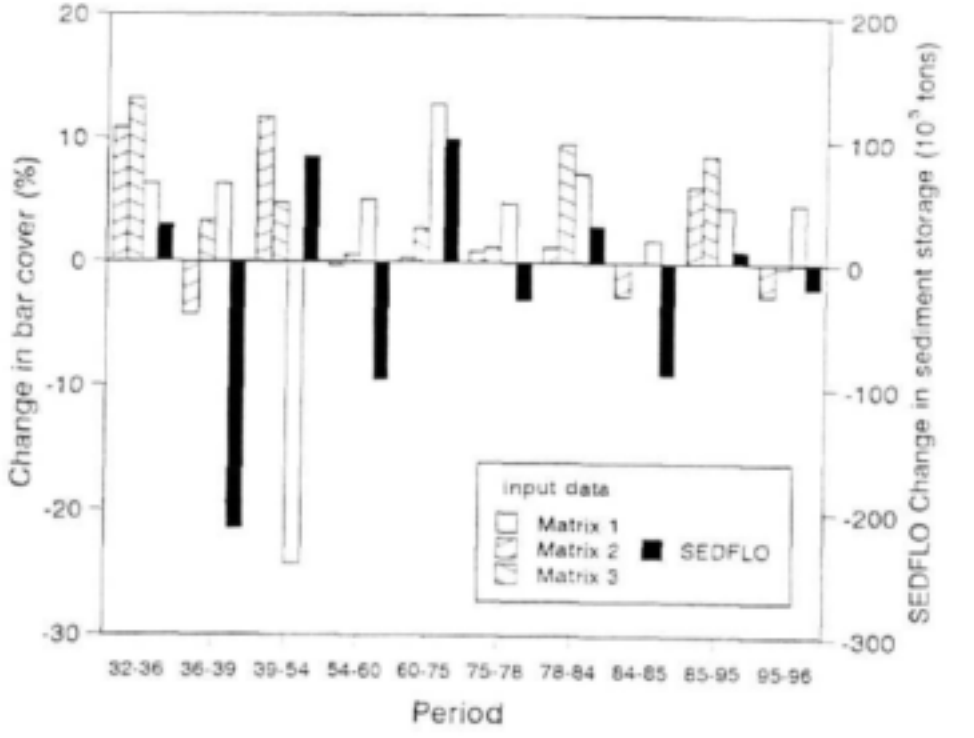

Figure 77 Comparison of trends in erosion and deposition predicted by SEDFLO and the rule based geomorphology model for the pool-rapid channel type cell

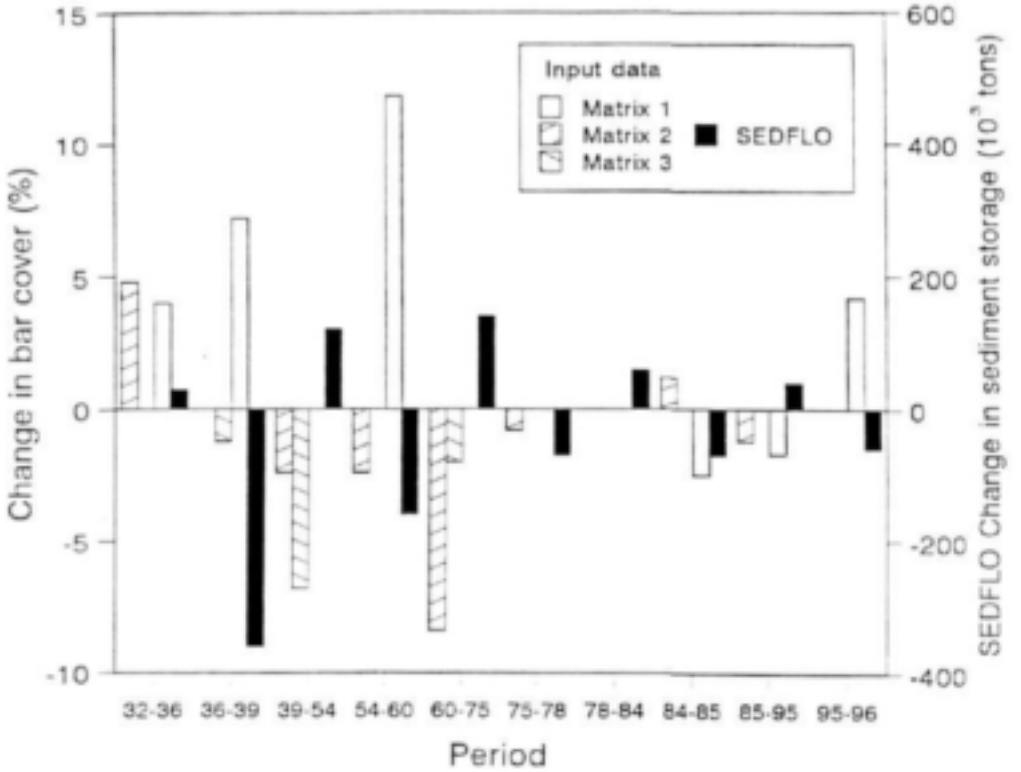

Figure 78 Comparison of trends in erosion and deposition predicted by SEDFLO and the rule based geomorphology model for the mixed-anastomosing channel type cell

7.6 Conclusions and recommendations

Overall, input matrix 1 appears to predict the trends in sedimentation most closely particularly in the pool-rapid and braided cells. Input matrices 2 and 3 perform less favourably and generally predict less variable changes. Only in the case of the mixed anastomosing cell are predictions consistently poor. It is suggested that this may be a result of inaccurate construction of the flow and sediment input matrix for the anastomosing generic channel type (Table 31)

The rule based geomorphological unit change model appears to predict the direction of change in unconsolidated sedimentary deposits satisfactorily. Results from the application of input matrix 3 indicate that sediment flux may have a greater influence on channel form than flow variability. Change to the macro-channel deposits would be expected during the erosive periods in 1936, 1954, 1975, 1985 and 1996. None of the input matrices provide results that confirm such changes, possibly due to the lack of knowledge concerning the change dynamics of these features over the longer timescale. In a number of instances, the morphological change predictions are not consistent with the historical aerial photographic data nor the bulk change in sediment storage modelled using SEDFLO. Furthermore, the degree of accuracy varies between the respective channel type cells. Possible reasons for the modelling inaccuracies include:

- Inaccurate matrix rules due to the poor quality of expert knowledge. This may explain the variable predictive accuracy for the channel type cells, since the knowledge base concerning channel change dynamics varies across channel types.

- Untested morphological change hierarchies.

- A single set of rules (comprising percentage changes) is invoked for each of the generic channel types. It will be more realistic to have separate morphological change rules for each channel type (e.g. alluvial vs. bedrock generic channel types), but this clearly requires an extensively improved knowledge base.

- Inadequate system of predicting the degree of local erosion and deposition at the channel type scale.

- Insufficient testing of the model predictions. The morphological unit dynamics within additional cells needs to be modelled, and further aerial photographic analysis is required to assess historical change. Methods for assessing the dynamics of consolidated sedimentary deposits also need to be developed.

Based on the application of the rule based geomorphological unit change model, it appears that there is encouraging evidence to support the further development of the rule based methodology as a predictive tool. Further development and refinement, however, requires supplementary observed data on morphological dynamics at the unit scale for a range of active and macro-channel features. The direct quantification of areal coverage by unit scale morphological features from aerial photographs over the period of record (1940 to 1996) was beyond the scope of this project and will require a protracted desktop study. These data are, however, imperative to any real further developments of the rule based methodology. Accurate quantification is restricted by the quality of the long-term aerial photographic record, although the more recent photographs are much improved in terms of both exposure scale (1:10 000) and time between flights (approximately ten years). Continuation of aerial photographic data collection will prove invaluable for providing historical records crucial for further model testing.

8 Conclusions and recommendations

The results of the sediment transport magnitude and frequency analysis (**chapter 2**) for the five major channel types along the Sabie River indicate that most sediment transport is associated with relatively frequent (up to 2-year return period) floods for the predominantly alluvial channel types. This is particularly evident for the braided channel type, where flows below the 1.1 year return period account for 39% of the potential bulk sediment transport. These findings are corroborated by studies reported in the literature for alluvial systems. As the influence of bedrock increases, the larger, less frequent floods become progressively more important for bulk sediment transport. Moderate and intermediate flood flows contribute significantly to sediment transport in the pool-rapid and bedrock anastomosing channels, with extreme flood events accounting for as much as 43% of the annual sediment movement in the bedrock anastomosing channels. Most of the potential sediment movement (80%) is accounted for by return period flows of less than 7.0 to 7.8 years in the pool-rapid and bedrock anastomosing channel types. Lower return period flows of up to 2.5, 3.7 and 3.8 are responsible for the bulk sediment movement in braided, single-thread and mixed anastomosing channel types, respectively. This illustrates the transport effectiveness of high-magnitude low-frequency flow events in bedrock influenced morphologies within semi-arid systems.

Analysis of the erodability of cohesive sediments along the Sabie River (**chapter 3**) shows that there is a 68% probability of the deposits being eroded by a discharge of approximately 2000 m^3/s. This value is similar (63% to 75%) for all the channel types with the exception of bedrock anastomosing, where the deposits have a 91% chance of being eroded at this discharge. The higher probability in the bedrock anastomosing channel types arises from the significantly elevated shear stresses. Field observations following a flood in February 1996 revealed that the removal of cohesive material was spatially isolated for the sites investigated along the length of the river, with vegetation cover on the macro-channel floor providing protection against erosive forces. The proportion of the cohesive bed material that was subjected to erosion during this flood appeared to be less than 68%, although it was difficult to assess due to spatial variability and the presence of recent overlying fluvial deposits.

Actual boundary shear stresses are likely to be considerably lower than those estimated in the analysis because of the assumption that the total resisting force is dissipated along the channel perimeter as boundary shear acting on the surface of the cohesive sediment. The Sabie River is characterised by well developed riparian vegetation (particularly in bedrock anastomosing channel type reaches) which, although increasing the total flow resistance by form drag, acts to reduce boundary shear. In addition, the root masses bind the sediments, further reducing entrainment. The proportion of the total resisting force that may be dissipated as vegetational form drag was apparent in the bedrock anastomosing channel type reaches, where extensive riparian tree mortalities were recorded with trees uprooted by the flow. The bed material along the Sabie River consists predominantly of non-cohesive medium to coarse sands and gravels. Granular material overlying cohesive soils provides protection of the cohesive bed, but mobile sediments act to rapidly abrade underlying cohesive material (Kamphuis, 1990).

The erosion of cohesive materials in a mixed alluvial-bedrock river containing mobile non-cohesive granular sediments and significant in-channel riparian vegetation, is therefore complex.

Quantification of the probability of eroding the cohesive sediments along the Sabie River is based on analyses of critical resistance of the local material and applied hydraulic stresses. Although the estimated probability of eroding cohesive material from the Sabie River bed for a large flood event appears to be higher than that observed following an extreme recent flood, the analysis nevertheless shows that there is considerable potential for large scale stripping of the macro-channel deposits. The reduction in hydraulic boundary shear stress resulting from in-channel vegetation is possibly the major reason for the erosion potential being higher than observed. This emphasizes the need to manage the riparian vegetation to enable it to continue providing protection to the cohesive bed during extreme flood events.

Hydraulics data corresponding to an extreme flood event have been used to extend the (low to intermediate) hydraulic relationships determined by Broadhurst *et al.* (1997) for the channel types along the Sabie River (**chapter 4**). The extended flow resistance relationships for the different types converge at high flows due to the reduced influence of channel type specific hydraulic controls. Although further development and validation of the "non-horizontal" model described by Broadhurst *et al.* (1997) was beyond the scope of this study, there is a need for more work on the hydraulics of bedrock dominated channels, since these morphologies occur widely in South African rivers. This need has become increasingly apparent during the course of hydraulic studies for instream flow requirement assessments for Southern African rivers.

The isolation and quantification of individual resistance components needs to be addressed in order to improve the transferability of channel type flow resistance values to similar channel environments. Consequently, a new project has been initiated to study the flow through reedbeds based primarily on experimental work within a controlled environment. *Phragmites maritianus* constitutes a large proportion of the in-channel riparian vegetation along the Sabie River, and this project provides the means to isolate and quantify the associated form and bed resistances.

Application of the sediment flux and storage model (SEDFLO) (**chapter 5**) indicates the long-term (1940 to 1986) change in sediment storage for the Sabie River within the KNP at approximately 3.5×10^3 tons/annum. Shorter-term changes in sediment storage are significantly more variable, reflecting periods of progressive sediment accumulation, interspersed by significant declines during years experiencing large flow events. The average increase in sediment storage during periods of progressive accumulation is as high as 40×10^3 tons/annum, while the loss of sediment during years experiencing large floods is generally greater than 200×10^3 tons.

Observed channel change on the Sabie River reveals that the system is not in a state of dynamic equilibrium, but rather that it is evolving (Heritage *et al.*, 1997a). Previous studies (Heritage *et al.*, 1997a; Vogt, 1992; Chunnett *et al.*, 1990) indicate that the river has experienced a net increase in sedimentation over the period 1940 to 1986, once again confirmed by the present analysis of change as reflected by bar dynamics. Aerial photographic data reveal that the change is spatially and temporally dynamic and complex.

The predicted changes in sediment storage are shown to be realistic when compared with changes in alluviation along the length of the Sabie River and the rate of siltation of the dam at Lower Sabie. The modelling of pre-1940 change within the bedrock anastomosing channel types shows significant losses of in-channel storage, and although there are no historical data to test this finding, a sequence of observed change suggests the recent occurrence of an extreme flood prior to 1940.

The scenario modelling of geomorphological change along the Sabie River using SEDFLO (**chapter 6**) shows that the long-term rates of alluviation increase approximately in proportion to reduced MAR. Dynamic sediment storage behaviour is reduced significantly by diminished flooding influence associated with upstream dam construction. Progressive sedimentation will systematically reduce the proportional occurrence of bedrock within the system and this is likely to impact significantly on the spatial and temporal assemblages of geomorphological features and associated aquatic and riparian habitats. The biodiversity of the system is a consequence of the mixed alluvial bedrock character and will be severely reduced if there is a loss of bedrock influence. In order to achieve a new dynamic equilibrium in response to a reduced flooding regime, alluvial channel types display a tendency to erode whilst pools and (to a lesser degree) mixed anastomosing channel types show a tendency to aggrade. Loss of storage within braided channel types is likely to result in a smaller active channel incised within the macro-channel infill. The scenario modelling carried out in this project was based directly on IFR recommendations and further modelling is recommended once system simulation modelling has been carried out to produce more realistic time series of Sabie River flows resulting from upstream water resources developments.

The modelling approach is based on the premise that dynamic sediment storage along a river can be quantified by assimilating models describing the two integral component processes, i.e. sediment production within the catchment and sediment transport in the river. It relies on the assumption that the form of the process descriptions developed from experiments are equally applicable to the system being considered. For the Sabie River, the application is for a scaled up system, almost infinitely more complex than that for which the process descriptions have been based. For example, the sediment transport equation (Ackers and White, 1973) was developed using data from flume experiments and sediment loads in alluvial river systems. Equally, the sediment yield analysis is based on data from experimental plots (located elsewhere), and any consideration of the sediment storage (catchment and tributary) and hence delivery ratio is nevertheless specific to the catchment.

The extent of calibration required by SEDFLO casts serious doubts on the advisability of using high resolution sediment production and transport models to describe bulk sediment movement and storage behaviour in large, complex systems such as the Sabie River. The contemporary approach under such circumstances is to increase the spatial resolution, and to develop and incorporate additional component models to account for those processes not adequately described. This generally results in an unwieldy model that is difficult to understand or apply and has large and often prohibitive data requirements.

SEDFLO has been developed and calibrated for the Sabie River within the KNP, and can be used operationally for prediction of bulk sediment movement in this system. It can also provide a basis for modelling other similar systems provided that the necessary field work is undertaken for its set up and calibration. The nature of the model, however, is such that this would take considerable effort and resources. It is recommended that research be carried out on alternative modelling approaches that would facilitate transferability.

Biota respond to morphological changes at smaller spatial scales than addressed by SEDFLO, which led to its use in combination with an alternative, rule-based modelling technique for predicting change at the morphological unit scale (**chapter 7**). This appears to predict the direction of change in unconsolidated sedimentary deposits satisfactorily, but the rules employed

need further refinement for confident application. It is recommended that further research be undertaken to improve understanding of channel adjustment at the morphological unit scale to enable more reliable rules to be formulated. Further development and refinement, however, requires supplementary observed data on morphological dynamics at the unit scale for a range of active and macro-channel features. The direct quantification of areal coverage by unit scale morphological features from aerial photographs over the period of record (1940 to 1996) was beyond the scope of this project and will require a protracted desktop study. These data are, however, imperative to any real further developments of the rule based methodology. Accurate quantification is restricted by the quality of the long-term aerial photographic record, although the more recent photographs are much improved in terms of both exposure scale (1:10 000) and time between flights (approximately ten years). Continuation of aerial photographic data collection is invaluable for providing historical records necessary for further model testing.

References

Ackers, P. and White, R. (1973). Sediment transport: new approach and analysis. *Jour. of the Hydraulics Division, ASCE*. Vol. **99** No. HY11, 2041-2060.

Amplett, M.B. and Dickenson, A. (1989). Dallao soil erosion study, Magat, Philippines. Summary report (1984-1987). Report No. OD 111, HR Wallingford in collaboration with the National Irrigation Administration, Government of Philippines.

Andrews, E.D. (1980). Effective and bankfull discharges of streams in the Yampa River Basin, Colorado and Wyoming. *Jour. of Hydrology* **46**, 311-330.

ASCE Task Committee on erosion of cohesive sediments (1968). Erosion of cohesive sediments. *Jour. Hydraulics Division, ASCE*. Vol. **94** HY4, 1017-1049.

Atkinson, E. (1991). Sediment delivery in river systems. Report No. OD/TN 48, HR Wallingford, UK.

Bagnold, R.A. (1966). An approach to the sediment transport problem form general physica. U.S. Geol. Survey, Prof. Paper 422-J.

Baker, V.R. (1977). Stream-channel response to floods, with examples from Central Texas. Geological Society of America Bulletin, **88**, 1057-1071.

Barnes, H.H. (1967). Roughness characteristics of natural channels, U.S. Geological Survey Water Supply Paper 1849, U.S. Geological Survey, Washington, D.C., 1-9.

Birkhead, A.L., Heritage, G.L. and van Niekerk, A.W. (1995). Techniques for evaluating river and reservoir sedimentation on the Sabie and Letaba River systems. In *Proc. seventh South African national hydrology symposium*, Grahamstown, South Africa, 4 to 6 September 1995.

Birkhead, A.L., Heritage, G.L., White, H., van Niekerk, A.W. (1996). Ground-penetrating radar as a tool for mapping the phreatic surface, bedrock profile and alluvial stratigraphy in the Sabie River, Kruger National Park. *Jour. Soil Water Cons.* Vol. **51** No. 3, 234-241.

Birkhead, A.L., Olbrich, B.W., James, C.S. and Rogers, K.H. (1997). Developing an integrated approach to predicting the water use of riparian vegetation. Water Research Commission Report No. 474/1/97, volume 1. Water Research Commission, Pretoria, South Africa. 292 pp.

Birkhead, A.L. and James, C.S. (1998). Synthesis of rating curves from local stage and remote discharge monitoring using nonlinear Muskingum routing. *Jour. of Hydrology* **205**, 52-65.

Bradbury, P.A. (1994). A catchment planning tool for simulating soil erosion and sediment yield. Report No. OD/P 122, Overseas development unit, HR Wallingford, UK.

Broadhurst, L.J., Heritage, G.L., van Niekerk, A.W, James, C.S. and Rogers, K.H. (1997). Translating local discharge into hydraulic conditions on the Sabie River. An assessment of channel flow resistance. Water Research Commission Report No. 474/2/96, volume 2. Water Research Commission, Pretoria, South Africa. 118 pp.

Carlson, E.J. and Enger, P.F. (1963). Studies of tractive forces of cohesive soils in earth canals. Hydraulic Branch Report No. Hyd-504, Bureau of Reclamation, Denver, Colorado.

Carter, A.J. and Rogers, K.H. (1995). A Markovian approach to investigating landscape change in the Kruger National Park rivers. CWE Report No. 2/1995, Centre for Water in the Environment, University of the Witwatersrand, Johannesburg.

Cheshire, P. (1994). Geology and geomorphology of the Sabie River, Kruger National Park and its catchment area. CWE Report No. 1/1994, Centre for Water in the Environment, University of the Witwatersrand, Johannesburg.

Chunnett, Fourie and Partners (1990). Water resources planning of the Sabie River catchment, South Africa Department of Water Affairs and Forestry Report No. P.X.300/00/0490. Vols. 1 to 10.

Colby, B.R. (1964). Practical computation of bed-material discharge. *Jour. Hydraulics Division, ASCE*. Vol. **90**, No. HY2, 217-246.

Crosby, C.T., McPhee, P.J. and Smithen, A.A. (1983). Introduction of the Universal Soil Loss Equation in the Republic of South Africa. Presentation to the American Society of Agricultural Engineers.

de Fontaine, M.L. (1995). Relationship between demographic structure of Breonadia Silicina (Delile) Ridsd sub-populations and geomorphic features of the Sabie River, Kruger National Park. Unpublished MSc thesis, University of the Witwatersrand, Johannesburg. 169 pp.

Department of Water Affairs and Forestry (1994). DWAF Eastern and Northern Transvaal Water Resource Development of the Sabie River. Issued by Prof. K. Asmal, Minister of Water Affairs and Forestry. In: River News, Newsletter No. 6, September 1994.

Department of Water Affairs and Forestry (1997). Sabie-Sand River System Instream Flow Requirements. Proceedings of IFR Workshop, 18-22 August 1996. DWAF, Pretoria, South Africa. 198 pp.

Donald, P.D. (1997). GIS modelling of erosion and sediment yield in a semi-arid environment. Unpublished MSc dissertation, University of the Witwatersrand, Johannesburg.

Donald, P.D., van Niekerk, A.W. and James, C.S. (1995). GIS modelling of sediment yields in semi-arid environments. *Proc. seventh South African national hydrology symposium*, Grahamstown, South Africa, 4 to 6 September 1995.

Dunn, I.S. (1959). Tractive resistance of cohesive channels. *Jour. of Soil Mechanics and Foundation Division, ASCE*. Vol. **85** No. SM3, Proc. Paper 2062, 1-24.

Einstein, H.A. (1950). The bed-load function for sediment transportation in open channel flows. U.S. Dept. Agr., Soil Conser. Serv., T.B. No. 1026.

Elwell, H.A. (1978). Modelling soil losses in Southern Africa, *Jour. of Agric. Eng. Res.* No. **23**, 117-127.

Engelund, F. and Hansen, E. (1967). A monograph on sediment transport in alluvial streams, Teknisk Forlag, Copenhagen.

Espey, W.H. Jr. (1963). A new test to measure the scour of cohesive sediment. Hydr. Eng. Lab., Department of Civil Engineering, Tech. Report No. HYD01-6301. The University of Texas, Austin, Texas.

Flaxman, E.M. (1963). Channel stability in undisturbed cohesive soils. *Jour. of the Hydraulics Division, ASCE*. No. HY2, 87-96.

Ghosh, J.K., Mazumder, B.S. and Sengupta, S. (1981). Methods of computation of suspended load from materials and flow parameters. *Sedimentology* Vol. **28** No. 6, 781-791.

Govers, G. (1990). Empirical relationships for the transport capacity of overland flow. *Proc. Jerusalem workshop on erosion, transport and deposition processes*, March 1987. *IAHS* Publication No. 189.

Graf, W.H. (1972). Hydraulics of sediment transport. McGraw-Hill series in water resources and environmental engineering. 513 pp.

Heritage, G.L. and van Niekerk, A.W. (1994). Morphological reponse of the Sabie River to changing flow and sediment regimes. In *Proc. South African Inst. of Civil Eng. conference on 50 years of water engineering in South Africa*. Johannesburg, South Africa. 389-403.

Heritage, G.L., van Niekerk, A.W., Moon, B.P. and Kapur, K. (1995). The influence of flow regime on the geomorphology of the Sabie River. In *Proc. seventh South African national hydrology symposium*, Grahamstown, South Africa, 4 to 6 September 1995.

Heritage, G.L., van Niekerk, A.W., Moon, B.P., Broadhurst, L.J., Rogers, K.H. and James, C.S. (1997a). The geomorphological response to changing flow regime of the Sabie and Letaba River systems. Water Research Commission Report No. 376/1/97, Water Research Commission, Pretoria, South Africa. 164 pp.

Heritage, G.L., Jewitt, G.P.W, van Niekerk, A.W. and Birkhead, A.L. (1997b). The geomorphology model. In: Modelling abiotic-biotic links in the Sabie River (Eds. Jewitt, G.P.W., Heritage, G.L. and Weeks, D.C.). Water Research Commission, Pretoria, South Africa. 124 pp.

Hey, R.D. (1975). Design discharges for natural channels, In R.D. Hey and J.D. Davies (Eds.) Science and Technology in Environmental Management. Farnborough, Saxon House, 73-88.

Hicks, D.M. and Mason, P.D. (1991). Roughness characteristics of New Zealand Rivers. Water Resources Survey, DSIR, 1-13.

Hughes, D.A., Sami, K. and Smakhtin, V. (1996). Sabie River Instream Flow Requirement Assessment Hydrology Starter Document. In: Starter Document for the Sabie Sand IFR Workshop, 18-22 August 1996. Department of Water Affairs and Forestry, Pretoria, South Africa.

Hughes, D.A., O'Keeffe, J.H., Smakhtin, V. and King, J.M. (1997). Development of an operating rule model to simulate time series of reservoir releases for instream flow requirements. *Water SA* Vol. **23** No. 1, 21-30.

Hunt, J.N. (1954). The turbulent transport of suspended sediment in open channels. *Proc.* Royal Society, London. Series A24.

James, C.S. (1987). Modelling the interaction between bed material and the different modes of transport. Report to Chamber of Mines Research Organization, 13 pp.

Jewitt, G.P.W., Heritage, G.L., Weeks, D.C., Mackenzie, J.A., van Niekerk, A.W., Gorgens, A.H.M., O'Keeffe, J., Rogers, K.H., Horn, M. (1997). Modelling abiotic-biotic links in the Sabie River. Water Research Commission, Pretoria, South Africa. 124 pp.

Kale, V.S., Baker, V.R., Mishra, S. (1996). Multi-channel patterns of bedrock rivers: An example from the central Narmada basin, India. *Catena* **26**, 85-98.

Kamphuis, J.W. (1990). Influence of sand or gravel on the erosion of cohesive sediment. *Jour. of Hydraulics Research* Vol. **28**, 43-53.

Kamphuis, J.W. and Hall, K.R. (1983). Cohesive material erosion by unidirectional current. *Jour. Hydraulic Engineering* Vol. **109** No. 1, 49-61.

Kochel, R.C. (1988). Geomorphic impact of large floods: review and new perspectives on magnitude and frequency. In: Flood geomorphology (Eds. Baker, V.R., Kochel, R.C. and Patton, P.C.), 169-188.

Kochel, R.C., and Baker, V.R. (1982). Palaeoflood hydrology. *Science* **215**, 353-361.

Leopold, L.B. and Maddock, T. (1953). The hydraulic geometry of stream channels and some physiographic implications. United States Geological Survey Professional Paper 252, 1-4, 9-16.

Lewin, J. (1989). Floods in fluvial geomorphology. In: Floods: Hydrological, Sedimentological and Geomorphological Implications, Beven, K. and Carling, P. (Eds.) John Wiley & Sons, 265-284.

Linsley, R.K., Franzini, J.B., Freyberg, D.L. and Tchobanoglous, G. (1992). Water Resources Engineering. Fourth Edition. McGraw-Hill Inc., US. 841 pp.

Lyle, W.M. and Smerdon, E.T. (1965). Relation of compaction and other soil properties to the erosion resistance of soils. *Trans. ASAE* Vol. **8**, 419-422.

McPhee, P.J. and Smithen, A.A. (1984). Applications of the USLE in the RSA. *Agric. Eng. in S.A.*, Vol. **18**, No. 1.

Meade, R.M. and Parker, R.S. (1989). Sediment in rivers in the United States. In: National Water Summary 1984, U.S. Geological Water Supply Paper, 2275, 49-60.

Meyer-Peter and Müller, R. (1948). Formulas for bed load or suspended load. *Jour. Hydraulic Engineering* Vol. **111** No. 1, 93-107.

Moon, B.P., van Niekerk, A.W., Heritage, G.L., Rogers, K.H. and James, C.S. (1997). A geomorphological approach to the ecological management of river in the Kruger National park: the case of the Sabie River. *Trans. Inst. Br. Geogr.*, NS **22**, 31-48.

Moore, W.L. and Masch, F.D. (1962). Experiments on the scour resistance of cohesive sediments. *Jour. of Geophysical Research* Vol. **67** No. 4, 1437-1449.

Moss, J.H. and Kochel, R.C. (1978). Unexpected geomorphic effects of the Hurricane Agnes storm and flood, Conestoga drainage basin, south-eastern Pennsylvania. *Jour. of Geology* **86**, 1-11.

Nanson, G.C. (1986). Episodes of vertical accretion and catastrophic stripping: a model of disequilibrium floodplain development. *Bulletin of the Geological Society of America* **97**, 1467-1475.

O'Keeffe, J.H., Weeks, D.C., Fourie, A. and Davies, B.R. (1996). A pre-impoundment study of the Sabie-Sand River System, Mpumalanga, with special reference to predicted impacts on the Kruger National Park. Volume 3: The proposed impoundments and management recommendations. WRC Report No. 294/3/96, Water Research Commission, Pretoria, South Africa. 111 pp.

Partheniades, E. and Paaswell, R.E. (1970). Erodability of channels with cohesive boundary. *Jour. of Hydraulics Division, ASCE*. Vol. **96**, No. HY3, 755-771.

Pickup, G. and Warner, R.F. (1976). Effects of hydraulic regime on magnitude and frequency of dominant discharge. *Jour. of Hydrology* **29**, 51-75.

Press, W.H., Flannery, B.P., Teukolsky, S.A. and Vetterling, W.T. (1989). Numerical Recipes: The Art of Scientific Computing (FORTRAN Version). Cambridge University Press.

Rectoric, R.J. and Smerdon, E.T. (1964). Critical shear stress in cohesive soils from a rotating shear apparatus. Paper No 64-216, ASCE, June 21-24.

Rooseboom, A., Verster, E., Zietsman, H.L. and Lotriet, H.H. (1992). The development of the new sediment yield map of Southern Africa. Water Research Commission report no. 297/2/92.

Rouse, H. (1937). Modern conceptions of the mechanics of turbulence. Trans. Am. Soc. Civil Engrs., Vol. **102**.

Schulze, R. (1989). ACRU: Background, concepts and theory. Water Research Commission Report No. 154/1/89.

Schumm, S.A. and Lichty, R.W. (1963). Channel widening and floodplain construction along the Cimarron River in south-western Kansas. United States Geological Survey Professional Paper 352-D, 71-88.

Smerdon, E.T. and Beasley, R.P. (1959). Tractive force theory applied to stability of open channels in cohesive soils. Research Bulletin No. 715, Agricultural Experimental Station, Univ. of Missouri, Colombia, Missouri.

Sunborg, A. (1956). The River Klareiven, a study of fluvial process. *Geografiska Annalen*, Stockholm, Sweden.

Thomas, C.W. and Enger, P.F. (1961). Use of a electric computer to analyse data from studies of critical tractive forces for cohesive soils. Intern. Assos. Hyd. Res. 9th Congress, Dubrovnik.

US Dept. of Interior, Bureau of Reclamation (1953). Interim Report on channel stability of natural and artificial drainageways in Republican, Loup and Little Sioux River Areas, Nebraska and Iowa. Hydrology branch, project planning div., Denver. 11 pp.

Vanoni, V.A. (Ed) (1975). Sedimentation Engineering. ASCE Manual and report No. 54., 745 pp.

van Coller, A.L. and Rogers, K.H. (1995). Riparian vegetation of the Sabie River: relating spatial distribution patterns to the characteristics of the physical environment. CWE report No. 1/1995, Centre for Water in the Environment, University of the Witwatersrand, Johannesburg, South Africa. 82 pp.

van Coller, A.L. and Rogers, K.H. (1996). A basis for determining the instream flow requirements for the riparian vegetation along the Sabie River within the Kruger National Park. CWE Report No. 2/1996, Centre for Water in the Environment, University of the Witwatersrand, Johannesburg.

van Coller, A.L., Rogers, K.H. and Heritage, G.L. (1997). Linking riparian vegetation types and fluvial geomorphology along the Sabie River within the Kruger National Park, South Africa. *African Jour. of Ecology*, **35**. 194-212.

van Niekerk, A.W. and Heritage, G.L. (1993). Geomorphology the Sabie River: Overview and Classification. CWE Report No. 2/1993, Centre for Water in the Environment, University of the Witwatersrand, Johannesburg.

van Niekerk, A.W. and Heritage, G.L. (1994). The use of GIS techniques to evaluate sedimentation patterns in a bedrock controlled channel in a semi-arid region. *Proc. international conference on integrated basin management*. Wallingford, England, UK. 13-16 September 1994. John Wiley, Chichester.

van Niekerk, A.W., Heritage, G.L. and Moon, B.P. (1995). River classification for management: The geomorphology of the Sabie River. *South African Geographical Jour.* Vol. 77 No. 2, 68-76.

van Rijn, L.C. (1984). Sediment transport, Part II: Suspended load transport. *Jour. of Hydraulic Engineering* Vol. **110** No. 11, 1613-1641.

van Rijn, L.C. (1986). Mathematical modelling of suspended sediment in non-uniform flows. *Jour. of Hydraulic Engineering* Vol. **112** No. 6, 433-455.

Vogt, I. (1992). Short-term geomorphological changes in the Sabie and Letaba Rivers in the Kruger National Park. Unpublished MSc thesis. University of the Witwatersrand, Johannesburg.

Weeks, D.C., O'Keeffe, J.H, Fourie, A. and Davies, B.R. (1996). A pre-impoundment study of the Sabie-Sand River System, Mpumalanga, with special reference to predicted impacts on the Kruger National Park. Volume 1: The ecological status of the Sabie-Sand River System. WRC Report No. 294/3/96, Water Research Commission, Pretoria, South Africa. 261 pp.

Williams, J.R. (1975). Sediment routing for agricultural watersheds. *Water Resources Bulletin*, Vol. **11** No 5, 965-974.

Williams, J.R. and Berndt, H.E. (1972). Sediment yield computed with universal equation. *Jour. Hydr. Div.*, Proc. Am. Soc. Civ. Eng., **98** No. HY2, 2087-2097.

Wischmeier, W.H. and Smith, D.D. (1978). Predicting rainfall erosion losses: a guide to conservation planning. USDA-SEA Agric. handbook 537, Agric. Research Service, USDA, Washington DC, USA.

Wolman, M.G. and Miller, J.C. (1960). Magnitude and frequency of forces in geomorphic processes. *Jour. of Geology* **68**, 54-74.

Wolman, M.G., and Gerson, R. (1978). Relative scales of time and effectiveness of climate in watershed geomorphology. *Earth Surface Processes* **3**, 189-203.

Yang, C.T. (1973). Incipient motion and sediment transport. *Jour. Hydraulics Division*, ASCE. Vol. **99** No. HY10, 1679-1704.

APPENDIX: A visual interface to the SEDFLO model

by

N.W. Quinn
Aqua Environmental
P O Box 100767
Scottsville 3209
South Africa

Table of Contents

List of Figures

List of Tables

Acknowledgements

The development of this interface formed a component of a Water Research Commission project entitled "Scenario Modelling for the Kruger National Park Rivers Research Programme Decision Support System", and was funded by the Water Research Commission. The support of the Water Research Commission and the contributions of Steering Committee members is gratefully acknowledged.

Chapter 1
Introduction

1.1 Purpose of the model

A semi-quantitative sediment flux and storage model was developed for predicting change at the channel type scale on an annual basis by Heritage *et al.* (1997). Birkhead *et al.* (1998) focusses on the refinement, calibration and verification of this model, based on historical data from aerial photographs spanning 56 years. The SEDFLO (SEDiment FLux and stOrage) Model consists of two integral components. The first component deals with the production of sediment across the catchment landscape and the delivery of this eroded source material to the study length of the river, including lateral inputs from tributaries. The second component of the model deals with the differential transport of sediment along the study river. Further details on the approach and theoretical background can be found in Chapter 5 of the main report (Birkhead *et al.* 1998). This document provides an overview of a graphical interface to the SEDFLO Model, outlining the format of required input files, the computational procedure and the output files which are produced. The interface also permits the viewing and plotting of files. Program control is through a menu screen (Figure 1.1)

1.2 Assumptions and limitations

The interface has been designed to be as generic as possible to permit application of the model to a river system other than the Sabie-Sand. Although this is possible within the current interface, it is likely that small changes to the program would have to be made. Of greater importance is the considerable calibration requirement; many of the calibration factors utilised in this version are for the Sabie-Sand system only. Application of SEDFLO to another catchment would thus require a considerable effort and it is strongly recommended that this is only undertaken in consultation with the authors of the main report (Birkhead *et al.* 1997).

1.3 Hardware requirements and installation

Running the SEDFLO Model interface requires Windows 95, 16Mb RAM, preferably a Pentium processor and approximately 150 Mb of space on a hard disk. The original set of programs were coded in QuickBasic, and integrated into Visual Basic 5.0 to form the interface and plotting facility. Installation is automated and is started by running SETUP.EXE. (See instructions on disk).

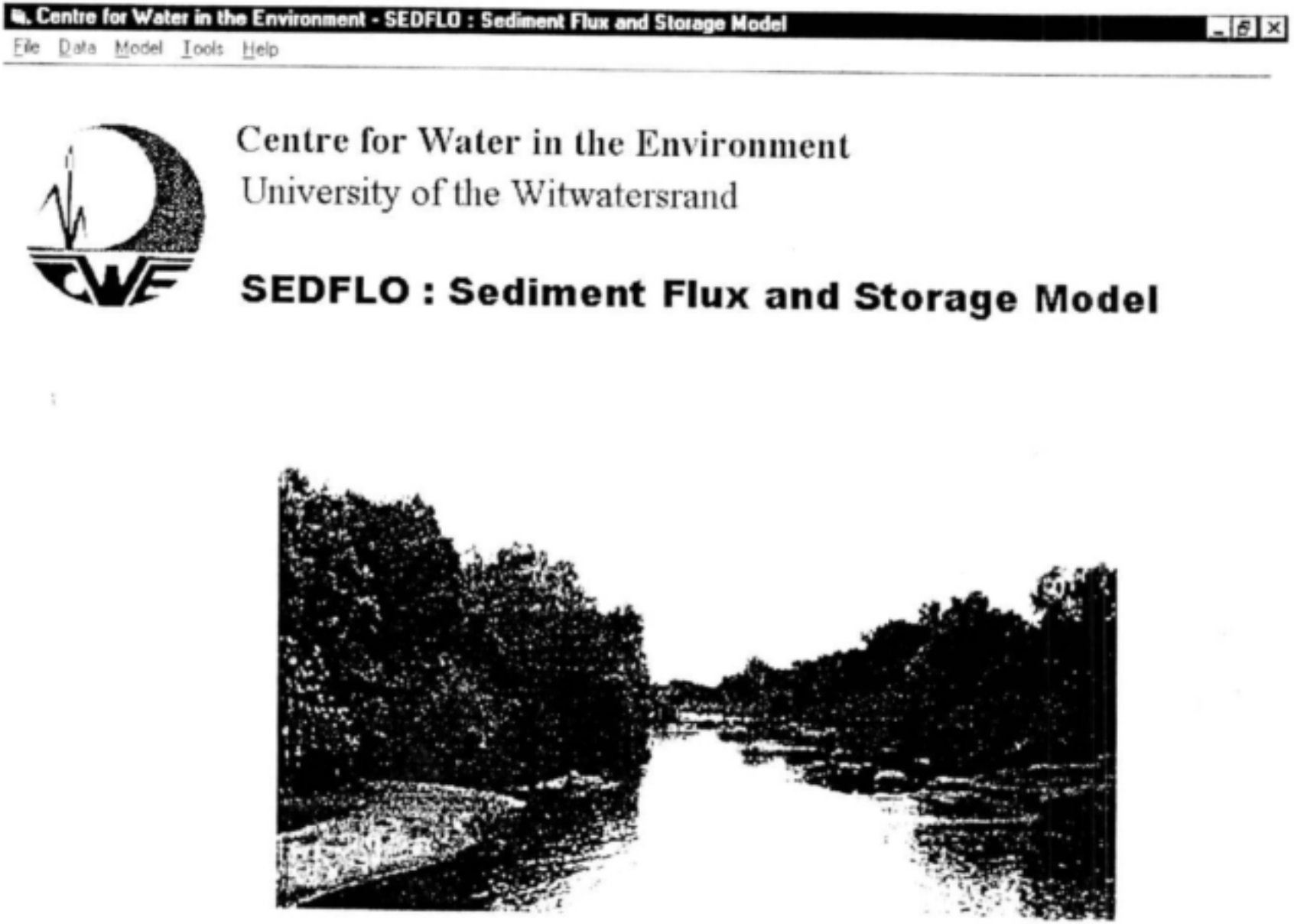

Figure 1.1 : Main navigation screen of the SEDFLO visual interface

1.4 Overview of the SEDFLO Model

The SEDFLO Model comprises five distinct modules (Figure 1.2). The first module (Chapter 2: Importing and converting ACRU data) imports and converts daily ACRU data files into a series of input files for the subsequent module. This module only needs to be run once for every set of ACRU scenario files. The second module (Chapter 3: Determining and calculating cell inputs) converts the catchment based runoff and sediment yield data into daily runoff and sediment yield for each of the defined river cells. The third module (Chapter 4: Calculating sediment transport) represents the core of the SEDFLO Model and calculates sediment transport capacity for each cell based on input data files (cross-sections, resistance and energy slope). The output of this process is then used to undertake a mass balance of sediment (Chapter 5: Mass balance sediment budget), based on the sediment transport capacity of individual reaches and the sediment inputs determined earlier. The final module (Chapter 6: Plotting and viewing results) comprises a suite of tools for graphing results and viewing files.

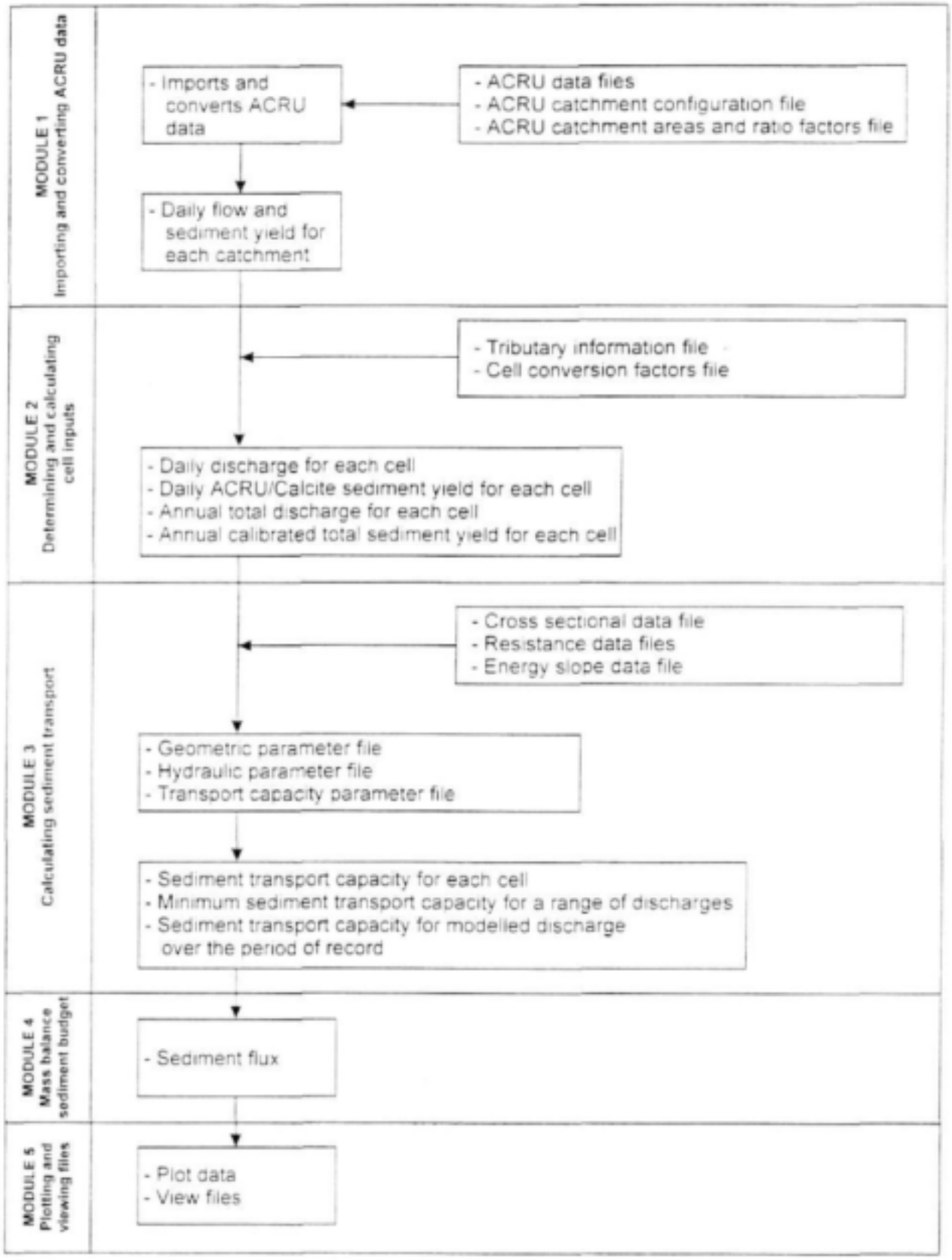

Figure 1.2 : Overview of the SEDFLO Model

Chapter 2
Importing and converting ACRU data

2.1 Purpose

This module of the program is the necessary first step in preparing data for the SEDFLO model and only needs to be run once per set of ACRU simulation data. This step converts ascii ACRU data files into daily ascii files of discharge and sediment yield according to various parameters contained in ancillary data files (`acrucon.dat` and `subareas.dat`)

2.2 Input files

Three types of input files are required; the first two are ascii comma delimited ancillary parameter files (`acrucon.dat` and `subareas.dat`) and the last type are the ascii ACRU data files (`s00x.day`). Specifications for each type of file are given below.

(a) ACRU data files (`s00x.day`)

An ascii ACRU output file for each sub-catchment in the catchment is required. These will have the extension (`.day`) and are numbered `s001.day` to `s0xx.day` where `xx` is the last subcatchment under consideration. In running the ACRU model only the following output variables should be requested : (`CELRUN, DAMPER, RFL, SEDYLD, SIMSQ, STRMFL`). *It is important to note that while sediment yield (tons.day^{-1}) is* calculated per catchment, runoff (mm.day^{-1}) is calculated to include upstream contributions as well.

(b) ACRU catchment configuration file (`acrucon.dat`)

The first line of this file specifies the number of catchments under consideration (`ncatch`), and for which an individual sediment yield file (`.Qs`) is calculated. As mentioned in (a) above, whilst sediment yield is calculated per catchment, the calculation for runoff includes the contribution of upstream catchments. For this reason, in this program a unique catchment discharge file is not output for each catchment. Discharge files are calculated only for those catchments where a tributary enters the main river stem. Thus the discharge contained in `s017.day` represents the total flow of the Sand River catchment (catchments 1 to 17) entering the Sabie River at that point.

The second line of the file thus specifies the number of tributaries (or catchments providing overland flow) providing lateral input of discharge into the main river stem (`nsubQ`). The third line is a comma delimited list of the catchment numbers providing lateral input. The number of catchments in this list must equal the value of `nsubQ` specified in line 2.

As sediment is calculated per catchment in ACRU, it is necessary to sum sediment delivery per contributing catchment. The fourth line thus specifies the number of contributing catchments (`nsubQs`) and is followed by a set of parameters which indicate the highest subcatchment (`subQsfrom`) to the lowest subcatchment (`subQsto`) and the numeric part of the file name which will be created by summing the individual catchment sediment yields together. The file format is summarised in Table 2.1 below.

Table 2.1 : Input file format for the ACRU catchment configuration file (`acrucon.dat`)

```
ncatch
nsubQ
subQ(1),.........subQ(nsubQ)
nsubQs
subQsfrom(1), subQsto(1),QsFileS(1)
.....
.....
.....
subQsfrom(nsubQs), subQsto(nsubQs),QsFileS(nsubQs)
```

Example from the Sabie-Sand catchment :

```
56
21
17,35,37,38,40,41,42,43,44,45,46,47,48,49,50,51,52,53,54,55,56
6
1,10,57
11,17,58
57,58,59
18,27,60
28,35,61
60,61,62
36,37,63
39,40,64
```

(c) ACRU catchment areas and ratio factors file (`subareas.dat`)

As indicated in (a) above, ACRU provides runoff output in units of $mm.day^{-1}$, and consequently it is necessary to convert these values to $m^3.s^{-1}$. In order to do this, the area of the catchment (or contributing catchments) is required. In addition to the catchment area and the upstream area for each catchment, a sediment ratio factor for each catchment is also provided. This factor adjusts the ACRU sediment yield as given in Table 7 of the main report (Birkhead *et al.* 1998). The file format is summarised in Table 2.2 below.

Table 2.2 : Input file format for the catchment areas and ratio factors file (`subareas.dat`)

```
catch, areasub(i),areaupsub(i),ratio(i)
.,.,.,
.,.,.,
.,.,.,
catch, areasub(ncatch),areaupsub(ncatch),ratio(ncatch)
```

Example from the Sabie-Sand catchment :

```
1,19.83,19.83,6.5
2,36.81,56.64,6.5
3,76.9,76.9,6.5
.,.,.,
.,.,.,
.,.,.,
56,25.01,6260.36,2.97
```

(d) Optional file (`rivernam.bat`)

In the case of the Sabie-Sand catchment, filenames relating to the tributary name rather than catchment numbers were considered more practical. A DOS batchfile thus renames certain catchment files to files bearing catchment tributary names (e.g. `s059.qs` to `Sand.qs`). This is an optional step and a separate batchfile outside of the visual interface would have to be created and executed. In the case of the Sabie-Sand catchment this file was named `rivernam.bat` and is provided with the programme files. If this is a preferred option, it is important to reflect the new file names in subsequent parameter and other files.

2.3 Running the program

In order to run this component select [DATA] from the main screen menu and [Import ACRU data] from the popup menu. The [IMPORTING AND CONVERTING ACRU DATA] screen will be displayed as in Figure 2.1 overleaf. Default input and output paths or files pertaining to the Sabie-Sand catchment are displayed. These can be changed using the [Change...] button. The [Viewfile...] button will load a simple text editor to enable one to view and edit the ancillary parameter files. The program is executed by the [Start...] button and the computational process is displayed in the bottom right of the screen. Depending on the number of catchment and the length of the daily record, this program may take a considerable period to complete (e.g. in the case of Sabie-Sand catchment approximately 40 minutes).

2.4 Computational sequence and output files

The two ancillary parameter files are read first and thereafter two ascii discharge files per contributing catchment are generated (`s0xx.Q` and `s0xx.Qc`). The number of (`.Q` and `.Qc`) files is determined by the parameter `nsubQ` in `acrucon.dat` and the daily discharge in the (`.Q`) files is discharge in $m^3.s^{-1}$ for the catchment including upstream contribution, whereas the data in the (`.Qc`) files do not. During execution the catchment number being currently processed is displayed as well as an indication of how many of the selected subcatchments for calculating `Q` and `Qc` have been completed.

The next stage of the process writes and ascii file (`.Qs`) daily sediment yield (tons.day^{-1}) for each of the subcatchments determined by the parameter (`ncatch`) in the file `acrucon.dat`. Progress is similarly displayed at the bottom of the screen.

The final stage of the program prepares accumulated sediment yield (tons.day^{-1}) for the contributing catchments. The number of files produced is determined by the parameter `nsubQs` in `acrucon.dat`. At the end of this stage [Process complete] is displayed and clicking on [Continue] will return the user to the main screen.

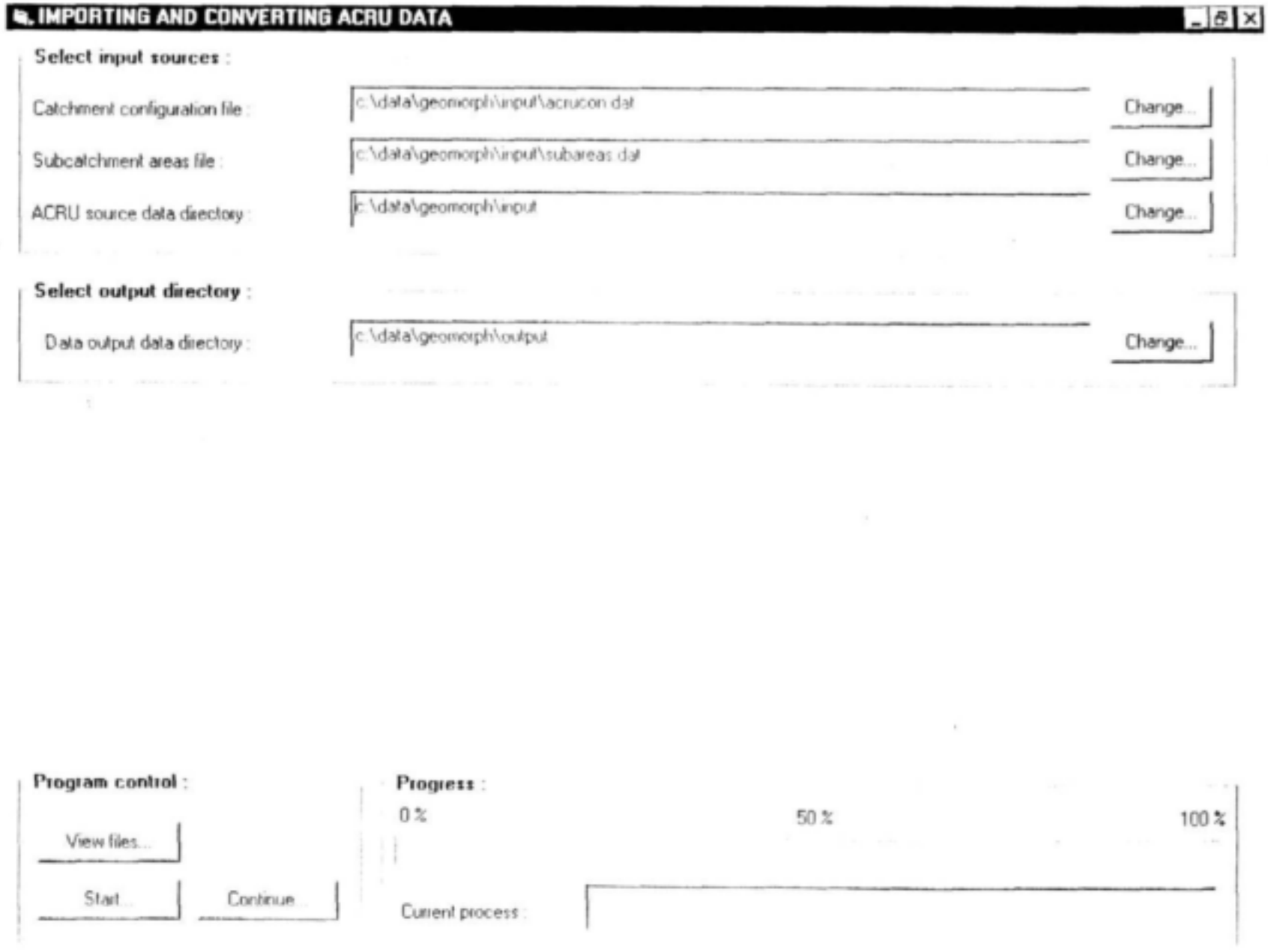

Figure 2.1 : Data input screen for the importing and converting of ACRU data

Chapter 3
Determining and calculating cell inputs

3.1 Purpose

The primary purpose of this module is the aggregation of the ACRU ascii daily flow and sediment files (`.Q`..`Qc` and `.Qs`) into separate files containing the daily flow and sediment inputs for, in the case of the Sabie-Sand, each of the 40 river cells defined along the main river stem. Prior to implementing this component of the program, the user must have discretised the river reaches to be modelled as cells. For each cell it is then necessary to determine which tributaries or portions of a catchment contribute flow and sediment into that cell.

3.2 Input files

In addition to the ascii output files generated in Chapter 2, two ascii comma delimited parameter files are required (`tribin.dat` and `celydfac.dat`). Specifications for each type of file are given below and the parameter files used in the simulation of the Sabie-Sand catchment are provided with the programme files.

(a) Tributary information file (`tribin.dat`)

The tributary information file indicates which tributaries and portions of a catchment provide flow and sediment into each cell. The first line of the file contains the character Q and indicates that parameters pertaining to flow will be read first. The first field of the second line (`cell`) refers to the cell number under consideration, whilst the second field (`notribQ(cell)`) indicates the number of tributaries or portions (proportion) of a catchment contributing flow to the cell. Thus if `notrib(cell)=3` then the program will expect to be able to read in weighting factors (`Qfact(cell,trib)`) and daily flow filenames (`Qtrib(cell,trib)`) for three tributaries or portions of a catchment. This sequence is repeated until factors and flow files have been determined for all cells. The input weightings and filenames for the last cell of the river segment are followed by the characters `99` on the next line to indicate the end of the input for flow. The file is continued for sediment weighting factors and filenames, with exactly the same layout. This set of input parameters also commences with the characters `Qs` and is terminated with `99`. The file format is summarised in Table 3.1 overleaf.

Table 3.1 : Input file format for the tributary information file (`tribin.dat`)

```
C
cell, nctribQ(cell)
Qfact(cell, trib),Qtrib(cell,trib)
.,.,.
99
Qs
cell, nctribQs(cell)
Qsfact(cell, trib),Qstrib(cell,trib)
.,.,.
99
```

Example from the Sabie-Sand catchment :

```
C
1,1
1,SABIE.Q
2,2
1,SABIE.Q
1,PHABENI.Q
3,3
1,SABIE.Q
1,PHABENI.Q
0.067,SC38.Qc
4,3
1,SABIE.Q
1,PHABENI.Q
0.133,SC38.Qc
...                    Continued to Cell 40
99
Qs
...                    Repeated for sediment factors and inputs
```

(b) Cell conversion factors file (`celydfac.dat`)

This file comprises a series of factors representing the ratio of ACRU/Calcsite modelled sediment yield to the calibrated sediment yield. Users are referred to Table 18 of the main report (Birkhead *et al.* 1998). Factors for each cell should be present (even if they are is 0) and each cell's factor should appear on a separate line. See `celydfac.dat` in the programme files for factors used in the Sabie-Sand case study.

3.3 Running the program

In order to run this component select [MODEL] from the main screen menu and [Compute cells] from the popup menu. The [CALCULATE CELL DATA] screen will be displayed as in Figure 3.1. Default input and output paths or files pertaining to the Sabie-Sand catchment are

displayed. These can be changed using the [Change...] button. The [Viewfile...] button will load a simple text editor to enable one to view and edit the ancillary parameter files. The program is executed by the [Daily...] button and the computational process is displayed in the bottom right of the screen. Having calculated the daily files it is then possible to produce annual summary files, and this is done by clicking the [Annual...] button. Depending on input files, this program may take a while to run (e.g. in the case of Sabie-Sand catchment approximately 20 minutes).

3.4 Computational sequence and output files

The tributary information file (`tribin.dat`) is read in first, and thereafter daily flow is calculated for each cell. For each cell the daily flow volume of each contributing source is multiplied by the area weighting factor for that source and summed to provide a total daily inflow for that cell. The first three lines of the output file specify a heading, the cell number and the units. The next line of the output file gives the starting year of the simulation, followed by the starting month on the next line. The discharge for each day in the month follows, with each daily value on a new line. Format of the remainder of the file for discharge (and sediment) follows the same pattern. Discharge is given in $m^3.s^{-1}$, and the output files are named `Cell01.Q` to `Cell40.Q`. After calculating daily discharge per cell, daily sediment yield for each cell is calculated in the same manner. Sediment yield is given in tons.day^{-1}, and the output files are named `Cell01.Qs` to `Cell40.Qs`. Once the calculation of daily discharge and sediment yield for each cell is complete [Completed calculating daily data. Click 'Annual...' to complete.] is displayed and clicking on [Annual...] will begin the next phase of the process. Calculation of annual totals begins with summing daily discharge for each cell over a year and converting daily values from $m^3.s^{-1}$ to million m^3. The resultant output file is named (`riverQ.ann`). A similar approach is adopted in the calculation of annual totals for sediment yield, except that in this case the factors representing the ratio between the ACRU/Calsite modelled sediment yields and the calibrated yields (from `celydfac.dat`) are used as multipliers in calculating annual totals. Annual sediment yield is expressed in thousand tons.year^{-1} and the resultant output file is named (`riverQscal.ann`). At the end of this stage [Process complete.] is displayed and clicking on [Continue...] will return the user to the main screen. In summary, during this phase of the modelling process the following files are produced:

`Cell01.Q..Cell40.Q` : Daily discharge for each cell ($m^3.s^{-1}$)
`Cell01.Qs..Cell40.Qs`: Daily ACRU/Calcite sediment yield for each cell (tons.day^{-1})
`riverQ.ann` : Annual total discharge per cell (million m^3)
`riverQs.ann` : Annual total calibrated sediment yield per cell (thousand tons)

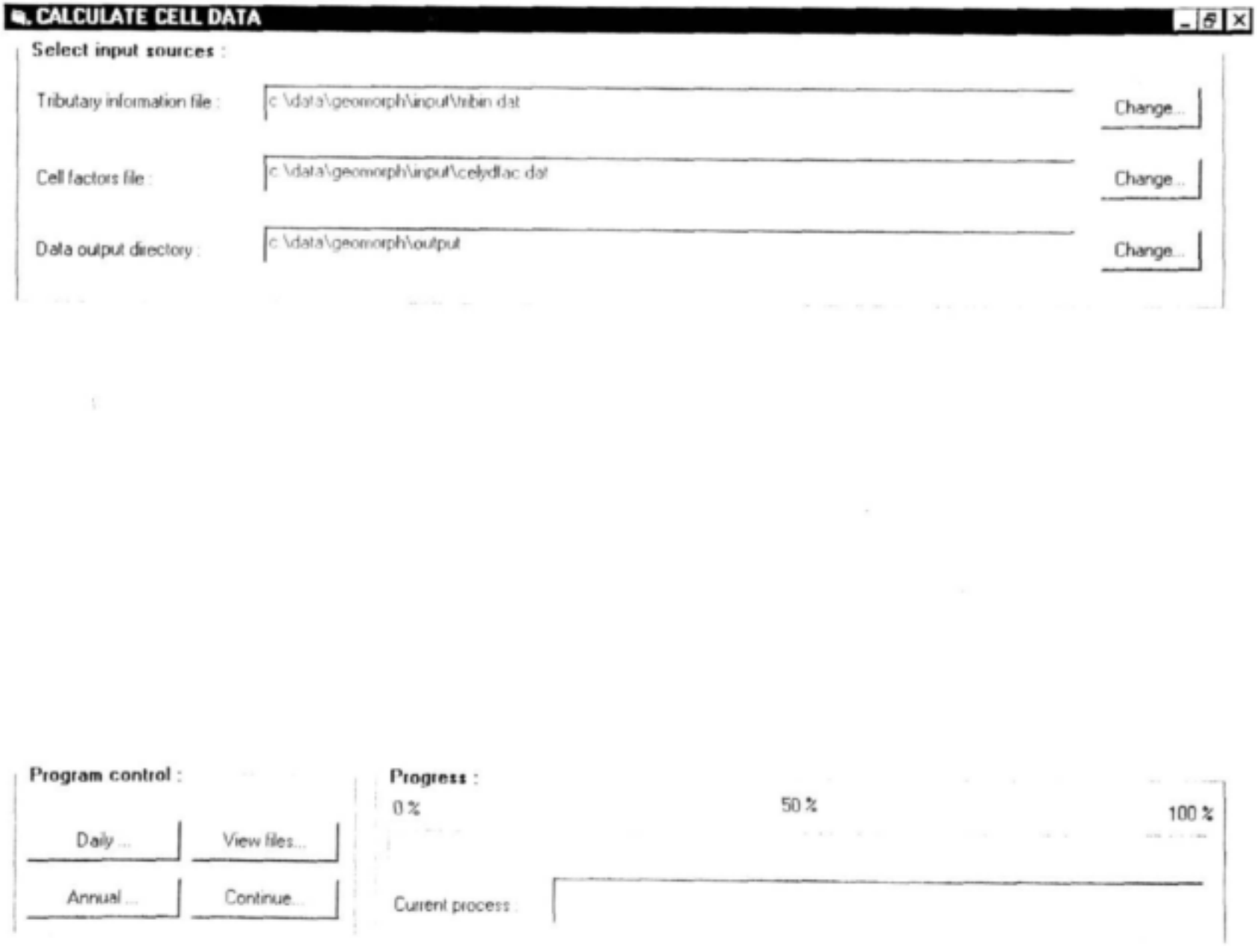

Figure 3.1 : Data input screen for determining and calculating cell sediment and flow inputs

Chapter 4
Calculating sediment transport

4.1 Purpose

This module is the core component of the SEDFLO model and deals with the differential transport of sediment along the study river system. The approach adopted is based on the Ackers and White (1973) method and is comprehensively discussed in Section 5.3 of the main report (Birkhead *et al.* 1998).

4.2 Input files

The time series of sediment transport capacities are computed by developing characteristic transport potential relationships for each of the five channel types identified by Heritage *et al.* (1997). Three categories of input data are required, corresponding to cross-sectional, resistance and slope parameters respectively. Specifications for each category of file are given below and the parameter files used in the case study simulation are provided with the programme files.

(a) Cross-sectional data files (`..xs.dat`)

For each of the five principal channel types, 3 or 4 cross-sections from representative channel type reaches have been used. Table 4.1 below summarises the required file names for each cross-section.

Table 4.1 : Required filenames for cross-sectional data corresponding to the five channel types

Channel type	File name
Single-thread	`stxs.dat`
Braided	`brxs.dat`
Pool-rapid	`prxs.dat`
Mixed anastomosing	`maxs.dat`
Bedrock anastomosing	`baxs.dat`

As all the cross-sectional input files follow the same format, only one (`stxs.dat`) will be discussed in detail. The first line indicates the type of channel, while the second line is a prompt for indicating the number of cross-sections (`nxs (chtype)`) which are included for this channel type and must be indicated on the third line. The next line is a prompt indicating that the distance

between cross-sections (`dy(count1)`) must be entered on the next line. The number of data points (separated by commas) will be one less than the total number of cross-sections. The following line (5) represents the first of the data pertaining to the first cross-section, indicating the cross-section name followed by 3 parameters on the next line. These parameters indicate the cross-section number (`xs`), the number, and a control parameter which is not used in this version of the model (`yo(chtype,count2)`). A list of comma delimited points follows, corresponding to the x and z ordinates along the cross-sections. The number of pairs in the list must equal the number of datapoints (`nxzdatapts(chtype,xs)`). Table 4.2 below summarises the format of this series of files.

Table 4.2 : Input file format for the cross-sectional data (e.g `stxs.dat`)

```
Single Thread Channel Type
No. of cross-sections
nxs chtype
Distance between cross-sections (m)
dy count1),...., dy(nxs(chtype)-1)
Reach cross-section 1x.x
xs,nxzdatapts(chtype,xs), yo(chtype,count2)
x chtype,xs,count3), z(chtype,xs,count3)
.
.
.
x chtype,xs,nxzdatapts(chtype,xs)), z(chtype,xs,nxzdatapts(chtype,xs))
Reach cross-section 2x.x
.....
```

Example from the Sabie-Sand catchment (single thread channel) :

```
Single Thread Channel Type
No. of cross-sections
4
Distance between cross-sections (m)
61,171,237
Reach cross-section 0.3
1,22,0
    0.000,409.362
    1.188,409.033
    8.616,406.964
    7.117,404.678
    ...
    ...                                    For 22 x and z points
Reach cross-section 0.4
...
```

(b) Resistance data files (`..res.dat`)

The second category of data files are those for determining resistance for each of the five channel types. The required filenames for these files are indicated in Table 4.3 below.

Table 4.3 : Required filenames for cross-sectional data corresponding to the 5 channel types

Channel type	File name
Single-thread	`stres.dat`
Braided	`brres.dat`
Pool-rapid	`prres.dat`
Mixed anastomosing	`mares.dat`
Bedrock anastomosing	`bares.dat`

The first three lines are the headings indicating which channel type the data is for, as well as the units (Table 4.4). The first important parameter occurs on the fourth line and indicates the number of discharge (Q) versus Manning's 'n' points (`nQndatapts(chtype)`) in the file. The indicated number of data pairs then follows.

Table 4.4 : Input file format resistance data (e.g `stres.dat`)

```
Manning's flow resistance data
Single Thread Channel Type
Q(m3/s), n
nQndatapts(chtype)
   Q(chtype, count1) Manning(chtype,count1)
   .      .
   .      .
   Q(chtype, nQndatapts(chtype)) Manning(chtype,nQndatapts(chtype))
```

Example from the Sabie-Sand catchment (single thread channel) :

```
Manning's flow resistance data
 Single Thread Channel Type
 Q(m3/s), n
       12
        1  0.077322
        2  0.066756
        5  0.05402
       10  0.045239
     1000  0.04721
        . .
        . .
     3000  0.06397
```

(c) Energy slope data (`riversf.dat`)

This file contains the energy slope data for each of the 40 cells, providing an energy slope during high and low flow conditions (the parameter values are identical for the calibrated model). The channel type of each cell is also indicated (Table 4.5)

Table 4.5 : Input file format for energy slope data (`riversf.dat`)

```
Description of datafile
Order of parameters
cell    chantype(cell)   Sflow(cell)   Sfhi(cell)
.            .              .            .
.            .              .            .
ncells  chantype(ncells) Sflow(ncells) Sfhi(ncells)
```

Example from the Sabie-Sand catchment (single thread channel) :

```
    Sabie River cell channel type and energy slope data
    cell chtype Sflowflow   Sfhighflow
    1       1    0.00126 0.00126
    2       2    0.00136 0.00136
    3       3    0.00216 0.00216
    .       .      .            .
    .       .      .            .
   40       5    0.00314 0.00314
```

4.3 Running the program

In order to run this component select [MODEL] from the main screen menu and [Sediment transport capacity] from the popup menu. The [CALCULATE SEDIMENT TRANSPORT CAPACITY] screen will be displayed as in Figure 4.1. Default input and output paths or files pertaining to the Sabie-Sand catchment are displayed. These can be changed using the [Change...] button. The [Viewfile...] button will load a simple text editor to enable one to view and edit the ancillary parameter files. The program is executed by the [Daily...] button and the computational process is displayed in the bottom right of the screen. Having calculated the daily files it is then possible to produce annual summary files, and this is done by clicking the [Annual...] button. Depending on input files, this program may take a few minutes to run (e.g. in the case of Sabie-Sand catchment approximately 10 minutes).

4.4 Computational sequence and output files

(a) Calculating geometric (`xxXSx.geo`) **and hydraulic** (`Cellxx.hyd`) **parameters**

The first part of this module reads in the cross-sectional and resistance data from the 10 parameter files described in 4.2(a) and (b) above. The next phase then computes the

geometric parameters for each of the cross-sections and for each of the channel types. As there are 4 cross-sections for each channel type except bedrock anastomosing where there are only 3 cross-sections, this results in 19 files containing geometric parameters. Thus for each of the 5 principal channel types, three or four cross-sections from the representative channel type reaches have been used to compute the *cross-sectional flow areas*, and *wetted perimeters* corresponding to a range of *flow depths* up to the macro-channel bank-full levels. In addition, the values of the parameter representing the *geometric determinants* in the Manning's resistance relationship are also calculated (See Maun Report, Section 5.5.2). The 19 files containing these data are named `ctXSx.GEO`, where `ct` refers to the naming convention for the channel type (see Table 4.1) and `XSx` refers to the cross-section number. Thus for cross-section 3 of the single-thread channel, the corresponding file will be `stxs3.geo`. Based on the energy slope parameters (`riversf.dat`), hydraulic variables are then computed for each cross-section of each cell resulting in a file for each cell (`Cellxx.hyd`) containing these parameters (See Section 5.5.2.1, Main Report).

(b) Solving Manning's equation and calculating potential sediment transport capacity

Manning's equation is solved for every cross-section within each of the 40 river cells, using the hydraulics data parameters (`Cellxx.hyd`) for each cell and also the geometric data for each cross-section of the specified channel type. Thus for Cell 1 (a single thread cell) it reads in the 4 cross-sections (`STXS1.GEO` to `STXS4.GEO`), matches geometric and hydraulic parameters and interpolates area, width and perimeter data. The *shear stress*, *average velocity*, *shear velocity* and *Froude number* are then calculated.

Based on the Ackers and White (1973) method, sediment transport capacity is then calculated (See Section 5.3.2 of Main Report (Birkhead *et al.* 1998). In this approach, sediment transport is determined as a function of sediment mobility, which depends on grain size and density, as well as the flow condition. The latter aspect is defined in terms of shear velocity, and whilst total shear velocity is used when considering fine or suspended sediments, effective shear stress is used for coarser sediments. For intermediate grain sizes an weighted combination is used, depending on grain and fluid characteristics. Section 5.3.2.2 (Main Report) defines the computational procedure whereby sediment transport is determined by combining the efficiency of the applied stream power (the rate of work done in moving bed load or maintaining suspension) with the mobility number.

Output files resulting from this process include a series of files (`CellxxSx.qy`), with one file for each cross-section within a cell. In calculating sediment transport, the calculated sediment transport is multiplied by the channel type scaling factors required as user input on the screen (See Table 17, Main Report), the purpose of which is to derive a more realistic long-term sediment discharge function. The next series of files in this section are (`Cellxxtr.cap`). This represents the minimum transport capacity as a function of discharge, and the data for all cells are written to the file (`allcell.qs`). The final sequence in this section is the calculation of annual sediment transport capacity (`riversdtr.ann`) based on the modelled discharge (`Cellxx.Q`) for each cell over the length of record.

In summary the following output files are produced in the calculation of sediment transport capacity :

`ctXSx.geo`: 19 geometric parameter files where `ct` refers to the naming convention for the channel type and `XSx` refers to the cross-section number

`Cellxx.hyd`: 40 files (one for each cell) of cell hydraulic parameters

`CellxxSx.qy` 151 files (one for each cross-section in each cell) of transport capacity factors

`Cellxxtr.cap`: 40 files (one for each cell) of sediment transport capacity for that cell

`allcell.qs`: 1 file with the minimum transport capacities for each cell over a range of discharges

`riversdtr.ann`: 1 file providing the actual sediment transport capacity predicted for the modelled discharge over the period of record

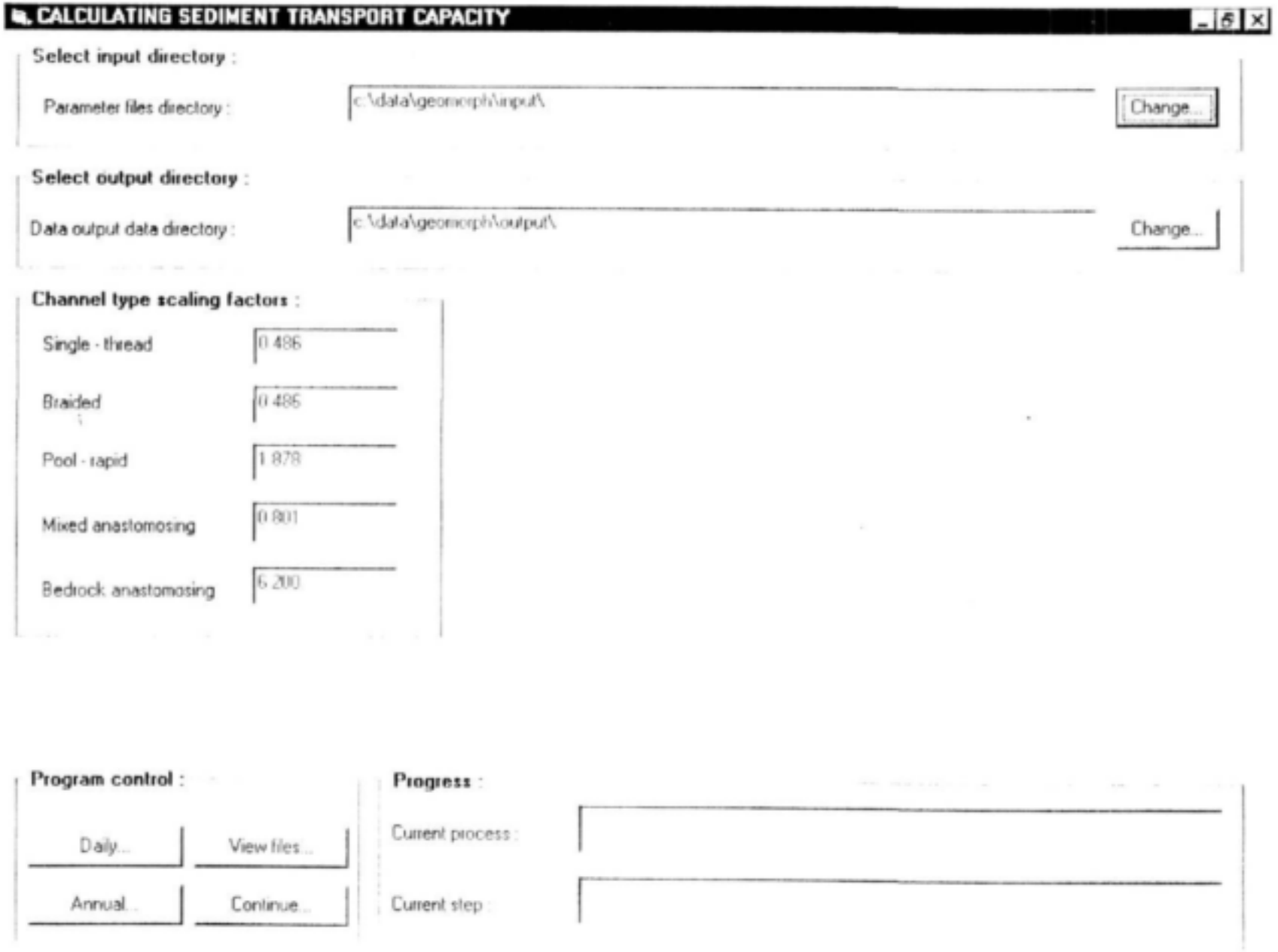

Figure 4.1 : Data input screen for sediment transport capacity calculation

Chapter 5
Mass balance sediment budget

5.1 Purpose

The primary purpose of SEDFLO is to predict the temporal change in storage for the 40 linked cells. This module undertakes a simple mass balance on the basis of the calculated sediment transport capacity for each cell and the predicted sediment yield for each cell, as determined in previous modules and discussed in previous Chapters. The final product of this module is a graph showing change in storage for the river system over the simulation study period, and a corresponding data file.

5.2 Input files

Only two files are required, the file containing the calculated minimum sediment transport capacities for each cell over the range of discharges (`riverQscal.ann`), and the file containing the annual sediment delivery to each cell (`riversdtr.ann`). The calibration factor entered on the data input screen adjusts the predicted sediment yields.

5.3 Running the program

In order to run this component select [MODEL] from the main screen menu and [Mass balance sediment] from the popup menu. The [SEDIMENT MASS BALANCE] screen will be displayed as in Figure 5.1 overleaf. Default input and output paths or files pertaining to the Sabie-Sand catchment are displayed. These can be changed using the [Change...] button. The program is executed by the [Plot...] button and a graph displayed once the sediment mass balance has been completed Changing the start or end of the plotting period will require the [Plot...] button to be clicked to show the new graph.

5.4 Computational sequence and output files

Figure 29 of the Main Report (Birkhead *et al.* 1998) provides an overview of the computational approach. This figure shows the sediment mass balance for three linked cells over two discrete time-steps. This process is followed to calculate sediment flux for the whole river reach and the results are displayed graphically as well as being written to file (`massbalance.txt`).

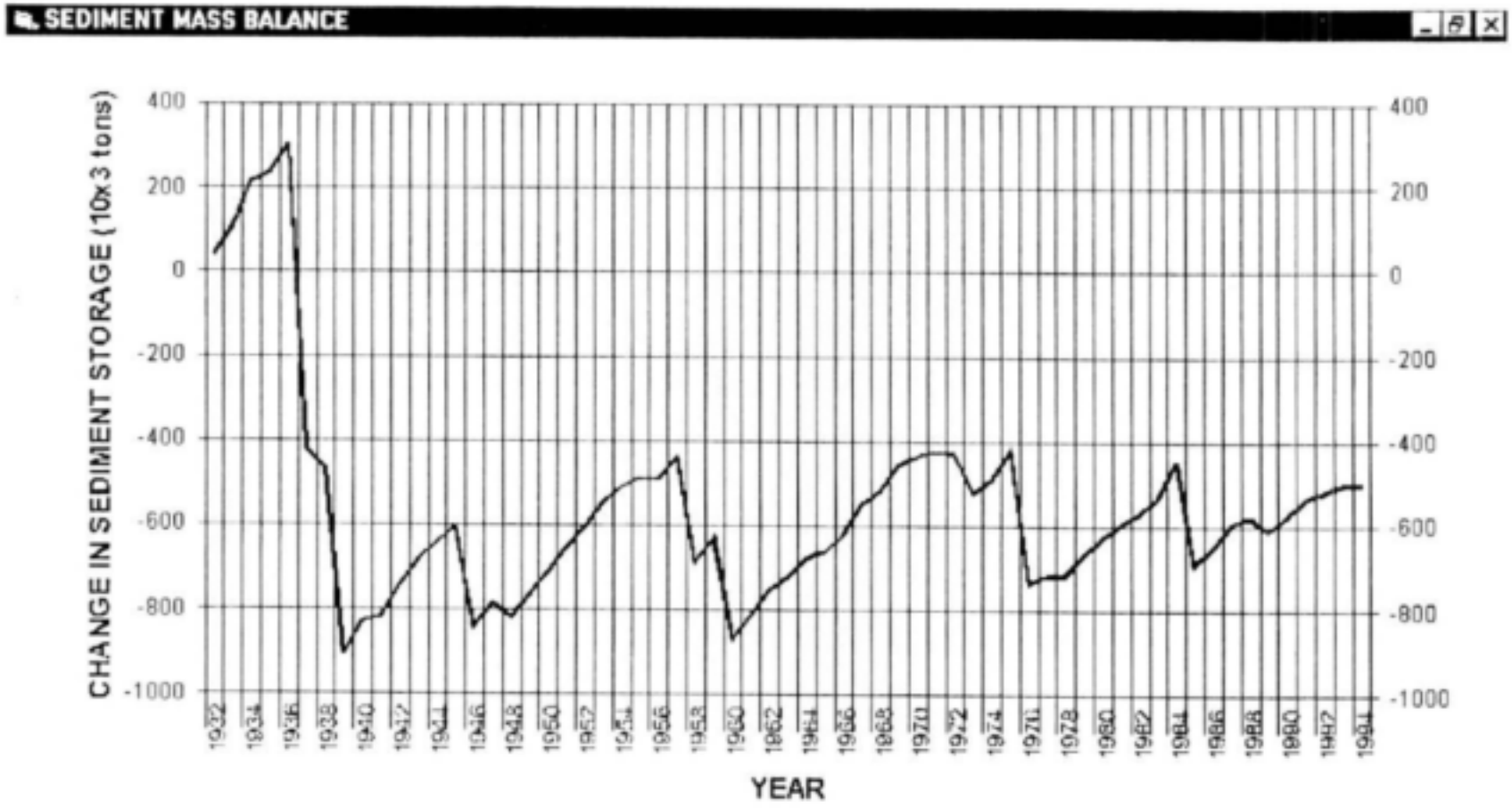

Figure 5.1 : Data screen for calculating and plotting the sediment mass balance

Chapter 6
Plotting and viewing results

6.1 Plotting and viewing daily data

Select [Tools] from the main menu screen and [Graph] from the pop-up menu. A further pop-up menu will be displayed: select [Daily] to load the daily data plotting screen. Several categories of daily data are written during the course of the modelling process. However all of these files have the extension .Q, .Qc or .Qs. The file to be plotted must be displayed in the left hand corner of the screen and can be changed by clicking the [Change...] button and selecting from the available files. The period over which you wish to plot the data must be entered on the two right hand text boxes. The default is 10 years. The graph can be viewed by selecting [Plot...] (Figure 6.1). Changing any of the output options will result in the graph disappearing and the [Plot..] button will have to be clicked again to view the new graph.

6.2 Plotting and viewing annual data for all cells

Select [Tools] from the main menu screen and [Graph] from the pop-up menu. A further pop-up menu will be displayed: select [Annual], [All cells] to load the annual data plotting screen. The three files used in the plotting must be displayed in the left hand corner of the screen and can be changed by clicking the [Change...] button and selecting from the available files. The year for which you wish to plot the data must be entered in the right hand text boxes. The graph can be viewed by selecting [Plot...] (Figure 6.2). Changing any of the output options will result in the graph disappearing and the [Plot..] button will have to be clicked again to view the new graph. Alternatively the user may 'step' forward or backward through the annual time series by clicking the [Next year...] or [Last year...] buttons respectively.

6.3 Plotting annual data for selected cells

Select [Tools] from the main menu screen and [Graph] from the pop-up menu. A further pop-up menu will be displayed: select [Annual], [Some cells] to load the annual data plotting screen. The three files used in the plotting must be displayed in the left hand corner of the screen and can be changed by clicking the [Change...] button and selecting from the available files. The cells and years for which you wish to plot the data must be entered in the right hand text boxes. The graph can be viewed by selecting [Plot...] (Figure 6.3). Three graphing options are available; annual discharge, annual sediment yield or discharge vs. sediment transport capacity.

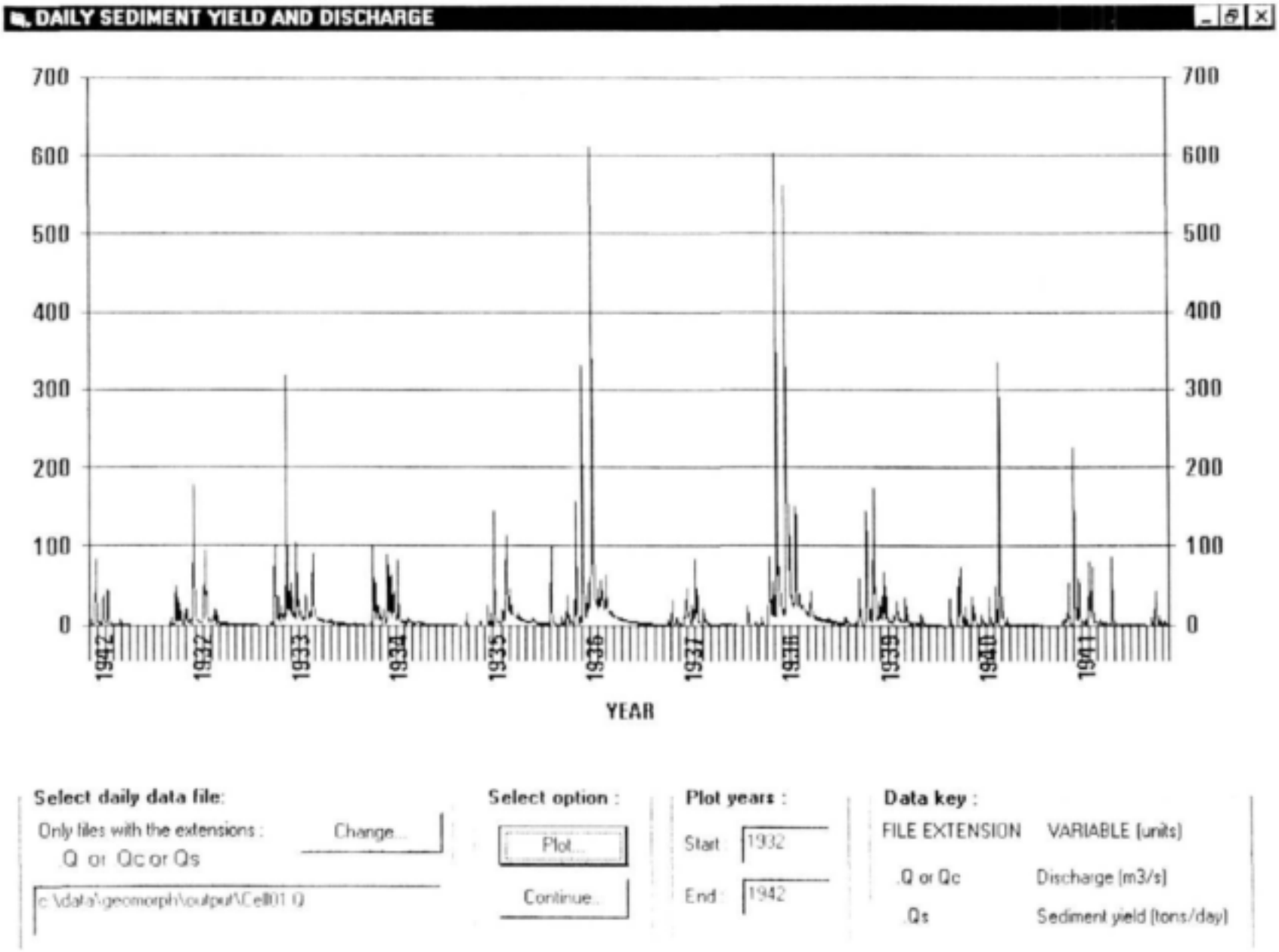

Figure 6.1 : Daily graphing screen

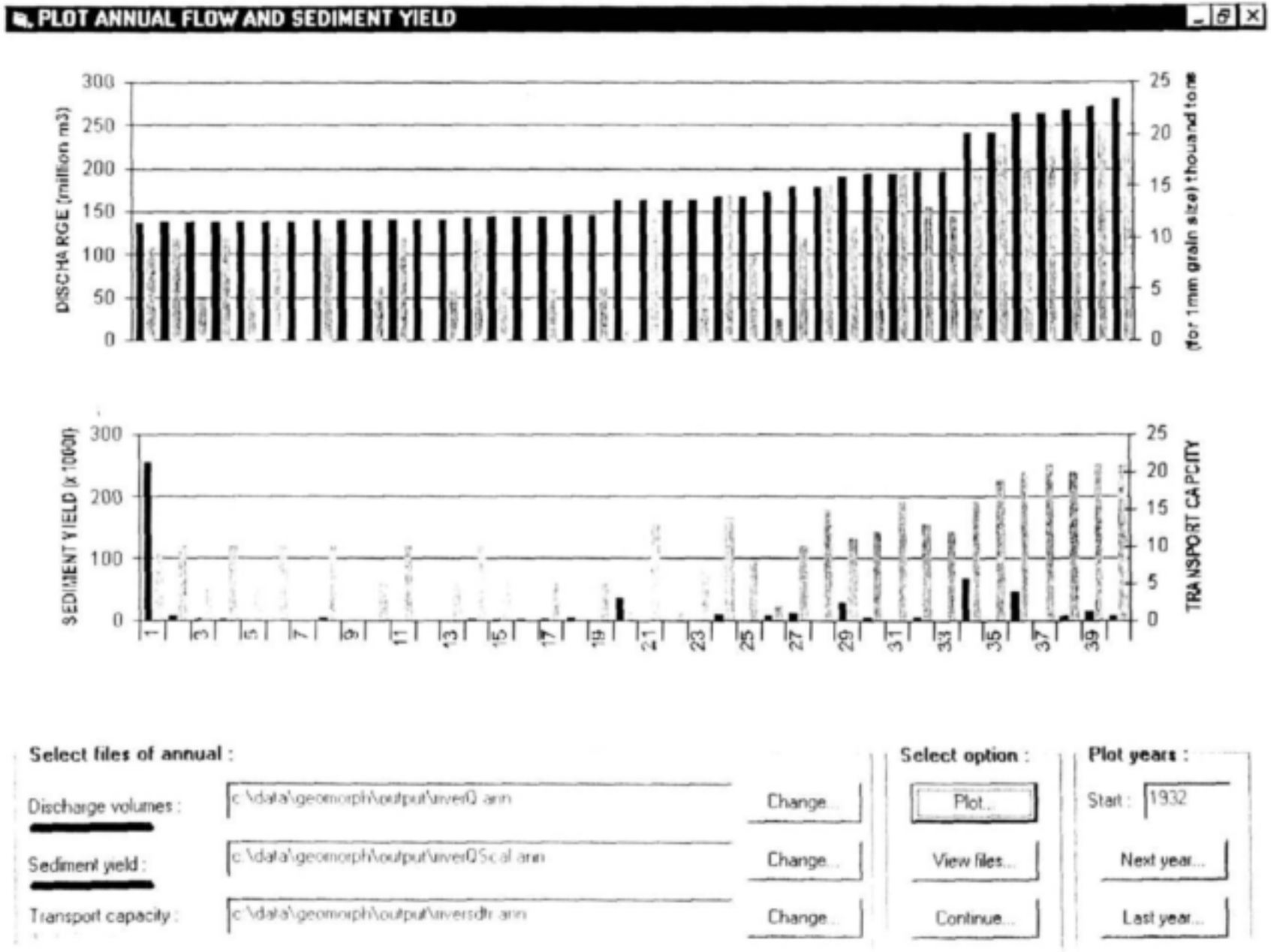

Figure 6.2 : Annual graphing screen

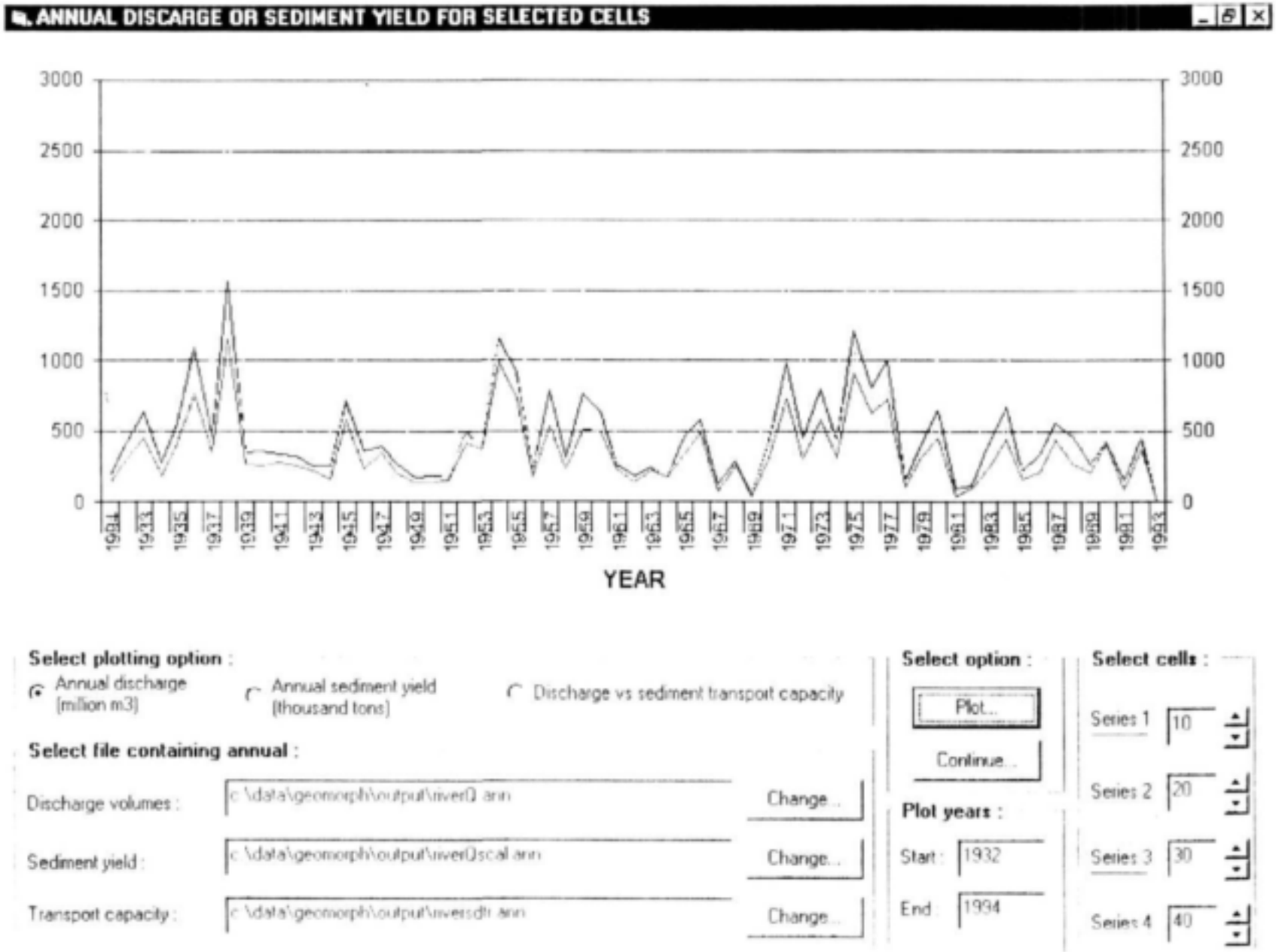

Figure 6.3 : Annual discharge or sediment yield for selected cells

Chapter 7
Concluding remarks and references

7.1 Concluding remarks

This User Manual is not intended as a comprehensive guide to the SEDFLO Model, and is only intended to provide an overview of the graphical interface to the SEDFLO Model. As discussed previously, the SEDFLO Model was developed, tested and calibrated for the Sabie-Sand catchment and has not been applied to any other catchment. To do so would require considerable data collection and calibration.

For further information consult the references below or contact the Centre for Water in the Environment, University of the Witwatersrand.

7.2 References

Ackers, P. and R. White. 1973. Sediment transport: new approach and analysis. *Journal of the Hydraulics Division, ASCE*. 99, HY11: 2041 - 2060.

Birkhead, A.L., G.L. Heritage, C.S. James, K.H. Rogers and A.W. van Niekerk. 1998. Geomorphological change models for the Sabie River in the Kruger National Park. WRC Report No. 782/1/98. Water Research Commission, Pretoria.

Heritage, G.L., A.W. van Niekerk, B.P. Moon, L.J. Broadhurst, K.H. Rogers and C.S. James. 1997. The geomorphological response to changing flow regime of the Sabie and Letaba River Systems. WRC Report No. 376/1/97. Water Research Commission, Pretoria.

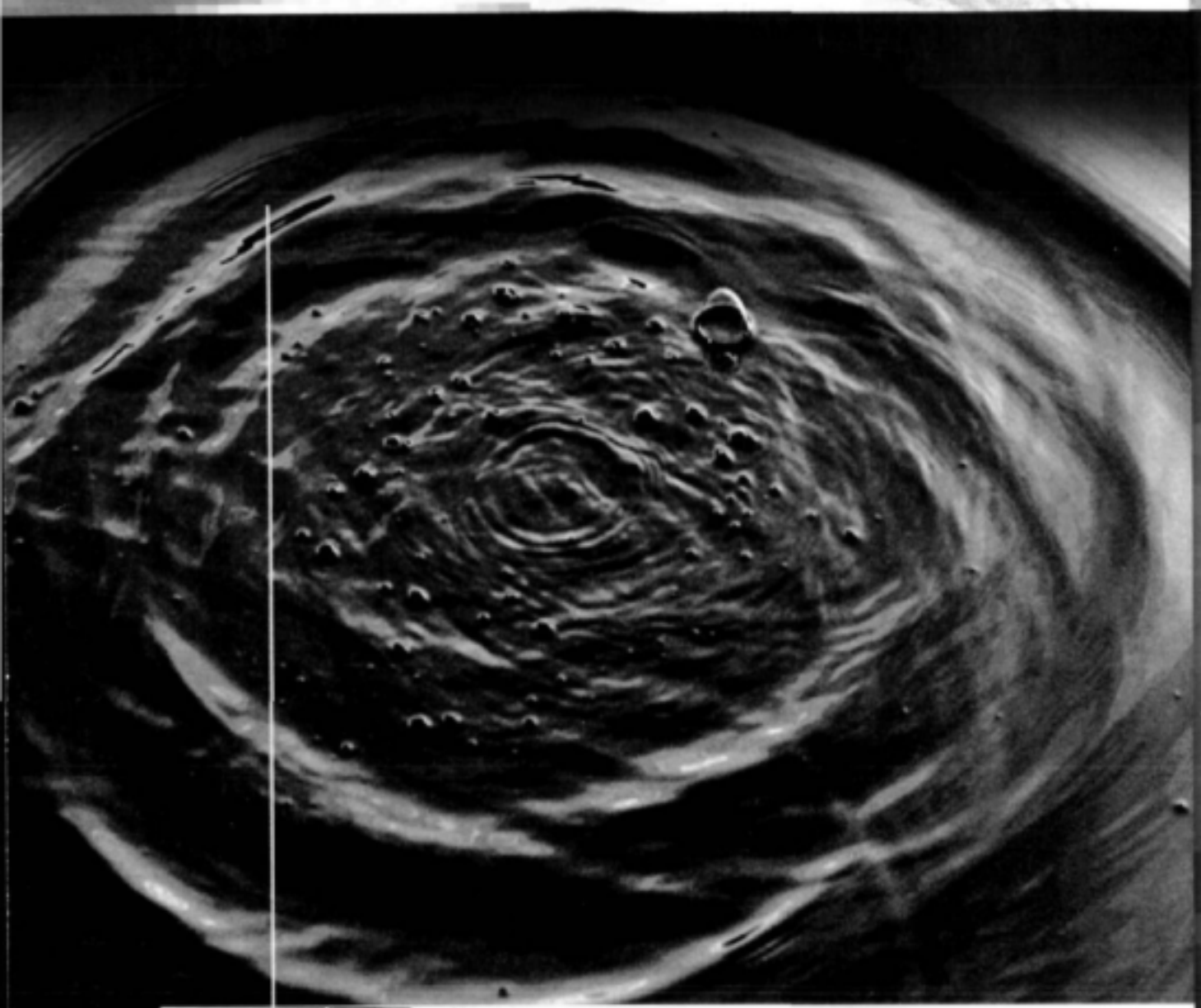

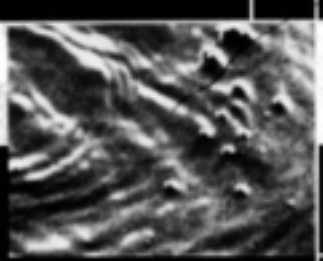

Water Research Commission
PO Box 824, Pretoria, 0001, South Africa
Tel: +27 12 330 0340, Fax: +27 12 331 2565
Web: http://www.wrc.org.za

1868453170